FINAL REPORT

RPSEA Project Number: 11122-27

Title: Relationships between Induced Seismicity and Fluid Injection: Development of Strategies to Manage Fluid Disposal in Shale Hydrocarbon Plays

Institution: Jackson School of Geosciences, University of Texas at Austin

Funding Active: 11 March 2013 – 10 March 2015

Principal Investigators:

Cliff Frohlich (cliff@ig.utexas.edu)
Institute for Geophysics
University of Texas at Austin
10100 Research Blvd (R2200)
Austin, TX 78758-4445

Julia Gale (julia.gale@beg.utexas.edu)
Bureau of Economic Geology
University of Texas at Austin
10100 Research Blvd (R2200)
Austin, TX 78758-4445

Peter Eichhubl (peter.eichhubl@beg.utexas.edu)
Bureau of Economic Geology
University of Texas at Austin
10100 Research Blvd (R2200)
Austin, TX 78758-4445

LEGAL NOTICE

This report was prepared by The University of Texas at Austin as an account of work sponsored by the Research Partnership to Secure Energy for America, RPSEA. Neither RPSEA, members of RPSEA, the National Energy Technology Laboratory, the U.S. Department of Energy, nor any person acting on behalf of any of the entities:

a. MAKES ANY WARRANTY OR REPRESENTATION, EXPRESS OR IMPLIED WITH RESPECT TO ACCURACY, COMPLETENESS, OR USEFULNESS OF THE INFORMATION CONTAINED IN THIS DOCUMENT, OR THAT THE USE OF ANY INFORMATION, APPARATUS, METHOD, OR PROCESS DISCLOSED IN THIS DOCUMENT MAY NOT INFRINGE PRIVATELY OWNED RIGHTS, OR

b. ASSUMES ANY LIABILITY WITH RESPECT TO THE USE OF, OR FOR ANY AND ALL DAMAGES RESULTING FROM THE USE OF, ANY INFORMATION, APPARATUS, METHOD, OR PROCESS DISCLOSED IN THIS DOCUMENT.

Table of Contents

1. Executive Summary 3
2. Barnet Shale Seismicity/injection Well Results 8
3. Eagle Ford Seismicity/injection Well Results 21
4. Bakken Seismicity/injection Well Results 39
5. Haynesville Seismicity/Injection Well Results 51
6. 17 May 2012 M4.8 Earthquake near Timpson, Texas 60
7. Geomechanics of the 17 May 2012 Timpson, Texas, M4.8 Seismic Event 79
8. Geomechanical Modeling of the Fort Worth Basin 104
9. Geological Synthesis 117

Appendix I: Earthquake Locations Determined in this Project 139

Appendix II. Publications Resulting from this Project 144

Appendix II. Technology Transfer Efforts Undertaken During this Project 145

1. Executive Summary

As stated in the Statement of Work of the subcontract agreement for this project, the primary objectives of this program were to:

(1) Determine the relationships between fluid injection practices, regional geology and stress regime, and the occurrence of earthquakes;

(2) Identify waste-disposal strategies for injection that reduce and minimize the triggering of seismic activity, or that ensure that seismic activity is confined to low-magnitude, harmless events.

The Statement of Work outlined the following tasks to be performed:

Task 1.0 – Project Management Plan

Task 2.0 – Technology Status Assessment

Task 3.0 – Technology Transfer

Task 4.0 – Other Reports and Special Items

Task 5.0 – Two-Year Surveys of Natural and Induced Seismicity in Four Shale Plays

Task 6.0. – Compilation of Injection Well Information

Task 7.0. – Statistical Comparison of Seismicity to Injection Data

Task 8.0. – Building Fault Models in Selected Areas: Data Acquisition and Integration

Task 9.0. – Analysis of Fault Reactivation Potential for Selected Areas

Task 10.0 – Synthesis and Development of Improved Injection Strategies

This Final Report will focus on summarizing research progress related to Tasks 5.0 to 10.0. However, Appendices II and III of this report present summaries of publications completed and presentations given during the active period of the project, and as such constitute a record of results associated with technology transfer Tasks 2.0 and 3.0.

Sections 2-5 of this report relate to Tasks 5.0 and 6.0, describing two-year surveys of earthquake activity in the Fort Worth Basin of Texas (section 2), the Eagle Ford of Texas (section 3), the Bakken/Williston Basin of North Dakota and Montana, (section 4) and the Haynesville of Texas and Louisiana (sections 5 and 6). Each section also includes an assessment of the relationship between seismic activity and injection wells.

In the Fort Worth Basin (Section 2), we identified 67 earthquakes occurring during the 2009-2011 survey period, of which only eight were reported by the U.S. Geological Survey. Of these 67 earthquakes, all the reliably-located events occurred in eight clusters, and each of these clusters was situated within 3.2 km of one or more high-volume injection disposal wells, i.e., wells having maximum monthly injection rates exceeding 150,000 barrels/month. This suggests that higher-volume injection wells in the Fort Worth Basin did trigger earthquakes; however, there

were numerous such high-volume wells that did not have earthquakes nearby. Thus it is unclear why earthquakes occurred near some high-volume wells and not others.

In the Eagle Ford (Section 3), we identified 62 earthquakes occurring during the 2009-2011 survey period, of which only four were reported by the U.S. Geological Survey. Of these 62 earthquakes, the majority (47 events) occurred following increases of fluid extraction (not injection) at nearby wells. The most reasonable conclusion is that most earthquakes identified in the Eagle Ford are triggered by petroleum operations—mostly by production/extraction of petroleum and water. But the triggering mechanism is clearly different than in the Fort Worth Basin, where earthquakes are associated with injection wells.

In the Bakken/Williston Basin (Section 4), we identified only nine earthquakes occurring during the 2008-2011 study period. Of these, only three were near injection wells. Thus earthquakes generally and possibly-triggered earthquakes in particular were far rarer in the Bakken/Williston Basin region than in the Fort Worth Basin or the Eagle Ford regions of Texas.

In the Haynesville of Texas and Louisiana (Section 5), we identified 50 earthquakes from the February 2010 through 2012 study period. We identify a cluster of activity near Bienville Parish, LA that has not been previously reported. This included 16 earthquakes between magnitudes 1.2-2.7 occurring over just a few months (August-October 2011). These smaller magnitude earthquakes without a preceding larger event for the Bienville Parish activity are most consistent with classification as a seismic swarm.

Data is available concerning monthly injection volumes, injection intervals, etc., for wells in Texas, but as yet we have been unable to obtain information about injection disposal volumes for wells in Louisiana. That is, within a few km of two high-volume injection wells in Texas, a series of earthquakes occurred which included the M4.8 17 May 2012 earthquakes south of Timpson, Texas. With collaborators from Stephen F. Austin University and the U.S. Geological Survey, we operated temporary seismograph stations and located numerous aftershocks the 2012 earthquake (Section 6). The locations and focal depths of these earthquakes suggest they occurred at and deeper than the depths of injection along a mapped basement fault. The evidence strongly suggests the sequence was triggered by injection.

When we conceived of this project, we anticipated that the relationship between seismicity and injection would be similar in the four geographic regions studied, and thus it would be reasonable to use statistical tools to assess salient features of the relationship (Task 7.0). However, to our surprise the relationship was hugely different in each of the four geographic regions: injection disposal triggered nearby earthquakes in the Fort Worth Basin; fluid extraction triggered earthquakes in the Eagle Ford; earthquakes were virtually non-existent in the Bakken; and two earthquake sequences within the Haynesville including an M4.8 triggered event, but otherwise little apparent triggered activity. Thus we did not pursue a statistical assessment of the relationship. However, the observation that the injection/seismicity relationship is significantly different in different geographic

regions is important and has implications for managing injection waste disposal operations. For example, it implies that before crafting regulations or implementing hazard-reduction actions in any particular local, surveys should be undertaken to assess the relationship between injection and seismicity within that local.

Sections 7 and 8 of this report concern developing geomechanical models to better understand the subsurface conditions where injection/extraction leads to seismic activity (Tasks 8.0 and 9.0). The most detailed, focused modeling effort was applied to the subsurface surrounding the epicenter of the 17 May 2012 M4.8 Timpson, TX earthquake (Section 7). The modeling indicated that the injection in two wells near the epicenter changed Coulomb stresses sufficiently to cause failure along a mapped (but previously unnoticed) fault. A practical implication of this work is that for proposed injection disposal operations, it indicates geomechanical modeling to evaluate Coulomb stress levels is a reasonable tool to apply to assess the geographic extent and location of possible earthquake activity, especially if there is information about rock properties and subsurface faulting near the proposed well.

The geomechanical model for the Fort Worth Basin described in Section 8 is considerably less detailed than the Timpson model of Section 7. The modeling approach here made very general assumptions about subsurface properties, and found that the areas where earthquakes occurred (especially in Johnson County TX) mostly coincided with areas of high fluid pressures in the subsurface. Previously, it had been puzzling why earthquakes occurred in several locations in Johnson County but not near many high-volume wells elsewhere in the Fort Worth Basin. The geomechanical modeling of Section 8 indicates that the greater injection volumes in Johnson County were sufficient to raise subsurface fluid pressures higher than in most other locations.

Section 9 also focuses on the Fort Worth Basin, evaluating publicly available information about mapped regional faults, the distribution of fault lengths, stratigraphy, and the properties of salt water disposal wells. The most detailed information came from analysis of reflection seismic images in Wise County, TX. Unfortunately, this was not an area where there was significant earthquake activity. Although proprietary data sets are know to exist in Johnson and Tarrant Counties where the highest rates of apparently-induced earthquakes occurred, we were unable to get access to these data.

Resulting from our research efforts, we here formulate several conclusions concerning the phenomenon of injection-triggered earthquakes, and associated recommendations concerning appropriate management strategies (Task 10.0).

• Conclusion #1: *The relationship between earthquake activity and injection/extraction varies greatly among different geographic environments*, ranging from "earthquakes are often associated with high-volume injection" in the Fort Worth Basin, to "earthquakes are often associated with increases in fluid extraction" in the Eagle Ford, to "injection/extraction is seldom associated with earthquake activity" in the Bakken. Retrospectively this is perhaps unsurprising from a geological perspective, as subsurface geology/rock type, porosity/permeability, and

thus hydrology/rock physics are known to vary greatly among different injection/production environments.

• Recommendation #1: *The above variability in response to injection/extractions suggests that prior to crafting detailed regulations or formulating an effective hazard reduction strategy at any specific location, it is desirable to evaluate the nature of the relationship (if any) between earthquake activity and injection/production.* This involves performing a survey to identify small-magnitude earthquakes and locating them with respect to injection/production operations. Because of the paucity of seismograph stations in many locations, performing a survey will require installation/operation of a seismic network.

• Conclusion #2: *When triggered earthquakes occur in environments where there is adequate seismic monitoring, knowledge of injection volumes at nearby locations, and sufficient information about subsurface structure, the earthquakes tend to occur approximately at depths at or beneath the depths of injection (often apparently in the basement), injection volumes tend to be relatively high (100,000 barrels/mo or more), and there is likely to be a fault situated within a few km of the epicenters and the injection wells.* Unfortunately, in most situations where there is an apparent association between earthquake activity and injection/extraction operations, there is little publically available information about subsurface faulting, and there is insufficient seismic monitoring to accurately determine earthquake focal depths.

• Recommendation #2: *Because of the possible association of triggered seismicity with higher-volume injection wells and subsurface faulting, we recommend that injection well operators focus attention on higher-volume injection wells, and make efforts to acquire and evaluate proprietary information about subsurface faulting near these wells, if such information is available*. Obviously, proprietary data concerning subsurface structure is often not available to researchers investigating the relationship between seismic activity injection/production. It could significantly improve our knowledge about this relationship if some way were found to encourage sharing of this information.

• Conclusion #3: *Where there is adequate information available concerning subsurface rock properties, structure and injection/extraction history including volumes and pressures, geomechanical modeling to evaluate Coulomb stresses provides a valuable tool for assessing whether past seismicity may have been triggered or whether future seismicity is likely to be triggered.* Geomechanical modeling has been applied in only a few cases. For injection well operators, it is a relatively cost-efficient means for gaining some insight into whether, when, and where a proposed operation may trigger seismic activity.

• Recommendation #3: *In our experience, available information concerning injection pressures is generally inadequate or barely adequate for geomechanical modeling; we thus suggest that operators of higher-volume injection wells be encouraged to collect and provide information about injection pressures sampled on at least an hourly basis*. Requirements for reporting injection pressures and volumes differ among the United States. In Texas, only monthly volumes and average and maximum pressure

levels are required, and it is often unclear what time intervals these pressure values represent. Moreover, controlled pressure tests administered at regular intervals (annually?) over the life of injection wells could provide critical information about reservoir volume and permeability; this information would be highly useful for contraining geoechanical models and (possibly) for identifying when an injection operation had reached a condition where seismic activity might be imminent.

• Conclusion #4: *The most significant still-unresolved research question concerning injection-triggered seismicity is why earthquakes occur near some injection wells and not near other wells having similar injection volumes*. We can hypothesize that earthquakes only occur at wells when there are suitably-oriented nearby faults, and a well-to-fault path with high enough permeability to raise pressure and reduce friction on the fault and allow failure. However, the presently available data isn't sufficient to prove this hypothesis.

• Recommendation #4: *We encourage efforts to obtain more information about subsurface structure and faulting near injection wells, including data both for wells that apparently trigger earthquakes and those that apparently do not*. It is desirable to obtain more detailed information about subsurface structure, information that is currently proprietary in most of the locations we studied, if we hope to reach a level of knowledge where we can quantitatively assess the relationship between subsurface faulting, injection volumes and pressures, and induced seismic activity.

2. Barnett Shale Seismicity/Injection Well Results

The material in this section was prepared by Cliff Frohlich and was published in 2012 in the *Proceedings of the National Academy of Sciences*, vol. 109, pp. 13934-13938, with the title "Two-year survey comparing earthquake activity and injection well locations in the Barnett Shale, Texas". Although this was published prior to the active funding period of this RPSEA project, the research here was undertaken as a pilot study to support our proposal to RPSEA, and included followup research completed after proposal submission but prior to the commencement of funding.

Abstract: Between November 2009 and September 2011, temporary seismographs deployed under the EarthScope USArray program were situated on a 70-km grid covering the Barnett Shale in Texas, recording data that allowed sensing and locating regional earthquakes with magnitudes M1.5 and larger. I analyzed these data and located 67 earthquakes, more than eight times as many as reported by the National Earthquake Information Center. All 24 of the most-reliably-located epicenters occurred in 8 groups within 3.2 km of one or more injection wells. These included wells near Dallas-Fort Worth and Cleburne, TX, where earthquakes near injection wells were reported by the media in 2008 and 2009, as well as wells in six other locations, including several where no earthquakes have been reported previously. This suggests injection-triggered earthquakes are more common than is generally recognized. All the wells nearest to the earthquake groups reported maximum monthly injection rates exceeding 150,000 barrels of water per month (24,000 m^3/mo) since October 2006. However, while 9 of 27 such wells in Johnson County were near earthquakes, elsewhere no earthquakes occurred near wells with similar injection rates. A plausible hypothesis to explain these observations is that injection only triggers earthquakes if injected fluids reach and relieve friction on a suitably-oriented, nearby fault that is experiencing regional tectonic stress. Testing this hypothesis would require identifying geographic regions where there is interpreted subsurface structure information available to determine whether there are faults near seismically active and seismically quiescent injection wells.

2.1 Introduction

It has been recognized since the 1960's that fluid injection into the subsurface can trigger earthquakes (Nicholson & Wesson, 1990; Suckale, 2009). Injection-triggered earthquakes have accompanied injection projects undertaken for various purposes, including the production of geothermal energy (Majer et al., 2007), secondary recovery in oil and gas fields (Davis & Pennington, 1989), the disposal of fluid wastes, and (very rarely) hydrofracturing (Kanamori & Hauksson, 1992; Holland, 2011).

Recently several widely publicized earthquake sequences have occurred near injection wells disposing of fluid wastes in Texas (Howe et al., 2010; Frohlich et al., 2011; Howe, 2012), Arkansas (Horton, 2012), West Virginia, Ohio and elsewhere. These fluid wastes are a byproduct of hydrofracturing; hydrofracturing has been an essential technology contributing to the development of unconventional gas

resources ongoing in several locations in the U.S. including the Barnett and Eagle Ford Shales in Texas, the Haynesville Shale of Texas and Louisiana, the Bakken Shale in North Dakota, and the Marcellus Shale in Pennsylvania, New York and West Virginia. Although this development has enormously increased domestic energy reserves, it may have contributed to an observed increase since 2009 in the number of small-magnitude earthquakes in the central and eastern U.S (Ellsworth et al., 2012). It has also raised policy concerns about possible seismic hazards associated with the practice of disposing of hydrofracture flowback fluids in injection wells (National Research Council, 2012).

Most investigations of induced or triggered earthquakes take place only after an earthquake occurs that is severe enough to be felt by nearby residents and receive media attention. Such events usually have magnitudes M~3 or greater and occur in populated areas. Limiting research only to these events doesn't help us understand why some injection wells trigger seismic activity and others do not. I am unaware of any previous investigation comparing the properties of injection wells that do and do not induce earthquakes.

In the present study I evaluate seismic activity occurring between 15 November 2009 and 15 September 2011 within the Barnett Shale of Texas (Fig. 2.1). During this interval the NSF-funded USArray program emplaced several hundred continuously-recording three-component broadband seismometers on a 70-km grid covering a 400-km-wide swath extending from the Canadian border to the Gulf of Mexico. In Texas, about 25 stations from this network were in or near the Barnett Shale, recording data allowing me to locate small regional earthquakes .

An important objective of this study is to assess the relationship between the presence/absence of earthquakes and the characteristics of nearby injection wells. In Texas, the vast majority of injection wells are Class II wells used to stimulate oil or gas production or to dispose of wastes associated with petroleum production such as hydrofracture fluids; the Texas Railroad Commission (RRC), which no longer regulates railroads, is responsible for regulating activity related to petroleum production. The RRC issues permits for drilling wells, and by law petroleum producers also provide the RRC with certain information concerning fluid injection, both when it is used to stimulate production and also when it used to dispose of fluid wastes.

2.2 Results

Seismic Data: Quarry Blasts and Earthquakes. Using a method to identify seismic phase arrivals by comparing short-term to long-term amplitude ratios, over the two-year study period I found 1330 seismic events with arrivals at four or more USArray stations. Of these, 319 were events occurring outside the study area, often because their arrival times were within a few seconds of predicted arrivals for NEIC-reported distant earthquakes, or because the (S-P) intervals or other features of their seismograms indicated they weren't local.

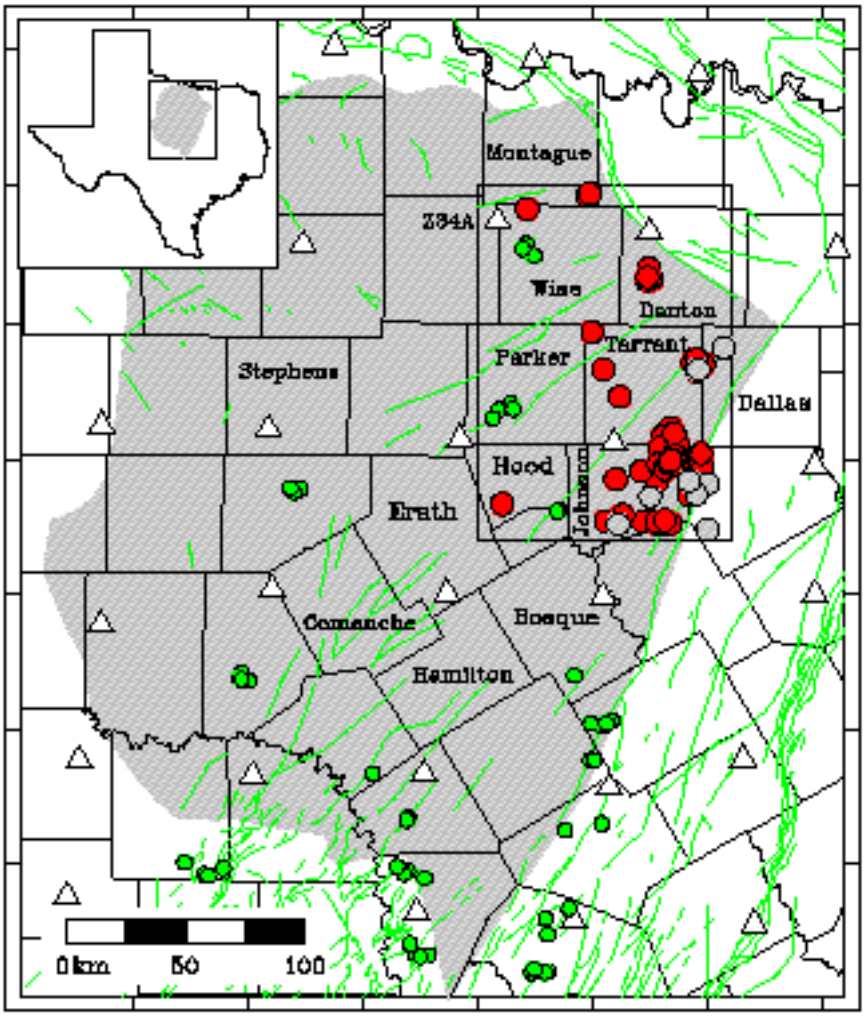

Fig. 2.1. Map of Barnett Shale study area; the inset and rectangle at upper left show area in Texas included in this map. Triangles are locations of USArray temporary seismic stations, red circles are earthquakes located in this study, green circles are quarry blasts located in this study, and white circles are epicenters reported by the National Earthquake Information Center (NEIC) during study interval (15 Nov 2009 to 15 Sept 2011). Gray shaded area is approximate extent of the Barnett Shale, green lines are mapped faults (Ewing, 1990); black lines are boundaries of Texas counties; labels indicate names of counties mentioned in the text. Dallas and Fort Worth are situated in Dallas and Tarrant Counties, respectively; the town of Cleburne is in Johnson County. Rectangle in upper right of figure indicates region mapped in Fig. 2.2.

I identified an additional 507 events as quarry blasts. The appearance of seismograms for quarry blasts and earthquakes is different, as quarry blasts typically have much larger, more prominent surface waves, and relatively weaker P and S arrivals except at the closest stations (distances of 30 km or less). Most quarries blast repeatedly, and thus the characteristic appearance of their seismic signals becomes familiar to an analyst. In some cases seismograms at the nearest

USArray station exhibited an unusual, high-frequency, radially-polarized arrival that traveled at 300 m/s, undoubtedly an air-wave. Moreover, inspecting occurrence times for any characteristic group reveals that the events never occur at night or on weekends. I located representative events for 52 blasts from about a dozen groups (Fig. 2.1). In most cases, inspecting the locations on GoogleMap revealed a quarry nearby; all quarry blast epicenters that had azimuthal gaps of 120° or smaller (all the 'A' quality locations, and some 'B' quality locations) were situated within 1.5 km from a visible quarry.

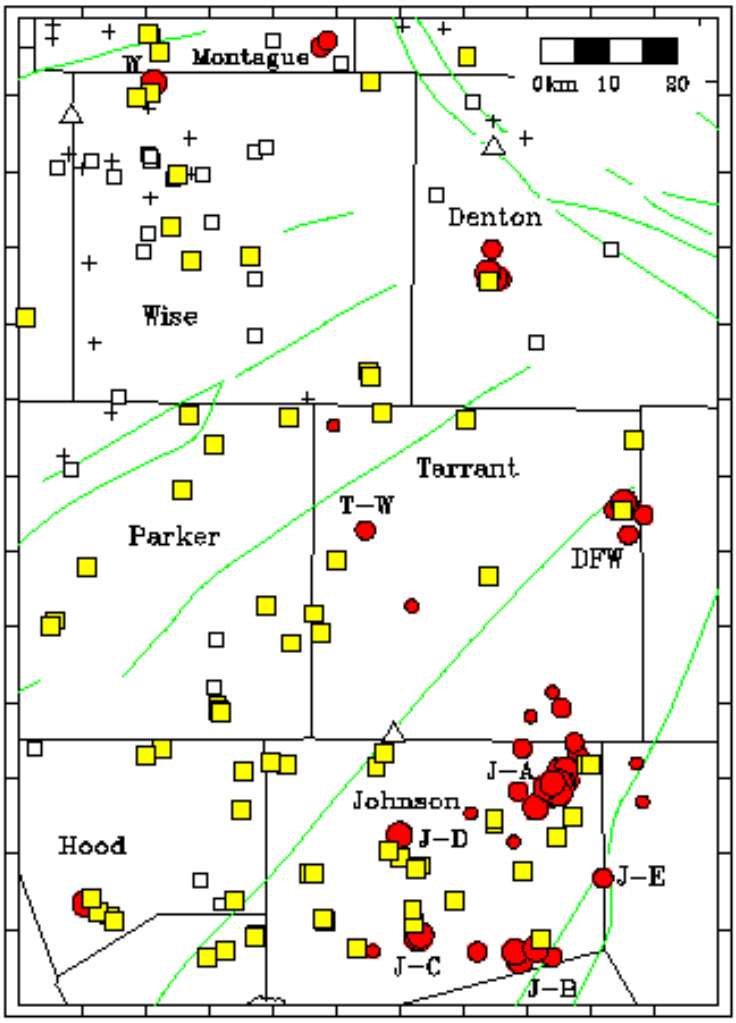

Fig. 2.2. Map showing earthquake epicenters determined in this study (red circles), injection wells (squares and '+' symbols) in use since October 2006, seismograph stations (white triangles), and mapped faults (green lines, from Ewing, 1990). Circle sizes indicate quality of epicentral location, with large, medium and small sizes indicating qualities 'A', 'B' and 'C'. Labels designate events or clusters in Table 2.1. For injection wells, yellow squares are wells with maximum monthly injection rates exceeding 150,000 BWPM (24,000 m^3/mo); white squares, exceeding 15,000 BWPM (2,400 m^3/mo) ; '+' symbols; exceeding 1500 BWPM (240 m^3/mo).

Table 2.1. Earthquake groups as located in this study and as reported by the NEIC and the ANF. Table reports number of earthquakes in each group and quality category. Quality is assigned considering number and geographic distribution of seismic data used for location, with 'A' indicating best locations. Distances listed are for all injection wells within 5 km, if such exist, from closest 'A' quality epicenter in each group, if such exists.

county and Fig. 2.2 label of group	*quakes rept. by NEIC*	*quakes rept. by ANF*	*quakes identified in this study*				*distance : nearest wells (km)*
			quality A	*quality B*	*quality C*	*cross-correlation*	
Wise W	-	1	1	-	-	1	1.6, 3.4, 4.5
Montague	-	1	-	2	-	2	3.9
Denton	-	4	3	4	1	40	0.9
Tarrant T-W	-	2	-	1	2	3	5.5
Tarrant DFW	2	3	2	4	-	3	1.3
Hood	-	1	1	-	-	-	1.1, 2.4, 4.0
Johnson J-A	3	6	8	15	9	24	3.2, 3.6, 5.0
Johnson J-B	-	-	3	4	0	3	1.6
Johnson J-C (Cleburne)	2	3	5	-	1	6	1.8, 3.8
Johnson J-D	-	-	1	-	-	-	2.9*, 2.9, 3.3
Johnson J-E	1	1	-	1	-	-	9.2
totals	8	22	24	30	13	82	

*All injection listed injection wells are Class II wells except for one Class I well 2.9 km from the J-D epicenter; this well's location and injection history is virtually identical to a the Class II well near J-D.

Among the remaining ~500 events, I was able to identify pickable P and S arrivals and determine epicenters for 67 earthquakes occurring within the study area (Figs. 2.1 and 2.2; Table 2.1). Of these, 46 were in Johnson County; most within three clusters (J-A, J-B, and J-Cleburne). In addition, there was a tightly clustered group of eight earthquakes in Denton County, and a cluster of six near the Dallas-Fort Worth airport between Tarrant and Dallas Counties. Finally, there were three isolated earthquakes in western Tarrant County, two events in Montague County, and single earthquakes in Wise and Hood Counties.

Only eight of these 67 located earthquakes were reported by the U.S. Geological Survey's National Earthquake Information Center (NEIC); only 22 are in the catalog compiled by the USArray's Array Network Facility (ANF), the organization that manages USArray seismograph stations. The differences between NEIC epicenters and those determined in this study ranged between 4 and 32 km, with five of the eight differences being between 9 and 16 km.

A reasonable estimate of location accuracy for the 'A' quality epicenters in this study is 1.5 km. This is consistent with the identification of quarries near 'A' quality blasts as mentioned above. And my locations for the five 'A' quality epicenters in the J-Cleburne group were all within 1.0 km of 2009 Cleburne epicenters located using a 5-station temporary local network (Howe et al., 2010; Howe, 2012).

Using signals recorded at the stations closest to several of the earthquake groups described above, I performed an autocorrelation analysis to search for additional unlocatable events too small to provide pickable P- and S arrivals at three or more USArray stations. This search identified an additional 82 earthquakes (Table 2.1), with 40 of these associated with the Denton group.

The analysis of USArray data allowed me to locate more than eight times as many earthquakes are reported by the NEIC. For the earthquakes in Fig. 2.1, the eight events reported by the NEIC had magnitudes between M2.1 and M3.0 with a median of M2.5; the 59 additional earthquakes located using USArray data had magnitudes between M1.4 and M2.5 with a median of M2.0; and the 82 earthquakes identified by cross-correlation analysis had magnitudes between M1.4 and M1.8 with a median of M1.6.

Injection Well Locations and Characteristics. Within the Barnett Shale neighborhood mapped in Fig. 2.1 there are 2458 injection wells reporting maximum monthly injection rates of 1500 barrels of water per month (BWPM; 1500 BWPM is 240 m^3/mo) or greater since October 2006 (Table 2.2). Of these, 125 are within the seismically active area mapped in Fig. 2.2.

Most of the earthquakes identified in this study are situated close to injection wells. Eight of the epicenter groups possess 'A'-quality epicenters (Table 2.1). All eight of these better-located groups have epicenters situated within 3.2 km of one or more of these injection wells; and, six of these groups include epicenters within 2.0 km.

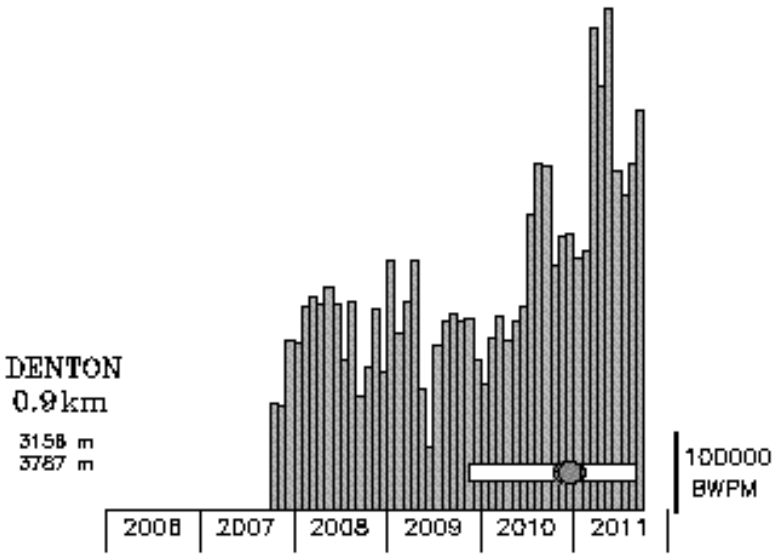

Fig. 2.3. Monthly injection rates the injection well near the Denton earthquake group identified in this study. Scale bar at right of each histogram is 100,000 BWPM (16,000 m³/mo). Rectangle shows time period of study; dark circles indicate earthquakes located in this study. Labels at left indicate distance to epicenter and depth interval of injection.

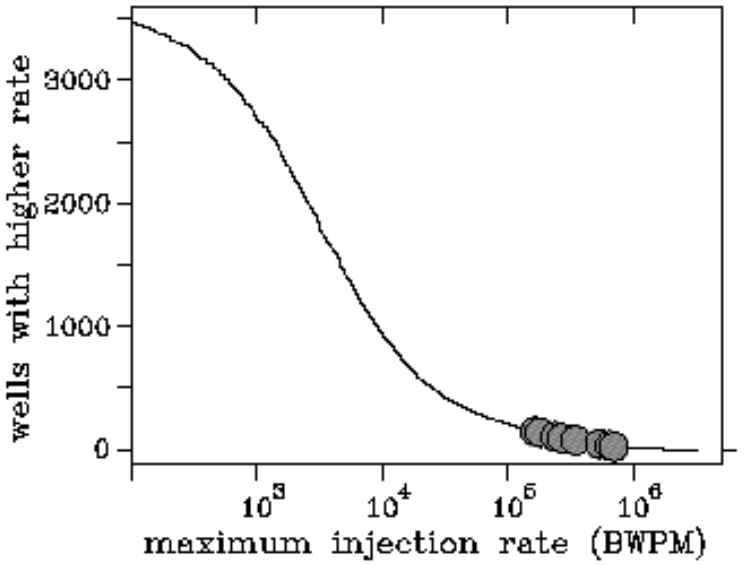

Fig. 2.4. Cumulative distribution of highest monthly injection rates for wells in the region mapped in Fig. 2.5. Horizontal axis is highest monthly injection rate between October 2006 and September 2011; vertical axis is number of wells exceeding plotted value. Dark circles correspond to maximum values for wells closest to the eight earthquake groups with 'A'quality epicenters identified in Fig. 2.2 and Table 2.1. Note that all eight have maximum injection rates exceeding 150,000 BWPM (24,000 m³/mo), a value exceeded by 160 wells in the mapped region (Figs. 2.1 and 2.5).

Table 2.2 Characteristics of injection wells/leases in selected regions. Table values are number of permitted wells/leases; values in the 'near EQ' column are number of wells where this study identified 'A' quality earthquake epicenters within 5 km; remaining columns are number of wells where maximum monthly injection rate between October 2006 and September 2011 exceeded specified value. Units for injection rates are barrels of water per month (BWPM); 1500 BWPM is 240 m³/mo.

geographic region	*near EQ*	*>150,000 BWPM*	*>15,000 BWPM*	*>1500 BWPM*
Parker County	0	14	20	24
Stephens County	0	24	77	165
Tarrant County	1	8	8	8
Wise County	3	9	27	36
Johnson County	9	27	27	27
Seismic region (Fig. 2.2)	17	74	106	125
Barnett Shale (Figs. 2.1, 2.5)	17	161	715	2458
Texas		1161	5017	9052

Injection had been ongoing at the wells near all eight of these epicentral groups prior to the known occurrence of earthquakes. Injection at all but one of these wells was at depths between 2 km and 4 km (see Fig. 2.3). And all had maximum monthly injection rates exceeding 150,000 BWPM (24,000 m^3/mo), and generally these injection rates had been maintained for a year or more prior to the onset of earthquake activity (Figs. 2.3 and 2.4). The Dallas-Fort Worth (DFW) group is an exception: earthquake activity began in October 2008 after only six weeks of injection at a nearby well (7); DFW earthquakes have continued into 2011 even although injection ceased in August 2009.

However, wells having sustained injection rates of 150,000 BWPM (24,000 m^3/mo) are common; there were 161 such wells in the region mapped in Fig. 2.1, and almost 90 per cent of these had no locatable earthquakes nearby (Table 2.2). For example, there are 14 such wells in Parker County with no nearby earthquakes, and 24 in Stephens County (see Fig. 2.5). In Wise County there are 9 such wells and only one locatable earthquake.

2.3 Discussion

Discovery of Previously Unknown Triggered Earthquakes. The most significant result of this investigation is that all of the better-located epicenters were situated within a few km of one or more injection wells. This is important because it suggests that small triggered earthquakes, M~2 and smaller, occur more often than reported previously. Most of these wells associated with earthquakes were not suspected of triggering earthquakes prior to this study: the NEIC had reported no earthquakes

near Denton, Hood, J-B, and Wise groups. And for the J-A and J-D groups, the NEIC locations had too-large uncertainties to identify individual wells; this study's more accurate locations are essential for identifying the responsible wells. Only the DFW and J-Cleburne groups had been confidently associated with particular wells prior to this study (Howe et al., 2010; Frohlich et al., 2011); in both areas this association had been confirmed only because temporary local seismograph networks had been installed.

It is possible that some of these earthquakes have a natural origin, but it is implausible that all are natural. The strongest candidate for a natural event is J-E in Fig. 2.2, a single earthquake that occurred on 0530 UT on 5 December 2009, and was situated ~9 km from the nearest injection well. Although the NEIC reported this earthquake and assigned it magnitude M2.9, this study assigned the location a 'B' quality because the earthquake occurred early in the study period and at that time USArray stations to the east had not yet been installed. Nevertheless it seems unlikely the location is inaccurate by more than a few km.

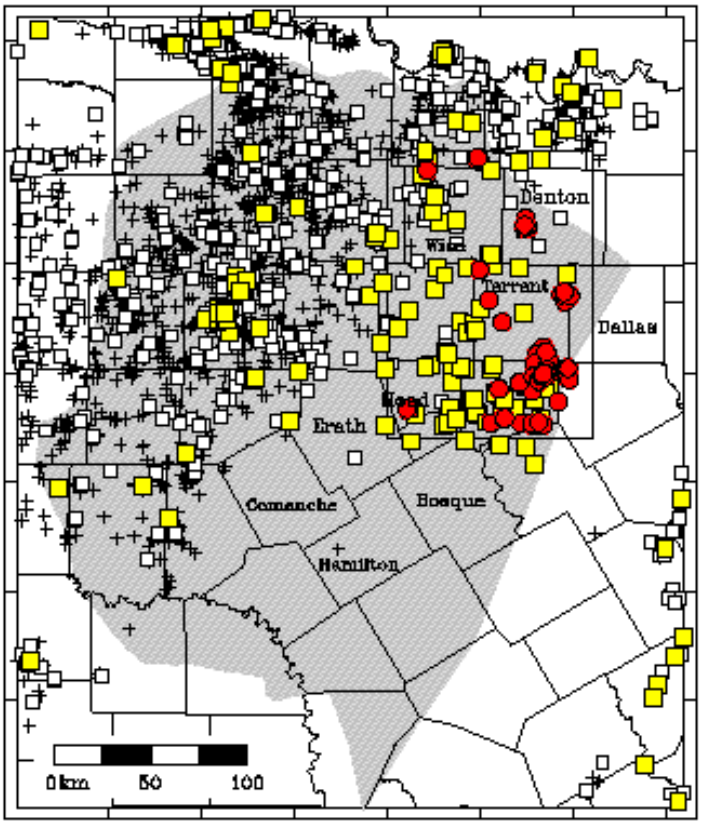

Fig. 2.5. Map of Barnett Shale area as in Fig. 2.1, showing earthquakes located in this study (red circles) and injection wells in use since 2006 (squares and '+' symbols). Yellow squares are wells reporting maximum monthly injection rates exceeding 150,000 BWPM (24,000 m^3/mo); white squares, exceeding 15,000 BWPM (2,400 m^3/mo); '+' symbols; exceeding 1500 BWPM (240 m^3/mo).

Characteristics of Earthquake-Triggering Wells. A second significant result of this study is that maximum injection rates exceeded 150,000 BWPM (24,000 m^3/mo) at the wells nearest all of the eight earthquake groups described above. Although this suggests that earthquakes are more likely to be triggered if injection reaches a critical rate, this critical rate may well depend on local subsurface conditions and thus vary in different geographic regions. In the Barnett Shale fluids are injected into the highly permeable Ellenburger formation; critical rates might be different under conditions where the permeability and other subsurface properties are different.

Moreover, it is unclear why earthquakes occur near some high-rate injection wells and not near other wells having apparently similar characteristics. Within the Barnett Shale there are more than 100 similar wells with injection rates exceeding 150,000 BWPM (24,000 m^3/mo) that experienced no nearby identifiable earthquakes during the study period (Figs. 2.4 and 2.5).

A plausible explanation is that injection-triggering only occurs if fluids reach suitably oriented, nearby faults (Frohlich et al., 2011). Surveys of crustal stress and observations from deep boreholes at several locations worldwide indicate that: 1) stress in continental interiors is fairly uniform within regional provinces having dimensions of hundreds of km (Zoback & Zoback, 1980); 2) the brittle crust is in a state of failure equilibrium (Zoback & Townend, 2001); with 3) the stress levels being controlled by networks of pervasive naturally-occurring faults; 4) where failure, enhanced by fluid flow, occurs according to Coulomb frictional failure theory along optimally oriented, critically stressed faults (Barton et al., 1995). Thus fluid injection may trigger earthquakes if pressures, rates, and permeability are sufficient to allow fluid to reach a favorably oriented fault and reduce the normal stress, decreasing fault strength.

There is evidence supporting this hypothesis for the DFW earthquakes (Frohlich et al., 2011). Here the relocated epicenters were situated along a NE-SW trend, and both proprietary seismic data and regional tectonic maps (Ewing, 1990) indicated a NE-SW trending subsurface fault within 1 km of the epicentral region (Fig. 2.2). Studies of regional stress (Sullivan et al., 2006) find that the present-day regional stress system favors normal-faulting motion along NE-SW trending faults.

Some of the non-proprietary fault map data (Ewing, 1990) is consistent with this hypothesis. It shows NE-SW trending faults in the area where earthquakes occur (Fig. 2.2). And where no earthquakes occur there is: 1) an absence of mapped faults in Stephens County where there are high-rate wells; 2) an absence of high-rate wells in Comanche and Hamilton County, where there are NE-SW-trending faults; and 3) an absence of both in Bosque County. However, there are no mapped faults near several of the earthquake groups in Fig. 2.2 (the Denton, Hood, J-A, J-C, and J-Cleburne groups).

Unfortunately, the quality of the available non-proprietary fault information is variable, and was collected well before the present development in the Barnett Shale. Thus near both seismically active and inactive wells, faults may exist that are

absent in Figs. 2.1 and 2.2. What is desirable would be collaborative investigations with industry allowing a more thorough evaluation of the presence/absence of faulting near active and inactive injection wells.

Within the study area, the fraction of wells associated with earthquakes depends on the geographical region chosen. For wells having maximum injection rates exceeding 150,000 BWPM (24,000 m^3/mo) in Johnson County, this fraction is 0.33 (9 of 27 high-rate wells; see Table 2.2); within the seismically active area of Fig. 2, it is 0.23 (17 of 74); within the Barnett Shale neighborhood of Figs. 2.1 and 2.5, the fraction is 0.11 (17 of 161).

Utility and Limitations of USArray Data. This study is an apt example of a positive but unanticipated benefit of the USArray Temporary Array, part of the NSF-funded EarthScope program. EarthScope was conceived and funded prior to most of the recent development of unconventional gas resources, and before the public realization that this development might trigger seismic activity. The present study's success at identifying previously unreported seismicity in the Barnett Shale suggests that an analysis of USArray data could provide similar information about triggered earthquakes elsewhere, as in the Bakken, Eagle Ford, and Haynesville Shales.

However, for analyzing triggered seismicity the USArray data does have limitations, and it doesn't replace the need for additional, focused monitoring efforts. The deployment of USArray stations is ephemeral, lasting only two years in any one location. While this interval provides a snapshot of seismic activity, its duration and timing isn't optimal for investigating the before, during, and after phases of an injection program. Moreover, the 70-km station spacing makes it difficult to accurately assess the depths of triggered earthquakes. In the present study I fixed earthquakes depths at 5 km to stabilize the determination of epicenters; this depth is arbitrary although plausible, considering the differing appearance of earthquakes and quarry blasts.

2.4 Data and Methods

Deep injection wells are categorized as Class I, which are used to dispose of hazardous, industrial or municipal wastes; or Class II, which inject fluids associated with oil and gas production. In Texas Class I injection wells are regulated by the Texas Commission on Environmental Quality, who provides information about wells upon request. Information about Class II injection well locations, depth, permitting history, and monthly injection rates is archived by the Texas Railroad Commission (RRC). The RRC issues permits for individual wells and for leases having numerous wells; these include injection wells used for waste disposal as well as for waterflooding and secondary recovery. The RRC's database is publically available online and includes monthly injection information for individual wells and leases which is mostly complete for the past two decades. This study also utilized RRC data as compiled by the company IHS Inc.

All USArray-station seismograms analyzed for this investigation are archived at the IRIS Data Management Center and freely available. To identify seismic events, I identified candidate phase arrivals by comparing short-term and long-term

averages at all seismic stations, inspecting arrivals for events identified at four or more network stations, then eliminating teleseisms and non-regional seismic events. For the remaining regional events, I picked P- and S arrival times and/or identified events as quarry blasts. I then located events using a standard iterated least-square method using a flat-layered velocity model (Frohlich et al., 2011). Depths for quarry blasts were fixed at 300 m; earthquake depths were fixed at 5 km, the depth determined for DFW hypocenters using temporary local network data. All earthquake and quarry blast locations mapped in Figs. 2.1, 2.2 and 2.5 were determined using arrival picks from at least three nearby stations, including one or more stations with both P and S picks. I graded all locations as 'A', 'B' or 'C', with the A-grade given to epicenters determined using numerous impulsive P- and S-arrivals and with an azimuthal gap of 120° or less. To estimate magnitudes for regional earthquakes, I fit the magnitudes M_{NEIC} for events reported by the NEIC to the equation:

$$M_{NEIC} = a \log_{10}(A_{Max}) + b/D,$$

where A_{Max} is maximum signal amplitude and D is event-to-station distance. I then used the coefficients a and b to calculate M for events not reported by the NEIC.

Greater detail concerning this investigation is provided in the SI Appendix file linked to the online version of this paper. This file provides a list of earthquake epicenters determined in this investigation, figures corresponding to Fig. 2.3 showing monthly injection volumes for all injection wells within 5 km of epicenters, and a discussion comparing epicenters determined in this study to those reported by the ANF.

2.5 References

Barton CA, Zoback MD, Moos D (1995) Fluid flow along potentially active faults in crystalline rock: *Geology* 23: 683-686.

Davis SD, Pennington WD (1989) Induced seismic deformation in the Cogdell oil field of West Texas. *Bull Seismol Soc Amer* 79: 1477-1495.

Ellsworth WL, Hickman SH, Lleons AL, McGarr A, Michael AJ, Rubinstein JL (2012) Are seismicity rate changes in the midcontinent natural or manmade? *Seismol Res Lett 83*: 403.

Ewing T (1990) *Tectonic Map of Texas*. University of Texas Bureau of Economic Geology.

Frohlich C, Hayward C, Stump B, Potter E (2011) The Dallas-Fort Worth earthquake sequence: October 2008 through May 2009. *Bull Seismol Soc Amer* 101: 327=340 doi:10.1785/0120100131.

Holland A (2011) *Examination of Possibly-induced Seismicity from Hydraulic Fracturing in the Eola Field, Garvin County, Oklahoma*: Open File Rept. OF1-2011, Oklahoma Geol. Survey, 28 pp.

Horton S (2012) Disposal of hydrofracking waste fluid by injection into subsurface aquifers triggers earthquake swarm in central Arkansas with potential for

damaging earthquake. *Seismol Res Lett* 83: 250-260, doi:10.1785/gssrl.83.2.250.

Howe AM (2012) *Analysis of Cleburne Earthquakes from June 2009 to June 2010*, M.S. thesis, Southern Methodist University, 102 pp.

Howe AM, Hayward CT, Stump BW, Frohlich C (2010) Analysis of recent earthquakes in Cleburne, Texas. *Seismol Res Lett* 81: 379.

Kanamori H, Hauksson E (1992) A slow earthquake in the Santa Maria Basin, California. *Bull Seismol Soc Amer* 82: 2087-2096.

Majer EL et al. (2007) Induced seismicity associated with Enhanced Geothermal Systems. *Geothermics* 36: 185-222, doi:10.1016/j.geothermics.2007.03.003.

National Research Council (2012) *Induced Seismicity Potential in Energy Technologies*, National Academies Press, 225 pp.

Nicholson C, Wesson RL (1990) *Earthquake hazard associated with deep well injection: A report to the U.S. Environmental Protection Agency*. U.S. Geol Surv Bull 1951, 74 pp.

Suckale J (2009) Induced seismicity in hydrocarbon fields. *Adv Geophys* 51: 55-106, doi:10.1016/S0065-2687(09)05107-3.

Sullivan EC, Marfurt KJ, Lacazette A, Ammerman M (2006) Application of new seismic attributes to collapse chimneys in the Fort Worth Basin. *Geophysics* 71, B111–B119, doi 10.1190/1.2216189.

Tingay MRP, Muller B, Reinecker J, Heidbach O (2006) State and origin of the present-day stress field in sedimentary basins: New results from the World Stress Map Project. in *Proc 41st U.S. Symposium on Rock Mechanics: 50 Years of Rock Mechanics: Landmarks and Future Challenges*: Golden, Colorado, CD-ROM ARMA/USRMS06-1049: 14 pp.

Zoback MD, Townend J (2001) Implications of hydrostatic pore pressure and high crustal strength for the deformation of intraplate lithosphere. *Tectonophysics* 336: 19-30.

Zoback ML, Zoback MD (1980) State of stress in the conterminus United States. *J Geophys Res* 85: 6113-6156

3. Eagle Ford Seismicity/Injection Well Results

The material in this section was prepared by Cliff Frohlich and Michael Brunt and was published in 2013 in *Earth and Planetary Science Letters*, vol. 379, pp. 53-63, with the title "Two-year survey of earthquakes and injection/production wells in the Eagle Ford Shale, Texas, prior to the MW4.8 20 October 2011 earthquake". The article was then reprinted in 2014 in *Earth and Planetary Science Letters*, vol. 402, pp. 257-264.

Abstract: Between November 2009 and September 2011 the EarthScope USArray program deployed ~25 temporary seismograph stations on a 70-km grid in south-central Texas between 27°N-31°N and 96°W-101°W. This area includes the Eagle Ford Shale. For decades this geographic region has produced gas and oil from other strata using conventional methods, but recent developments in hydrofracturing technology has allowed extensive development of natural gas resources from within the Eagle Ford. Our study surveys small-magnitude seismic events and evaluates their correlation with fluid extraction and injection in the Eagle Ford, identifying and locating 62 probable earthquakes, including 58 not reported by the U.S. Geological Survey. The 62 probable earthquakes occur singly or in clusters at 14 foci; of these foci, two were situated near wells injecting recently increased volumes of water; eight were situated near wells extracting recently increased volumes of oil and/or water; and four were not situated near wells reporting significant injection/extraction increases. Thus in this region, while the majority of small earthquakes may be triggered/induced by human activity, they are more often associated with fluid extraction than with injection. We also investigated the M_W4.8 20 October 2011 Fashing earthquake—the largest historically reported earthquake in south-central Texas—that occurred two weeks after the removal of the temporary USArray stations. A field study indicated that the highest-intensity (MMI VI) region was about 10 km south of 2010-2011 foreshock activity, and that there were no high-volume injection wells within 20 km of the MMI V-VI region or the foreshocks. However, the 20 October 2011 earthquake did coincide with a significant increase in oil/water extraction volumes at wells within the MMI V-VI region, and this was also true for previous earthquakes felt at Fashing in 1973 and 1983. In contrast, our study found significant increases in injection prior to an m_{bLG}3.6 20 July 1991 earthquake near Falls City, Texas. Thus the Eagle Ford geographic region, with seismic activity associated both with extraction and injection, appears to be more complex than the Barnett Shale of northeast Texas, where a similar survey found possible correlations only with fluid injection.

3.1. Introduction

While earthquake seismologists have long recognized that fluid injection into the subsurface sometimes triggers earthquakes (Healy et al., 1968; Hsieh and Bredehoeft, 1981; Nicholson and Wesson, 1990; Suckale, 2009), this phenomenon has gained attention recently (e.g., National Research Council, 2012; Ellsworth, 2013) because earthquakes near injection disposal wells have occurred in several locations where no previous seismicity had been reported historically. These

include Dallas-Fort Worth, TX (Frohlich et al., 2011; Janska and Eisner, 2012; Reiter et al., 2012), Cleburne, TX (Howe, 2012), Timpson, TX, and Youngstown, OH. In these cases the injected fluids were generated by shale-gas development projects where wells are hydrofractured to enhance subsurface permeability. The production of gas is accompanied by the flowback of hydrofracture fluids that require disposal, typically accomplished by injecting them elsewhere in designated Class II disposal wells.

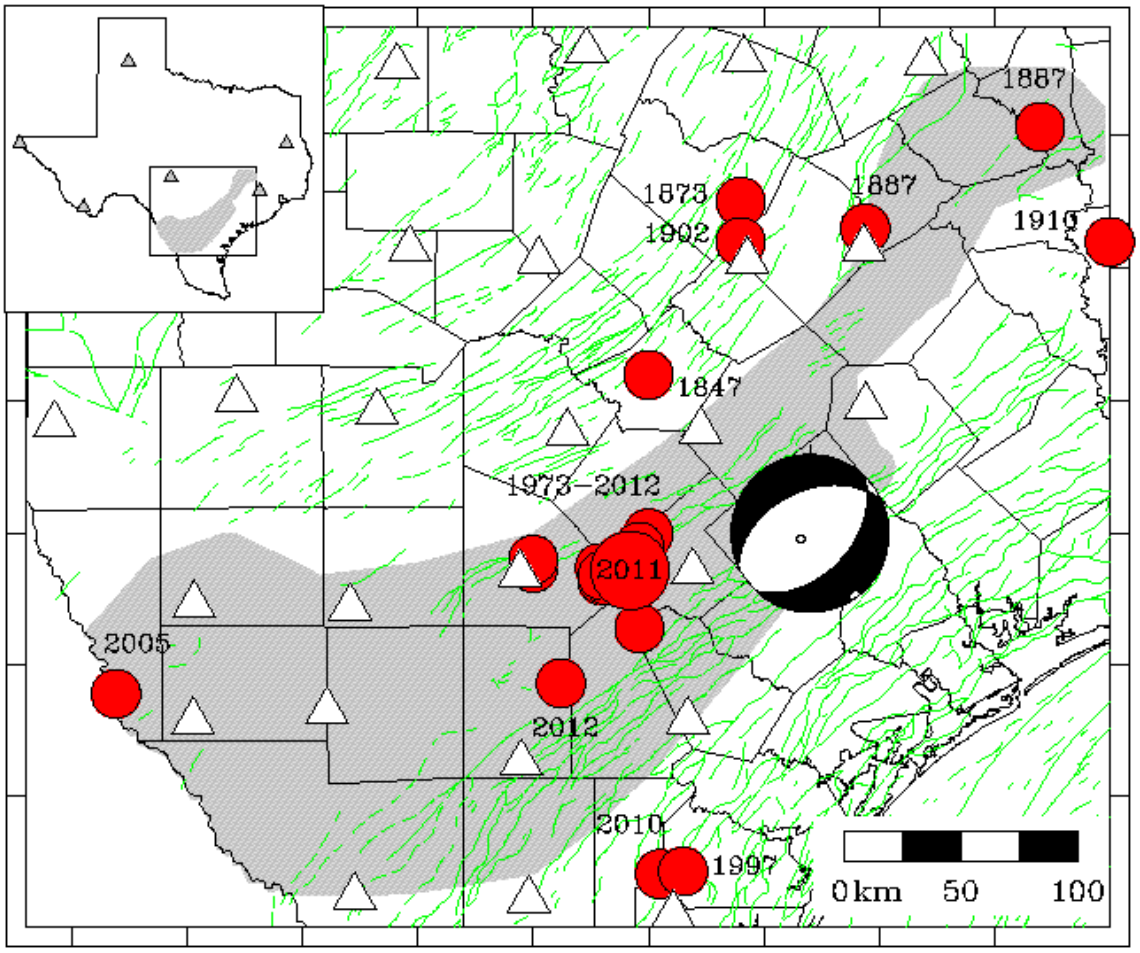

Fig. 3.1. Map showing extent of Eagle Ford Shale (shaded grey), USArray temporary seismograph stations operating during Nov 2009 to Sept 2011 period (triangles), historical seismicity (red circles; from Frohlich and Davis, 2002; and the NEIC), and mapped faults (green; from Ewing, 1990). Large red circle labeled "2011" is NEIC location for the 20 October 2011 M_W4.8 earthquake, and beachball at right is focal mechanism determined by the St. Louis group (Herrmann et al., 2011). Other labels indicate year of historical earthquakes. Inset with boundary of Texas shows mapped area and broadband seismograph stations (grey triangles) operating in 2005 prior to passage of the USArray.

This study investigates the relationship between seismicity, fluid injection, and fluid extraction in the Eagle Ford region of south central Texas (Fig. 3.1). Gas and oil have been produced extensively from this region since before 1950, mostly from the Edwards formation, a Lower Cretaceous limestone that underlies the Upper Cretaceous Eagle Ford Shale. A series of southwest-northeast fault systems (see Fig. 3.1), including the Fashing Fault Zone, cuts through much of the Eagle Ford region (Harbor, 2011). Most of these fault systems formed in the proximity of up-dip Triassic/Jurassic salt and result from basinward salt movement (Montgomery, 1990). In some regional fields these faults provide the trap that makes petroleum production viable.

Earthquakes with epicenters within or on the boundaries of producing fields have occurred since a tremor was reported by residents of Fashing, TX, on 25 December 1973 (e.g., Pennington et al., 1986; Olson and Frohlich, 1992; Davis et al., 1995; Frohlich and Davis, 2002). The largest of these earthquakes, with M_W4.8, occurred on 20 October 2011 near the Fashing Gas Field. Since 2008 the Eagle Ford has been an intense focus of shale gas development involving extensive hydrofracturing; this raises two questions: (1) Are small earthquakes within the Eagle Ford region associated either with fluid extraction or injection? And (2) Does the evidence indicate the M_W4.8 20 October 2011 earthquake is of natural origin, triggered by fluid extraction, or triggered by the injection to dispose of flowback brines associated with production and hydrofracturing?

Only a handful of seismograph stations operated in south central Texas prior to 2009 (Fig. 3.1); however, the passage of the EarthScope USArray transportable array between 2009 and 2011 provided an unprecedented opportunity to identify and accurately locate earthquakes. The present study will survey seismic activity during this period and evaluate its relationship to both injection and extraction wells. We will compare results from the Eagle Ford region to results from a companion study of the Barnett Shale (Frohlich, 2012). We also present a summary of felt reports for the 20 October 2011 Fashing earthquake.

The present survey searches for possible correlations between seismicity and extraction/injection rates in the Eagle Ford region. Interpreting the significance of these correlations will require a more thorough analysis of local geology as well as physical modeling of subsurface hydrological/stress. This is the focus of an ongoing companion study for which we hope to enlist industry cooperation concerning the details of subsurface structure.

3.2. Data and methods

3.2.1. Felt reports for the 20 October 2011 Fashing earthquake

We gathered felt report information (Fig. 3.2) in two ways. Following the 20 October 2011 earthquake one of the authors (M.B.) spent three days in the epicentral region interviewing residents, concentrating his efforts in the higher-intensity areas. We augmented these data with “Did you feel it?” (DYFI) information provided by the National Earthquake Information Center (NEIC). The DYFI program (Atkinson and

Wald, 2007; Wald et al., 2011) is an internet-based program where individuals can provide unsolicited responses to questions about their experiences and location during an earthquake. The responses are assigned a modified Mercalli intensity (MMI) value; the NEIC routinely presents summary online maps of the MMI distributions. For this study the DYFI data were especially useful for establishing boundaries for the MMI III and MMI IV regions, whereas the in-person interviews constrained the MMI V and MMI VI boundaries that had smaller areal extents but were situated in regions where population was sparse.

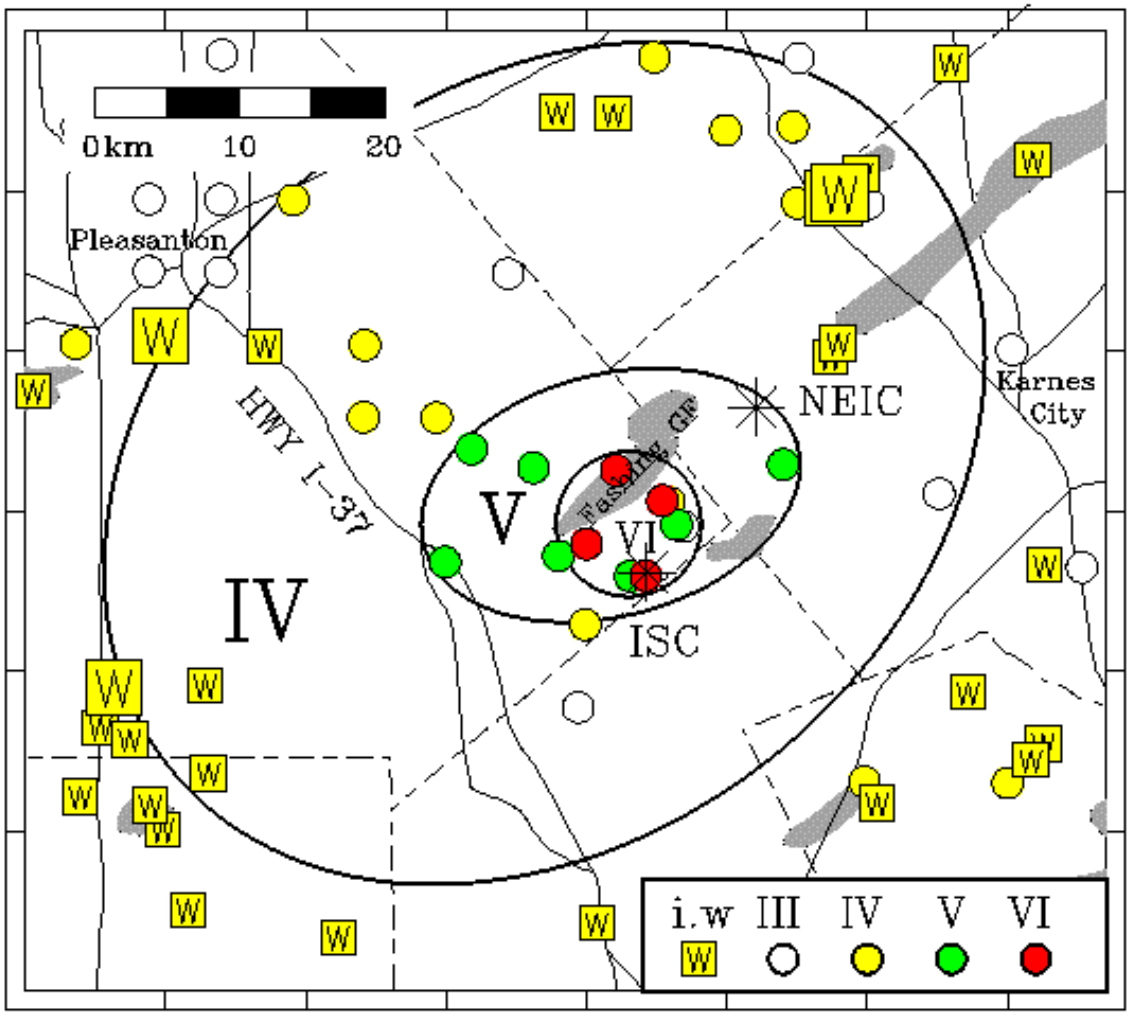

Fig. 3.2. Map of locations of felt reports (circles) defining the boundaries of regions experiencing modified Mercalli intensity (MMI) IV, V, and VI during the 20 October 2011 earthquake. Yellow squares labeled "W" are injection wells: larger symbols – wells with maximum monthly rates > 100,000 BWPM (16,000 m^3/mo); smaller symbols; wells with maximum monthly rates > 10,000 BWPM (1600 m^3/mo). Stars '' indicate 20 October 2011 epicenter as reported by the NEIC and ISC. Shaded gray regions are producing oil and gas fields from Galloway et al. (1983) and Kosters et al. (1989). Note that there are no injection wells within ~20 km of center of MMI VI area.*

3.2.2. Seismic data and earthquake location

Our procedure for identifying seismic events involved three steps. The first step was to acquire vertical-component seismograms for the ~25 USArray stations operating in the study area between November 2009 and September 2011. Then, to identify time intervals when locatable seismic events might have occurred, we applied a filter that compared the ratio of the signal short-term average (STA; 4-sec interval) and long-term-average (LTA; one-hour interval) of the vertical-component signal. We thus identified 2252 intervals where the STA/LTA ratio exceeded 5.0 during a 30-sec interval at four stations.

The second step was to inspect arrivals for these signals, eliminating obvious teleseisms and non-regional seismic events. For this we calculated predicted phase arrival times for phases from selected earthquakes reported by the National Earthquake Information Center (NEIC), the Array Network Facility (ANF) and the Oklahoma seismic network. The third step was to acquire 3-component seismograms for the remaining intervals. For these intervals we picked P- and S arrival times using Seismic Analysis Code (SAC) software. After some experience had been gained and after making some preliminary locations, we picked only representative events from groups of apparent quarry blasts, i.e., groups of numerous similar seismograms, all occurring during daytimes hours, with identical S-P times, large surface waves, and epicenters in or near quarries as identified on GoogleMap.

We located the remaining events using standard iterated least-squares methods and appropriate flat-layered velocity models. The crustal velocity varies significantly within the study area, and thus we obtained the most accurate locations when we used phase arrivals only from the 4-6 nearest USArray stations surrounding each epicenter. When events occurred in clusters, we reread the P- and S-arrivals within each cluster to ensure that we were picking the same arrival feature for the various events. The distances separating stations (~70 km) was too large to permit accurate determination of focal depths; thus we fixed focal depths at 5 km for all events. With these procedures we obtained locations for 245 seismic events (Fig. 3.3).

All earthquake and quarry blast locations in Fig. 3.3 were determined using arrival picks from at least three nearby stations, including one or more stations with both P and S picks. We graded all locations as 'A' or 'B', with the A-grade given to epicenters determined having an azimuthal gap of 200° or less and residuals of 1.0 sec or smaller. We estimate that 'A' quality epicenters are accurate to within about 2 km, and 'B' quality epicenters to within about 4 km. Both are significantly more accurate than NEIC locations for small-magnitude (~M3) Texas earthquakes.

To estimate earthquake magnitudes, we fit the magnitudes M_{NEIC} for events reported by the NEIC to the equation:

$$M_{NEIC} = a \log_{10}(A_{Max}) + b/D,$$

where A_{Max} is maximum peak-to-peak signal amplitude as measured in this study and D is event-to-station distance. We then used the coefficients obtained (*a=0.854*

and *b=-34.5 km)* to calculate M for events not reported by the NEIC, obtaining magnitudes ranging from ~1.5-3.0.

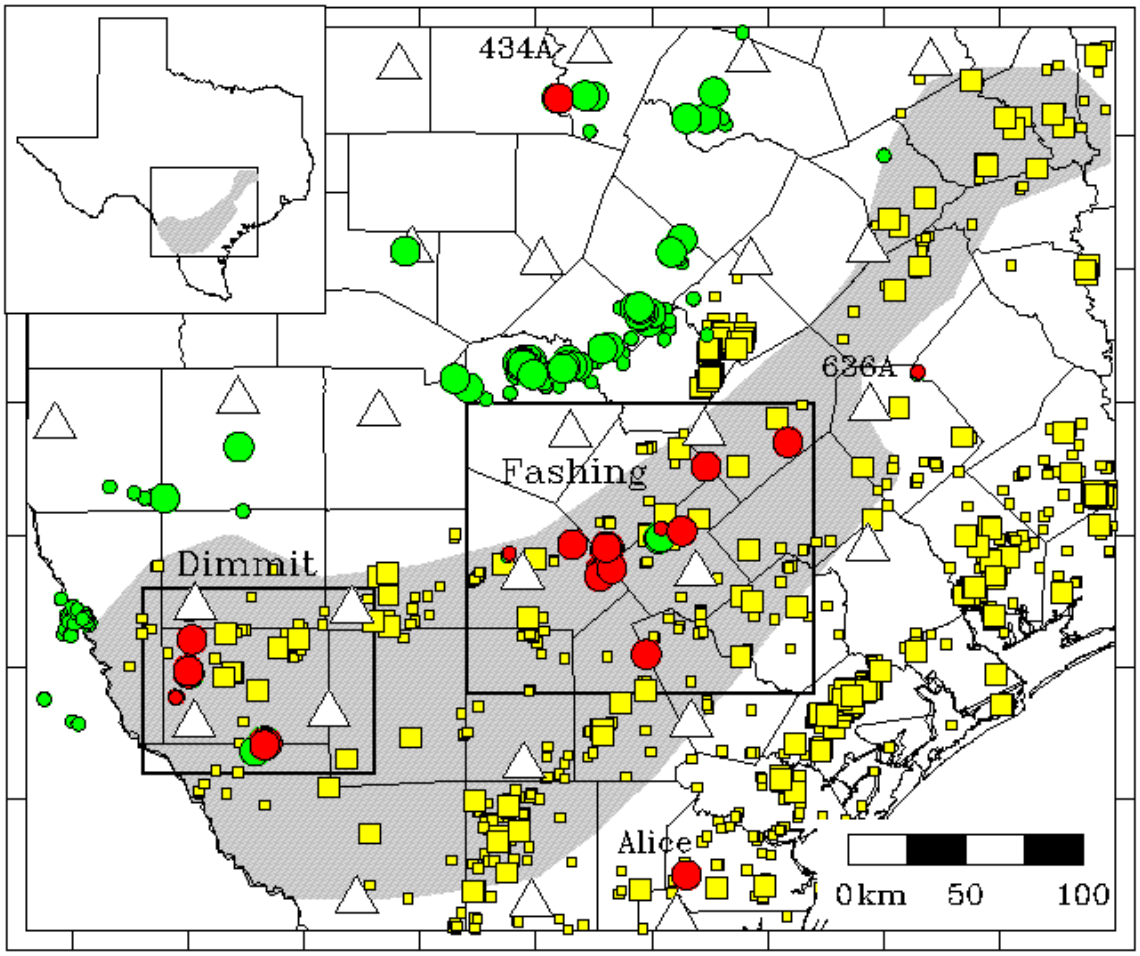

Fig. 3.3. Map of seismic events (circles) located in this study, injection disposal wells (yellow squares) active October 2006 to November 2009, and USArray temporary stations (triangles). For seismic events, green circles have origin times between 1300 and 2400 hours, corresponding to local daylight work hours 7 AM to 6 PM; red circles occur at other times; larger circles are 'A' quality locations (see text); smaller circles are 'B' quality locations. In several areas events occur only during daylight work hours and are presumably quarry blasts. For injection wells: small symbols – maximum monthly volume > 10,000 BWPM (1600 m^3/mo); large symbols – maximum monthly volume > 100,000 BWPM (16,000 m^3/mo). Rectangles labeled 'Dimmit' and 'Fashing' show areas mapped in Figs. 3.4 and 3.8; labels near some USArray stations indicate stations mentioned in the text.

3.2.3. *Injection of water; extraction of petroleum and water*

Within the Eagle Ford there are thousands of wells drilled for producing oil and natural gas, for injecting water to enhance petroleum production, and for disposing of flowback brines associated routinely with production operations and

hydrofracturing. The Texas Railroad Commission (RRC) regulates petroleum wells of all types; they also archive information about permitting history, well locations, depth, and monthly production/injection rates for oil, gas, and water. The RRC database is publically available online and for individual wells includes monthly injection/production information that is mostly complete for approximately the past three decades. For this study we used RRC data as supplied in more user-friendly form by the company IHS Inc.

3.3. Results

3.3.1. Felt reports for the 20 October 2011 Fashing earthquake

The felt area of the Fashing earthquake extended over approximately 11,000 km^2 (MMI III area), from about 40 km south of Fashing to 90 km north. The north boundary of the felt area included heavily populated San Antonio; the southern boundary is sparsely populated.

The most intense shaking (MMI VI) occurred within a 64 km^2 area that extended across the Fashing Gas field (Fig. 3.2). Here residents reported pictures falling off walls, items falling out of cupboards, and some cracking in masonry and sheet rock. The center of the MMI VI area was at 28.79N 98.17W, 12 km southwest of the epicenter determined by the NEIC (28.865N 98.079W), but only about 3 km from the prime epicenter reported by the International Seismological Center (28.7616N 98.1572W).

3.3.2. Seismic events: quarry blasts and earthquakes

The majority of events located in this study are probably quarry blasts. Of the 245 seismic events located in this study, 201 (82 per cent) occurred between hours 1300 and 2400; this corresponds to local times 7 AM to 6 PM, i.e., daylight working hours. These daylight events often occurred in clusters; e.g., in Fig. 3.3 note the cluster north of the 'Fashing' label, the cluster on the U.S.-Mexico border west of the 'Dimmit' label, and the clusters south and east of station 434A. Inspection of GoogleMap revealed crushed rock quarries near all of these clusters.

Elsewhere seismic events occurred during both daylight and nighttime hours. We have identified 62 as probable earthquakes. All but five of these occurred in two areas—near Fashing, TX, in Atascosa and Karnes Counties; and in Dimmit County.

3.*3.3. Fashing area: probable earthquakes and injection/production wells*

We located 35 probable earthquakes in the Fashing area (Figs. 3.3 and 3.4). Since 1982 the International Seismological Centre (ISC) has reported 15 earthquakes within the area mapped in Fig. 3.4; if we combine these with the probable earthquakes identified in this study, their magnitude-frequency distribution is consistent with a b-value of ~1.0 (Fig. 3.5).

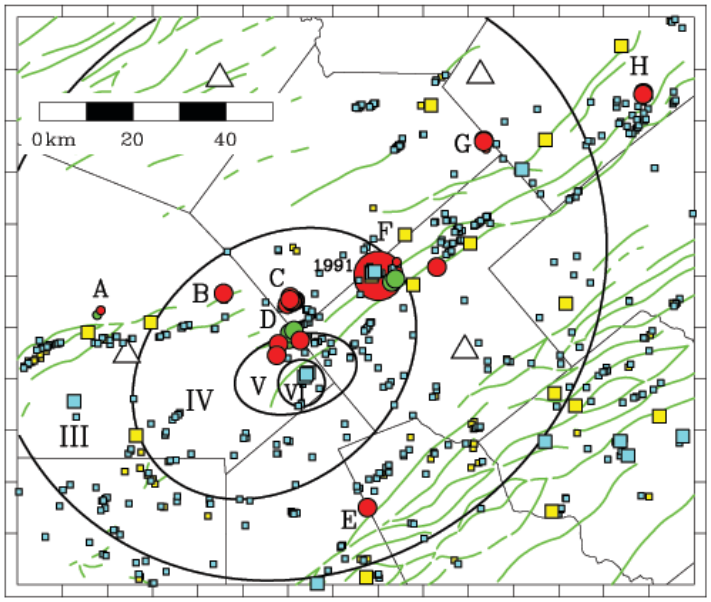

Fig. 3.4. For Fashing region, map of seismic events (circles, symbols as in Fig. 3.3), Class II injection wells (yellow squares, symbols as in Fig. 3.3), wells producing/extracting water (blue squares), USArray stations (triangles), and mapped faults (green; from Ewing, 1990). Ellipses labeled with Roman numerals III-VI are boundaries of MMI felt areas for the 20 October 2011 M_W4.8 earthquake (see Figs. 3.2 and 3. 3).

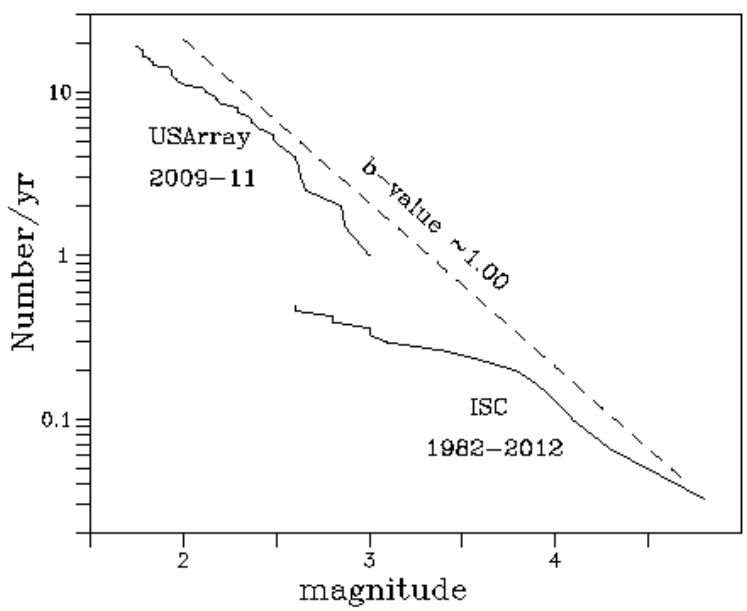

Fig. 3.5. Magnitude-frequency plots for earthquakes located in Fashing area (Fig. 3.4). Events labeled 'USArray 2009-11' are as identified in this study; events labeled 'ISC 1982-2012' are as reported by the International Seismological Centre (ISC). Note that a b-value (slope of magnitude-frequency line) of ~1.0 is consistent with both event groups.

The Fashing events we identified occurred within eight clusters (labeled A-H in Fig. 3.4), broadly distributed over a ~100km-long SW-NE trending zone. None of the clusters were situated within the highest-intensity (MMI VI) region of the 20 October 2011M_W4.8 earthquake; the closest cluster D was about 10 km northward.

All but three of the Fashing events occurred during the second year of this project, after 20 December 2010—ten months prior to the 20 October 2011 earthquake, and 22 occurred in April or May of 2011, approximately six months prior. These 22 were broadly distributed geographically, including events in clusters A, C, D, G and H. The last event we located occurred on 22 September 2011 (Event #6750, in cluster F). There were no USArray stations in the Fashing area to record the 20 October 2011 earthquake or its aftershocks, as the array moved eastward during the first week of October.

Two of the event clusters, cluster A and cluster F, were situated within 5 km of recently active injection wells (Table 3.1). Cluster A consists of two earthquakes with magnitude ~M1.8 occurring in May and August of 2011. Since 2000 production of oil and gas has been negligible within 5 km of cluster A, but there are several nearby active injection wells. The closest high-volume injection well [API 14201007611 at ~5 km distance] commenced injecting at rates of 10,000-70,000 BWPM (1600-11,200 m^3/mo) in 2004. Then in March 2011, two months prior to the occurrence of event #6063 on 21 May 2011, injection rates increased to 262,344 BWPM (42,000 m^3/mo), and rates exceeded 190,000 BWPM (30,400 m^3/mo) until November 2011.

The epicenters in cluster F coincide with the maximum-intensity area of the 20 July 1991 m_{bLG}3.6 Falls City earthquake as determined by Olson and Frohlich (1992). The 1991 earthquake occurred following a large increase in monthly injection rates that began in 1990 (Fig. 3.6) and exceeded 500,000 BWPM (80,000 m^3/mo) for all but two months between October of 1990 December 1993. There is no obvious relationship to injection rates for cluster F epicenters that began occurring in March of 2010. However, the extraction of water for wells within 5 km of F events did increase to nearly 100,000 BWPM between Jan-Mar of 2010 when the events began.

There are no recently active injection wells nearby clusters B, C, D, E, G and H; however, all but E coincide with increases in production of oil and/or water (Table 3.1). The B epicenter (event #5220) occurred two months following a two-month spike in water production at wells within 5 km. And the G and H activity only began after marked increases in production of oil and water at wells within 10 km (Figs. 3.7).

The C and D clusters are closest geographically to the highest-intensity region of the 20 October 2011 M_W4.8 earthquake. Oil and water production increased sharply near clusters D early in 2011 and near cluster C before April 2011 when the activity occurred. Rates of oil+water production remained high throughout most of 2011 and 2012. Although the 20 October 2011 earthquakes occurred following a peak in water production, the D-cluster events began well before the increase commenced.

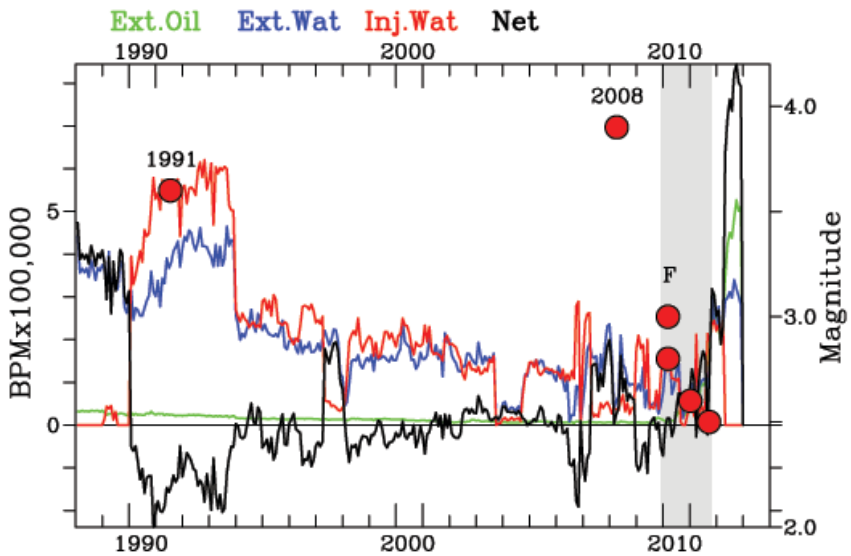

Fig. 3.6. For wells within 10 km of cluster F (29°N 98°W; see Fig. 3.4), monthly volumes (left axis) for the extraction of oil (green) and water (blue), injection of water (red), and the net (black: oil + water extracted – water injected). Red circles and right axis indicate occurrence and magnitude of earthquakes; gray shaded area indicates time interval when USArray station data was available. Note that m_{bLG}3.4 23 July 1991 Falls City earthquake followed significant increases in injection beginning in 1990, and the m_b4.1 7 April 2008 earthquake followed increases in production and injection in late 2006-2007. However, there is no obvious injection/production relationship with cluster F earthquakes.

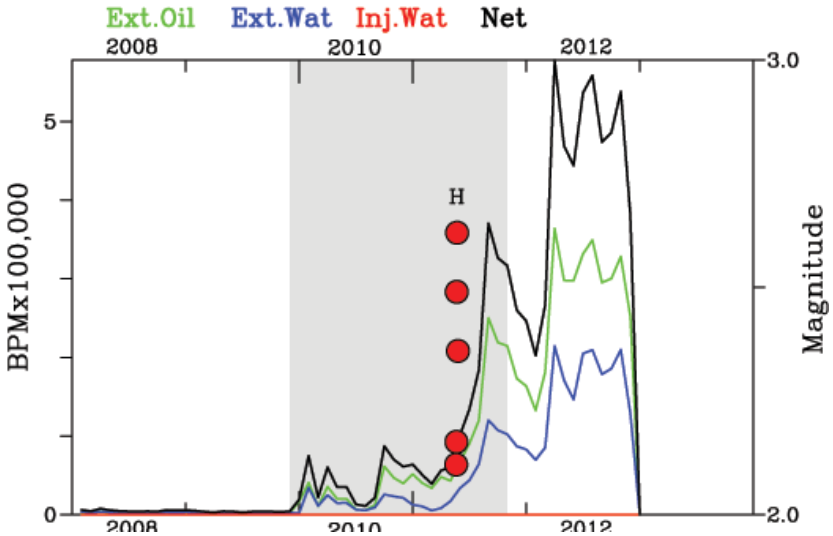

Fig. 3.7. For wells within 5 km of cluster H (29.353°N 97.413°W; see Fig. 3.4), monthly volumes (left axis) for the extraction of oil (green) and water (blue), injection of water (red), and the net (black: oil + water extracted – water injected). Red circles and right axis indicate timing and magnitudes of cluster H events; gray shaded area indicates time interval when USArray station data was available.

Table 3.1. Relationship of seismic events/event clusters to injection/extraction. Events/clusters are as labeled on Figs. 3.3, 3.4, and 3.8. Injection/extraction increase columns describe monthly sums for all wells within included radius.

Fashing clusters	*number of events*	*1st event*	*injection increase*	*wells included radius (km)*	*oil/water extraction increase*	*no increase*
A	2	May 2011	Feb 2011: ~200,000 BWPM increase	5		
B	1	Jan 2011		5	Oct-Nov 2010: produced water doubles to 28,000 BWPM	
C	12	Apr 2011		5	Mar 2011: oil+water doubles to ~70,000 BPM	
D	6	Aug 2010		5	Apr 2011: oil+water increases to ~100,000 BPM and more	note increase is <u>after</u> D begins
E	1	Feb 2011				none
F	4	Mar 2010	Jun 2011: ~200,000 BWPM inj. begins	5	Jan-Mar 2010: water increases to 90-100,000 BPM	
G	4	Apr 2011		10	Mar 2011: oil+water increases to ~80,000 BPM	
H	5	May 2011		5	Sep 2010-May 2011: oil+water increases to ~100,000 BPM	

If we consider size and time dependence of the clusters A-F, none would be characterized as mainshock-aftershock sequences, with a large earthquake followed by numerous smaller-magnitude events. Instead, when there were several events in a cluster the times were generally swarm-like, with all events having similar magnitudes and occurring within a one- or two-month period (e.g., see clusters C, G, and H.

3.*3.4. Dimmit area: probable earthquakes and injection/production wells*

Our investigation identified 22 probable earthquakes (Fig. 3.8) in Dimmit County, an environment where no earthquakes had previously been reported. Except for one isolated event (labeled J in Fig. 3.8 ; #4728) all occurred in three clusters (K, L and M). The northern cluster K consisted of seven events, and began in January 2010. There were five events in cluster L, all occurring during April 2010, and nine events in cluster M, all in June and July, 2011.

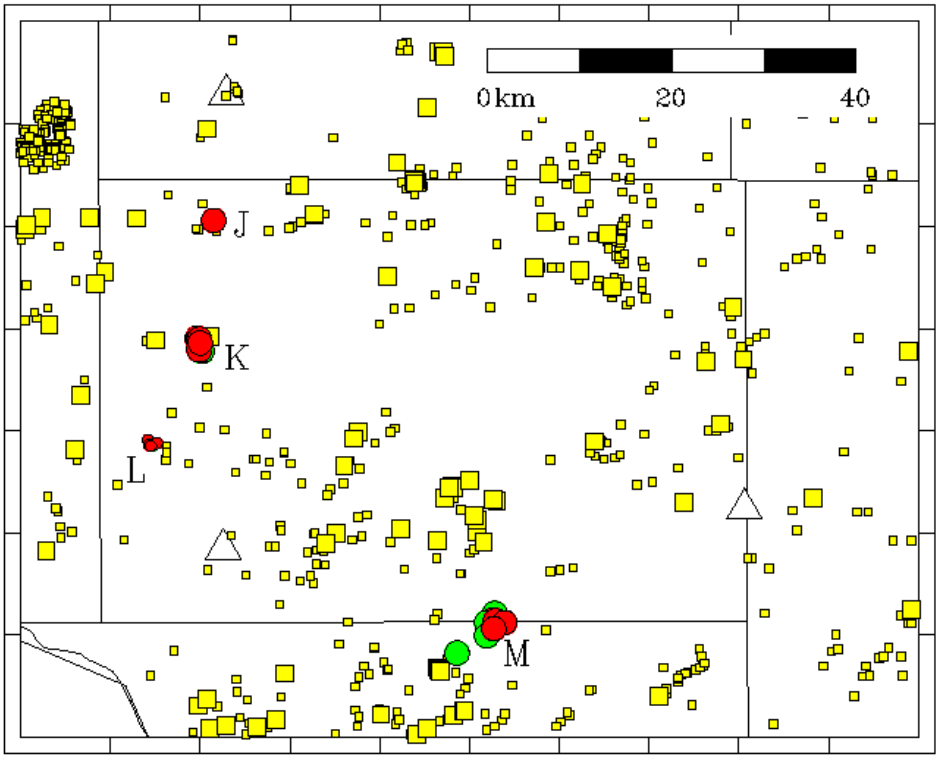

Fig. 3.8. For Dimmit County and neighboring region (see Fig. 3.3), map of seismic events (circles; symbols as in Fig. 3.3), USArray stations (triangles) and wells injecting water (yellow squares) and producing water (blue squares). For wells: small symbols – maximum monthly volume > 10,000 BWPM (1600 m^3/mo); large symbols – maximum monthly volume > 100,000 BWPM (16,000 m^3/mo). Labels 'J', 'K', etc. indicate event groups discussed in the text.

Of these events none except event J occurred near active high-volume injection wells (Table 3.1). Wells within 5 km of J's location had been injecting at volumes of ~100,000 BWPM since 1996.

In contrast, clusters K, L, and M all are within 5-10 km of wells producing water or oil that reported significant increases in 2009 or 2010. For example, water wells within 5 km of cluster K produced 169,000 BWPM (27,000 m^3/mo) in November 2009; the K events began in January 2010. Wells within 10 km of M all began producing early in 2010; and for the two months prior to June 2011 when M activity began, their combined extraction of oil and water exceeded 270,000 BPM. As in the Fashing area, the size and time dependence of Dimmit clusters was more swarm-like than aftershock-like, e.g., all the events in cluster M had magnitudes between 1.9 and 2.7, and all occurred within a three-week period.

3.*3.5. Other probable earthquakes*

The remaining probable earthquakes include the m_{bLG}3.9 25 April 2010 earthquake felt widely near Alice, TX (see Fig. 3.3 and Event #1986) that was the subject of an investigation by Frohlich et al. (2012). Two other isolated events that are probable earthquakes occurred on 18 September 2010 (Events #3906 and #3909 south of station 434A in Fig. 3.3). Although there are stone quarries that do sometimes generate quarry blasts near this location (a nearby city is named Marble Falls) the seismograms for these two events were distinct, with higher-frequency body waves and smaller surface waves than regional quarry blasts. Finally, two probable earthquake events occurred east of station 636A on 2 November 2010 and 9 December 2010 (Events #4484 and #4828). None of these remaining events are near active production or injection wells.

3.**4. Discussion**

3.4.1. Possibly-induced earthquakes and USArray

Like Frohlich's (2012) survey of earthquakes and injection wells in the Barnett Shale of northeast Texas, the present investigation of the Eagle Ford analyzed seismograms collected by the USArray stations to identify small-magnitude seismic events and evaluate their relationship to the extraction/injection of fluids in wells operated by the petroleum industry. Both studies surveyed seismicity in an area undergoing intensive petroleum operations, and evaluated possible relationships between seismicity and human activities. By surveying small-magnitude events, most too small to be reported by the NEIC or felt by local residents, these studies contrast with many investigations of induced/triggered seismicity that are initiated only after an earthquake occurs that is large enough to be felt by local residents and provoke media attention.

Both this study and Frohlich's (2012) survey were possible only because the USArray stations improved event-detection thresholds and increased accuracy of epicenter determination. The USArray program was conceived and funded before there was widespread public concern concerning possible human-caused earthquakes in Texas and elsewhere. Thus these investigations provide apt examples of the potential unanticipated benefits that can follow from large-data gathering programs like USArray, especially when the data are made freely available to all.

From an analysis of USArray data, the present investigation was to able to identify 62 small-magnitude events classified as probable earthquakes occurring in/near the Eagle Ford during the November 2009 to September 2011 survey period. Of these events, only four were reported by the NEIC. There were also five earthquakes outside the boundaries of the Eagle Ford (see events near stations 434A and 636A in Fig. 3.3) including the previously-studied m_{bLG}3.9 earthquake occurring in April 2010 near Alice, TX (see Frohlich et al., 2011).

For earthquakes occurring prior to the deployment, and following the removal of the USArray stations, there is often 10 km or more uncertainty in their epicentral location unless felt reports are available to better constrain the epicenter. For example, maximum-intensity foci were established for the m_{bLG}3.6 23 July 1991 and m_{bLG}4.3 9 April1993 earthquakes near Falls City and Fashing (Olson and Frohlich, 1992; Davis et al., 1995). In contrast, no felt-report survey was undertaken for the the m_b4.1 7 April 2008 earthquake and although it was felt in Falls City its exact location is uncertain.

3.4.2. Relationship of seismicity to injection/extraction

The principal result of this study was that the majority (~90 per cent) of the identified probable earthquakes occurred as single events or clusters at foci near active production or injection wells. Of these foci near active wells, 85 percent occurred near wells where injection or extraction had undergone a significant increase within a year or less prior to the beginning of seismic activity.

However, increases in fluid extraction, rather than injection, occurred prior to the majority of these events and foci (47 of 62 events; 8 of 14 foci). For example, in Dimmit County since 2008 production of water for hydrofracturing and agriculture has increased significantly (Nicot and Scanlon, 2012); 21 of the 22 events (3 of 4 foci) we identified in the Dimmit area (Fig. 3.8 and Table 3.1, clusters J-M) appear to be within 5-10 km of such wells. In the Fashing area (Fig. 3.4 and Table 3.1, clusters A-F) 28 of the 35 events (5 of 8 foci) identified are near wells showing increases in oil/water production.

Fluid injection increases at nearby wells did occur prior to seismic events at two foci—foci A in the Fashing region and J in Dimmit County. In addition, our investigation found that the m_{bLG}3.6 20 July 1991 Falls City earthquake followed an 18-month interval where injection at nearby wells had increased substantially.

These associations between seismic activity and increases in injection/production volumes imply that many of the Eagle Ford earthquakes were triggered/induced. Of course, injection/production activity is nearly ubiquitous throughout much of the Eagle Ford, and in many areas this activity increased markedly in 2010. Thus it is possible that earthquakes of natural origin may occur coincidentally near active wells. However, the observation that most earthquakes identified in this study occurred during the second year of the survey, when regional injection/production rates were generally higher, favors an induced/triggered origin.

The results of this survey indicate the relationship between seismicity and injection/extraction is more complex in the Eagle Ford than in the Barnett. In the

Barnett, Frohlich's (2012) two-year survey found that seismic activity was clustered near injection wells, and these were wells having monthly injection rates exceeding 150,000 BWPM (24,000 m^3/mo). In the Eagle Ford, our survey finds that seismicity is associated with increases of both injection and extraction, and we were unable to identify a critical monthly rate. In both the Barnett and Eagle Ford there are numerous high-volume production and injection wells with no nearby seismicity.

There are geological and historical differences between the Barnett and the Eagle Ford that may explain the differences in their induced seismicity. In the Eagle Ford region petroleum has been produced by conventional means from various other strata, notably the Edwards formation, for more than 60 years. The plays are fault bounded and some have been associated with extraction-related earthquakes since the 1970's (Pennington et al., 1986; Davis et al., 1995). In contrast, the induced earthquakes in the Barnett have mostly occurred areas where widespread development took place only within the past ten years (Frohlich, 2012). Thus the differences in Eagle Ford/Barnett induced seismicity may arise partly because human intervention affects a broader variety of geological formations in the Eagle Ford, and partly because features of induced seismicity can change over time scales of decades when injection/extraction is ongoing. This is certainly true for the seismicity associated with injection in Paradox Valley, CO, which has been ongoing for more than 20 years (Ake et al., 2005).

In both the Eagle Ford and Barnett, as well as many other petroleum-producing regions in the U.S., the sparseness of permanent seismic station coverage is inadequate if we hope to understand why some operations induce earthquakes and others do not. The two-year coverage provided by USArray allows us to identify earthquakes with magnitudes of 2 and smaller and obtain epicenters with uncertainties of ~2 km—often good enough to associate them with particular wells. However, two years is not a sufficiently long interval to obtain unequivocal statistical evidence that particular wells are or are not inducing earthquakes, nor was the station spacing of the USArray network adequate to obtain focal depth information. To better understand the scientific basis of induced earthquakes, for crafting effective policies regulating injection/extraction wells, and for developing effective strategies so that well operators can manage and mitigate the associated hazards, it is desirable to deploy more permanent regional seismic stations, including some densely instrumented networks in targeted areas where induced earthquakes are known to occur.

3.*4.3. Was the M_W4.8 20 October Fashing earthquake induced/triggered?*

We find no evidence that fluid injection is responsible for the 20 October 2011 earthquake. Injection is absent or negligible at wells within the MMI-V felt area, and at wells near foreshock clusters D and E. The nearest active high-volume injection wells are about 20 km distant near the site of the 1991 Falls City earthquake—it seems implausible that injection at this distance would induce/trigger the 2011 event.

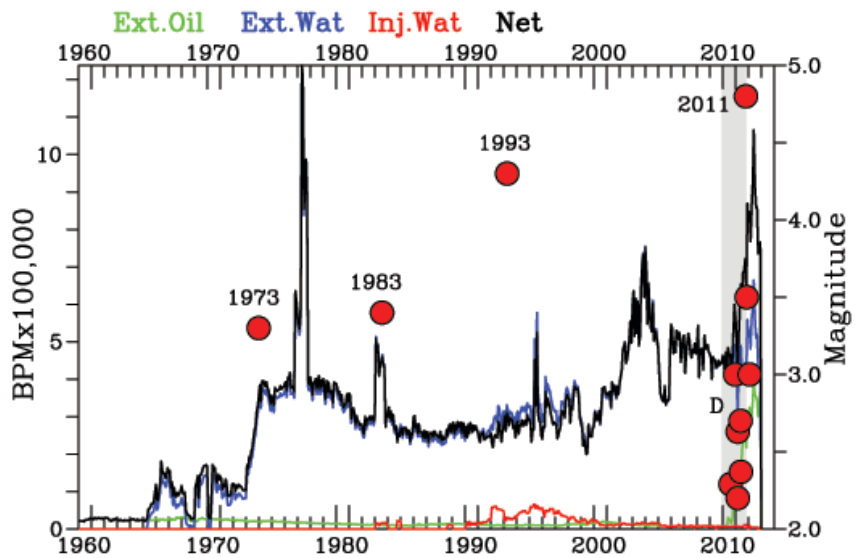

Fig. 3.9. Fashing earthquakes (red circles, right axis) and monthly volumes (left axis) for the extraction of oil (green) and water (blue), injection of water (red), and net (black: extraction oil + water – injection water) for wells within MMI V region of the 20 October 2011 earthquake (see Fig. 3.4). Note that earthquakes in 1973, 1983 and 2011 coincide with significant increases in extraction volumes. Gray shaded area indicates time interval when USArray station data was available.

A comparison of Fashing seismic activity with the 50-year record of production of petroleum and water in the MMI-V region of the 20 October 2011 earthquake (Fig. 3.9) suggests there is a relationship between seismic activity and the extraction of fluids (oil+water). The first known Fashing earthquake occurred on 25 December 1973 and followed a marked increase in the production of water at nearby wells that began late in 1971 and first reached 300,000 BWPM (48,000 m^3/mo) in November 1973. The m_{bLG}3.4 earthquake of 23 July 1983 occurred during a nine-month period beginning in January 1983 when water production exceeded 400,000 BWPM (64,000 m^3/mo). There is no apparent water-production anomaly associated with the m_{bLG}4.3 Fashing earthquake of 9 April 1993.

Finally, the M_W4.8 20 October 2011 earthquake followed increases in the production of oil and water that began in 2010. In fact, it was in October 2011 that the sum of oil+water extraction first exceeded its highest level of the previous three decades (750,000 BPM, or 120,000 m^3/mo, in December 2003).

Thus it is plausible that extraction of oil and water induced/triggered the M_W4.8 20 October 2011 earthquake. This is consistent with the previous studies Fashing-area earthquakes by Pennington et al. (1986) and Davis et al. (1995), who concluded that depressuring of subsurface fluids associated with the extraction of oil and water caused Fashing 1973-1993 earthquakes activity. It is notable that the centers of the maximum-intensity felt areas are virtually identical for the Fashing events of 23 July 1983 (m_{bLG}3.4), 9 April 1993 (m_{bLG}4.3), and 20 October 2011 (see Davis et al., 1995; Frohlich and Davis, 2002).

3.5. References

Ake, J., K. Mahrer, D. O'Connell and L. Block, 2005. Deep-injection and closely monitored induced seismicity at Paradox Valley, Colorado, Bull Seismol Soc Amer 95, 664-683, doi:10.1785/0120040072.

Atkinson, G.M., Wald, D.J., 2007. "Did you feel it"? intensity data: A surprisingly good measure of earthquake ground motion. Seismol Res Lett 78, 362-368, doi:10.1785/gssrl.78.3.362.

Davis, S.D., Nyffenegger, P., Frohlich, C., 1995. The 9 April 1993 earthquake in south-central Texas: Was it induced by fluid withdrawal? Bull Seismol Soc Amer. 85, 1888-1895.

Ellsworth, W., 2013. Injection-induced earthquakes, Science 341, 142-149, doi:10.1126/science.1225942.

Ewing, T., 1990. Tectonic map of Texas, published by Univ. Texas Bureau of Economic Geology.

Frohlich, C., Glidewell, Brunt, M., 2012. Location and felt reports for the 25 April 2010 mbLG3.9 earthquake near Alice, Texas: Was it induced by petroleum production? Bull Seismol Soc Amer 102, 457-466, doi:10.1785/0120110179.

Frohlich, C., Hayward, C., Stump, B., Potter, E., 2011. The Dallas-Fort Worth earthquake sequence: October 2008 through May 2009. Bull Seismol Soc Amer 101, 327-340, doi:10.1785/0120100131.

Frohlich, C., 2012. Two-year survey comparing earthquake activity and injection-well locations in the Barnett Shale, Texas. Proc Nat Acad Sci 109, 13934-13938, doi: 10.1073/pnas.1207728109.

Frohlich, C., Davis, S.D., 2002. Texas Earthquakes, Univ Texas Press, Austin, Texas, 275 pp.

Galloway, W.E., Ewing, T.E, Garrett, C.M., Tyler N., Bebout, D.G., 1983. Atlas of Major Texas Oil Reservoirs, University of Texas Bureau of Economic Geology, Austin, TX.

Harbor, R.L., 2011. Facies Characterization and Stratigraphic Architecture of Organic-Rich Mudrocks, Upper Cretaceous Eagle Ford Formation, South Texas. M.S. thesis, University of Texas at Austin, 184 pp.

Healy, J.H., Ruby, W.W., Griggs, D.T. Raleigh, C.B., 1968. The Denver earthquakes. Science 162, 1301-1310.

Herrmann, R.B., Benz, H., Ammon, C.J., 2011. Monitoring the earthquake source process in North America. Bull Seismol Soc Amer., 101, 2609-2625, doi:10.1785/0120110095.

Howe, A.M., 2012. Analysis of Cleburne Earthquakes from June 2009 to June 2010. M.S. thesis, Southern Methodist University, 102 pp.

Hsieh, P.A., Bredehoeft, J.S., 1981. A reservoir analysis of the Denver earthquakes—A case of induced seismicity. J Geophys Res 86, 903-920.

Janska, E., Eisner, L., 2012. Ongoing seismicity in the Dallas-Fort Worth area. Leading Edge 31, 1462-1468.

Keller, G.R., Shurbet, D.H., 1975. Crustal structure of the Texas Gulf Coastal Plane. Geol Soc Amer. Bull 86, 807-810.

Kosters, E.C., Bebout, D.G., Seni, S.J., Garrett, C.M., Brown, L.F., Hamlin, H.S., Dutton, S.P., Ruppel, S.C., Finley, R.J., Tyler, N.,1989. Atlas of Major Texas Gas Reservoirs, Univ. Texas Bur Econ Geol. Austin, TX, 161 pp.

Mitchell, B.J., Landisman, M., 1971. Geophysical measurements in the southern great plains, in The Structure and Physical Properties of the Earth's Crust, ed. By J. G. Heacock, AGU Monograph 14, 77-92.

Montgomery, S.L., 1990, Horizontal drilling in the Austin Chalk; Part 1, Geology, drilling history and field rules. Petroleum Frontiers 7, no. 3, 44 p.

National Research Council (2012). Induced Seismicity Potential in Energy Technologies, National Academies Press, 225 pp.

Nicholson C, Wesson R.L., 1990. Earthquake hazard associated with deep well injection: A report to the U.S. Environmental Protection Agency. U.S. Geol Surv Bull 1951, 74 pp.

Nicot, J.P, Scanlon, B.R., 2012. Water use for shale-gas production in Texas. Env Sci Technol 46, 3580-3586, doi:10.1021/es204602t.

Olson, D.R., Frohlich, C., 1992. Felt reports from the 20 July 1991 Falls City earthquake, Karnes County, Texas. Seismol Res Lett 63, 5030604, 1992.

Pennington, W.D., Davis, S.D., Carlson, S.M., Dupree, J., Ewing, T.E., 1986. The evolution of seismic barriers and asperities caused by the depressuring of fault planes in oil and gas fields of south Texas. Bull Seismol Soc Amer 76, 939–948.

Reiter, D., Leidig, M., Yoo, S.-H., Mayeda, K., 2012. Source characteristics of seismicity associated with underground wastewater disposal: A case study from the 2008 Dallas-Fort Worth earthquake sequence. Leading Edge 31, 1454-1460.

Suckale J (2009) Induced seismicity in hydrocarbon fields. Adv Geophys 51: 55-106, doi:10.1016/S0065-2687(09)05107-3.

Wald, D.J., Quitoriano, V., Worden, B., Hopper, M., Dewey, J. W., 2011. USGS "Did you feel it?" internet-based macroseismic intensity maps. Annals Geophys 54, 688-707, doi:10.4401/ag-5354

4. Bakken Seismicity/Injection Well Results

The material in this section was prepared by Cliff Frohlich, Jacob Walter and Julia Gale and was published in 2015 in *Seismological Research Letters* vol. 86, pp. 492-499, with the title "Analysis of transportable array (USArray) data shows arthquakes are scarce near injection wells in the Williston Basin, 2008-2011".

Abstract: We investigate possible links between seismicity and fluid injection in the Williston Basin in the north central U.S., focusing on the region around the Bakken Formation unconventional hydrocarbon play. Here we show that earthquakes are rarer near injection wells in the Williston Basin than in the Fort Worth Basin of Texas or in central Oklahoma. To identify earthquakes we analyze seismograms collected by EarthScope USArray temporary stations, deployed on a grid with 70-km spacing. During the September 2008 – May 2011 study period we identified only nine regional earthquakes; of these only three were situated near injection wells. The reason why Williston Basin earthquakes are so scarce is unclear. In both the Bakken and Barnett Shale play regions, injection volumes increased significantly in late 2007, and both areas have very low levels of natural seismicity. Oklahoma has experienced much higher rates of apparently-induced seismicity than either region, possibly because injection volumes are higher in some wells in Oklahoma.

4.1 Introduction

It is well-established that fluid injection into deep (~1-5 km) wells sometimes induces earthquakes (Suckale, 2009; Ellsworth, 2013; National Research Council, (2013). Since 2008 this has been investigated at several sites in the Midwestern U.S. where there is wastewater disposal to support hydrofracturing operations (Horton, 2012; Frohlich et al., 2011; 2014; Justinic et al., 2013; Keranen et al., 2013; 2014; Kim, 2013).

Over much of the Midwestern United States it can be difficult to assess whether detected earthquakes are natural, or instead caused by regional petroleum production or fluid injection operations at nearby wells. This is because there are few continuously-operating seismograph stations in the Midwest, and the U.S. Geological Survey's National Earthquake Information Center (NEIC) does not routinely detect and locate earthquakes smaller than approximately magnitude 2 (Ellsworth, 2013). Moreover, epicentral uncertainties are often as large as 10-15 km; this complicates associating earthquakes with particular wells unless temporary seismograph networks are deployed. However, for the two-year duration of deployments in the USArray program (Witze, 2013), high-quality seismograph stations operated continuously on a grid with 70-km spacing, making it possible to detect and locate earthquakes as small as M1-5-2.0 with an epicentral accuracy of 1-2 km.

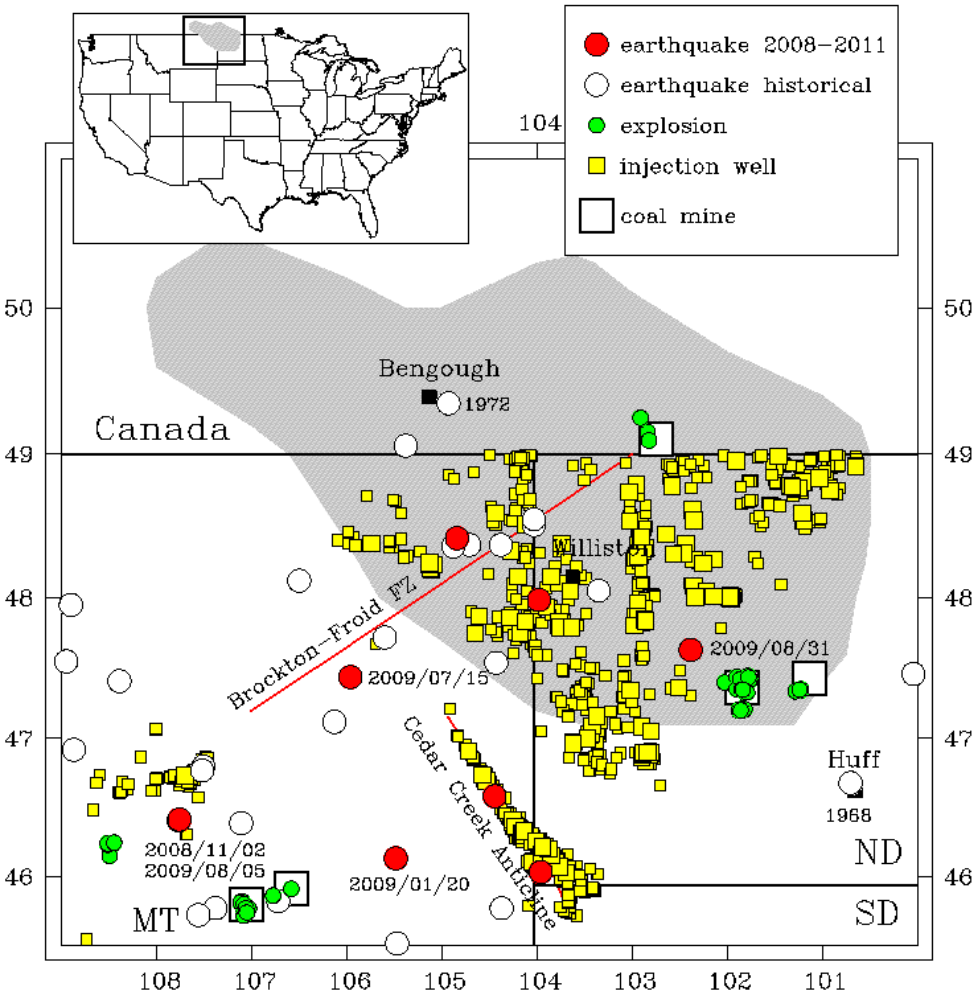

Fig. 4.1. Map of earthquakes and injection wells in the Bakken region. Red circles are earthquakes located in this study, white circles are historical earthquakes, green circles are mine blasts. Coal mines are large white squares, labeled black squares are towns mentioned in the text, and injection wells are yellow squares. All plotted wells reported monthly injection volumes exceeded 1600 m^3/mo for one or more months since 2000; larger symbols are wells where monthly injection volume exceeded 16,000 m^3/mo. Grey region shows the extent of the Bakken Formation. Labeled events are earthquakes mentioned in the text (see also Fig. 4.3).

In the present study we investigate the relationship between seismicity and injection/production in the Williston Basin (Fig. 4.1), which recently has undergone a massive boom of production in one of its units, the Bakken Formation (Fig. 4.2). The methods utilized in this study to analyze USArray data to identify and locate earthquakes are similar to those we applied in surveys of three regions in Texas: the Barnett Shale play in northeast Texas (Frohlich, 2012), the Eagle Ford play of south central Texas (Frohlich and Brunt, 2013) and the Cogdell Field in west central Texas (Gan and Frohlich, 2013). We shall show that the relationship between seismicity and injection is different in each of the four regions; of the four regions, there are the fewest apparently-induced earthquakes in the Williston-Bakken region. Seismic

activity is also considerably lower in the Williston-Bakken region than in Oklahoma (Keranen et al., 2013; 2014) or Arkansas (Horton, 2012).

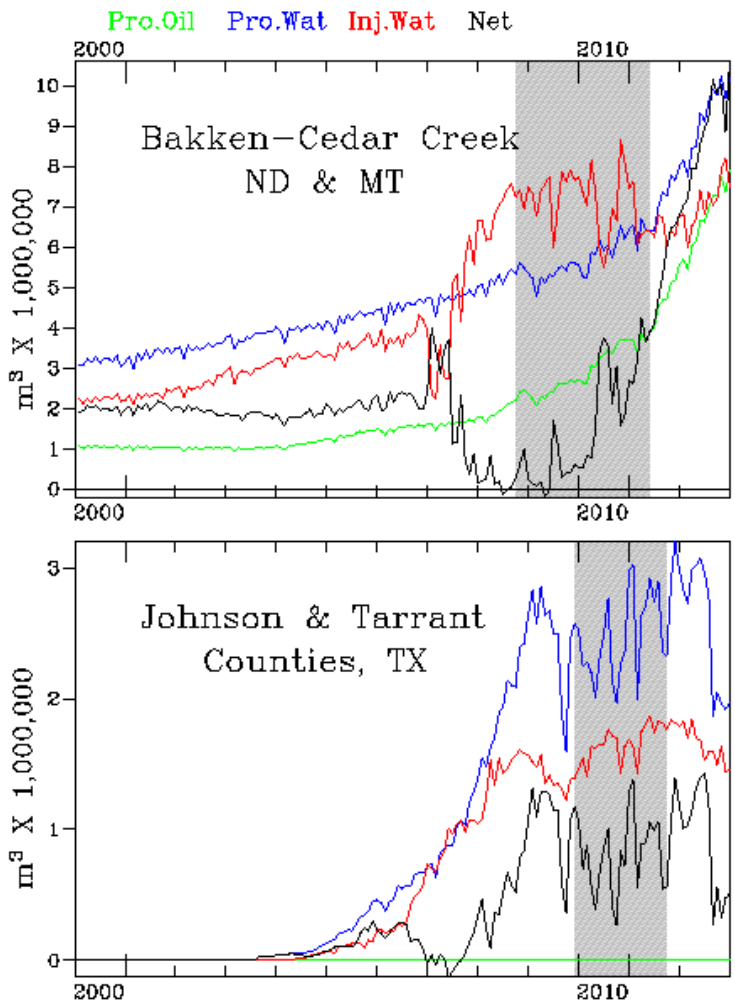

Fig. 4.2. Regional monthly injection and production volumes in two geographic regions. Top graph shows monthly volumes for all Bakken-Cedar Creek wells in ND and MT; bottom graph is for all Johnson and Tarrant County wells in TX. Green and blue lines are oil and water produced, red line is water injected, and black line is net volume (oil + water produced – water injected). Note that injection volumes in both regions experience significant increases in 2007. Area shaded gray indicates interval when presence of USArray seismograph stations allowed detailed surveys of regional earthquake activity.

4.2 The Williston Basin and the Bakken Formation

The Williston Basin is a roughly circular depression covering about 500,000 km^2 across parts of North and South Dakota, Montana, Manitoba and Saskatchewan. The deepest point, where the Precambrian basement depth is about 5 km, is near Williston, ND. The Williston Basin began to subside during the Ordovician and has undergone episodic subsidence subsequently (Polastro et al., 2013). Basin stratigraphic sequences record several cycles of marine transgression and

regression. Petroleum production has been ongoing in the Williston Basin since oil was discovered along the Cedar Creek Anticline the 1920's, with significant development phases occurring in the 1950's, and then again in the 1970's.

The Bakken Formation is currently the most commercially important stratigraphic sequence in the Williston Basin (Polastro et al., 2013). The Bakken, which is upper Devonian and Lower Mississippian in age, is entirely in the subsurface with no surface outcrop. It has three members, an upper and lower black, organic-rich shale, separated by a dolomitic siltstone. Petroleum has been produced from the Bakken Formation for more than 50 years; however, the application of hydraulic fracturing and horizontal drilling technologies has recently augmented Bakken oil and gas production, both which have increased approximately exponentially since 2006 (Fig. 4.2). As a result, by 2013 North Dakota was the second-largest petroleum-producing state in the U.S., behind only Texas.

Historically, the largest earthquake reported in the Williston/Bakken region was assigned magnitude 5½ and occurred on 15 May 1909, with a reported epicenter that "could have been located in southern Saskatchewan, northeastern Montana, or northwestern North Dakota" (Horner and Hasegawa, 1978). Subsequently the largest earthquakes were a M4.4 on 8 July 1968 near Hough in North Dakota and a M4.3 on 26 July 1972 near Bengough in Saskatchewan (Horner et al., 1973).

A second, roughly linear group of epicenters is situated in northern Montana and North Dakota. There are historical reports of earthquakes felt in Williston in 1915 and 1946, and instrumentally-located epicenters occurred in 1975 (M3.9), 1982 (M 3.3), 1998 (M3.5), 2012 (M3.3) and 2014 (M4.1). Due to the absence of regional seismic stations most of these locations are poorly determined, but they lie approximately along the SW-NE-trending Brockton-Froid fault zone. Dip and sense of movement on the fault zone are not well constrained. It shows evidence of Quaternary deformation but it is not clear if it extends to the basement (Wheeler, 1999).

4.3 Data and Methods

We identified seismic events for this study using data recorded by the three-component seismographs in the USArray temporary network, an NSF-supported program that deployed stations for intervals of two years on a grid with spacing ~70 km. For the region surrounding the Bakken, USArray data was available between September 2008 and May 2011, allowing us to locate seismic events occurring during this period. At each station we filtered the seismograms and identified candidate phase arrivals using a short-term/long-term average method; we analyzed events when there were phase arrivals identified at three or more stations.

We personally inspected the seismograms, reread P and S phases for, and relocated all events that appeared to be regional earthquakes as well as representative mine blasts from each mine we identified. For most of the relocations we only used phases recorded at stations within 1° of the epicenter; for the relocations we arbitrarily fixed the depths of earthquakes at 5 km. In this study, with seismographs

located on a 70-km grid, we estimate that earthquake epicenters determined in this study are accurate to within ±2 km or less.

The information in this study concerning well locations and depths of production or injection, monthly volumes of oil produced, and water and gas produced and injected, was from the database of IHS, Inc. IHS, Inc. is a private company that compiles information about petroleum operations available from public sources, and provides them by subscription to the public.

In the literature, the great majority of earthquakes reported as induced have epicenters within a few km of an active injection well (Suckale, 2009). Exceptions at distances exceeding 10 km occurred in situations like Paradox Valley, CO, where injection has been ongoing for as much as 20 years (Block et al., 2014), or as in Oklahoma where injected volumes are extremely high (Keranen et al., 2014). In the Bakken widespread injection began increasing only in 2007, and thus in this study we evaluate injection volumes primarily within 5 km of earthquake epicenters.

4.4 Results

By far the most abundant seismic signals recorded were mine blasts at regional strip mines that produce coal, mostly to be consumed electric power plants. The ten largest coal mines in the U.S. are in northwestern Wyoming (U.S. Energy Information Administration, 2013); some of these mines regularly generate explosions assigned m_b3.5-4.0 by the NEIC.

Table 4.1. Locations of earthquakes identified in this study. Key: ID is identification number; dep is focal depth (fixed at 5 km for location); mag is magnitude; rms is root mean square residual; gap is azimuthal gap. Column labeled loc is location; events labeled Bk have epicenters within the shaded region in Fig. 4.1; events labeled CC are along the Cedar Creek Anticline.

ID	*year*	*mo*	*da*	*hr*	*mi*	*sec*	*lat*	*long*	*dep*	*mag*	*rms*	*gap*	*loc*
200	2008	11	02	22	49	19.48	46.410	-107.766	5	1.9	0.39	75	
360	2009	01	20	20	49	26.03	46.134	-105.484	5	1.8	0.21	107	
640	2009	07	15	5	14	7.15	47.439	-105.961	5	1.9	0.49	60	
680	2009	08	05	6	5	45.68	46.416	-107.760	5	1.9	0.36	76	
826	2009	08	31	1	24	22.78	47.632	-102.382	5	1.9	0.50	94	Bk
2090	2010	03	21	16	56	40.55	47.984	-103.978	5	2.5	0.27	72	Bk
2175	2010	04	27	5	7	58.84	46.585	-104.445	5	2.1	0.30	66	CC
2306	2010	06	14	7	58	3.46	46.034	-103.960	5	1.4	0.51	64	CC
2720	2011	04	06	11	23	49.39	48.418	-104.841	5	2.6	0.21	304	Bk

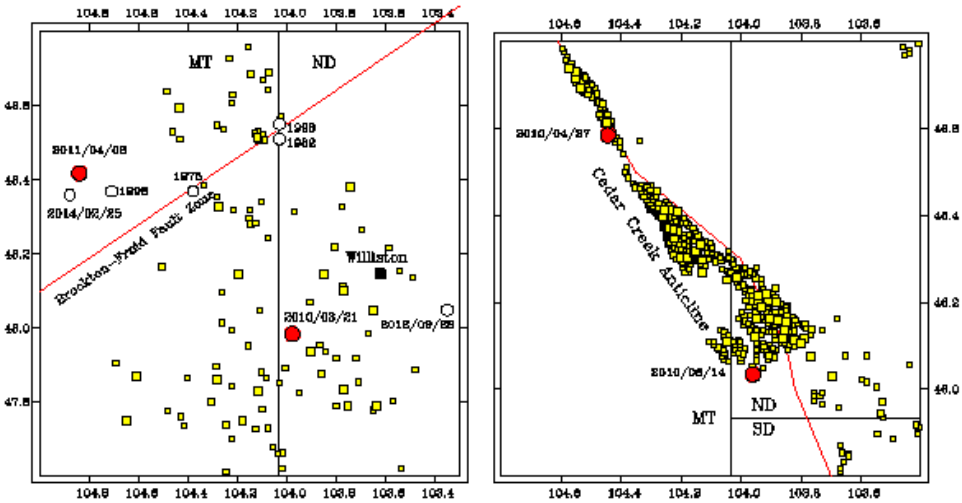

Fig. 4.3. Detail maps of earthquakes and injection wells investigated in this study. Map at left is region near Williston and the Brockton-Froid fault zone; map at right shows area along the Cedar Creek Anticline. Red circles are earthquakes located in this study; white circles are historical earthquakes. All plotted wells reported monthly injection volume exceeded 1600 m³/mo for one or more months since 2000; larger symbols are wells where monthly injection volume exceeded 16,000 m³/mo.

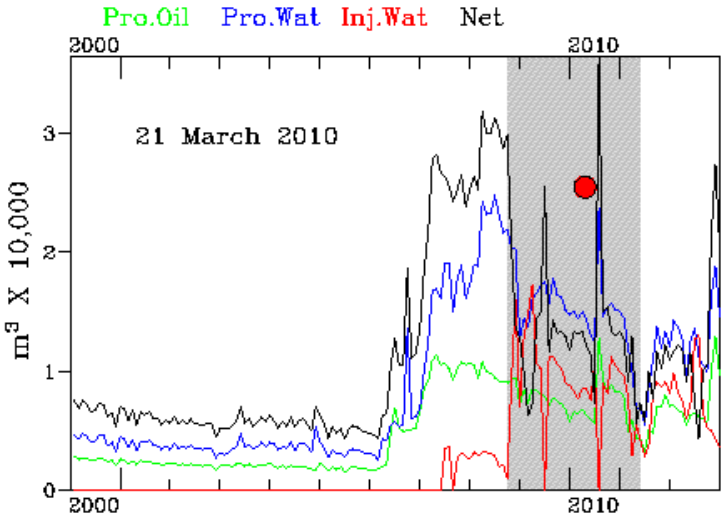

Fig. 4.4. Injection and production volumes for wells near the earthquake of 21 March 2010. Graph shows monthly volumes for wells within 5 km of the epicenter (see Table 4.1 and Fig. 4.3 left). Green and blue lines are oil and water produced, red line is water injected, and black line is net volume (oil + water produced – water injected). Note that production volumes experienced significant increases in 2006, and injection volumes increased in 2008. Red circle indicates time when earthquake occurred; area shaded gray indicates interval when presence of USArray seismograph stations allowed our detailed survey of regional earthquake activity.

Within the region mapped in Fig. 4.1, our analysis of USArray data detected only nine earthquakes (Table 4.1) occurring between September 2008 and May 2011. Three of these epicenters lie within the mapped extent of the Bakken, two occurred south of the Bakken along the Cedar Creek Anticline, and four were to the west of the Bakken in Montana.

Within the Bakken area only one of the three earthquakes identified is probably induced/triggered. For the earthquake of 21 March 2010 southwest of Williston (Fig. 4.3, left), at wells within 5 km of the epicenter there was a significant increase in oil and water production at the end of 2006, and a significant increase in injection near the end of 2008 (Fig. 4.4). In contrast, although the earthquake of 31 August 2009 (Fig. 4.1) was well-recorded so its location should be accurate, there were no active injection or production wells within 5 km. Similarly, there were no wells nearby the northeastern Montana earthquake of 6 April 2011 (Fig. 4.3, left). Moreover, it occurred in roughly the same area as the apparently natural earthquakes of 1975, 1998 and 2014 associated with the Brockton-Froid fault zone.

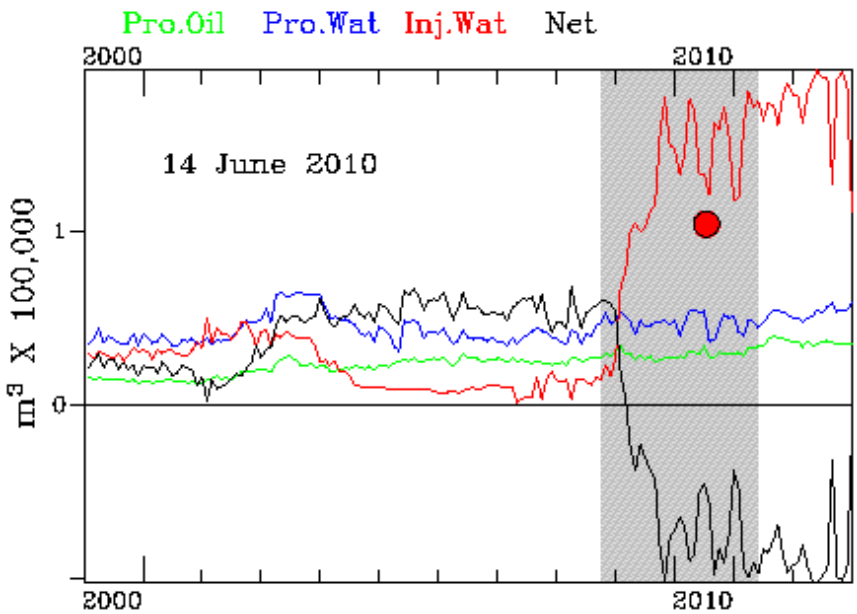

Fig. 4.5. Injection and production volumes for wells near the earthquake of 14 June 2010. Graph shows monthly volumes for wells within 10 km of the epicenter (see Table 4.1 and Fig. 4.3 right). Green and blue lines are oil and water produced, red line is water injected, and black line is net volume (oil + water produced – water injected). Note that injection increased significantly in 2009 prior to the earthquake. Red circle indicates time when earthquake occurred; area shaded gray indicates interval when presence of USArray seismograph stations allowed our detailed survey of regional earthquake activity.

Further south, two earthquakes detected along the Cedar Creek Anticline may be induced/triggered. The event of 14 June 2010 (Fig. 4.3 right) followed an overall increase in injection rates to about 150,000 m^3/mo in mid-2009 at wells within a radius of 10 km (Fig. 4.5). For the earthquake of 27 April 2010 (Fig. 4.3 right),

injection volumes from 2003 onward averaged more than 100,000 m^3/mo at wells within 5 km of the epicenter (Fig. 4.6); however, volumes for extraction of water were approximately the same, so that net volume of fluid extracted was considerably less.

It is implausible that injection triggered any of the four remaining earthquakes we detected, all located in eastern Montana (Fig. 4.1). There are no injection or production wells within 10 km of the earthquakes of 20 January 2009 or 15 July 2009. For the earthquakes of 2 November 2008 and 5 August 2009 which had nearly identical epicenters, there were no nearby injection wells although since 2000 there have been producing wells within 5 km that regularly extract water at rates of ~15,000 m^3/mo.

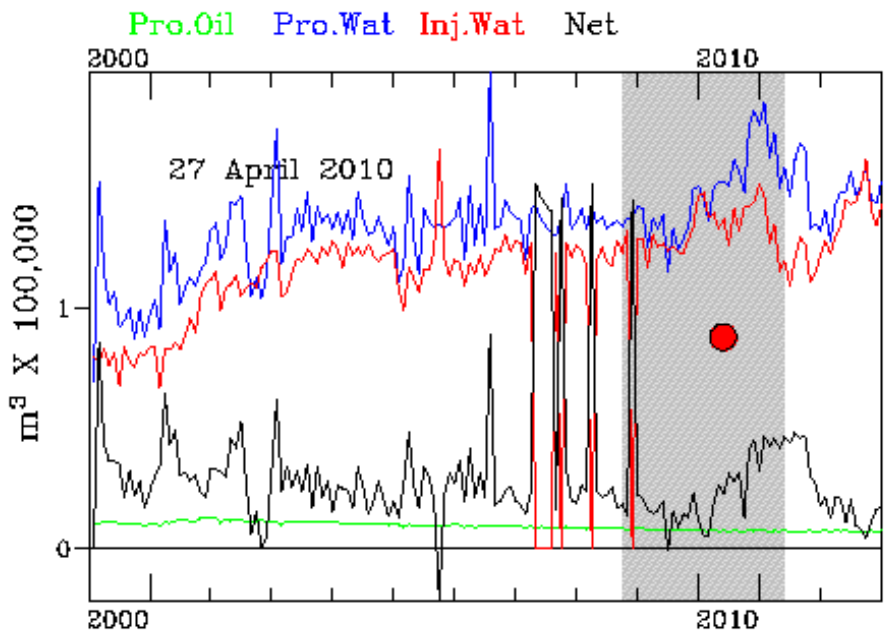

Fig. 4.6. Injection and production volumes for wells near the earthquake of 27 April 2010. Graph shows monthly volumes for wells within 5 km of the epicenter (see Table 4.1 and Fig. 4.3 right). Green and blue lines are oil and water produced, red line is water injected, and black line is net volume (oil + water produced – water injected). Note that injection and water production volumes were consistently high in the decade prior to the earthquake, but that there are no unusual changes in 2009 or 2010. Red circle indicates time when earthquake occurred; area shaded gray indicates interval when presence of USArray seismograph stations allowed our detailed survey of regional earthquake activity.

4.5 Discussion

The principal result of this study is that an intensive search finds significantly fewer injection-caused earthquakes in the Bakken region than identified in a similar search in the Barnett Shale region of Texas (Frohlich, 2012), or as reported by NEIC in central Oklahoma (Keranen et al., 2013; 2014). The Oklahoma situation, especially for events reported near Oklahoma City, may differ because injection

volumes there are massive, with four high-volume injection wells within 20 km of the reported earthquake activity, including two where injection rates exceeded a million barrels per month (160,000 m^3/mo). Within the Barnett Shale of Texas, earthquake activity associated with injection was concentrated in a few areas, notably in Johnson and Tarrant Counties, and elsewhere there were few or no earthquakes even in counties where injection wells were numerous. Yet, the time history of injection in the Bakken and Barnett regions are similar, with both experiencing significant increases in injected volumes since 2006 (Fig. 4.2).

Triggered earthquakes are thought to occur when injected fluids reduce the normal stress and thus friction across faults, allowing them to slip in response to regional tectonic stress (Zoback and Townend, 2001; National Research Council, 2013). The in-situ stress state, orientation of pre-existing faults and changes in fluid pressure are needed to assess the likelihood of fault reactivation. In the Williston Basin, Zhou et al. (2008) argue that maximum stress is vertical; the Bakken Formation is overpressured (Burris et al., 1996) but otherwise the stress profile relates simply to depth and density with a gradient of 1 psi/ft (Zhou et al., 2008). The horizontal stresses are poorly constrained, but Williams-Stroud and Billingsley (2010) note the low stress anisotropy and comment that this produces a wider range of fracture orientations than would be found in basins where the differential stress is higher. The World Stress map (Heidbach et al., 2009) shows one data point in Saskatchewan with maximum horizontal stress oriented N-S. Ling (2014) show highly variable orientations in North Dakota, with NE-SW predominant.

The Bakken play and neighboring regions are remarkable for their low level of historical seismicity. This may be partly because of the absence of "felt" seismicity, due to historically low populations densities coupled with the near-absence of regional seismograph stations. The occurrence of regional earthquakes with M5½ in 1909 and M4.4 in 1972 suggests higher natural seismic activity than occurs in the Fort Worth Basin of northeast Texas, where no natural historical earthquakes with magnitudes this large have occurred (Frohlich et al., 2011; Frohlich and Davis, 2002). If the 1909 estimate of magnitude M5½ is accurate, maximum earthquake size for the Bakken region is more comparable to Oklahoma, where the largest natural historical earthquakes (in 1882 and 1952) had magnitudes of ~5.7.

An important result of this and previous surveys is that the relationship between seismicity and injection/production activities varies considerably in different geographic areas. In the Williston Basin and western counties of Texas' Fort Worth Basin (Frohlich, 2012), there is very little seismic activity near injection wells. In Oklahoma (Keranen et al, 2013; 1014), Arkansas (Horton, 2012), in Johnson and Tarrant counties in the Fort Worth Basin (Frohlich et al., 2011; Frohlich, 2012: Justinic et al., 2013), and near Timpson in east Texas (Frohlich et al., 2014), there are earthquakes associated with high-volume injection wells. In the Eagle Ford play region of Texas earthquakes are associated primarily with production (not injection) (Frohlich and Brunt, 2013). In the Cogdell Field of Texas increased seismic activity since 2006 coincided with a massive CO_2 gas injection program to enhance production (Gan and Frohlich, 2013).

Two unresolved questions raised by these investigations are: (1) why does injection or production enhance seismic activity near some wells and fields and not others?; and (2) what differences in geology and/or in injection/production practices explain the difference response of the various regions? This variability in response to injection complicates efforts to come up with sensible uniform policies and regulations to mitigate potential seismic hazards associated with injection practices. At a minimum it suggests that within any particular geographic region it is important to survey the relationship between seismicity and injection before considering possible policy responses or regulations.

4.6 Data and Resources

All seismograms evaluated in this study are archived at the IRIS Data Management Center and freely available. Information about injection well locations, volumes, etc., were obtained by subscription from IHS, Inc., is a private company that compiles information about petroleum operations available from public sources.

4.7 References

Block, L. V., C. K. Wood, W. L. Yeck and V. M. King (2014). The 24 January 2013 M_L 4.4 earthquake near Paradox, Colorado, and its relation to deep well injection. *Seismol. Res. Lett.* **85**, 609-624.

Burrus J., K. Osadetz, S., Wolf, B., Doligez, K., Visser and D Dearborn (1996). A two-dimensional regional basin model of Williston Basin hydrocarbon systems. *AAPG Bulletin* **80**, 265–29.

Ellsworth, W. L. (2013). Injection-induced earthquakes. *Science* **341**, doi:10.1126/science.1225942.

Frohlich, C., C. Hayward, B. Stump and E. Potter (2011). The Dallas-Fort Worth earthquake sequence: October 2008 through May 2009. *Bull. Seismol. Soc. Amer.* **101**, 327-340.

Frohlich, C., W. Ellsworth, W. A. Brown, M. Brunt, J. H. Luetgert, T. MacDonald and S. Walter (2014). The 17 May 2012 M4.8 earthquake near Timpson, east Texas: An event possibly triggered by fluid injection. *J. Geophys. Res. Solid Earth* **119**, 581-593.

Frohlich, C. (2012). Two-year survey comparing earthquake activity and injection well locations in the Barnett Shale, Texas. *Proc. National Acad. Sci.* **109**, 13934-13938.

Frohlich, C. and M. Brunt (2013). Two-year survey of earthquakes and injection/production wells in the Eagle Ford Shale, Texas, prior to the M_W4.8 20 October 2011 earthquake. *Earth Planet. Sci. Lett.* **379**, 53-63.

Frohlich, C. and S. D Davis (2002). *Texas Earthquakes*. Univ. Texas Press, 275 pp.

Gan, W. and C. Frohlich (2013). Gas injection may have triggered earthquakes in the Cogdell oil field, Texas. *Proc. National Acad. Sci.* **110**, 18786-18791.

Heidbach, O., M. Tingay, A., Barth, J., Reinecker, D., Kurfeß and B. Müller (2009). *The World Stress Map*, equatorial scale 1:46,000,000: Commission for the Geological Map of the World, doi:10.1594/GFZ.WSM.Map2009.

Horner, R. B. and H. S. Hasegawa (1978). The seismotectonics of southern Saskatchewan. *Canadian J. Earth Sci.* **15**, 1341-1355.

Horner, R. B., A. E. Stevens and H. S. Hasegawa (1973). The Bengough, Saskatchewan, earthquake of July 26, 1972. *Canadian J. Earth Sci.* **10**, 1805-1821.

Horton, S. (2012). Disposal of hydrofracking waste fluid by injection into subsurface aquifers triggers earthquake swarm in central Arkansas with potential for damaging earthquake. *Seismol. Res. Lett.* **83**, 250–260.

Justinic, A. H., B. Stump, C. Hayward and C. Frohlich (2013). Analysis of the Cleburne, Texas, earthquake sequence from June 2009 to June 2010. *Bull. Seismol. Soc. Amer.* **103**, 3083-3093.

Keranen, K. M., H. M. Savage, G. A. Abers and E. S. Cochran (2013). Potentially induced earthquakes in Oklahoma, USA: Links between wastewater injection and the 2011 Mw 5.7 earthquake sequence. *Geology* **41**, 699-702.

Keranen, K. M., M. Weingarten, G. A. Abers, B. Bekins B. and S. Ge, (2014). Sharp increase in Oklahoma seismicity since 2008 triggered by massive wastewater injection, 10.1126/science.1255802, *Science* **345**, 448-451.

Kim, W.-Y. (2013). Induced seismicity associated with fluid injection into a deep well in Youngstown, Ohio. *J. Geophys. Res. Solid Earth* **118**, 3506-3518.

Ling, K. (2014). *Geomechanical Study of Bakken Formation for Improved Oil Recovery*. http://www.netl.doe.gov/research/oil-and-gas/project-summaries/enhanced-oil-recovery/05643_geomech_bakken.

National Research Council (2013). *Induced Seismicity Potential in Energy Technologies*, National Academies Press, 248 pp.

Pollastro, R. M., L. N. R. Roberts and T. A. Cook (2013). Geologic assessment of technically recoverable oil in the Devonian and Mississippian Bakken formation. Chap. 5 of *Assessment of Undiscovered Oil and Gas Resources of the Williston Basin province of North Dakota, Montana, and South Dakota, 2010*, U.S. Geol. Survey Digital Data Series DDS-69-W. 34 pp.

Suckale, J. (2009). Induced seismicity in hydrocarbon fields. *Adv. Geophys*. **51**, 55-106.

U.S. Energy Information Administration (2013). *Annual Coal Report 2012*. U.S. Dept. of Energy. 59 pp.

Wheeler, R. L., compiler (1999), Fault number 707, Brockton-Froid fault zone, in Quaternary fault and fold database of the United States: U.S. Geological Survey website, http://earthquakes.usgs.gov/hazards/faults, accessed 07/23/2014 08:49 AM.

Williams-Stroud, S. and R. L Billingsley (2010). Techniques to estimate fracture effectiveness when mapping low-magnitude microseismicity. *SEG Technical Program Expanded Abstracts 2010*, 2075-2079. doi: 10.1190/1.3513253.

Witze, A. (2013). USArray eyes its final frontier. *Nature* **503**, 16-17.

Zhou, X. J., Z. Zeng, M., Belobraydic, M. and Y. Han (2008). Geomechanical Stability Assessment of Williston Basin Formations for Petroleum Production and CO2 Sequestration. *Proceedings, American Rock Mechanics Association, 42nd US Rock Mechanics Symposium and 2nd U.S.-Canada Rock Mechanics Symposium*, San Francisco, CA.

Zoback, M. D. and J. Townend (2001). Implications of hydrostatic pore pressure and high crustal strength for the deformation of intraplate lithosphere. *Tectonophysics* **336**, 19-30.

5. Haynesville seismicity report

The material in this section was prepared by Jake Walter, Cliff Frohlich and Peter Dotray.

5.1. Introduction

In the last decade, incidences of increased seismicity throughout the central United States have been correlated with wastewater disposal to support hydrofracturing operations (Frohlich et al., 2011; Frohlich et al., 2014; Keranen et al., 2014; Rubinstein et al., 2014). The paucity of permanent seismic stations in the area of the Haynesville shale play makes it exceedingly difficult to establish any evidence for historical seismicity over the last century. Without this historical context, it is difficult to determine whether earthquakes are natural or induced in regions of increasing energy production, especially those associated with wastewater disposal and/or production enhancements related to hydrofracturing operations in the last decade. Nonetheless, we investigate recent seismicity near the Haynesville shale play, which encompasses parts of eastern Texas and northwestern Louisiana.

Similar to our investigation of seismicity near the Bakken play and within the Williston Basin (Section 4), we utilize temporary (~2 years) deployments of seismographs during the USArray Transportable Array (TA) experiment. We analyze the seismicity from February 2010 through the end of 2012 using this denser instrumentation.

Sometimes seismicity catalogs can be woefully incomplete due to myriad reasons including high station noise, earthquakes occurring closely spaced in time, and other factors. These factors contribute to incomplete seismicity catalogs. An effective way to identify possible "missing" events is the waveform matched-filter technique (e.g. Shelly et al., 2007). Waveforms from earthquakes that are undetected but close-by cataloged events may transmit waveforms that appear similar or upon inspection by cross-correlation are similar. In this way, we are able to use existing waveforms to search for other earthquakes that were previously undetected. We use the matched-filter to detect earthquakes not detected by our initial automatic detection. With these methods, we build a more comprehensive seismicity catalog with geographic emphasis near the Haynesville shale play.

5.2. Methods

5.2.1. Automatic earthquake detection

We first build a catalog utilizing standard passive seismological techniques for identifying earthquakes along continuous seismograms. We identify phase arrivals utilizing an automatic short-term average/long-term average (STA/LTA) ratio filter whose threshold we identify based on our previous experience working with TA data. We catalog picks and origin information within Antelope Seismic Database software. The phase arrivals and event associations are analyst-reviewed and in all

cases re-picked. The phase information is used to locate the events with hypoDD utilizing a generic 1-dimensional velocity model.

We utilize the events identified in this way as templates for the next step in the analysis.

5.2.2. Waveform matched-filter detection of "missing" earthquakes

We next augment that catalog significantly with a matched-filter technique, which is an effective way to identify possible "missing" events. This technique utilizes waveforms or travel time information of known events as a template, or "matched-filter," to search for similar patterns in the continuous recordings that suggest the presence of a smaller event. It has been successfully applied to detect many unreported events that occurred at mid-ocean ridges and transform faults (Shearer, 1994), track low-frequency earthquakes within the deep tectonic tremor signals (Shelly et al., 2007; Brown et al., 2008; Shelly and Hardebeck, 2010) and earthquake swarms (Shelly and Hill, 2011), detect early aftershocks (Peng and Zhao, 2009; Lengliné and Marsan, 2009; Lengline et al., 2012), triggered earthquakes (Meng et al., 2012), and foreshocks (Bouchon et al., 2011; Kato et al., 2012).

In order to run the matched-filter technique, we use the picked waveforms as initial templates. In order to focus on regional waveforms, we bandpass filter these data between 1 to 5 Hz and cut the waveforms 1 s before and 5 s after the phase arrival (P or S). We utilize template events that consist of phase arrivals for at least 5 stations within the network. The matched-filter technique computes the cross-correlation coefficient between the template and continuous data at each sample point through time to determine the cross-correlation coefficient time series. The cross-correlation functions for each component are then time-shifted back to the origin time and stacked for each component. Detection occurs when the stack exceeds 9 times the median absolute deviation (MAD), a threshold similar to other studies utilizing a network-based matched-filter (e.g. Shelly and Hill, 2011; Meng et al., 2013). We first examine these detections and after careful analyst scrutiny, choose a threshold of 12 times the MAD, to ensure that visible body waves are present at a least a few stations.

One method of identifying whether a seismic network captures all the seismicity that is actually occurring is the magnitude of completeness (M_c). The M_c value is the magnitude where the Gutenberg-Richter empirical relationship becomes depleted in events below that magnitude. Thus, a seismicity catalog can be considered "complete" for earthquakes with magnitudes greater than M_c. We will utilize M_c to determine the degree to which our method improves the seismicity catalog.

5.3. Results

We identify 19 earthquakes using the methods described in Section 5.2.1. When we augment the catalog with the matched-filter technique, we identify a total of 50 earthquakes. Most of the newly identified earthquakes are of smaller magnitude than the original 19 template events. Note that the cluster of seismicity in East

Texas adjacent to Timpson is similar to findings of Frohlich et al. (2014). One contribution of this investigation is the newly identified cluster of earthquakes identified in the northeastern portion of Louisiana, which occurred within in the Bienville Parish. These earthquakes were not reported by other agencies.

Given the small amount of earthquakes identified in this study, it is difficult to accurately assess the magnitude of completeness (M_c). Nonetheless, the matched-filter appears to indicate a value of M_c of approximately 2. This is compared to the earthquakes obtained with our automatic detector, which yielded a M_c value of approximately 3. Thus, the ability to detect earthquakes is greatly improved and is comparable to order-of-magnitude M_c improvement from previous studies (i.e. Schaff and Waldhauser, 2010).

The greatest spatial correlation of seismicity is mostly concentrated in the areas of Timpson, TX, and within the Bienville Parish, LA, between the towns of Jamestown and Ringgold. The seismicity detected in these regions is shown in Figure 5.3. While the Timpson sequence has already been discussed by Frohlich et al. (2014), we also identify additional earthquakes with magnitudes 2-3 in the year preceding the M4.8 event on 17 May 2012. This may indicate sustained triggering of earthquake activity in the year prior to the larger sequence.

The Bienville Parish seismic activity has hitherto been unreported. Of particular note is the number of smaller magnitude earthquakes without a preceding larger event for the Bienville Parish activity. Clearly these events are not part of some aftershock sequence and are instead most consistent with classification as a seismic swarm. A total of 20 earthquakes between magnitudes 1-2.5 occurred over just a few months (August-September 2011).

At this time, we are not able to directly compare seismicity with injection well information for Bienville Parish due to incomplete archives at the Louisiana Department of Natural Resources. For example, their records indicate the existence of 51 active injection wells in Bienville Parish, though the data is inconsistently reported and appears to be missing for most wells in 2012 and all wells prior to 2012. We are currently investigating this issue.

5.4. Conclusions

We identified many earthquakes in eastern Texas and Louisiana that had not been previously identified. While some earthquakes exist outside two distinct zones, most seismicity is confined to zones near Timpson, TX, and Bienville Parish, LA. The Timpson sequence has been studied and discussed extensively by Frohlich et al. (2014), while we are currently investigating the environmental conditions associated with the Bienville Parish sequence. This work highlights the continued need for investments in monitoring seismicity in areas of active oil and gas activities.

5.5. References

Bouchon, M., H. Karabulut, M. Aktar, S. Özalaybey, J. Schmittbuhl, and M.-P. Bouin (2011), Extended nucleation of the 1999 Mw 7.6 Izmit earthquake, Science, 331, 877–880, doi:10.1126/science.1197341.

Brown, J. R., G. C. Beroza, and D. R. Shelly (2008), An autocorrelation method to detect low frequency earthquakes within tremor, Geophys. Res. Lett., 35, L16305, doi:10.1029/2008GL034560.

Frohlich, C., C. Hayward, B. W. Stump, and E. Potter (2011), The Dallas-Fort Worth earthquake sequence: October 2008 through May 2009, Bull. Seismol. Soc. Amer., 101, 327-340

Frohlich, C., W. Ellsworth, W. A. Brown, M. Brunt, J. H. Luetgert, T. MacDonald, and S. Walter (2014), The 17 May 2012 M4.8 earthquake near Timpson, east Texas: An event possibly triggered by fluid injection, J. Geophys. Res. Solid Earth, 119, 581-593, doi:10.1002/2013JB010755.

Kato, A., K. Obara, T. Igarashi, H. Tsuruoka, S. Nakagawa, N. Hirata (2012), Propagation of Slow Slip Leading Up to the 2011 Mw 9.0 Tohoku-Oki Earthquake, Science, DOI: 10.1126/science.1215141.

Keranen, Kathleen, Matthew Weingarten, Geoffrey A. Abers, Barbara Bekins, Shemin Ge. 2014. "Sharp increase since 2008 induced by massive wastewater injection." Science 345 (6195): 448-451.

Lengliné, O. and D. Marsan (2009), Inferring the coseismic and postseismic stress changes caused by the 2004 Mw = 6 Parkfield earthquake from variations of recurrence times of microearthquakes, J. Geophys. Res., 114, B10303, doi:10.1029/2008JB006118.

Lengliné, O., B. Enescu, Z. Peng, and K. Shiomi (2012), Decay and expansion of the early aftershock activity following the 2011, Mw9.0 Tohoku earthquake, Geophys. Res. Lett., 39, L18309, doi:10.1029/2012GL052797.

Meng, X., Z. Peng, and J. L. Hardebeck (2013), Seismicity around Parkfield correlates with static shear stress changes following the 2003 Mw6.5 San Simeon earthquake, J. Geophys. Res. Solid Earth, 118, 3576–3591, doi:10.1002/jgrb.50271.

Peng, Z., and P. Zhao (2009), Migration of early aftershocks following the 2004 Parkfield earthquake, Nature Geosci., 2, 877–881, doi: 10.1038/ngeo697.

Rubinstein, J.L., W.L. Ellsworth, A. McGarr, and J. Benz, (2014), The 2001-Present induced earthquake sequence in the Raton Basin of Northern New Mexico and Southern Colorado, Bull. Seism. Soc. Am., 104 (5), 1-20.

Schaff, D. P. and F. Waldhauser (2010). One magnitude unit reduction in detection threshold by cross correlation applied to Parkfield (California) and China seismicity, Bull. Seismol. Soc. Am. 100:6, 3224–3238.

Shearer, P. M. (1994), Global seismic event detection using a matched filter on long-period seismograms, J. Geophys. Res., 99, 13,713–13,725.

Shelly, D. R., G. C. Beroza, and S. Ide (2007), Non-Volcanic Tremor and Low Frequency Earthquake Swarms, Nature, 446, 305-307, doi:10.1038/nature05666.

Shelly, D. R. and J. L. Hardebeck (2010), Precise tremor source locations and amplitude variations along the lower-crustal central San Andreas Fault, Geophys. Res. Lett., 37, L14301, doi:10.1029/2010GL043672.

Shelly, D. R. and D. P. Hill (2011), Migrating swarms of brittle-failure earthquakes in the lower crust beneath Mammoth Mountain, California, Geophys. Res. Lett., 38, L20307, doi:10.1029/2011GL049336.

Shelly, D. R., Z. Peng, D. P. Hill and C. Aiken (2011), Triggered creep as a possible mechanism for delayed dynamic triggering of tremor and earthquakes, Nature Geosci., 4, 384-388, doi: 10.1038/ngeo1141.

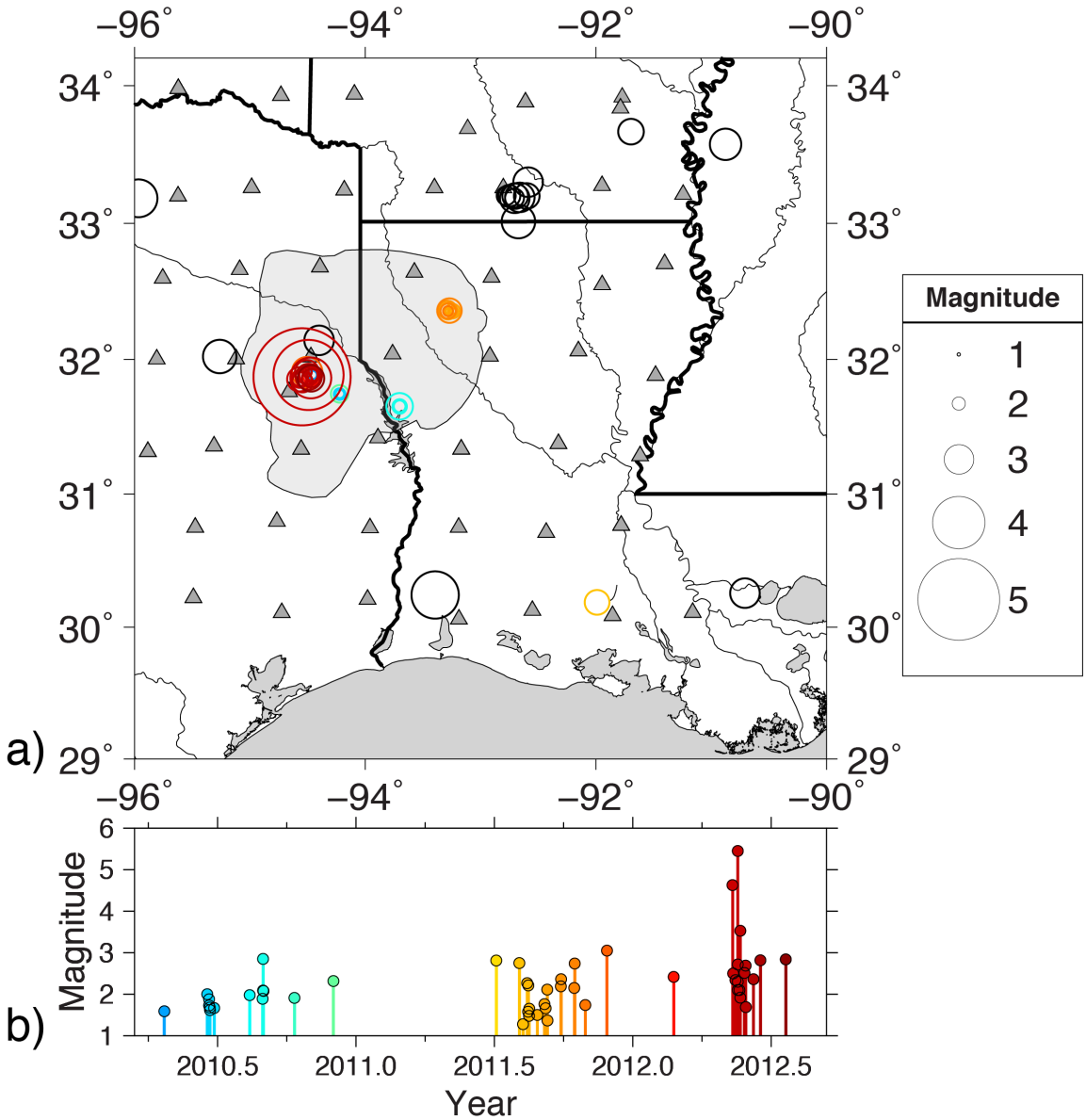

Figure 5.1: (a) Map of study area including identified earthquakes in this study. Color scheme is linear beginning in early 2010 through 2013 progressing from blue to red. Open circles denote previous historical earthquakes identified by the USGS in the years 1980-February 2010. (b) Local magnitude over time period of this study for earthquakes shown in (a).

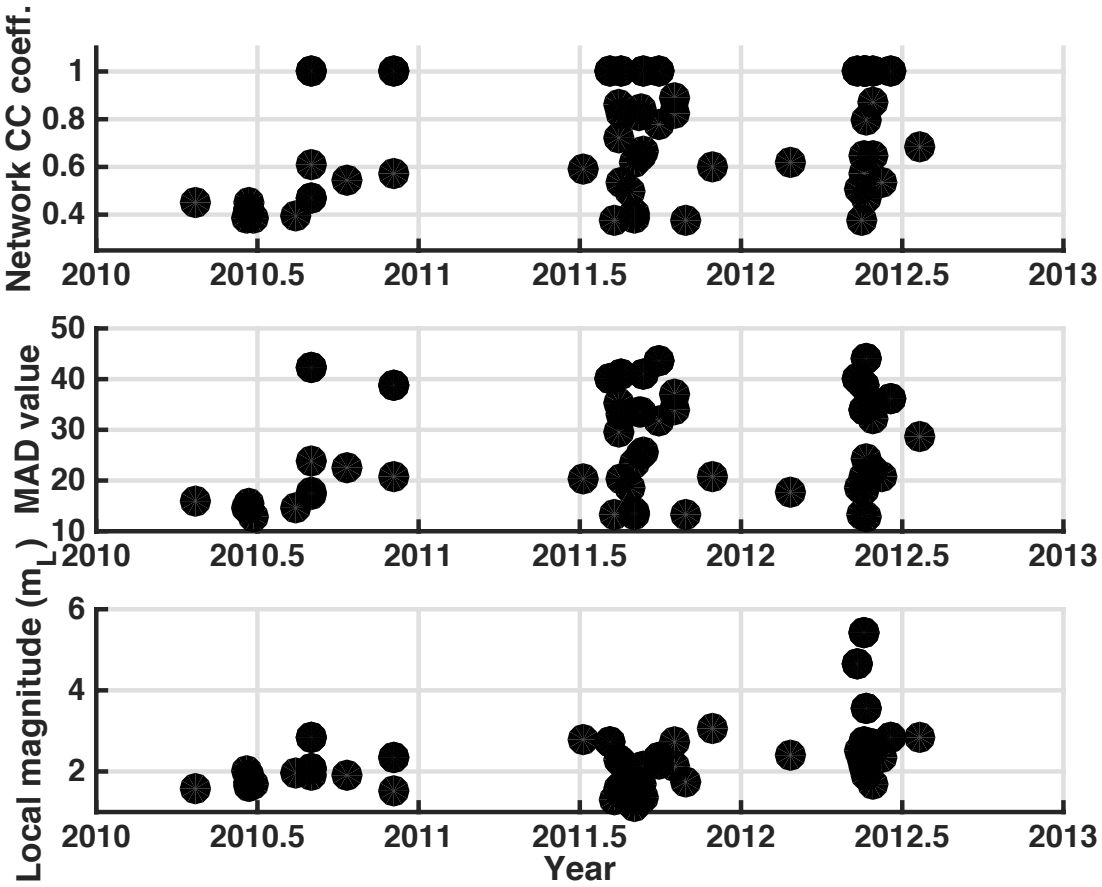

Figure 5.2: Matched-filter results. (a) The network-average cross-correlation coefficient where a value of 1 indicates a self-detection of a template event. (b) Median absolute deviation of the stacked cross-correlation. (c) Local magnitude of both template and matched-filter events.

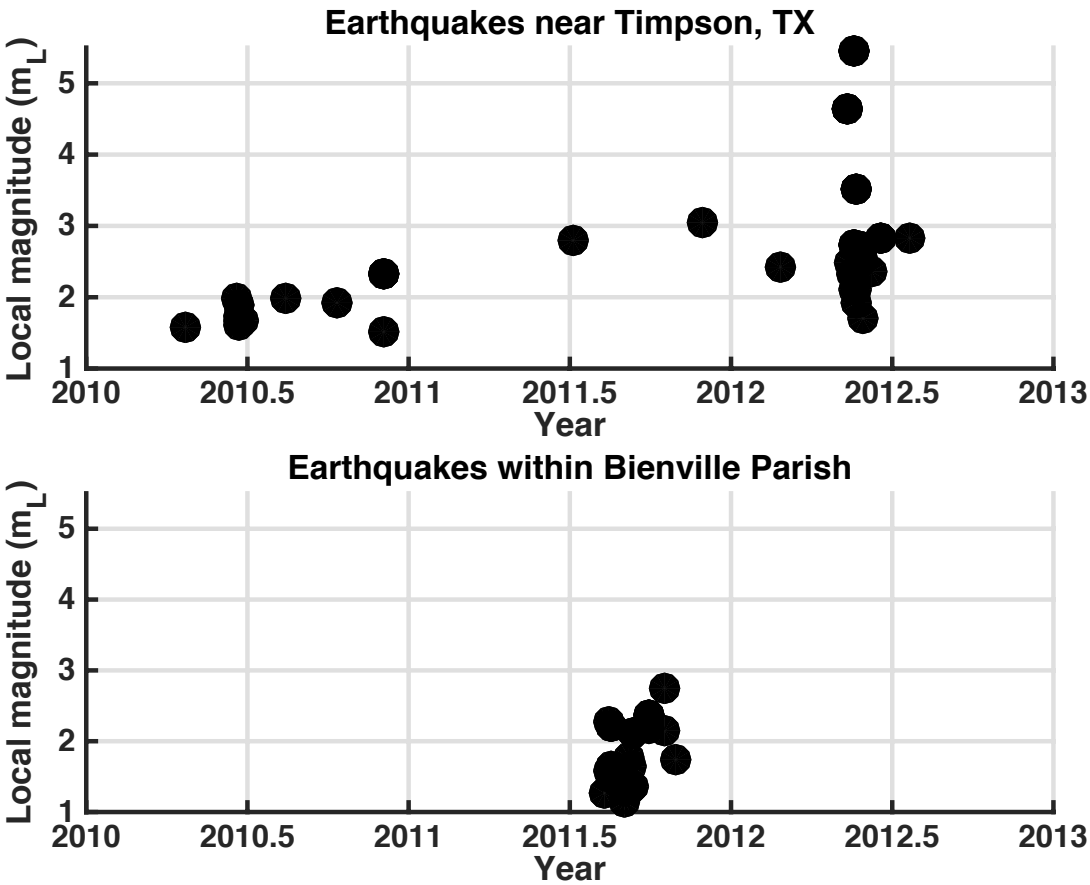

Figure 5.3: Earthquakes within two distinct regions of (a) East Texas and (b) Bienville Parish, Louisiana.

Table 5.1. Haynesville area events

Year	Month	Day	Hour	Min.	Sec.	Latitude	Longitude	Depth	Mag
2010	4	22	3	0	40.26	31.884224	-94.456665	1.88	1.59
2010	6	17	20	5	26.64	31.884182	-94.457186	1.953	2
2010	6	20	6	17	15.77	31.744706	-94.220117	7.581	1.88
2010	6	20	9	23	27.02	31.744702	-94.220093	7.576	1.73
2010	6	21	4	42	28.72	31.744686	-94.220125	7.576	1.68
2010	6	21	7	36	36.67	31.744718	-94.220117	7.569	1.62
2010	6	27	3	8	6.82	31.744722	-94.220036	7.574	1.67
2010	8	12	19	0	21.24	31.884204	-94.459318	2.153	1.98
2010	8	29	19	58	25.06	31.65259	-93.701172	1.764	1.89
2010	8	30	14	5	31.12	31.652464	-93.701465	1.759	2.85
2010	8	30	15	7	3.79	31.652629	-93.700944	1.764	2.09
2010	8	30	21	38	39.32	31.652572	-93.701237	1.734	2.08
2010	10	10	21	11	13.96	31.884267	-94.457275	1.979	1.91
2010	12	1	4	5	47.52	31.745003	-94.221566	8.25	2.32
2011	7	4	2	36	36.4	31.871753	-94.490999	13.50	2.81
2011	8	3	11	8	50.49	30.187105	-91.988721	27.36	2.75
2011	8	8	9	18	11.64	32.356769	-93.281144	5.948	1.28
2011	8	13	18	15	8.84	32.356419	-93.281177	6.068	2.27
2011	8	14	21	53	37.24	32.356732	-93.281315	6.08	1.58
2011	8	15	4	12	30.05	32.356989	-93.280623	6.378	2.21
2011	8	16	0	56	31.89	32.356791	-93.281396	6	1.48
2011	8	16	8	48	26.64	32.356722	-93.281104	6.055	1.65
2011	8	27	3	53	54.9	32.356858	-93.281226	6.054	1.5
2011	9	5	11	52	14.53	32.356486	-93.24091	9.682	1.76
2011	9	7	3	24	45.17	32.355516	-93.244775	5.987	1.66
2011	9	9	4	48	35.52	32.356423	-93.240991	9.721	2.11
2011	9	9	9	34	2.46	32.356242	-93.241227	9.894	1.37
2011	9	27	6	39	43.29	32.356852	-93.281063	6.117	2.19
2011	9	27	9	17	36.08	32.364537	-93.285107	13.39	2.36
2011	10	14	22	31	22.94	32.356801	-93.280981	6.063	2.15
2011	10	15	10	55	43.7	32.360225	-93.271395	2.419	2.74
2011	10	29	9	19	28.68	32.356639	-93.281217	6.014	1.74
2011	11	26	21	22	13.84	31.905288	-94.503035	17.78	3.05
2012	2	23	1	21	3.16	31.884127	-94.457959	1.991	2.42
2012	5	10	15	15	40.86	31.88395	-94.492098	14.11	4.63
2012	5	11	8	35	45.87	31.883734	-94.491895	13.89	2.5
2012	5	14	7	37	9.37	31.883811	-94.491895	13.9	2.34
2012	5	17	8	12	2.46	31.871297	-94.547599	20.13	5.45
2012	5	17	8	46	6.63	31.856077	-94.571672	22.69	2.1
2012	5	17	10	58	54.13	31.852708	-94.571118	22.81	2.72
2012	5	17	14	9	21.29	31.855332	-94.571411	22.73	2.3
2012	5	19	16	37	12.87	31.88387	-94.457926	1.947	2.1
2012	5	20	18	28	35.24	31.862244	-94.470524	13.35	3.53
2012	5	20	19	8	58.46	31.883927	-94.456323	1.935	1.92
2012	5	26	5	42	24.76	31.832074	-94.545345	27.87	2.51
2012	5	27	17	35	28.44	31.907774	-94.505005	17.67	2.69
2012	5	28	3	31	23.25	31.905904	-94.50271	17.73	1.69
2012	6	7	0	34	48.31	31.861226	-94.470719	13.53	2.36
2012	6	16	8	58	13.3	31.871682	-94.490194	13.39	2.82
2012	7	19	19	8	0.3	31.861208	-94.470638	13.53	2.84

6. 17 May 2012 M4.8 Earthquake near Timpson, Texas

The material in this section was prepared by Cliff Frohlich, William Ellsworth, Wesley Brown, Michael Brunt, Tim MacDonald and Steve Walter and was published in 2014 in the *Journal of Geophysical Research*, vol. 119, pp. 581-593, with the title "The 17 May 2012 M4.8 earthquake near Timpson, east Texas: An event possibly triggered by fluid injection".

Abstract: This study summarizes our investigation of the 17 May 2012 $M_{W\text{-}RMT}$4.8 earthquake near Timpson, Texas, the largest earthquake recorded historically in eastern Texas. To identify pre- and aftershocks of the 17 May event we examined the arrivals recorded at Nacogdoches (NATX) 30 km from the 17 May epicenter, at nearby USArray Transportable Array stations, and at eight temporary stations deployed between 26 May 2012 and mid-2013. At NATX we identified seven preshocks, the earliest occurring in April 2008. Reliably-located aftershocks recorded by the temporary stations lie along a 6 km-long NW-SE linear trend corresponding to a previously mapped basement fault that extends across the highest-intensity (MMI VII) region of the 17 May main shock. Earthquakes in this sequence are relatively shallow—with focal depths ranging from 1.6-4.6 km. Evidence supporting these depths include: hypocentral locations of exceptionally well-recorded aftershocks, S-P intervals at the nearest stations, and comparisons of synthetics and observed seismogram. Within 3 km of the linear trend of aftershock activity there are two Class II injection disposal wells injecting at 1.9 km depth beginning in August 2006 and February 2007, with injection rates averaging 42,750 m^3/mo and 15,600 m^3/mo respectively. Several observations support the hypothesis that fluid injection triggered the Timpson sequence: well-located epicenters are situated near a mapped basement fault and near high-volume injection wells, focal depths are at or below the depths of injection, and the earliest preshock (April 2008) occurred after the onset of injection in 2006.

6.1. Introduction

On 17 May at 0812 UTC a $M_{W\text{-}RMT}$4.8 earthquake occurred near Timpson, Texas. The quake awoke numerous residents of Nacogdoches, Texas, 50 km to the southwest of Timpson, and caused significant damage to chimneys, fireplaces, and brick veneer siding 5 km southwest of Timpson. The 17 May earthquake is the largest earthquake in the historical record in east Texas (Fig. 6.1). This paper discusses this earthquake and the sequence of pre- and aftershocks, including an $M_{W\text{-}RMT}$4.0 foreshock on 10 May 2012 at 1515 UTC, and aftershocks occurring on 25 January 2013 at 701 UTC (m_{bLg}4.1) and 2 September 2013 at 1652 (m_{bLg}4.1) and 1851 ($M_{W\text{-}RMT}$4.3).

Regional tectonics in eastern Texas is dominated predominately by salt bodies; however, the Mt. Enterprise fault zone, a system of approximately east-west trending Cretaceous-Paleogene faults, is situated north and west of the epicentral area (see Fig. 6.1; also *Ewing,* 1990). In the epicentral area of the 2012 earthquake *Jackson* (1982) and *Geomap Company* (2012) also indicate a northwest-southeast-trending fault that is roughly parallel to, and slightly east of the Rusk-Shelby county line.

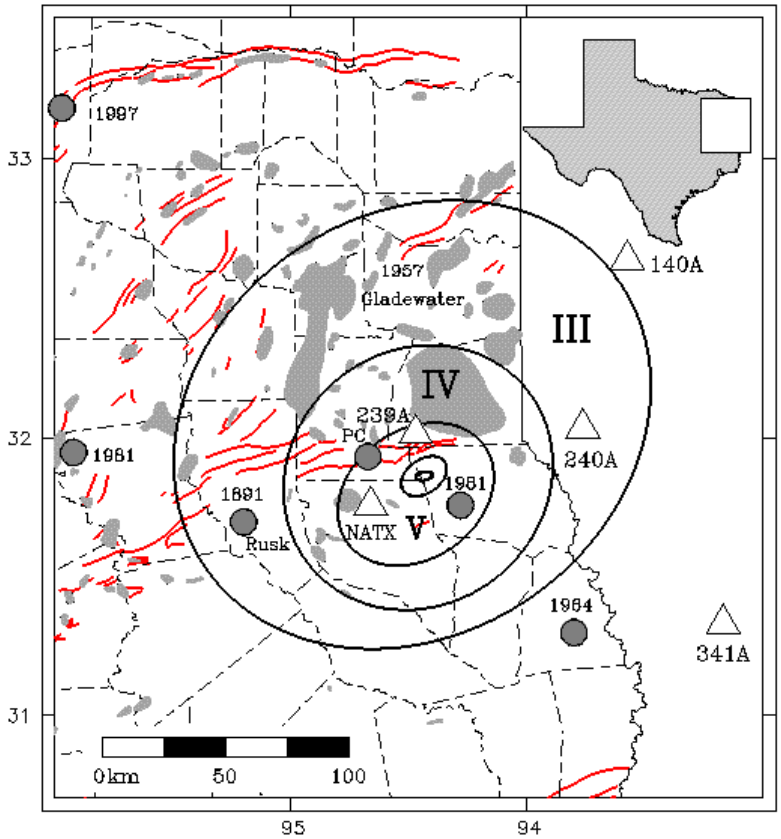

Fig. 6.1. Felt area of 17 May 2012 $M_{W\text{-}RMT}$4.8 earthquake. Roman numerals indicate regions experiencing modified Mercalli intensities MMI III, MMI IV, and MMI V; unlabeled regions within MMI V ellipse experienced MMI VI and MMI VII. Grey circles are historically reported earthquakes from Frohlich and Davis (2002); labels indicate year of occurrence. Also plotted and labeled "PC" is 11 December 1981 microearthquake located by Pennington and Carlson (1984). Red lines are regional faults as mapped by Ewing (1990); the fault system north and west of the highest-intensity region is the Mt. Enterprise fault zone. Triangles are regional seismic stations nearest the 17 May epicenter; all but 239A, which closed December 2011, were used to locate it. Gray shaded regions are oil and gas fields as described by Galloway et al. (1983) and Kosters et al. (1989). Dashed lines are county boundaries. Rectangle within Texas icon at upper right indicates area mapped in this figure.

Seismicity was rare in this region prior to the events analyzed in this study. The nearest events discussed by *Frohlich and Davis* (2002) were a M4.0 8 January 1891 Rusk, Texas, event, 80 km to the west of the epicentral region; and the M3.0 9 June 1981 Center, Texas, earthquake, 25 km to the southeast. However, some investigations have suggested the 1891 Rusk event might be spurious—a thunderstorm or a tornado—and the 1981 Center earthquake was only locatable because it was recorded by a temporary local network deployed between June 1981 and August 1982 (*Pennington and Carlson*, 1984). This network also recorded a

microearthquake occurring on 11 December 1981 and located 25 km west of the 2012 epicenter.

There are two high-volume injection disposal wells within 3 km of the highest-intensity region of the Timpson earthquakes, and it is possible that injection triggered them. Since 2008, fluid injection appears to have triggered several earthquake sequences in Texas and elsewhere in the midwestern U.S. (*Frohlich et al*., 2011; *Frohlich*, 2012; *Horton*, 2012; *Keranen et al.,* 2013; *Ellsworth*, 2013; *Justinic et al.,* 2013).

We first present results from a felt-report survey for the 17 May 2012 earthquake. We then summarize our analysis of seismograms to identify and locate earthquakes in the sequence; nearby stations include U. S. National Network station NATX in Nacogdoches located 25 km from the epicenter, several nearby EarthScope Transportable Array stations, and eight temporary seismographs deployed following the 17 May earthquake. Finally, we describe the injection disposal wells situated near the epicentral area and discuss their possible relationship with seismicity.

6.2. Felt Reports from the May 2012 Earthquakes

The 10 May foreshock and 17 May main shock were strongly felt in the region around Timpson, TX, with the area of high intensities including the zip code for the town of Garrison to the southwest. Instrumental epicenters determined by the USGS, however, place the foreshock 10 km northwest of Timpson and the main shock 4 km to the northeast (Fig. 6.2). The ~10 km difference in their epicenters is consistent with the formal uncertainty in their locations, suggesting that they might be nearly co-located (as we might expect). To better constrain the epicentral area of these events we gathered felt report information (Figs. 6.2 and 6.3) from three different sources. Following the 17 May earthquake we contacted the *Nacogdoches Daily Sentinel* and the *Timpson & Tenaha News*, who published felt report questionnaires that respondents mailed either to us or to newspaper offices. Two of the authors (M.B. and W.A.B.) spent three days in the epicentral region interviewing residents, concentrating their efforts in the higher-intensity areas.

We augmented these data with "Did you feel it?" (DYFI) information provided by the National Earthquake Information Center (NEIC). The DYFI program (*Atkinson and Wald*, 2007; *Wald et al.,* 2011) is an internet-based program where individuals can provide unsolicited responses to questions about their experiences and location during an earthquake. The responses are analyzed to assign a modified Mercalli intensity (MMI) value; the NEIC routinely presents summary online maps of the MMI distributions. For this study the DYFI data were especially useful for constraining boundaries for the MMI III and MMI IV regions (Fig. 6.1).

We interviewed residents at eight locations who experienced the most severe intensities (MMI VII); these occurred within a 5.7 km X 2.3 km area (~10 km^2) about 6 km southwest of Timpson, TX in the direction of Garrison (Fig. 6.3). These individuals reported significant damage to chimneys, fireplaces, or masonry; objects such as pictures, mirrors, or deer heads fell off walls; objects fell off shelves or out of

cabinets and often broke. One respondent reported his fireplace came down inside his residence and his south exterior brick wall "blew off" the house.

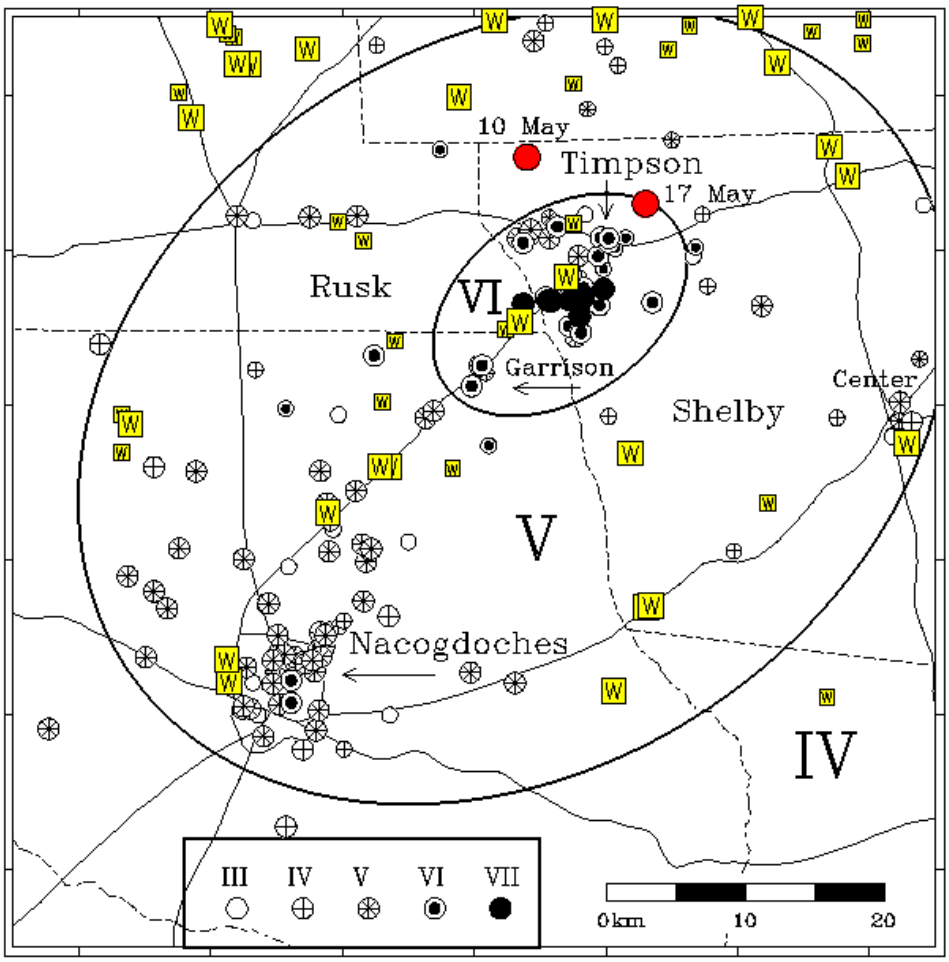

Fig. 6.2. Locations of felt reports for the 17 May 2012 earthquake. Key at bottom of Fig. shows symbols for felt intensities MMI III to MMI VII; larger symbols are reports collected by the authors; smaller symbols are DYFI reports provided by the NEIC. Yellow squares labeled "W" indicate the location of Class II injection wells; larger (smaller) symbols are wells with maximum monthly injection volumes exceeding (less than) 100,000 BWPM (16,000 m^3/mo). Red circles are NEIC epicenters determined for the 10 May and 17 May 2013 earthquakes. Solid lines are regional roads; broken lines are county boundaries.

People experienced intensities of MMI VI and MMI V over areas of approximately 170 km^2 and 2200 km^2, respectively. Since the earthquake occurred at 3:12 AM local time, in the MMI V region typical respondents noted that they were awakened by the earthquake, and realized that furniture was moving or objects were rattling. The MMI IV and MMI III felt areas covered approximately 7000 km^2 and 20,000 km^2 respectively.

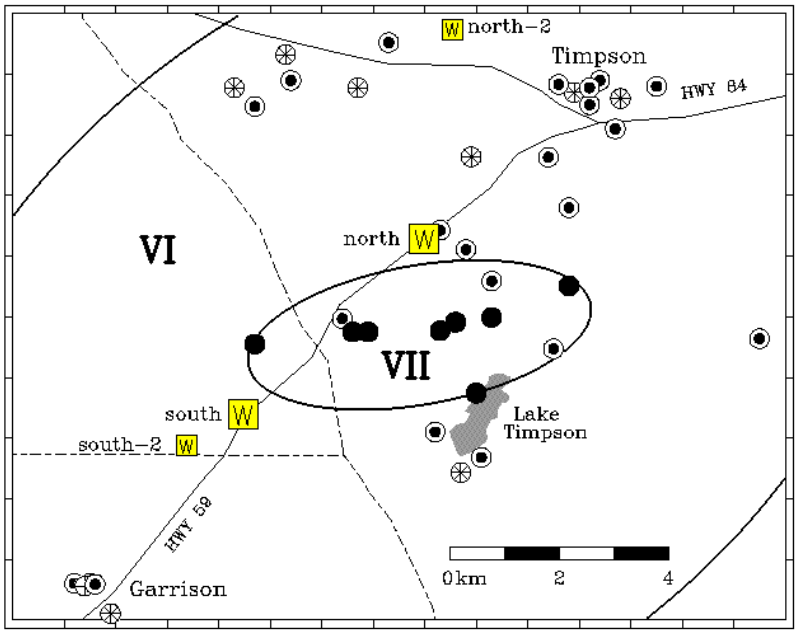

Fig. 6.3. Locations (circles) of felt reports and injection wells (squares) near the 17 May 2012 epicenter. County lines, highways, and key for MMI level are as in Fig. 6.2. Ellipse labeled "VII" shows approximate extent of MMI VII area. Squares labeled "W" are locations of Class II injection disposal wells. The town of Timpson is at the junction of state highways 59 and 84.

We also collected felt report information for the 10 May M_W3.9 earthquake. This was much less severe than the 17 May earthquake, and took place in the morning, 10:15 local time. Several residents of Timpson and the region approximately 5-10 km to the southwest experienced intensities of MMI V; the region of highest intensity for the 10 May event coincided roughly with the highest-intensity region for the 17 May main shock.

6.3. Analysis of Seismograms: Origin Times and Epicenters

6. 3.1 Seismic station coverage

Seismic station coverage in this part of east Texas has varied considerably over the past few years. The nearest permanent seismic station is the U.S. National Network station NATX in Nacogdoches, operational since 2004, and situated approximately 25 km southwest of the highest-intensity region (Fig. 6.1). Between 2009 and 2011 EarthScope USArray Transportable Array (TA) stations were deployed in eastern Texas; until December 2011 TA station 239A operated 15 km north of the epicentral region. TA stations 140A, 240A, and 341A were installed some 65-140 km to the east between February 2011 and February 2012. Because of the absence of stations in the epicentral area, we fixed focal depths at 2.5 km to locate earthquakes occurring prior to 26 May 2012 (white circles in Fig. 6.4) and their epicentral uncertainties are several km. In particular, for the 2011- May 2012 earthquakes, our relocations found a median value for the largest axis of the uncertainty ellipse to be ±2.9 km.

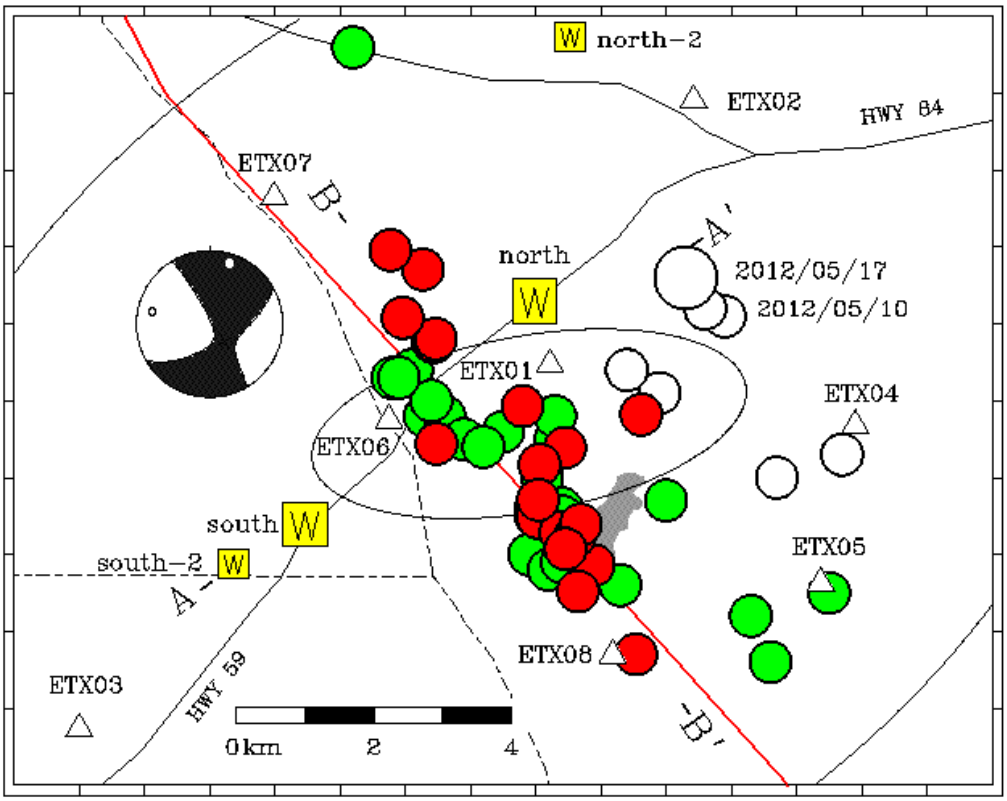

Fig. 6.4. Epicenters (circles) determined in this study. White circles are epicenters occurring before 26 May 2012 when the first temporary stations (triangles) were deployed. Green circles are epicenters occurring between 26 May 2012 and 5 February 2013; red circles are best-recorded hypocenters occurring after 22 February 2013. Red line indicates basement fault from Jackson (1982). Yellow squares labeled "W" are locations of injection disposal wells as in Figs. 6.2 and 6.3. Ellipses indicate MMI VI and MMI VII areas as in Fig. 6.3. Beach ball is global centroid moment tensor reported by Columbia group (see www.globalcmt.org); note that the best recorded hypocenters (red circles) lie along a NW-SE trend approximately parallel to one nodal plane. Labels A, A', B and B' indicate locations of cross sections (Fig. 6.6).

Following the 17 May 2012 earthquake we installed three temporary NetQuakes accelerometers (ETX01, ETX02, and ETX03; see Fig. 6.4) between 26 May and 15 June. Because these instruments required access to power and an internet connection, we only were able to find sites for them along HWY 59 between Nacogdoches and Timpson. Thus for aftershocks occurring between 26 May 2012 and February 2013, the stations closest to the highest-intensity region (NATX, ETX01, ETX02 and ETX03) were situated approximately along a northeast-trending straight line. Two stations somewhat to the east (140A and 240A) lay approximately along an extension of this line. Thus, arrivals at the remaining, relatively distant station 341A (distance ~ 1.2°) were critical for constraining aftershock locations along the northwest-southeast direction. There were readable P and S phases at 341A for only three earthquakes detected during the 26 May 2012 –February 2013

period. For earthquakes during this period we determined locations (green circles in Fig. 6.4) with focal depths fixed at 2.5 km, and their epicentral positions along the NW-SE direction are poorly determined.

The region was shaken strongly a third time on January 25 at 0701 UTC by a m_{bLg}4.1 aftershock. This event was well-recorded by the three NetQuakes accelerometers. Peak acceleration and peak velocity at the closest instrument ETX01 were 62% of gravity and 22 cm/s, respectively (Fig. 6.5).

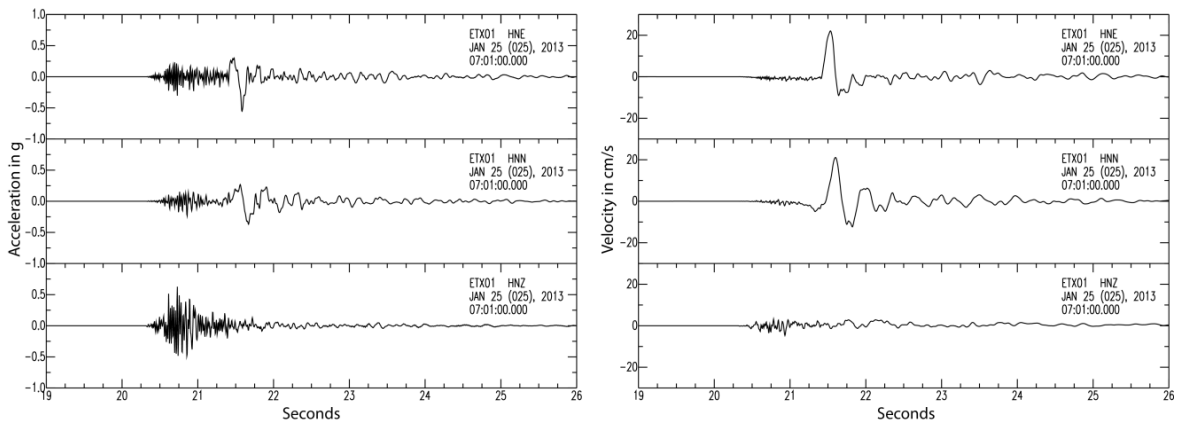

Fig. 6.5. Accelerations (left) and velocities recorded at ETX01 for the 25 January 2013 0701 UTC m_{bLg}4.1 aftershock. The 1.08 s S-P time at this closest station to the event requires a shallow focal depth for the earthquake.

In response to this earthquake we installed five additional stations (ETX04 – ETX08, see Fig. 6.4) equipped with both broad band seismometers and accelerometers to surround the epicentral area. These stations were operational starting on 22 February 2013 and remained in the field until early August, 2013. For this paper, we have analyzed a subset of the earthquakes recorded by the combined network of temporary stations and NATX, to determine hypocenters with free depths (red circles in Figs. 6.4 and 6.6). We consider the epicentral locations and focal depths to be reliable for these events because they are located within the network—median values are ±0.3 km for the largest axis of the epicentral uncertainty ellipsoid, and ±0.6 km for focal depth. These error estimates refer to the precision of the relative location only, as we lack a calibration shot to constrain the absolute location uncertainty. Absolute errors are likely less than 1 km, considering the network geometry, timing precision and uncertainty in crustal velocity model.

On 2 September 2013 two more earthquakes occurred, at 1652 UTC with m_{bLG}4.1 and at 1851 UTC with $M_{W\text{-}RMT}$4.3. Because ETX04-ETX08 had been removed we don't have accurate locations for these events. However, they are clearly in the same epicentral zone as the earlier events, with S-P times of ~1.0 sec at ETX01. These earthquakes also produced excellent records at NATX that we have modeled to evaluate focal depth (see section 6.3.4).

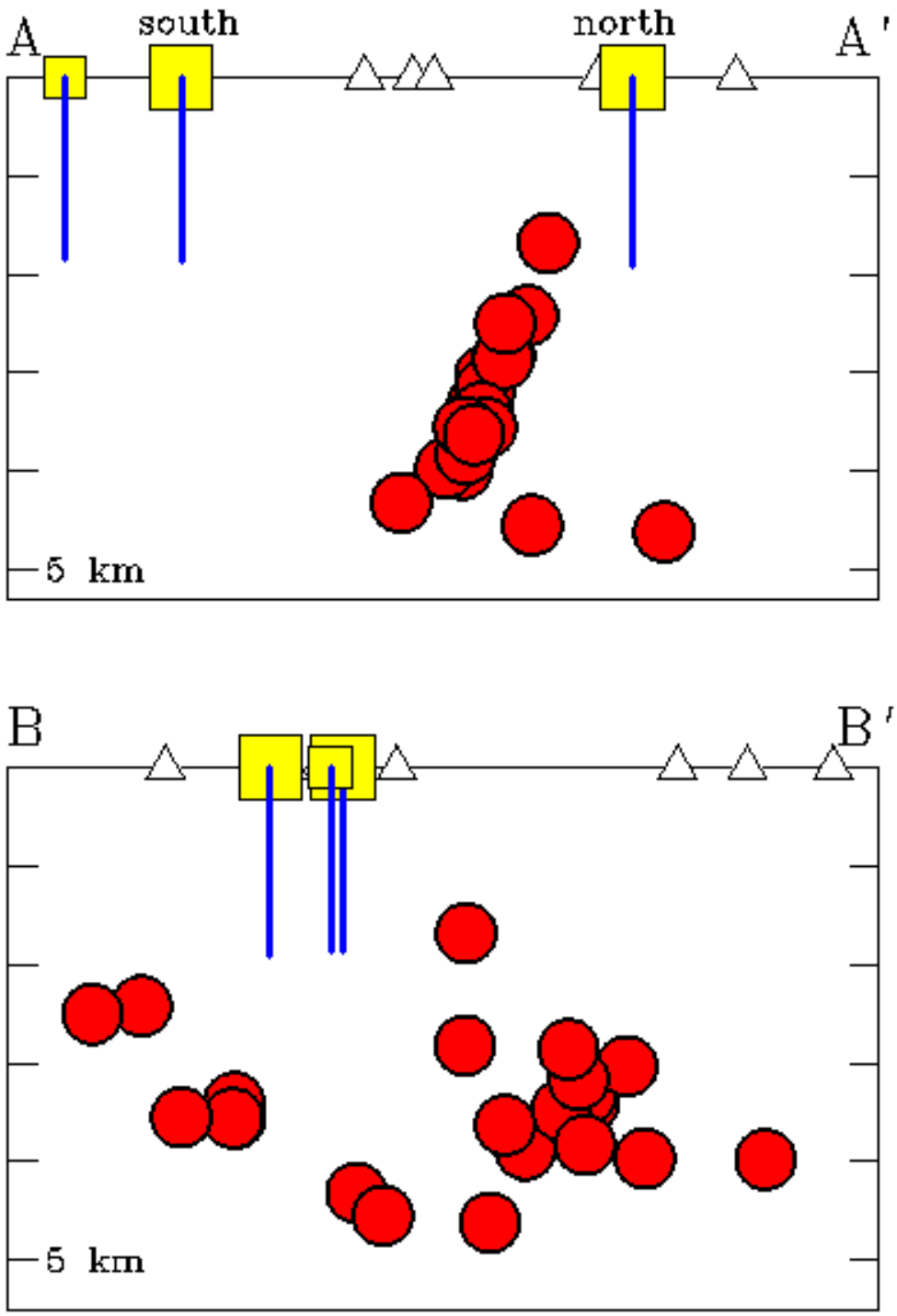

Fig. 6.6. Cross sections A-A' and B-B' (see Fig. 6.4) of best recorded hypocenters (red circles) determined in this study. Symbols are as in Fig. 6.4; blue lines extending beneath injection wells (yellow squares) indicate depth extent of injection wells. Note that hypocenters in section A-A' form a linear group extending from ~2.5-4.5 km depth, suggesting they may occur along a southwest-dipping planar surface trending ~35° west of north.

6.3.2 Fore- and aftershocks; (S-P) times

NATX is the only regional station that has been continuously operational for more than two years. Using a seismogram from the 10 May 2012 event as a cross-correlation template, we searched NATX records from January 2005 to through May 2012 and identified seven preshock events with magnitudes 0.5-2.2. All the events found had (S-P) times of 4.0-4.5 sec at NATX (Fig. 6.7, top), similar to that of the 10 May 2012 foreshock and the 17 May 2012 mainshock, which had (S-P) times of 4.30 and 4.20 sec, respectively. The earliest event (with S-P of 4.35 sec) occurred in April 2008 and apparently went unnoticed by local residents.

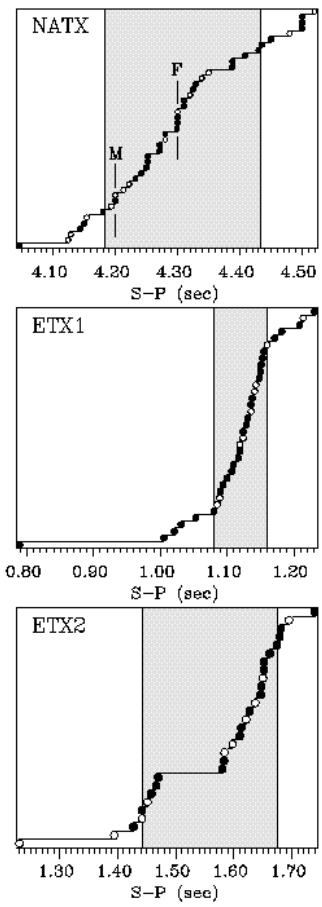

Fig. 6.7. Cumulative distribution of S-P intervals observed at three stations recording the Timpson sequence. Open circles indicate less-reliable data where either the S or P reading was of lower quality. Grey area between vertical lines indicates the middle two-thirds of the distribution. (Top panel) S-P intervals at station NATX; times labeled M and F are S-P intervals for 17 May 2012 mainshock and 10 May 2012 foreshock. (Middle panel) S-P intervals at ETX01. The observation that S-P intervals are ~1.1 sec indicates focal depths must be ~4 km or shallower (see text). (Bottom panel) S-P intervals at ETX02. The observation that S-P intervals form two groups suggests that the earthquakes originate from at least two distinct clusters.

For all Timpson earthquakes recorded by NATX we determined magnitudes. We performed a linear least-squares fit between the logarithm of the peak-to-peak amplitudes and NEIC-reported magnitudes for ten of the Timpson earthquakes reported by the NEIC. A frequency-magnitude plot of these data (Fig. 6.8) indicates that NATX detects all Timpson earthquakes with magnitudes of ~2.0 and greater. The b value for the sequence is 0.570 ± 0.17 (95% confidence interval) as determined using *Aki's* (1965) method for events having magnitude of 2.0 and larger.

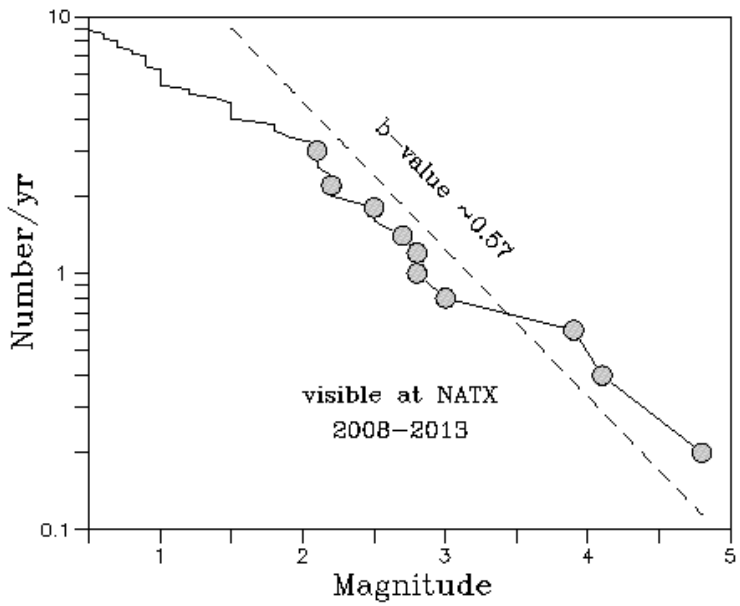

Fig. 6.8. Magnitude distribution of Timpson earthquakes recorded at station NATX. Circles indicate events assigned magnitudes by NEIC; other magnitudes are as determined in this study.

In the year following the 17 May 2012 main shock we recorded 55 aftershocks; many were well-recorded on the temporary stations ETX01 and ETX02. At ETX01, the station recording the smallest S-P intervals, all but one interval fell between 1.00 and 1.23 seconds (Fig. 6.7, middle). At ETX02 the intervals formed two distinct groups (Fig. 6.7, bottom), one clustered at 1.45 seconds, and the other at 1.65 seconds.

6.3.3 Velocity Model and Locations

Historically, earthquakes have been rare in east Texas and regional station coverage has been poor; thus there is no well-established velocity model for location. For the 17 May 2012 earthquake the St. Louis group (see *Hermann et al.*, 2011) obtained a better fit to regional seismograms using their model WUS (western U.S.) than with model CUS (central U.S). In comparison with the CUS model, the WUS model has significantly lower velocities in the uppermost 8 km. Velocity logs for the depth interval ~1.0-3.5 km, including one well situated about 3 km north of the town of Timpson (API: 42-41931360), indicated that P velocity increased approximately linearly from about 3 km/s to 5 km/s in this depth range.

We developed a starting location model based on this information, and then modified it to obtain a final model by applying the VELEST computer program to the best-recorded Timpson earthquakes. VELEST solves the simultaneous hypocenter and 1-D velocity model tomography problem for local earthquakes as initial reference models for 3-D seismic tomography (*Kissling et al.,* 1994). Our final model has relatively low velocities with $V_P/V_S \sim 2$ to depths of 2.5 km, and then $V_P/V_S \sim 1.72$ at greater depths. Because of the limited station coverage and relatively restricted range of focal depths, the model is determined only to about 4 km depth.

The deepest horizon plotted on *Jackson's* (1982) summary cross sections of east Texas regional geology is the top of the Louann Salt at 4.5 km; the Louann is only a short distance above Paleozoic Ouachita basement. This is in general agreement with *Lutter and Novack's* (1990) analysis of the PASSCAL Ouchita experiment that found Mezozoic sediments extending to a depth of 5 km, and also well logs shown by *Hammes et al.* (2011) from two wells about 20-30 km south of the 2012 epicenter.

For the 22 best-recorded earthquakes in Group 3, locations determined with this model had small residuals (average RMS error 0.02 s), with epicenters extending along a NW-SE line approximately 6 km long through the center of highest-intensity region (Figs. 6.4 and 6.6, red circles). Focal depths are well constrained and ranged between 1.6 and 4.6 km. For our preferred velocity model the observed S-P intervals ranging from 1.0-1.2 sec at ETX01 (Figs. 6.5 and 6.7) are inconsistent with any focal depths exceeding 3.3-4.6 km.

We fixed focal depths at 2.5 km for the 30 epicenters in Group 2 (green circles in Fig. 6.4. These were events with fewer observations at temporary local stations than the Group 3 earthquakes. Although the station distribution for Group 2 earthquakes provided relatively poor constraint along the NW-SE direction, our preferred locations were generally situated along the same NW-SE linear trend as the well-constrained Group 3 earthquakes.

Epicenters determined for earthquakes occurring before the installation of local stations (white circles in Fig. 6.4) were about 3 km east of the better-recorded events. These locations are not considered reliable; they are controlled by stations 140A and 341A situated 110-130 km east of the highest-intensity area; it is thus plausible that Group 1 locations are systematically mislocated by ~ 3 km as the velocity model is uncalibrated along their ray paths. The (S-P) intervals observed at station NATX for Group 1 earthquakes, including the 10 May foreshock and 17 May aftershock, were similar to (S-P) intervals observed after installation of the local network (see Fig. 6.7, top panel). This observation suggests that the Group 1 earthquakes occurred in nearly the same location as the later Group 2 and Group 3 events with better-constrained locations.

6.3.4 Modeling Seismograms Recorded at NATX

A notable feature of the transverse horizontal broadband seismograms recorded at NATX for the 17 May 2012 main shock are several high-amplitude phases arriving in the 20-sec interval following the S arrival (Figs. 6.9 and 6.10) on the transverse

component of motion. Similar phases are visible on seismograms of the 10 May 2012 $M_{W\text{-}RMT}$ 3.9 and 25 January 2013 m_{bLg}4.1 earthquakes.

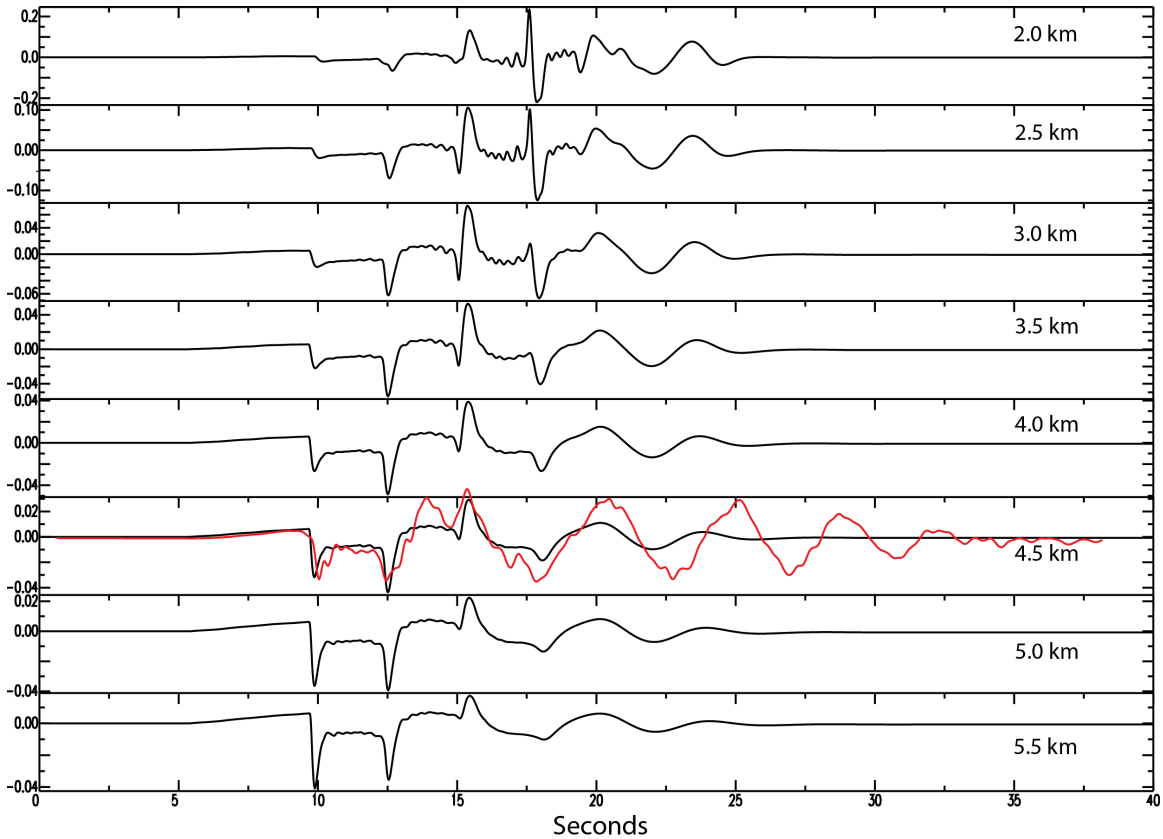

Fig. 6.9. Transverse component displacement seismograms (black) for a double couple point source (strike=330, dip=85, rake=-15) at a range of 24.5 km and azimuth of 240 degrees for depths between 2 and 5.5 km. The near-field ramp begins at the P-wave arrival at approximately 5 s and is interrupted by the S-wave arrival at approximately 10 s travel time. It is followed by multiple, impulsive arrivals, corresponding to whispering gallery arrivals from waves trapped in the sediments above basement. Note the sensitivity of the relative amplitudes of the whispering gallery phases to focal depth. Later arrivals have the largest amplitude at shallow depth while the first arrival has the largest amplitude for deeper focal depths. Observed transverse displacement at NATX (red) for the 17 May 2012 main shock best matches a focal depth of 4.5 km. Both observed and synthetic displacements were low-pass filtered at 2 Hz.

We interpret these arrivals as crustal reverberations—sometimes called "whispering gallery phases" (*Aki and Richards*, 1980) —generated when a shallow source lies near the boundary between a low-velocity gradient overlying a higher-velocity layer, and significant amounts of energy become trapped in the upper layer. We modeled the seismograms recorded at NATX for the 10 May 2012 foreshock, the 17 May main shock, the 25 January 2013 aftershock, and both 2 September 2013 aftershocks using the velocity model obtained with VELEST and the Global CMT focal mechanism (Fig. 6.4). Synthetic seismograms were computed using program

FK (*Zhu and Rivera*, 2002) at the appropriate epicentral distance for a range of focal depths. Both the synthetic and observed seismograms were low-pass filtered at 2 Hz and integrated to displacement for comparison. We obtained the best match between the NATX displacement seismograms and the relative amplitudes of the whispering gallery phases for synthetic sources (Fig. 6.9) at depths of 3.5, 4.5, 2.75, 4.0, and 4.5 km for these five events, respectively (Fig. 6.10).

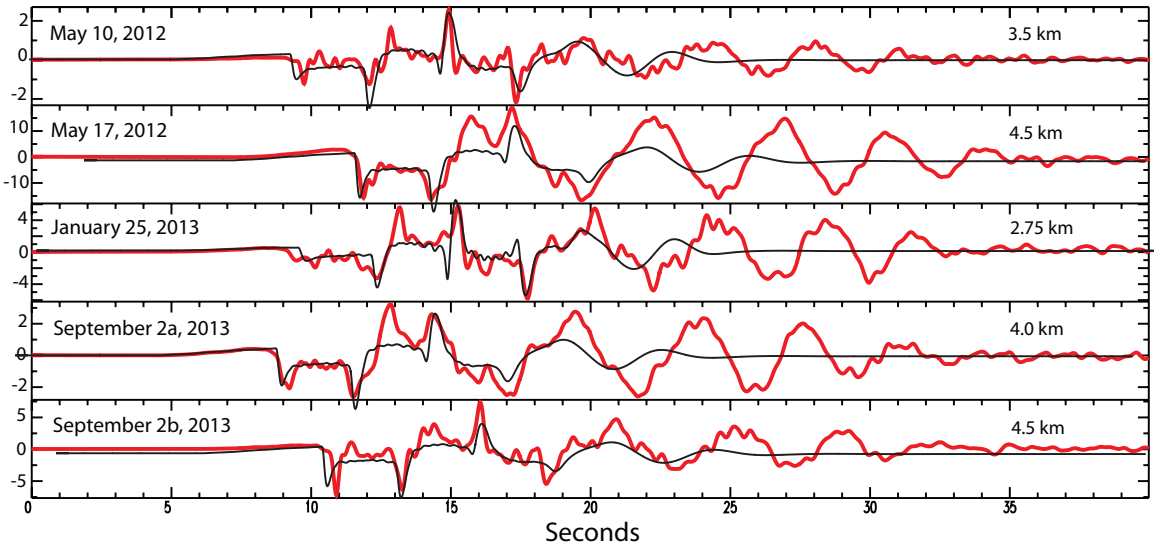

Fig. 6.10. Transverse component displacement seismograms recorded at NATX (red) for the five principal earthquakes. Synthetic seismograms (black) are shown for the best-fitting point source focal depth for the double-couple orientation used in Fig. 6.9. Both observed and synthetic displacements were low-pass filtered at 2 Hz.

6.4. Injection Wells

In Texas, the Texas Railroad Commission (RRC), which no longer regulates railroads, is responsible for regulating activity related to petroleum operations in the state. The RRC issues permits for drilling wells, and monitors production and underground disposal activities. By law operators annually provide the RRC with certain information concerning fluid injection, both when it is used to stimulate production and also when it used to dispose of fluid wastes. The RRC's database is publically available online and includes information for individual wells and leases which is mostly complete for the past two decades; for each well the data includes monthly volumes of water and gas injected and volumes of oil, water and gas extracted.

Although east Texas has been the focus of recent unconventional gas development, in the immediate vicinity of the epicenters located in this study there were no wells actively producing petroleum between 2000-2011. However there were several such wells situated several km to the southeast in Rusk and Nacogdoches Counties. Many of the gas wells began operation in 2005 or later and produced from formations within the Trinity at depths of 2.2-2.9 km.

There are, however, two relatively high-volume and two lower-volume injection disposal wells situated within several km of the highest-intensity region of the 17 May 2012 earthquake (Figs. 6.4 and 6.11). All four wells injected at depths of about 1.8-1.9 km.; here Paleozoic basement is at ~5 km depth (*Jackson*, 1982; *Lutter and Novack*, 1990; *Hammes et al*., 2011). The highest injected volumes, averaging 269,000 BWPM (42,750 m^3/mo) since September 2006, were at a well at 4 km southwest of the center of the MMI VII region (API 42-40133833; labeled 'south' in Fig. 6.4); RRC data indicates that injection was into the Rodessa of the Trinity formation. At a well about 2 km north of the MMI VII centroid (API 42-41931083; labeled "north" in Fig. 6.4) monthly volumes averaged 98,000 BWPM (15,600 m^3/mo); injection here was also into the Rodessa. The total injected volumes for the "north" and "south" wells were 1.05 million m^3 and 2.90 million m^3, respectively.

While these are relatively high-volumes wells, they are not unusual for Texas injection wells. There are more than 10,000 injection wells in Texas that have been active since 2000; of these more than 1300 have reported injection volumes exceeding 100,000 BWPM (16,000 m^3/mo) for 12 or more months since 2000.

Injection volumes were considerably less at two other regional wells. At well API 42-40131974 (labeled "south"2" in Fig. 6.4) injection took place only from April 2009 to January 2010, and injection volumes never exceeded 50,000 BWPM (8000 m^3/mo). At a fourth well (API 42-41931287; labeled "north-2" in Fig. 6.4) injection began in March 2009 and volumes averaged about 50,000 BWPM. .

The RRC also reports monthly values for maximum and average injection pressures at disposal wells (Fig. 6.11). At both the higher-volume wells, in 2010 and afterwards injection volumes decrease even as injection pressures hold steady, as at the "south" well, or increase, as at the "north" well. Variations in the injected volume presumably reflect demand, and nothing more. Increasing injection pressure with decreasing volume injected could mean that the well bore has become constricted from a build-up of scale or plugging of a screen, or it could reflect increased resistance from the formation to accept additional fluid.

Modeling of subsurface hydrology and stress conditions in response to the pressure/volume histories at individual wells would help achieve a more complete understanding of the relationship between fluid injection and seismicity However, this will require more information about injection pressures and well properties than is available from RRC data. The RRC-reported pressures are average and maximum surface pressures; these data don't reflect whether injection was episodic or continuous throughout the month. Moreover, the surface pressures for a pumping system don't account for frictional losses depending on casing diameters, etc., and thus aren't related simply to the pressures at depth where well perforations permit fluid to disperse into subsurface strata.

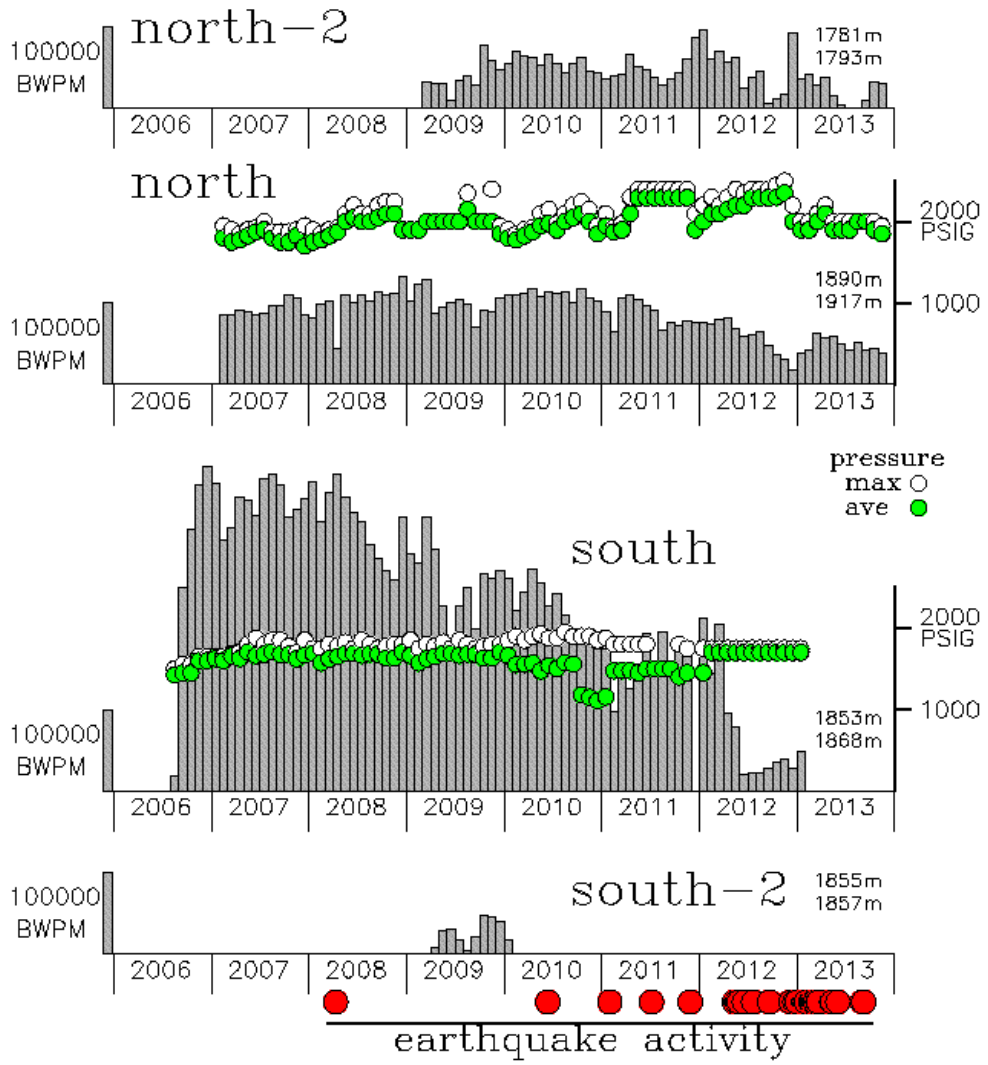

Fig. 6.11. Monthly injection volumes for the wells indicated labeled 'north-2', 'north', 'south' and 'south-2' in Fig. 6.4. Scale bar at left of histograms is 100,000 BWPM (16,000 m³/mo). Green and white circles and right scale are average and maximum monthly injection pressures (1000 PSIG is 6895 kPa). Red circles indicate times of earthquakes identified in this study. Labels at right indicate depth interval of injection. At time of publication, information for February 2013 and later was not yet available concerning monthly injection volume and pressures for 'south' well.

6.5. Discussion

The most significant conclusions of the present study are that:

(1) Epicenters of aftershocks of the 17 May 2012 earthquake occurred along a ~6 km-long N35°W-striking linear zone that coincides with a mapped basement fault (see *Jackson*, 1982; *Geomap*, 2012).

(2) The epicentral area extends across the highest-intensity region of the 17 May 2012 $M_{W\text{-}RMT}$4.8 main shock, where local residents experienced intensities of MMI

VII. Moreover, the aftershocks trend parallel to one nodal plane of the predominantly strike-slip focal mechanisms reported for this event by both the Columbia (Fig. 6.4) and the St. Louis groups (*Ekstrom et al.,* 2010; *Herrmann et al*., 2011).

(3) The better-determined focal depths of sequence events are relatively shallow, with depths ranging from 1.6-4.6 km as determined by a network of temporarily deployed stations. For the five largest earthquakes in the sequence, modeling of the seismograms recorded at station NATX at a distance of 24.5 km indicate focal depths between 2.75 and 4.5 km.

(4) Two relatively high-volume injection disposal wells are situated within ~3 km of the linear trend of epicenters and near the highest-intensity region of the 17 May main shock. Injection at these wells began in 2006-2007 prior to the first recorded sequence earthquake in April 2008.

6.5.1 Origin: Human-Triggered or Natural?

The above observations demonstrate that the Timpson earthquakes share many features in common with recent earthquakes elsewhere in the Midwestern U.S that are have been inferred to be triggered or induced. Like the 1962-1968 earthquakes in Denver (*Healy, et al.*, 1968; *Herrmann and Park*, 1981) the 2008-2009 earthquakes in Dallas-Fort Worth (*Frohlich et al*., 2011), the 2009 earthquakes near Cleburne, TX (*Justinic et al.,* 2013) and the 2011 earthquake in Youngstown, OH (*Kim*, 2013), the Timpson earthquakes are the first known earthquakes in this location, and began only after injection began. As in Denver, Dallas-Fort Worth, Cleburne, 2011 in Arkansas (*Horton*, 2012), and 2011 in Youngstown OH (*Kim*, 2013), the Timpson earthquakes had focal depths at or exceeding the depths of injection, and occurred along a linear trend situated within only a few km of the site of injection. Elsewhere in Texas *Frohlich* (2012) found that seismic activity at distances of ~3 km is sometimes associated with wells having maximum monthly rates exceeding 150,000 BWPM (24,000 m^3/mo); in Timpson, injection rates averaged 269,000 BWPM (43,000 m^3/mo) since 2007 at the "south" well (Figs. 6.4 and 6.11). All the above observations are consistent with the hypothesis that the Timpson earthquakes were triggered by nearby injection disposal wells; the likelihood that Timpson earthquakes are induced is comparable to that for the Denver, Dallas-Fort Worth, Cleburne and Arkansas sequences.

Like the Dallas-Fort Worth earthquake sequence, the linear trend of aftershocks in Timpson approximately coincides with a mapped fault. In both cases we have been unable to locate the primary evidence confirming the faults' existence and location. The fault location indicated in Fig. 6.4 is from *Jackson* (1982), as plotted on his map of faults at the top of Paleozoic basement; he doesn't place the fault on maps of faulting at shallower depths. *Geomap* (2012) shows the fault 2-3 km east of Jackson's location. The Timpson region has been the focus of recent exploration efforts and we are seeking more recent data that might fix the location and dip of this fault, and thus resolve the possible discrepancy.

Although the preponderance of evidence favors the conclusion that the Timpson earthquakes were induced or triggered by fluid injection, our investigation cannot rule out the possibility that they are of natural origin. The historical record (*Pennington and Carlson*, 1984; *Frohlich and Davis*, 2002) indicates that in 1891 and 1981, well before injection began, M4.0 and M3.2 earthquakes occurred at Rusk, Texas, 80 km west of Timpson, and at Center, Texas, 25 km to the southeast (Fig. 6.1). These could not have been triggered by human activity; rather, they have been attributed to the Mt. Enterprise fault zone (Fig. 6.1). One of the focal planes for a focal mechanism reported for the 17 May 2012 earthquake (see Fig. 6.4) is parallel to faults in the Mt. Enterprise fault zone as mapped by *Ewing* (1990)); the other focal plane is parallel to the mapped fault reported by *Jackson* (1982) and *Geomap* (2012).

6.5.2 Magnitude and Scalar Moment

The 17 May 2012 Timpson earthquake, with magnitude $M_{W\text{-}RMT}$4.8 and scalar moment M_o of 2.21×10^{23} dyne-cm, is the largest earthquake to have occurred in eastern Texas. The largest previous earthquakes in eastern and central Texas are the 19 March 1957 M4.7 Gladewater earthquake, attributed to extraction in the east Texas oil field by several investigators, including *Frohlich and Davis* (2002); and the 20 October 2011 $M_{W\text{-}RMT}$4.8 Fashing earthquake (M_o 1.8×10^{23} dyne-cm), with an epicenter that coincides with several previous earthquakes that *Pennington et al.* (1986), *Davis et al.* (1995) and *Frohlich and Brunt* (2013) attributed to extraction in the Fashing gas field. The nearest historical earthquakes larger than the 17 May 2012 Timpson event are more than 400 km distant; e.g., in Oklahoma earthquakes with magnitudes of 5.5, 5.7 and 5.6 occurred in 1882, 1952, and 2011.

The magnitudes of both the 17 May 2012 earthquake and 10 May foreshock were adjusted upward several days after they occurred. That is, the 17 May magnitude was initially reported as m_{bGS}4.3 from short-period body waves, and the 10 May foreshock magnitude as m_{bGS}3.7. Then, following analysis of broadband regional signals to determine the scalar moments and focal mechanisms for both events, the magnitudes were upgraded to $M_{W\text{-}RMT}$4.8 and $M_{W\text{-}RMT}$3.9. This suggests that the body-wave amplitudes at frequencies of ~1 sec used to determine m_{bGS} give magnitude values somewhat smaller than predicted by the *Atkinson and Boore* (2006; 2011) Central U.S. strong motion model. It also suggests that the magnitudes catalogued for some historical earthquakes in east Texas and along the Gulf Coastal Plain—determined from body waves—might be smaller than moment magnitudes that might have been determined using modern methods had broad-band observations been available.

6.6 References

Aki, K. (1965), Maximum likelihood estimate of b in the formula log N = A – bM and its confidence limits, *Bull. Res. Inst. Tokyo Univ., 43*, 237-239.

Aki, K, and P. G. Richards (1980), *Quantitative Seismology*, Freeman and Co, San Francisco.

Atkinson, G. M. and D. M. Boore (2006), Earthquake ground-motion prediction

equations for eastern North America, *Bull. Seismol. Soc. Amer., 96*, 2181–2205.

Atkinson, G. M. and D. M. Boore (2011) Modifications to existing ground-motion prediction equations in light of new data, *Bull. Seismol. Soc. Amer, 101*, 1121-1135.

Atkinson, G. M. and D. J. Wald (2007), "Did you feel it"? intensity data: A surprisingly good measure of earthquake ground motion, *Seismol. Res. Lett., 78*, 362-368, doi:10.1785/gssrl.78.3.362.

Davis, S. D., P. Nyffenegger and C. Frohlich (1995), The 9 April 1993 earthquake in south-central Texas: Was it induced by fluid withdrawal? *Bull. Seismol. Soc. Amer., 85*, 1888-1895.

Ekström, G., M. Nettles and A. M. Dziewonski (2012), The global CMT project 2004-2010: Centroid-moment tensors for 13,017 earthquakes, *Phys. Earth Planet. Inter., 200-201*, 1-9, doi:10.1016/j.pepi.2012.04.002.

Ellsworth, W. L. (2013), Injection-induced earthquakes, *Science,* 341, 1225924, doi: 10.1126/science.1225942.

Ewing, T. (1990), *Tectonic Map of Texas*, published by Univ. Texas Bureau of Economic Geology.

Frohlich, C. (2012), Two-year survey comparing earthquake activity and injection-well locations in the Barnett Shale, Texas, *Proc. Nat. Acad. Sci., 109*, 13934-13938, doi: 10.1073/pnas.1207728109

Frohlich, C. and M. Brunt (2013), Two-year survey of earthquakes and injection/production wells in the Eagle Ford Shale, Texas, prior to the M_W4.8 20 October 2011 earthquake, *Earth Planet. Sci. Lett.*, *379*, 53-63, doi:10.1016/j.epsl.2013.07.02.

Frohlich, C. and S. D. Davis (2002), *Texas Earthquakes*, Univ. Texas Press, Austin, Texas, 275 pp.

Frohlich, C., C. Hayward, B. Stump and E. Potter, (2011), The Dallas-Fort Worth earthquake sequence: October 2008 through May 2009, *Bull. Seismol. Soc. Amer.*, *101*, 327-340.

Galloway, W. E., T. E. Ewing, C. M. Garrett, N. Tyler and D. G. Bebout (1983), *Atlas of Major Texas Oil Reservoirs*, Univ. Texas Bureau Economic Geol., Austin, TX, 139 pp.

Geomap Company (2012), *Executive Reference Map 302: East Texas*, scale 1:386,000, Dallas, TX.

Hammes, U., H. S. Hamlin and T. E. Ewing (2011), Geologic analysis of Upper Jurrasic Haynesville shale in east Texas and west Louisiana, *AAPG Bull.*, 95, 1643-1666, doi:10.1306/02141110128.

Healy, J. H., W. W. Rubey, D. T. Griggs and C. B Raleigh (1968), The Denver earthquakes, *Science*, 161, 1301-1310.

Herrmann, R. B., H. Benz and C. J. Ammon (2011), Monitoring the earthquake source process in North America, *Bull. Seismol. Soc. Amer., 101*, 2609-2625, doi:10.1785/0120110095.

Herrmann, R. B. and S.-K. Park (1981), The Denver earthquakes of 1967-1968, *Bull. Seismol. Soc. Amer., 71*, 731-745.

Horton, S. (2012), Disposal of hydrofracking waste fluid by injection into subsurface aquifers triggers earthquake swarm in central Arkansas with potential for damaging earthquake. *Seismol. Re.s Lett., 83*, 250-260, doi:10.1785/gssrl.83.2.250.

Jackson, M. P. A. and B. D. Wilson (1982), *Fault Tectonics of the East Texas Basin*, Geol. Circular 82-4, Univ. Texas Bureau Economic Geol., 31 pp.

Justinic, A. H., B. Stump, C. Hayward and C. Frohlich (2013), Analysis of the Cleburne, Texas earthquake sequence from June 2009 to June 2010, *Bull. Seismol. Soc. Amer., 103*, 3083-3093, doi:10.1785/0120120336.

Keranen, K. M., H. M. Savage, G. A. Abers and E. S. Cochran (2013), Potentially induced earthquakes in Oklahoma, USA: Links between wastewater injection and the M_W 5.7 earthquake sequence, *Geology, 41*, 609-702, doi: 10.1130/G34045.1.

Kim, W.-Y. (2013), Induced seismicity associated with fluid injection into a deep well in Youngstown, Ohio, *J. Geophys. Res.*, 10.1002/jgrb.50247.

Kissling, E., W.L. Ellsworth, D. Eberhart-Phillips and U. Kradolfer (1994), Initial reference models in local earthquake tomography*, J. Geophys. Res., 99*, 19635-19646, 1994.

Kosters, E. C., D. G. Bebout, S. J. Seni, C. M. Garrett, L. F. Brown, H. S. Hamlin, S. P. Dutton, S. C. Ruppel, R. J. Finley and N. Tyler (1989), *Atlas of Major Texas Gas Reservoirs*, Univ. Texas Bur. Econ. Geol., Austin, TX, 161 pp.

Lutter, W. J. and R. L. Novack (1990), Inversion for crustal structure using reflections from the PASSCAL Ouachita experiment, *J. Geophys. Res., 95*, 4633-4646.

Pennington, W. D. and S. M. Carlson (1984), *Observations from the East Texas Seismic Network (June 1981-August 1982)*, Univ. Texas. Bureau Economic Geol. Circ. 84-3, 48 pp.

Pennington, W. D., S. D. Davis, S. M. Carlson, J. Dupree and T. E. Ewing (1986), The evolution of seismic barriers and asperities caused by the depressuring of fault planes in oil and gas fields of south Texas, *Bull Seismol. Soc. Amer., 76*, 939–948.

Wald, D. J., V. Quitoriano, B. Worden, M. Hopper and J. W. Dewey (2011), USGS "Did you feel it?" internet-based macroseismic intensity maps, *Annals Geophys., 54*, 688-707, doi:10.4401/ag-5354.

Zhu, L. and L. A. Rivera, (2002), A note on the dynamic and static displacements from a point source in multilayered media, *Geophys. J. Int.,* 148, 619-627.

7. Geomechanics of the Timpson, Texas, M4.8 Seismic Event

The material in this section has been prepared by Zhi-Qiang Fan, Peter Eichhubl and Julia Gale, and has been submitted for publication in *Earth and Planetary Science Letters*

Abstract. An earthquake sequence that culminated in a M_W4.8 strike-slip event near Timpson, east Texas, the largest documented earthquake to date in that region, had previously been attributed to waste water injection starting 69 months prior to the main seismic event. To assess the geomechanical relationships between fluid injection and seismic fault slip, we created a coupled poroelastic finite element model to simulate the spatial and temporal evolution of pore pressure and stress fields in the vicinity of the injection wells and of the Coulomb failure stress on the fault as a function of the permeability of the injection layer, fault orientation, fault permeability, and orientation and magnitude of the in situ stress state prior to injection. We find that fault slip is favored by low reservoir permeability, low fault permeability, and a favorable orientation of the fault relative to the in situ stress state. We also demonstrate that sensitivity of the Coulomb failure stress to variations in input parameters results in large uncertainties in correlating injection rate and volume with the onset of induced seismic events. These results demonstrate that geomechanical predictive algorithms used for assessment and management of induced earthquake risk can be highly sensitive on the quality of input parameters that include in situ stress, reservoir permeability, and fault orientation.

7.1. Introduction

Injection of wastewater including formation water produced from conventional hydrocarbon reservoirs and flow back after hydraulic fracturing of tight unconventional reservoirs is routinely practiced on a large commercial scale. In rare occurrences, increased rates of seismic activity are reported in the vicinity of injection wells and attributed to fluid injection (Horton, 2012; Ellsworth, 2013; Keranen et al., 2013; Kim, 2013; Frohlich et al., 2014). While the fundamental geomechanical processes linking fluid injection and seismic fault slip are well known and documented (Raleigh et al., 1972; Hsieh and Bredehoeft, 1981; National Research Council, 2013), the correlation between injection activity and the occurrence of seismic events is in many cases based on their spatial and temporal association but without a site-specific geomechanical analysis (Frohlich et al., 2011; Frohlich, 2012; Frohlich and Brunt, 2014; Frohlich et al., 2014). For evaluating the seismic risk during the design phase of injection programs, site assessments that consider the coupled geomechanical and reservoir flow processes are desirable to optimize fluid injection strategies while minimizing potential associated seismic hazards. Such a site assessment could consider rates and volume of fluid injection that the target formation can accommodate without attaining critical reservoir pressures for reactivation of nearby faults. This study provides such a coupled geomechanical and reservoir flow model for the 2012 Timpson M_W4.8 seismic event

to assess data needs and data quality requirements for seismic risk assessment for wastewater injection.

The May 17, 2012 M_W4.8 earthquake near Timpson, east Texas, occurred 69 months after wastewater injection commenced into two nearby Class II disposal wells, and following a sequence of smaller earthquakes that started in April 2008, 17 months after the start of wastewater injection (Frohlich et al., 2014). These wells, referred to as south and north well, are located within 3 km of the epicentral region and target the Rodessa Formation of the Trinity Group, an oolithic sandstone (Frohlich et al., 2014) (Fig. 7.1). The Rodessa Formation is overlain by fine crystalline anhydrite with interbedded limestone and dolomite of the Massive Anhydrite, and underlain by dense limestone of the James Lime. The south well became operational in August 2006, with an average injection rate of 42,750 m^3/mo at an average surface pumping pressure of 11.7 MPa, injecting at depths between 1853 and 1868 m (Frohlich et. al, 2014; Texas Railroad Commission, 2014). At the north well, wastewater is injected at depths between 1897 and 1910 m at an average surface pumping pressure of 13.6 MPa. As of December 2012, the total injected volume for the North and South wells are 1.05 and 2.9 million m^3, respectively. Epicenters of smaller events following the M_W4.8 event and located using a portable seismic array are aligned along a fault that was previously mapped using seismic data (Jackson, 1982; Frohlich et al., 2014). Focal depths of these events range in depth between 1.6and 4.6 km. The M_W4.8 event is the largest recorded earthquake to date within a region where historical earthquakes are extremely rare.

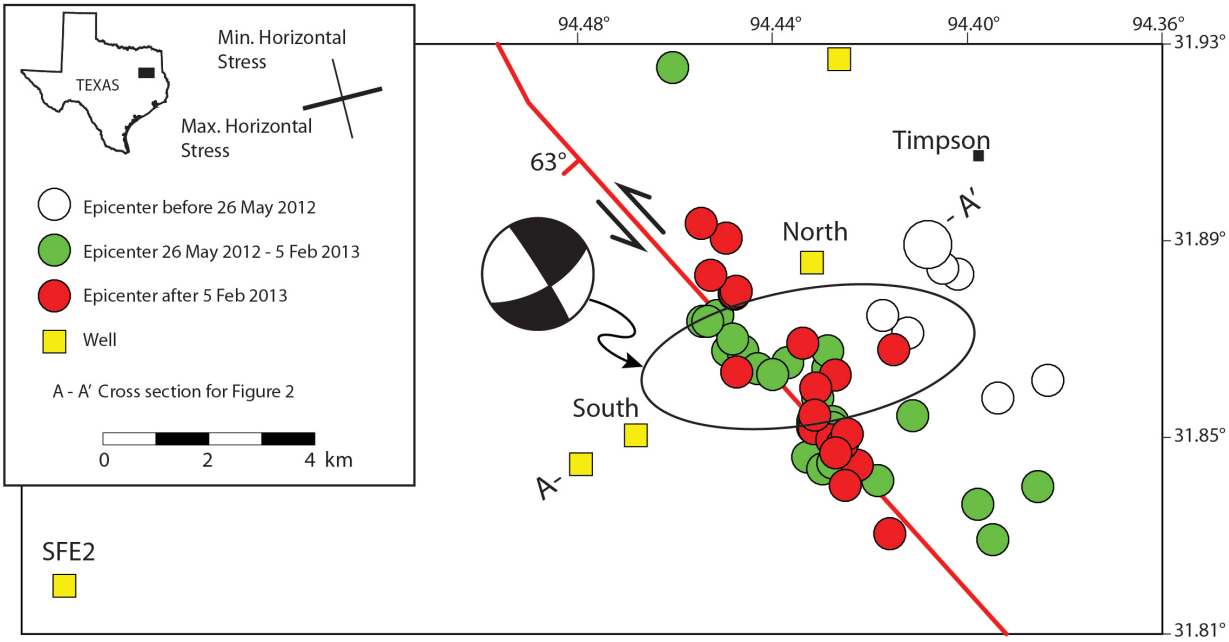

Fig. 7.1.Map of epicenters for the earthquake sequence near Timpson, east Texas (modified after Frohlich et al., 2014). Location of the main Mw4.8 event (beachball diagram) within the elliptical region approximately defined by the Mercalli intensity MMI VII area. Red circles are most reliable epicenter locations of aftershocks after deployment of temporary stations in February,

2013. These best located aftershocks align along a mapped fault striking about N42° W. In situ stress orientations are determined using wellbore breakout and drilling-induced fracture data from SFE2 well.

To investigate the causative relationship between fluid injection and initiation of seismic fault slip, we integrated geological and geophysical data into a finite element model and conducted coupled poroelastic simulations to estimate stress changes and pore pressure perturbations associated with waste water injection and evaluate the potential of fault reactivation. Through parametric studies we demonstrate the sensitivity of model results linking fluid injection and earthquake slip including the temporal and spatial evaluation of pore pressure and Coulomb failure stress, as a function of the permeability of injection layer, fault orientation, and in situ stress orientation and magnitude.

7.2. Methods

7.2.1 Model configuration and boundary conditions

Using the software package Abaqus we constructed a plane-strain poroelastic finite element model to simulate the time-dependent distributions of pore pressure and effective stress in the injection layer and in the over- and underlying units. The simulation plane is oriented NE-SW, perpendicular to the fault, and contains both injection wells (Fig. 7.1). The model extends from the surface to a depth of 4 km and consists of 14 layers (Fig. 7.2), with porosity, permeability, and poroelastic parameters listed in Table 7.1. Tops of formation were taken from logs of the south well obtained through the RRC database (Texas Railroad Commission, 2014).The distance between the two injection wells is 4.5 km. The regional dip is about 0.6° to the SW based on Ewing's (1990) tectonic map. We extend the model horizontally to 16km to minimize lateral boundary effects. The multilayered domain is intersected by the fault dipping about 63° to the southwest. In the base scenario of simulation, the fault is represented as an embedded interface with zero-thickness and mechanical properties equal to those of the surrounding formations and thus transparent to fluid flow. We have insufficient information about the dip-slip offset along the fault which we assume to be negligible. The effect of fault architecture and permeability structure on fluid flow and fault stability will be discussed in section3.3.

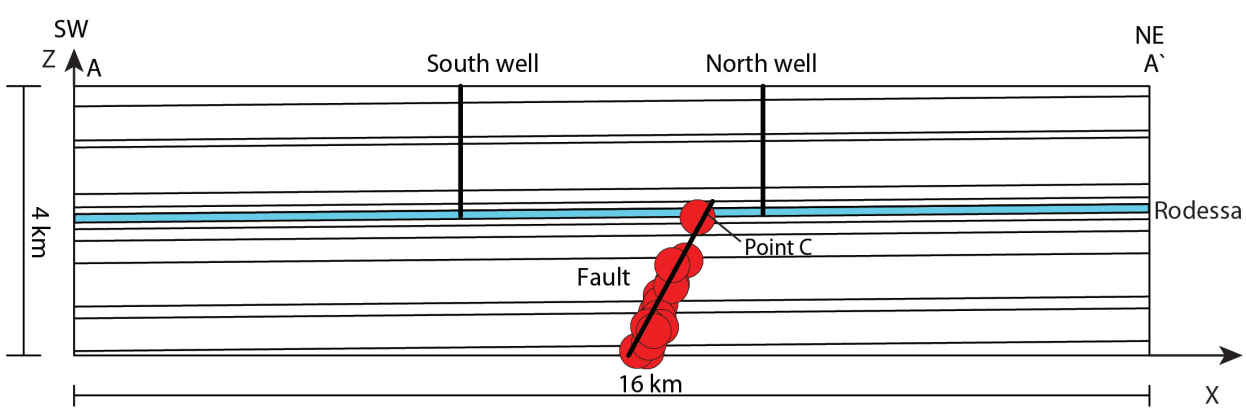

Fig. 7.2.Finite element model geometry. Red circles are reliably located hypocenters in section A-A' which coincide with the mapped fault dipping about 63° to the SW.

The injection is simulated by applying a constant flow rate to nodes in the injection zone at the wells. We approximate the 3D geometry of fluid injection into a vertical well in the 2D finite element simulation by assuming that the injection source extends for 3 km perpendicular to each side of the model plane, equivalent to the approximate distance of the well bore to the fault. We inject wastewater at a constant rate of 3.7×10^{-6} m/s, which is equivalent to a volumetric injection rate of 4.27×10^{5} m^3/month as reported for the south well. Because the two wells are aligned roughly orthogonally to the strike of the fault, and the fault extends along strike for a distance that is large relative to the spacing between the two wells, the computational model was set up in 2D for computational efficiency. The stress and stability analysis, however, was performed in three dimensions. The duration of fluid injection in our simulation is 8 years.

The full set of boundary conditions is given as follows.

Top: traction free, p=0

Bottom: v=0, p=0

Left and right: u = 0, p = 0

where u and v are horizontal and vertical displacements, respectively, and p is excess pore pressure. In situ stress conditions were determined as part of this study using image logs of the SFE2 well as described in section 2.3. Available reservoir pressure data (Texas Railroad Commission, 2014) indicate that the Rodessa Formation was slightly underpressured prior to injection, with a bottom hole pressure at a depth of 1844 m in the south well of 17.2 MPa. To create a pore pressure field matching these available data, we assume initial hydrostatic pore pressure and simulate continuous fluid production at a constant extraction rate (1/10 of the injection rate) at the two wells for 6 years. Free flow of fluid is then allowed to achieve equilibrium until the bottom hole pressure of 17.2 MPa is reached at the south well and fluid injection is initiated.

We assume that the onset of seismic fault slip is adequately described by the friction criterion

$$CFS = \tau + \mu(\sigma_n - p) > 0 \tag{1}$$

where CFS is the Coulomb failure stress, μ is coefficient of friction, p is pore fluid pressure, τ and σ_n are shear and total normal stresses acting on the fault, respectively, which in turn are affected by the pore fluid pressure diffusion due to the poroelastic effect. We assume negligible cohesion for seismic slip on a pre-existing fault surface.

7.2.2 Governing equations of poroelasticity

The governing equations for the poroelastic rock are given by (Wang, 2000)

$$G\nabla^2 u_i + \frac{G}{1-2\nu}\varepsilon_{kk,i} = \alpha p_{,i} \tag{2}$$

$$\alpha\frac{\partial\varepsilon_{kk}}{\partial t} + \frac{\alpha}{K_u B}\frac{\partial p}{\partial t} = \frac{k}{\mu_f}\nabla^2 p \tag{3}$$

where G is the shear modulus, ν is Poisson's ratio, α is the Biot coefficient, K_u is the undrained bulk modulus, B is the Skempton coefficient, t is time, k is the intrinsic permeability, and μ_f is the viscosity of pore fluid. Parameters u and p are coupled displacement and pore fluid pressure, respectively. Equation (2) is a natural extension of the Navier equation in linear elasticity where the pore pressure gradient effect is taken into account. Under uniaxial stain and constant vertical stress conditions with incompressible rock grains, a = 1, and equation (3) reduces to the standard pressure diffusion equation (Roeloffs, 1988). At the interface between two adjacent layers, displacement, total and effective stress, and pore fluid pressure are continuous.

7.2.3 In situ stress determination

We constrained the in situ stress using borehole televiewer images for the SFE2 well, located 14 km from the epicenter. The image logs recorded both wellbore breakouts and drilling induced fractures indicating that the well experienced both shear and opening-mode failure as it was drilled. The drilling-induced fractures are parallel to the axis of the vertical well which indicates that vertical stress σ_V is a principal stress and the minimum compressive horizontal stress σ_{hmin} is the least principal stress (Zoback, 2010). We measured 136 breakout azimuths and 408 breakout widths at 0.1 inch depth increments in five distinct breakout zones over a depth range of 514 m (2515- 3029 m), providing a minimum compressive horizontal principal stress orientation of N166±3° E (Fig. 7.3a). Hence the mean σ_{Hmax} orientation is N76° E. The angular breakout is 71°±13° (Fig. 7.3b). Four distinct drilling-induced fractures were detected covering a cumulative length of 17 m in the depth interval of 2950 and 3027 m, with 349 measurements yielding a mean orientation of σ_{Hmax} of N79° E± 11° (Fig. 7.3c). Combining the azimuth information of wellbore breakouts and drilling induced fractures in the SFE 2 well, we determined an average σ_{Hmax} azimuth of N 79± 11°E. The inferred directions of σ_{Hmax} derived from our measurement are consistent with the stress orientation independently determined by Laubach and Monson (1988) using coring-induced fractures observed in oriented core and with in situ stress data reported previously for east Texas (Heidbach et al., 2008).

An average gradient of the vertical stress s_v of 24 MPa/km was calculated by Thiercelin and Plumb (1994) through integration of the bulk density log of the SFE2 well. The gradient of the least compressive horizontal principal stress s_{hmin} was determined in the SFE2 well using the microfrac technique as 14MPa/km (Peterson, 1989; Thiercelin and Plumb, 1994). Utilizing breakout width determined above and unconfined compressive strength (UCS, also referred to as cohesive strength C_0) data reported by Plumb et al. (1992), and assuming a hydrostatic pore pressure

gradient, the magnitude of the maximum compressive horizontal principal stress s_{Hmax} is obtained through

$$\sigma_{Hmax} = \frac{C_0 + 2P - \Delta P_w - \sigma_h \left(1 - 2\cos\omega_{bo}\right)}{1 + 2\cos\omega_{bo}} \tag{4}$$

where ΔP_w is assumed to be negligible, and ω_{bo} is the breakout width (Zoback, 2010). Plumb et al. (1992) carried out triaxial tests to measure UCS for eight selected rock samples collected from the SFE2 well between the depths of 2513 and 3030 m. Their results range from 51 to 321 MPa. Presence of wellbore breakouts requires that the maximum hoop stress along the wellbore exceeds the UCS of the rock. Breakouts are expected to occur preferentially in weaker lithologies. We thus used the lower to intermediate range of measured UCS data to determine s_{Hmax}. The results, summarized in Table 7.2, suggest that the magnitude of σ_{Hmax} is approximately equal to σ_V when the lower range of measured UCS values is used. The strike-slip focal mechanism implies that $\sigma_{Hmax} \geq \sigma_V > \sigma_{hmin}$. For our simulations we combined the two lines of evidence, wellbore breakout and earthquake focal mechanism data, to take the magnitude of σ_{Hmax} to be equal to σ_V.

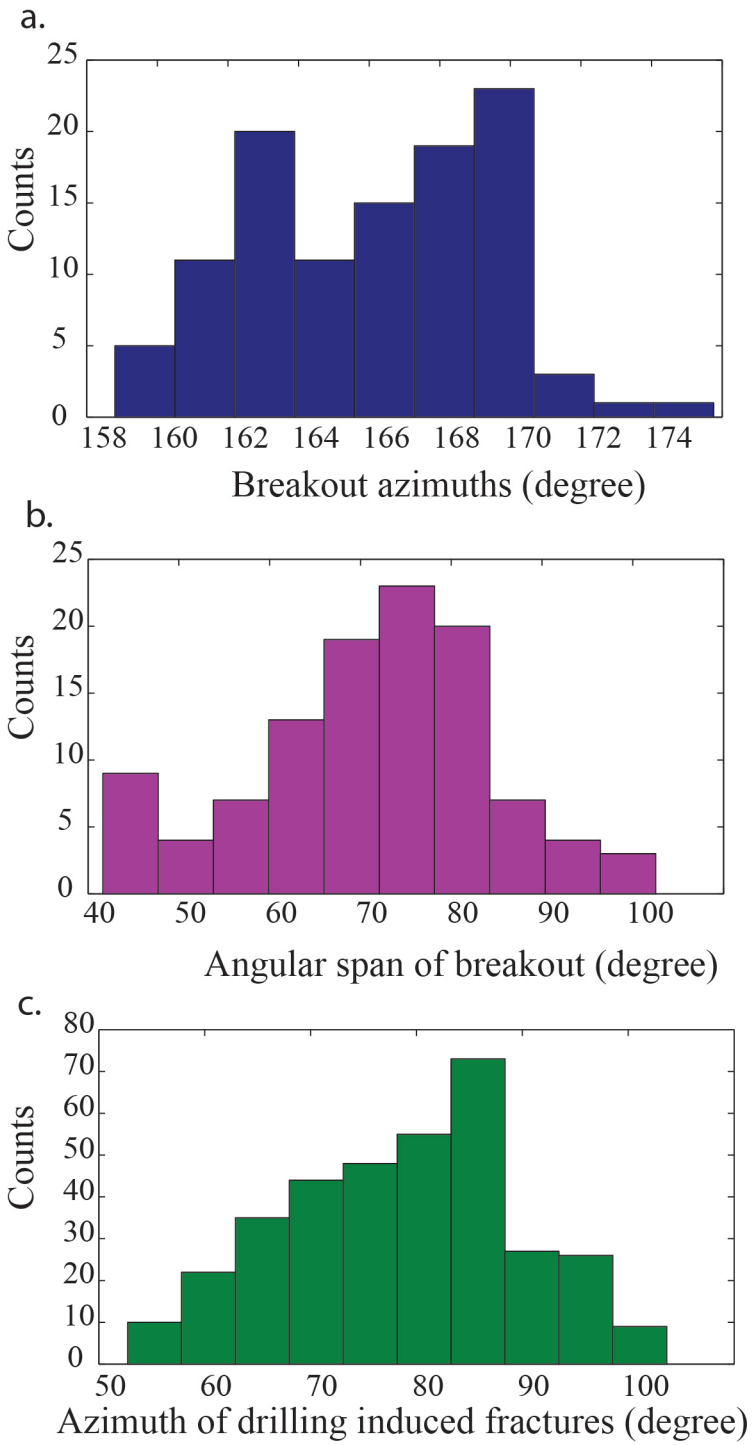

Fig. 7.3. Histograms of breakout angular span (a), breakout orientation (b), and azimuth of drilling induced fractures (c) in the SFE2 well.

Once the in situ stress tensor σ in the principal coordinate system is known, the stress in the modeling system (xyz) can be obtained via the tensor transformation

$$\sigma' = A^T \sigma A \tag{5}$$

where $A = \begin{bmatrix} \sin(az+st) & -\cos(az+st) & 0 \\ \cos(az+st) & \sin(az+st) & 0 \\ 0 & 0 & 1 \end{bmatrix}$ is the transformation matrix, with az and st denoting the azimuth of σ_{Hmax} and the fault strike, respectively.

$\sigma = \begin{bmatrix} \sigma_{H\max} & 0 & 0 \\ 0 & \sigma_{h\min} & 0 \\ 0 & 0 & \sigma_V \end{bmatrix}$ is the stress in the principal coordinate system. The normal stress σ_n and shear stress τ acting on the fault are given by

$$\sigma_n = n_1^2 \sigma_{H\max} + n_2^2 \sigma_{h\min} + n_3^2 \sigma_V \tag{6}$$

$$\tau = \sqrt{n_1^2 \sigma_{H\max}^2 + n_2^2 \sigma_{h\min}^2 + n_3^2 \sigma_V^2 - \left(n_1^2 \sigma_{H\max} + n_2^2 \sigma_{h\min} + n_3^2 \sigma_V\right)^2} \tag{7}$$

where n_1=cos(dip+90°)cos(az+st-90°), n_2=cos(dip+90°)cos(180°-az-st), and n_3=cos(dip) are the components of the unit normal to the fault plane with dip denoting the fault dip angle.

During fluid injection, total stress and pore pressure are coupled by the poroelastic effect with an increase in pore pressure causing a poroeastic increase in total compressive horizontal stresses, which in turn influences the normal stress acting on the fault. Because of the traction-free boundary condition at the Earth's surface, and the large width to height ratio of the pressure disturbance in the reservoir at advanced stages of fluid injection, the vertical total stress will remain constant. When the CFS at a point on the fault changes from negative to positive, shear failure is assumed to occur.

7.3 Results

7.3.1 Effect of permeability of injection layer

We first examine the effect of permeability of the injection layer on pore pressure diffusion, stress distribution in the reservoir, and Coulomb shear stress on the fault. Figs. 7.4a – 7.4c show the excess pore pressure profile after 69 months of fluid injection (August 2006 – May 2012) for a permeability of the injection layer of 100 md, 200 md, and 400 md. Under otherwise same conditions, pore pressure changes are higher in an injection layer of lower permeability compared to a layer of higher permeability. Higher permeability corresponds to a higher diffusivity, which allows faster diffusion of fluid. Because we assume a constant injection rate for the two injection wells, it will take longer for pore pressure to build up adjacent to the fault and thus trigger fault slip in an injection layer of higher permeability. Since the permeabilities of overlying and underlying strata are three to four orders of

magnitude lower than that of the injection layer, the migration of wastewater is mainly confined to the Rodessa layer. Downward migration from the injection horizon is limited to a depth of about 2700 m. We note that pore pressure decreases with increasing distance away from the injection well until it meets the diffusive fluid pressure front propagating from the second injection well. This decrease in pore pressure with increasing distance becomes more pronounced as permeability of the injection layer decreases. Consequently, two expanding pore pressure anomalies or bulbs form around the wells, which are commonly observed for high-volume fluid injection (Nicholson & Wesson, 1990). The bulbs are more evident for the case of lower permeability of the injection layer. For the base scenario with an injection layer permeability of 200 md, the simulated pore fluid pressure increase at the north well after 69 months of injection is 13.26 MPa and the maximum pore pressure perturbation along the fault (denoted by Point C in Fig. 7.2) is 12.54 MPa at a distance about 800 m from the north well.

Figs. 7.5a – 7.5c show the excess pore pressure, Terzaghi effective normal stress, and Coulomb failure stress plotted against time at Point C for different permeabilities of the injection layer. The following parameters are used in the numerical calculation: fault strike – N42°W, fault dip63° to the SW, azimuth of σ_{Hmax} N79°E, and coefficient of friction 0.6. For a given permeability of injection layer, the simulated pore pressure increases monotonically with time, which counteracts the normal stress and decreases the effective normal stress. As a result, the Coulomb failure stress also increases with time, which means the potential for fault reactivation is enhanced. We note that for the base scenario (k= 200 md) the Coulomb failure stress remains negative which means that the fault remains stable after 69 months of injection. We also observe an abrupt increase in pore pressure gradient after 6 months of injection into the south well which can be attributed to the contribution of the north well, which became operational in February 2007. Comparing the results in Figs. 7.5a- 7.5c, we observe that the general trends of evolution of excess pore pressure, effective normal stress, and Coulomb failure stress through time are quite similar. For any given time, the effect of lower permeability is to increase the pore fluid pressure, decrease the effective normal stress, and thus to increase the Coulomb failure stress. Thus, a lower permeability of the injection layers results in a higher potential of fault slip.

For the base scenario, although the pore pressure exceeded the initial least compressive principal stress at points below the injection zone after 69 months of injection, the effective least compressive principal stress remains compressive due to an increase in total minimum horizontal stress associated with the pore pressure increase (poroelastic effect). Therefore, no hydraulic opening-mode fractures are induced.

Fig. 7.5d shows the comparison of excess pore pressure at the bottom of two injection wells between the simulation results and measured surface pressures considering pressure loss due to friction. Following Economides and Martin (2007), we calculated the fluid pressure drop caused by friction as 3.16 MPa and 0.19 MPa for the south and north well, respectively. Numerical simulation, using a constant

injection rate equivalent to a six-year average, yields a smooth pore pressure response to continuous fluid injection, compared with the monthly varying field data.

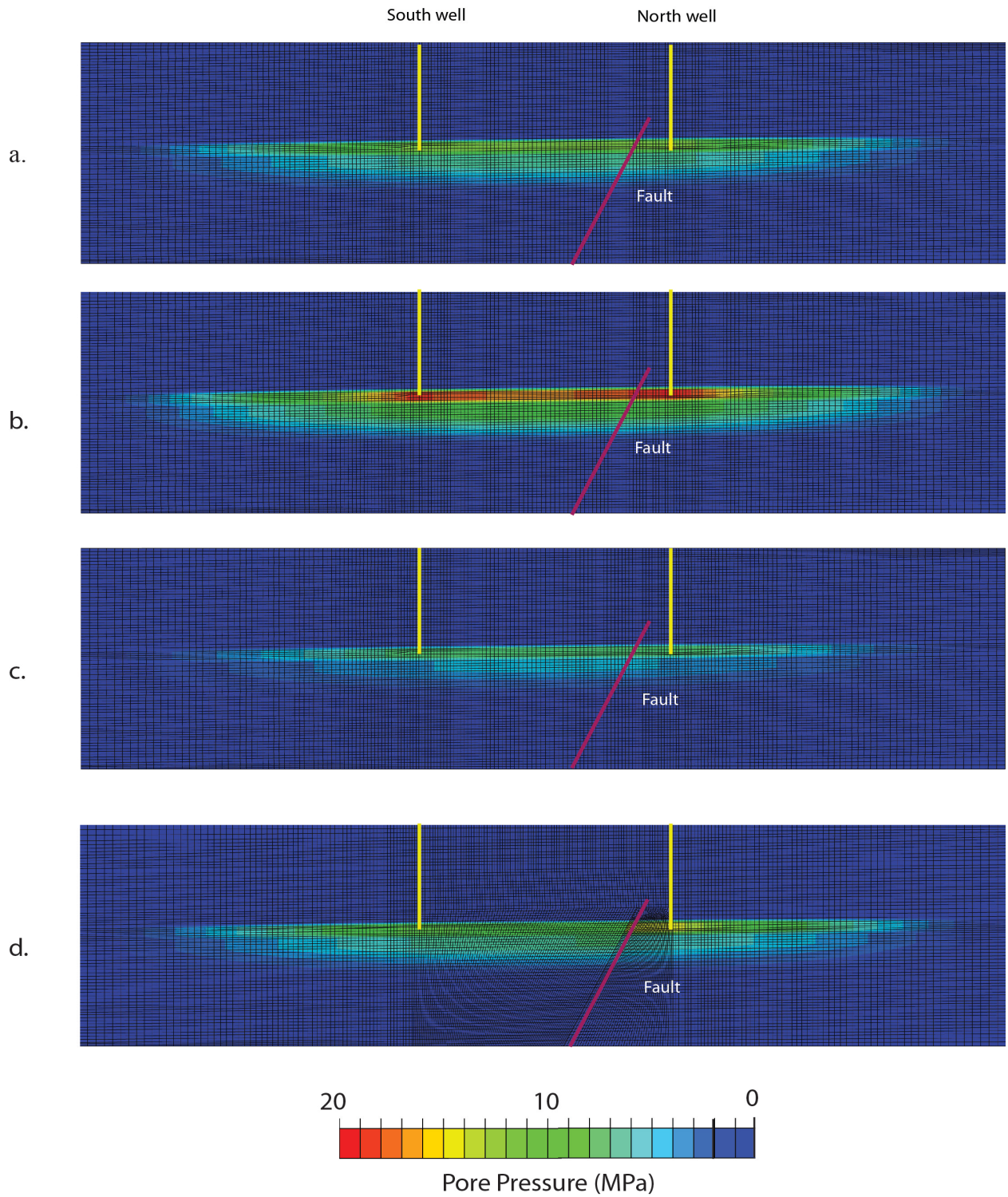

Fig. 7.4. Pore pressure profiles after 69 months of injection corresponding to different permeability k of injection layer. (a) k = 200 md, (b) k = 100 md, and (c) k = 400 md. (d) Pore pressure profile after 69 months of fluid injection for the case of sealing fault (k_{fault}= 0.01 md; $k_{formation}$ = 200 md)).

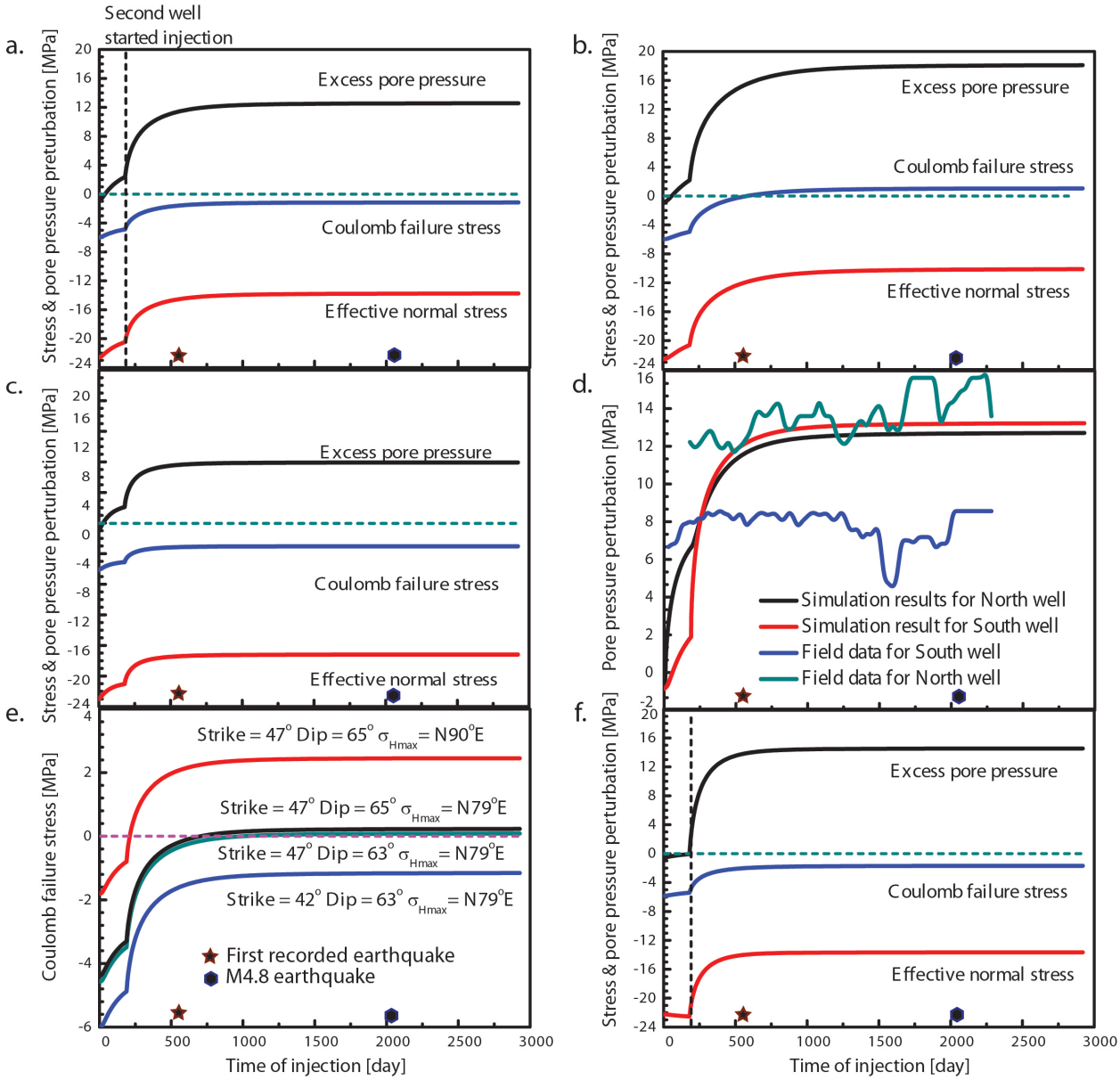

Fig. 7.5. Effect of permeability of injection layer on the temporal evolution of pore pressure and stress at point C along the fault in the injection layer. (a) k = 200 md , (b) k = 100 md and (c) k = 400md. (d) Comparison of excess pore pressure at the bottom of injection wells between field data and numerical simulation results; (e) Evolution of Coulomb failure stress over time at point C along the fault for different combinations of fault orientation and in situ stress orientation; (f) Effect of fault permeability on the pore pressure and stress evolution as a function of time at point C, located on the footwall of the low-permeability (k=0.01 md) fault. Formation permeability k = 200 md.

7.3.2 Effect of relative orientation of the preexisting fault and the in situ stress

Next we examine the effect of fault orientation and in situ stress orientation, assuming an injection layer permeability of 200 md. Based on the precision of aftershock hypocenter locations reported by Frohlich et al. (2014), we determined an admissible range of fault strike as N42°W ±5° and dip 63±2° to the SW. The orientation of σ_{Hmax} is N79°E±11°. Fig. 7.5e shows the evolution of Coulomb failure stress over time corresponding to four different admissible combinations of fault strike, fault dip, and azimuth of σ_{Hmax} within their range of uncertainties. Increasing fault strike azimuth, dip angle, or the azimuth of σ_{Hmax} will orient the fault more favorably for slip relative to the principal stress orientations, expressed as an increase of Coulomb failure stress. This can be explained by observing the normal and shear stress resolved across the fault in equations (6) and (7). We note that the Coulomb failure stress is highly sensitive to small variations in fault or stress orientation.

The effect of changing pore pressure and stress state at Point C along the fault is displayed in Fig. 7.6 using a 3D Mohr diagram for effective stress. The initial effective stress state, with $\sigma'_H = \sigma'_V$, is represented by a single Mohr circle, with the range in fault orientation relative to the principal stress orientations indicated by the bold segment of the stress circle. A decrease in pore pressure due to fluid withdrawal causes an increase in differential stress despite the increasing effective stress. The Mohr circle is driven to the right and closer to the friction line. Because the fault is unfavorably oriented relative to the in situ stress state, the fault is stable prior to injection. Favorably oriented faults would be unstable. We interpret these results to indicate that the stress state prior to injection is controlled by critically stressed faults that are located outside the area affected by fluid injection. After 69 months of injection, pore fluid pressure increases by 12.57 MPa, reducing the effective stress and shifting the stress state closer to the friction line. Because we assume isotropic poroelastic properties, total σ_{hmin} increases at the same rate of σ_{Hmax} while total s_v remains constant because of the traction-free Earth's surface. Effective stress s'_v after injection is thus lower than s'_{Hmax}. The tractions on the fault at Point C, shown for their admissible range of angles between the fault and the principal stresses (cross-hatch circle segment in Fig. 7.6b), fall to both sides of the friction line, indicating that fault slip would occur earlier than 69 months for more favorable orientations, while less favorable orientations would remain stable after 69 months of fluid injection.

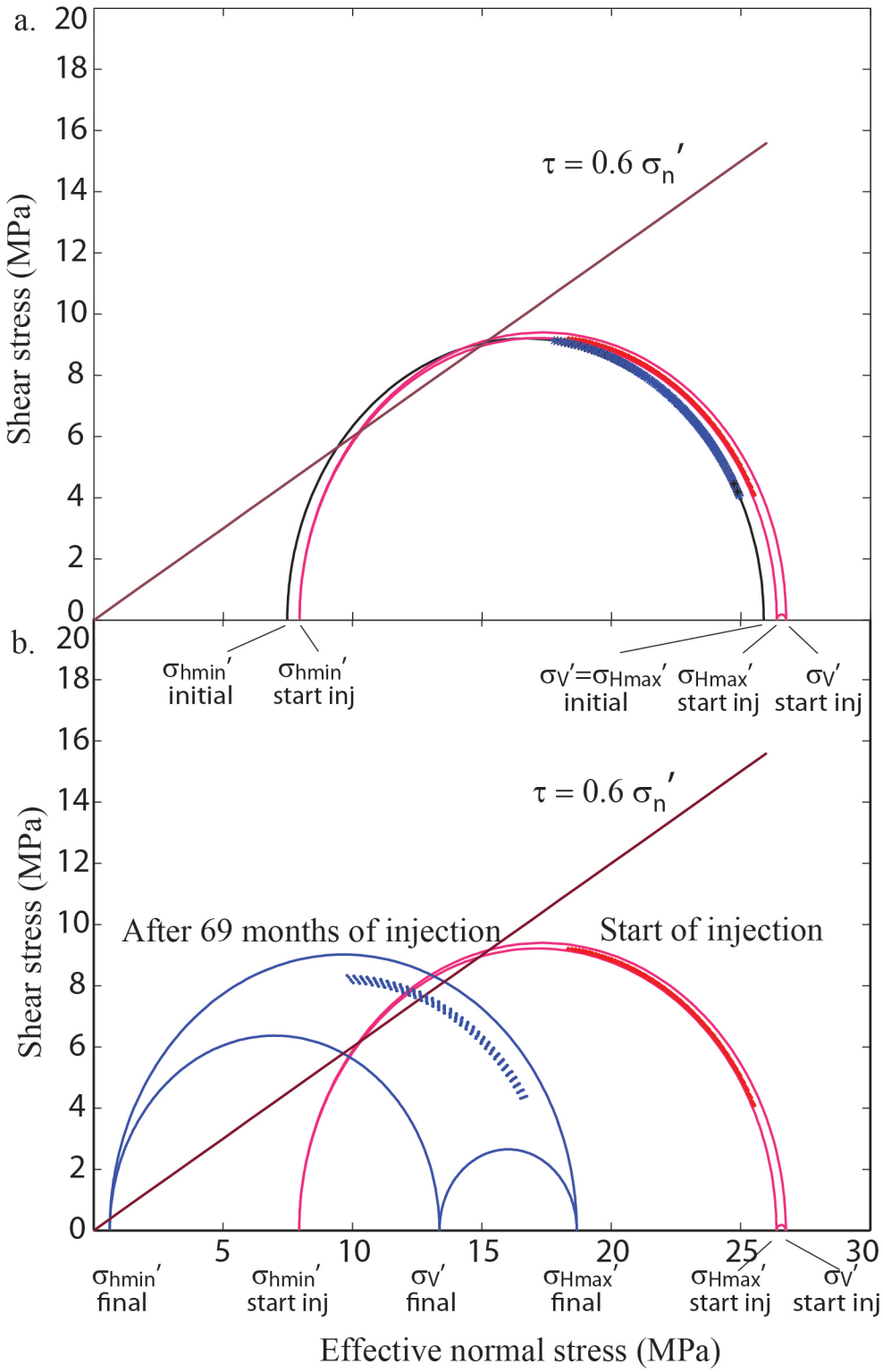

Fig. 7.6. Three dimensional Mohr diagram showing the change in stress state and tractions at point C along the fault (a) before (initial) and after (start inj) fluid withdrawl and (b) at the start of (start inj) and after 69 months (final) of fluid injection. Criterion for frictional slip on a cohesionless fault assumes a

Byerlee coefficient of 0.6. Heavy black circle segment in (a) represents initial tractions at point C along the fault for an admissible range of fault and stress orientations. Heavy red circle segment in (a) and (b) indicates tractions at point C along the fault prior to injection. Blue hatch pattern in (b) indicates stress states at point C along the fault after 69 months of fluid injection.

It is instructive to compare the changes in σ_h corresponding to the changes in pore pressure due to poroelastic coupling. A uniaxial strain simplification yields the following horizontal stress- pore pressure change ratio

$$\frac{\Delta\sigma_h}{\Delta p} = \alpha\frac{1-2\nu}{1-\nu} \tag{8}$$

(Zoback, 2010) which is a good estimate for a thin reservoir with large width to thickness aspect ratio (> 10:1) over- and underlain by non-permeable layers separated by frictional layer interfaces. A compilation of data by Engelder & Fischer (1994) and Hillis (2000) indicates that $\Delta\sigma_h/\Delta p$ falls in the range of 0.34-0.8. Our numerical simulations suggest that $\Delta\sigma_h/\Delta p = 0.45$ in the Rodessa layer compared to a value of 0.59 predicted by equ. 8 (with $\alpha = 0.79$, and $\nu = 0.2$ used in both the numerical simulation and in equ. 8). We attribute the discrepancy between the numerical and uniaxial strain values to poroelastic strains in the over- and underlying layers in the numerical simulation.

A suitable combination of in situ stress and fault orientations would yield that fault reactivation does not occur until 69 months after fluid injection commences. Table 7.3 lists the pressure changes at the fault and time lag between the onset of fluid injection and the initiation of fault slip for different combination of injection layer permeability, fault orientation and in situ stress orientation. The sharp contrast between the time delays serves to highlight the importance of detailed geomechanical site characterization to manage the seismic rick posed by waste water disposal.

7.3.3 Effect of fault permeability

So far, we considered the fault to be transparent to flow, with material properties equal to those of the host rock, equivalent to a zero-thickness interface. More realistically, we would consider a fault zone of finite width composed of a fault core bounded by a damage zone. Whether a fault act as conduits or barriers for fluid flow across or along the fault depends on the fault zone architecture and permeability structure of the fault core and damage zone (Caine et al., 1996; Bense et al., 2013), details that are not known for the fault of interest.

To assess the effect of fault zone properties on our model results, we consider the case of a 15 m thick "sealing" fault composed of a low-permeability core (k_{fault}=0.01 md; $k_{formation}$=200 md) (Fig. 7.4d).Compared to the transparent fault where the pore pressure fields starting from the two injection wells overlap to generate a combined smooth pore pressure field, we observe a sharp pore pressure discontinuity across the sealing fault resulting in an overall higher pore fluid pressure in the footwall of

the fault facing the North well, and lower pore fluid pressure in the hanging wall. Because the criterion for frictional slip needs to be met on only one side of the fault, with slip occurring along the interface of the fault core and footwall damage zone, a sealing fault is more favorable to fault reactivation. In our case, even though the excess pore pressure in the footwall of the sealing fault is higher than for the transparent fault (Fig. 7.5a), the Coulomb failure stress is still too low for fault slip to occur.

7.4 Discussion

7.4.1 Coupling between fluid flow and geomechanical deformation

Previous studies addressing fluid induced seismicity solved the standard fluid diffusion equation,

$$\frac{\partial p}{\partial t} = D\nabla^2 p \tag{9}$$

where D is the diffusivity, and then considered a critical pore pressure value that must be reached to induce seismic fault slip (Parotidis & Shapiro, 2004; Shapiro et al., 2013; Keranen et al., 2014). This approach differs from our fully coupled poroelastic approach by neglecting the coupling between fluid flow and poroelastic deformation leading to a lower diffusivity and thus slower fluid diffusion, hence a higher pore pressure distribution through the domain.

In some cases fault reactivation follows the fluid injection by several days or weeks (Zoback & Harjes, 1997). In others, the time gap may reach years or even decades (Healy et al., 1968; Keranen et al., 2014). The time required for the pore pressure at the fault to reach the threshold value depends on the reservoir permeability, injection rate and pressure, injection depth, fault permeability, and distance between the injection wells and the fault, which helps to explain the time lag between the start of injection and the onset of seismicity, as observed in our study and in other cases (Nicholson & Wesson, 1990). Because the poroelastic coupling between pore pressure and total stress, we propose that fully coupled modeling approach as followed in this study provides a closer prediction of the time delay between injection and fault instability.

7.4.2 Implications for fluid injection practices

Our in situ stress results suggest that the reservoir was critically stressed for favorably oriented faults prior to injection, with the in-situ stress field controlled by slip along critically stressed faults located outside the influence area of fluid injection. The delayed onset of seismicity after significant fluid injection indicates that no favorably oriented faults large enough to result in observable earthquake activity at the beginning of fluid injection are present in the influence area of fluid injection. The absence of such favorably oriented faults within the influence area of fluid injection and the highly unfavorable orientation of the fault relative to the in situ stress state allowed significant fluid injection prior to the onset of seismic activity.

Our results illustrate that presence of faults and their orientation within a targeted injection reservoir can significantly limit the injection capacity of the reservoir. While faults large enough to result in earthquakes of magnitudes larger than ~5 are generally resolvable in reflection seismic surveys (Gale et al., this report), smaller sub-seismic faults may still limit reservoir injection capacity, presenting challenges in planning fluid injection programs and assessing induced earthquake risk prior to the onset of seismic activity. Our results also demonstrate that the allowable injection volume prior to onset of induced seismicity is sensitive to small variations in geomechanical input parameters including fault and in situ stress orientation, and initial stress state and pore fluid pressure. Meaningful prediction of injection volume and induced seismic risk through geomechanical models prior to any observed seismic activity would therefore require detailed site-specific geomechanical and structural evaluation that, given limitations in seismic imaging technology, may still leave unacceptable predictive uncertainty.

7.5 Conclusions

To address the geomechanical link between fluid injection and initiation of seismic fault slip in Timpson, Texas, we numerically simulated the coupled processes of fluid diffusion and stress and pore pressure changes associated with fluid injection and their effects on fault reactivation. Published and newly calculated in situ stress data based on borehole breakouts and induced fractures in the nearby SFE2 well in combination with the focal mechanism of the M_w4.8 event indicate a normal/strike-slip faulting stress regime. While the initial stress state appears controlled by critically stressed favorably oriented faults, the seismically active fault near Timpson is unfavorably oriented for slip suggesting the absence of favorably oriented faults in the area affected by fluid injection. The model simulations suggest that pore pressure perturbation and thus the Coulomb failure stress and potential of the fault for shear reactivation, are sensitive to the permeability of the injection layer, fault orientation relative to the in situ stress orientation, and in situ stress magnitudes. Seismic fault reactivation is favored by low reservoir permeability and a favorable orientation of the fault relative to the in situ stress state. Fault permeability affects the pore fluid distribution across the fault, with a sealing fault potentially favoring fault instability. Assessment of fault stability and earthquake risk associated with fluid injection using geomechanical modeling prior to the onset of seismic activity requires the detailed site assessment of fault orientation, pore pressure prior to injection, and in-situ stress.

7.6 Acknowledgments

This research was funded by the Research Partnership to Secure Energy for America (RPSEA) subcontract 11122-27 through the "Ultra-Deepwater and Unconventional Natural Gas and Other Petroleum Resources" program authorized by the U.S. Energy Policy Act of 2005. RPSEA (www.rpsea.org) is a nonprofit corporation whose mission is to provide a stewardship role in ensuring the focused research, development, and deployment of safe and environmentally responsible technology that can effectively deliver hydrocarbons from domestic resources to the citizens of

the United States. RPSEA, operating as a consortium of premier U.S. energy research universities, industry, and independent research organizations, manages the program under a contract with the U.S. Department of Energy's National Energy Technology Laboratory. The views and conclusions contained in this document are those of the authors and should not be interpreted as representing the official policies, either expressed or implied, of the U.S. Government. We thank Jon Olson, Cliff Frohlich, Matthew Weingarten, and Ellen Rathje for discussion and suggestions for improvement and clarification. Valerie Gono is thanked for RRC database searches. Publication authorized by the Director, Bureau of Economic Geology.

7.7 References

Ake,J.,Mahrer,K.,O'Connell,D.,Block,L.,2005.Deep-injection and closely monitored induced seismicity at Paradox Valley, Colorado. Bull.Seismol.Soc.Am. 95, 664–683.

Balkey, J., 1989. Ann McKnight (Paluxy) field, Smith County, Texas, in East Texas Geological Society Publication Series: Occurrence of Oil and Gas in Northeast Texas, 1989 Edition, edited by Shoemaker, P. W., pp. 15-20.

Bense, V.F., Gleeson, T., Loveless, S.E., Bour, O., Scibek, J., 2013. Fault zone hydrogeology. Earth-Sci. Rev. 127, 171-192.

Berg, R. R., Gangi, A. F., 1999. Primary migration by oil-generation microfracturing in low-permeability source rocks: Application to the Austin chalk, Texas, AAPG Bulletin. 83, 727-756.

Boyd, R. F., White, L. P., 1989. Trawick (Travis Peak, James) field, Nacogdoches and Rusk counties, Texas, in East Texas Geological Society Publication Series: Occurrence of Oil and Gas in Northeast Texas, 1989 Edition, edited by Shoemaker, P. W., pp. 191-196.

Brogdon, D. R., 1962. Trawick field: Nacogdoches and Rusk counties, Texas,, in East Texas Geological Society Publication Number 5, Volume 1: Occurrence of Oil and Gas in Northeast Texas, edited by Nichols, P. H., pp. 96-102.

Caine, J. S., Evans, J. P., and Forster, C. B., 1996. Fault zone architecture and permeability structure. Geology 24, 1025-1028.

Cappa, F., Rutqvist, J., 2011. Modeling of coupled deformation and permeability evolution during fault reactivation induced by deep underground injection of CO2. Int. J. Greenh. Gas Control. 5, 336-346.

Dutton, S. P., Diggs, T. N., 1992. Evolution of porosity and permeability in the Lower Cretaceous Travis Peak Formation, east Texas, AAPG Bulletin. 76, 252-269.

Economides, M. J., Martin, T., 2007. Modern fracturing enhancing natural gas production, ET Publishing, Houston, TX.

Ellsworth, W. L., 2013. Injection-induced earthquakes. Science. 341, 142-149.

Engelder, T., Fischer, M. P., 1994. Influence of poroelastic behavior on the magnitude of minimum horizontal stress, Sh in overpressured parts of sedimentary basins. Geology. *22*, 949-952.

Ewing, T. 1990, Tectonic Map of Texas, Bureau of Economic Geology, The University of Texas, Austin, Texas.

Finley, R. J., Speer, S. W., and Diecchio, R. J. 1984. Geology and Engineering Characteristics of Selected Low-permeability Gas Sandstones: A National Survey. Bureau of Economic Geology, The University of Texas at Austin.

Jackson, M. P. A. 1982. Fault Tectonics of the East Texas Basin, Geol. Circular, vol. 82–4, p. 31, Bureau of Economic Geology, The University of Texas at Austin.

Frohlich, C., Hayward, C., Stump, B., Potter, E.,2011. TheDallas–Fort Worth earthquake sequence: October 2008through May 2009. Bull.Seismol.Soc.Am.101, 327–340.

Frohlich,C., 2012.Two-year survey comparing earthquake activity and injection-well locations in the Barnett Shale, Texas. Proc.Natl.Acad.Sci.109, 13934–13938.

Frohlich, C., Brunt, M. 2014. Two-year survey of earthquakes and injection/production wells in the Eagle Ford Shale, Texas, prior to the Mw4.8 20 October 2011 earthquake. Earth Planet. Sci. Lett., 402, 257-264,

Frohlich, C., Ellsworth W., Brown, W. A., Brunt, M., Luetgert, J., MacDonald T., and Walter, S. 2014. The 17 May 2012 *M*4.8 earthquake near Timpson, East Texas: An event possibly triggered by fluid injection. J. Geophys. Res. Solid Earth, 119, 581–593,

Grubbs, E. L., 1953. Variations in porosity and permeability in the Wilcox Group of the Texas Upper Gulf Coast, Gulf Coast Association of Geological Societies Transactions 3, 54-70.

Heidbach, O., Tingay, M., Barth, A., Reinecker, J., Kurfe, D. Müller, B., 2008. The World Stress Map database release 2008. doi:10.1594/GFZ.WSM.Rel2008.

Hillis, R., 2000. Pore pressure/stress coupling and its implications for seismicity. Explor. Geophys.31, 448-454.

Horton, S., 2012. Disposal of hydrofracking waste fluid by injection into subsurface aquifers triggers earthquake swarm in central Arkansas with potential for damaging earthquake. Seismol. Res. Lett.83, 250-260.

Hsieh,P.A., Bredehoeft,J.S.,1981.A reservoir analysis of the Denver earthquakes—A case of induced seismicity. J.Geophys.Res. 86,903–920.

Keranen, K. M., Savage, H. M., Abers, G. A., Cochran, E. S., 2013. Potentially induced earthquakes in Oklahoma, USA: Links between wastewater injection and the 2011 Mw 5.7 earthquake sequence. Geology. 41,699-702.

Keranen, K. M., Weingarten, M., Abers, G. A., Bekins, B. A., Ge, S., 2014. Sharp increase in central Oklahoma seismicity since 2008 induced by massive wastewater injection. Science 345, 448-451.

Kim, W. Y., 2013. Induced seismicity associated with fluid injection into a deep well in Youngstown, Ohio. J. Geophys. Res. Solid Earth. 118, 3506-3518.

Konstantinovskaya, E., Rutqvist, J., Malo, M., 2014. CO_2 storage and potential fault instability in the St. Lawrence Lowlands sedimentary basin (Quebec, Canada): Insights from coupled reservoir-geomechanical modeling. Int. J. Greenh. Gas Control.22, 88-110.

Laubach, S., Monson, E., 1988. Coring-induced fractures: Indicators of hydraulic fracture propagation in a naturally fractured reservoir, Society of Petroleum Engineers, SPE-18164-MS.

Mancini, E., Aharon, P., Goddard, DA, Horn, M., Barnaby,R., 2012. Basin Analysis and Petroleum System Characterization and Modeling, Interior Salt Basins, Central and Eastern Gulf of Mexico, Part 3: Tectonic / Depositional History, Resource Assessment, AAPG Search and Discovery Article #10395.

McGarr, A., 2014. Maximum magnitude earthquakes induced by fluid injection. J. Geophys. Res. Solid Earth. 119, 1008-1019.

National Research Council. 2013. Induced Seismicity Potential in Energy Technologies, National Academies Press, 248 pp.

Nicholson, C., and Wesson, R. L., 1990. Earthquake hazard associated with deep well injection: A report to the U.S. Environmental Protection Agency. U.S. Geol. Surv. Bull. 1951. 74 pp.

Nicholson, C., Wesson, R. L., 1992. Triggered earthquakes and deep well activities. Pure Appl. Geophys. 139, 561-578.

Parotidis, M., Shapiro, S. A., 2004. A statistical model for the seismicity rate of fluid-injection-induced earthquakes. Geophys. Res. Lett..31(17).

Peterson, R. E., 1989. Staged field experiment No. 2: Application of advanced geological, petrophysical and engineering technologies to evaluate and improve gas recovery from low permeability sandstone reservoirs- volume 1. Gas Research Institute GRI report 89/0140.

Plumb, R., Herron, S., Olsen, M., 1992. Composition and texture on compressive strength variations in the Travis Peak Formation, paper presented at SPE Annual Technical Conference and Exhibition, Society of Petroleum Engineers.

Pollard, N., 1989. Alabama Ferry (Glen Rose) field, Leon County, Texas, in East Texas Geological Society Publication Series: Occurrence of Oil and Gas in Northeast Texas, 1989 Edition, edited by Shoemaker, P. W., pp. 1-14.

Raleigh, C.B., Healy, J.H., Bredehoeft, J.D., 1972. Faulting and crustal stresses at Rangely, Colorado. American Geophysical Union Geophysics Monograph Series 16, 275-284.

Roeloffs, E. A., 1988. Fault stability changes induced beneath a reservoir with cyclic variations in water level. J. Geophys. Res. Solid Earth. 93, 2107-2124.

Shapiro, S. A., Kruger, O. S., Dinske, C., 2013. Probability of inducing given-magnitude earthquakes by perturbing finite volumes of rocks. J. Geophys. Res. Solid Earth. 118, 3557-3575.

Texas Railroad Commission, 2014. http://www.rrc.state.tx.us/about-us/resource-center/research/online-research-queries/, accessed Oct 1 2014.

Thayer, P. A., 1983. Relationship of porosity and permeability to petrology of the Madison Limestone in rock cores from three test wells in Montana and Wyoming, US Department of the Interior, Geological Survey Professional Paper 1273C, C1-C29.

Thiercelin, M., Plumb, R., 1994. A core-based prediction of lithologic stress contrasts in east Texas formations.SPE Form. Eval.9, 251-258.

Wang, H., 2000. Theory of Linear Poroelasticity with Applications to Geomechanics and Hydrogeology, Princeton University Press.

Zoback, M. D., 2010. Reservoir Geomechanics, Cambridge University Press.

Zoback, M. D., Harjes, H. P., 1997. Injection-induced earthquakes and crustal stress at 9 km depth at the KTB deep drilling site, Germany. J. Geophys. Res. Solid Earth. 102, 18477-18491.

Table 7.1. Mechanical and hydrological properties of rocks used in the finite element analysis to simulate the coupled stress and pore pressure changes due to fluid injection.

Unit	Lithology	Depth of formation tops for south well (m)	Permeability range and mean (md)	Porosity range and mean (percent)	References for permeability and porosity	Young's modulus (GPa)	Poisson's ratio	Biot coefficient	References for mechanical properties
Wilcox and sandy units above	Sand	0	114-908 400	21.6-25.5 25	Grubbs (1953)	1.0	0.35	0.9	Wang (2000)
Midway/ Navarro/ Taylor Marl	Shale and sandy shale/Marl	244	200-2500 300	20-28 22	Mancini et al. (2012)	24	0.25	0.9	Wang (2000)
Austin Chalk	Chalk/Marl couplets	747	<0.05 0.01	4-10 5	Berg &Gangi (1999)	18	0.25	0.95	Wang (2000)
Fredericksburg Group	Limestone/shale/marls	838	323	10-30 19.6	Balkey (1989)	40	0.25	0.85	Wang (2000)
Glen Rose	Limestone	1548	0.3-500 10	6-30 18	Pollard (1989)	58	0.19	0.69	Wang (2000)
Massive Anhydrite	Anhydrite with limestone stringers	1762	0.01-0.06 0.03	5-20 10	Thayer (1983)	57	0.2	0.69	Wang (2000)
Rodessa	Oolitic sand	1829	10-650 200	10-26 18	Brogdon (1962) Mancini et al. (2012)	40	0.2	0.79	Wang (2000)
James Lime	Limestone	1974	0.01-1.0 0.1	6-18 9	Boyd & White (1989)	60	0.27	0.69	Wang (2000)
Pettet (Sligo)	Interbedded limestone/shale/oolitic limestone	2047	142.97	16-20 19.26	Brogdon (1962)	36	0.27	0.69	Thiercelin &Plumb (1994)
Travis Peak (Hosston)	Sandstone	2234	0.01-50 0.026	4.4-10.67	Dutton & Diggs (1992)	42.4	0.23	0.38	Peterson (1989)
Cotton	Sandstone	2569	0.0053	6-10	Finley	62	0.13	0.44	Peterson

Valley			-0.042 0.015	8	(1984)				(1989)
Gilmer Limestone	Limestone	3179	0.1-1.0 0.5	5-15 8	Ahr (1981)	66	0.27	0.69	Thiercelin &Plumb (1994)
Buckner Fm. and "Paleozoics"	Various	3377	50-400 100	9-16 10	Mancini et al. (2012)	66	0.2	0.6	Wang (2000)
Volcanics (Basement)	Volcanics	3880	<1-100 10	11-22 15	Mancini et al. (2012)	66	0.17	0.23	Wang (2000)

Table 7.2. Magnitude of maximum horizontal stress obtained from SFE2 wellbore breakout data.

Depth (m)	P (MPa)	σ_V (MPa)	σ_{hmin} (MPa)	UCS (MPa)	σ_{Hmax} (MPa)
2516	24.7	60.4	35.2	64	56 - 70.7
				128	87.1 - 123.6
				197	120 – 180.7
3013	29.5	72.3	42.2	51	54.7 – 63.4
				74	65.8 – 82.4
				321	185.7 – 286.7
3029	29.7	72.7	42.4	51	54.8 – 63.5
				74	66 – 82.6
				321	185.9 – 286.9

Table 7.3: Variations of fluid pressure increase along the fault and time lag between start of fluid injection and fault reactivation for different combinations of injection layer permeability, fault orientation, and in situ stress orientation. 'No slip' indicates no slip occurring within 8 years of simulated injection.

Permeability of injection layer (Millidarcy)	Azimuth of fault strike (Degree)	Fault dip (Degree)	Azimuth of maximum horizontal stress (Degree)	Maximum pore pressure perturbation along the fault (MPa)	Time lag between start of fluid injection and initiation of fault slip (Month)
200	42	63	79	12.57	No slip
400	42	63	79	7.83	No slip
100	42	63	79	18.1	20
200	47	63	79	12.57	35
200	37	63	79	12.57	No slip
200	42	65	79	12.57	No slip
200	46	65	79	12.57	68
200	42	63	90	12.57	9
200	47	65	79	12.57	24
200	47	65	90	12.57	7

8. Injection Well Modeling of the Fort Worth Basin

This section was prepared by Valerie Gono. It is the basis for a manuscript to be submitted to the American Rock Mechanics Association annual meeting in June 2015.

8.1 Background

An increased number of earthquakes in the central and eastern United States within the last few years has caused concerns within the government, academia, and the public in general (Frohlich, 2012; Keranen, et al., 2014; USGS, 2015). Various articles in prominent newspapers and magazines speculated that the cause of the rise was due to increased oil and gas related activities (Panzar, 2014; Fountain, 2014). A leading theory is that the earthquakes are induced by the increasing amount of wastewater injection, a consequence of increased produced water from hydraulically fractured oil and gas wells (Zoback, 2012).

The thought that oil and gas activities can induce seismic events is not a new one. Fluid injection has been correlated to induced seismicity since the 1960s (van Poollen & hoover, 1970; Zoback, 2012). Furthermore, many studies correlating the location of earthquake activities and their proximity to injection wells have been done (Frohlich, 2012; Holland, 2013; Justinic, et al., 2013). Simulations correlating fluid injections and earthquakes have been performed on a local scale after the occurrences of uncharacteristically large magnitude earthquakes in various fields all over the world (Zoback, 1997; Jalali, et al., 2008; Kim, 2013). However, no basin-wide study correlating fluid injection and seismic activities have been performed. This could be attributed to the scarcity of accurately available public injection and geologic data related to the areas of interest.

The idea behind modeling the whole basin instead of just focusing on modeling injection wells in proximity to the earthquake locations is that, depending on the geology of the formation and the volume of fluid injected, the pore pressure front may extend farther than anticipated, providing the possibility of activations of various faults and fractures located farther away from the point of injection (Shapiro, et al., 2006). This may help explain why some seismic events are observed in areas where no injection wells are present.

Simulation Method

Using publicly available injection well data plus regional geology information, a flow simulation model was constructed of the Fort Worth Basin. The Implicit Explicit Black Oil (IMEX) finite difference simulator of the Computer Modeling Group (CMG) was used to model wastewater injection. The pore pressure increase at the end of the each injection period was observed and plotted. Then a spatial and temporal analysis between the increased pore pressure and seismic activities was performed.

Earthquake data were taken from the United States Geological Survey (USGS) National Earthquake Information Center (NEIC) database. The wastewater injection data were queried from the Railroad Commission of Texas (RRC). For all the injection wells located in the Fort Worth Basin within the focus area, the following information was obtained: well locations, injection volumes, and injection depths.

8.2 Simulation Domain

The simulated region includes Denton, Ellis, Erath, Hill, Hood, Jack, Johnson, Palo Pinto, Parker, Somervell, Tarrant, and Wise counties (Figure 1). The region is roughly bounded on the west by the Bend Arch, on the north by the Red River and Muenster Arches, and on the east by the Ouachita Thrust (Pollastro et al., 2007). The total number of injection wells was 374. The simulation grid blocks were cubes, 2,000 ft on a side, and the entire model included 342 by 330 by 9 grid cells in the x, y and z directions, respectively, for an areal extent of 130 by 125 miles and approximately 17,000 ft thick. The injection duration was 199 months (start date: 1997-12-01).

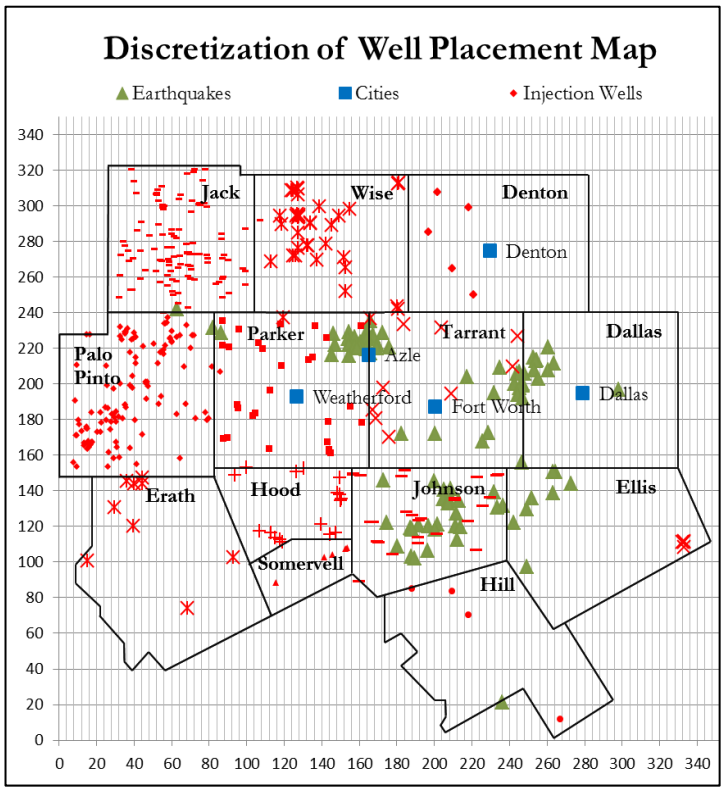

Figure 1. Discretized Well Placement Map

Based on published data available, the following porosity and permeability values were used in the simulation. When no data was available, an average between the known values was taken to represent the unknown porosity and permeability values. It was assumed that the porosity and permeability were constant in each layer in order to simplify the simulation.

Layer	k_{horiz} (md)	k_{vert} (md)	Porosity
1	75	7.5	0.20
2	40	4.0	0.13
3	1	0.1	0.05
4	5	0.5	0.07
5	9	0.9	0.06
6	13	1.3	0.11
7	16	1.6	0.09
8	16	1.6	0.07
9	16	1.6	0.07

Table 1. Porosity and Permeability of Each Layer

The well configuration in the simulator can be seen on Figure 2.

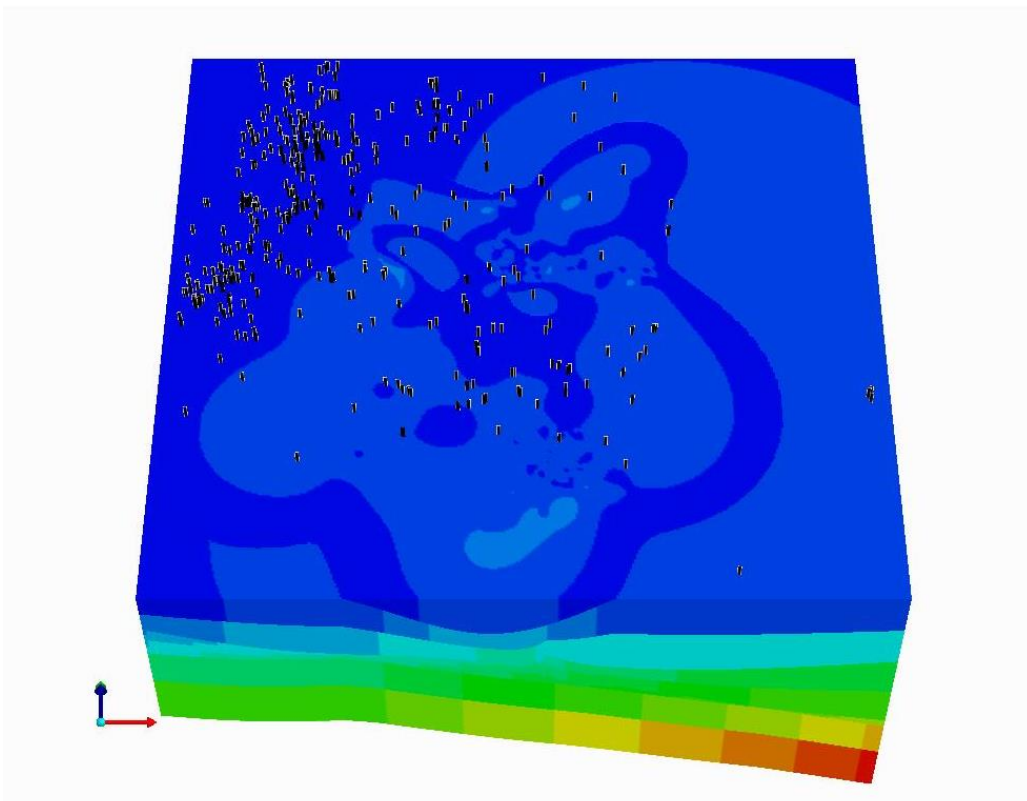

Figure 2. Well Configuration in CMG

Geologic Data

Geologic data plays a crucial role in the accuracy of the simulation results. However, it was quite difficult to obtain good data on the subsurface geology. Detailed geologic information is usually proprietary, and is obtained by private companies during the drilling operation. Obtaining geologic data is one of the major challenges faced in this research.

Formation Top

Formation tops helped constrain the vertical height of the model based on data from IHS Petra. Top for the following formations: Strawn, Marble Falls, Barnett, and Ellenburger, were interpolated to fit the simulation domain. These formations correspond to the top of layers 2, 4, 6, and 8 respectively. The top of the layer 1 is 0, and the top for layers 3, 5, and 7 were computed by taking an average between the top of the known layers where the unknown layer is sandwiched in between.

As can be seen in Figure 3, Petra has an extensive formation top data for a specific area. A built-in MATLAB interpolation scheme based on the Green's function interpolation method was then utilized to populate the whole region of interest with top data. The interpolated tops can be seen on Figure 4. From Figure 3 and Figure 4, it can also be observed that the top of the formations increases in depth as it moves to the East. This observation is especially prominent in the Barnett and the Ellenburger, which is consistent with the published structure contour map for the top of the Ellenburger and the top of the Barnett shale (Thompson, 1982; Pollastro, et al., 2007). However, the interpolation scheme show a tendency to make a bowl shape out of the layers for the Strawn and Marble Falls data in the regions outside the data. These bowl geometries should be considered artifacts and not representative of the real structure.

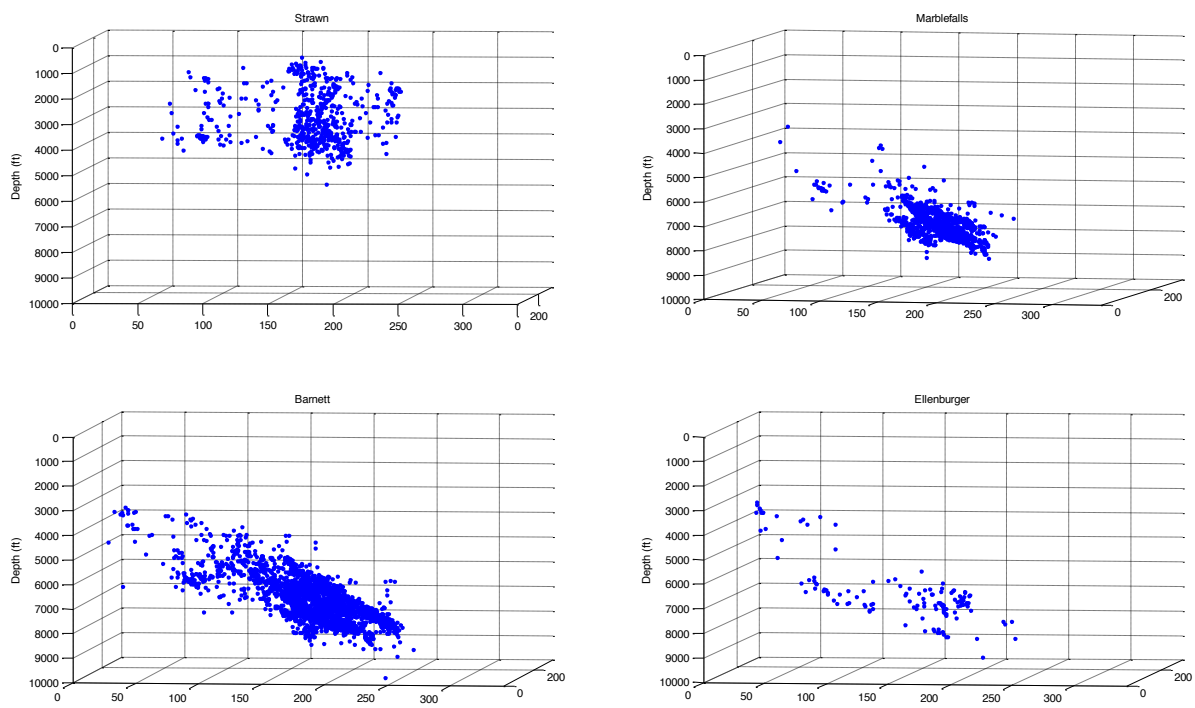

Figure 3. Formation Top Data Points from Petra

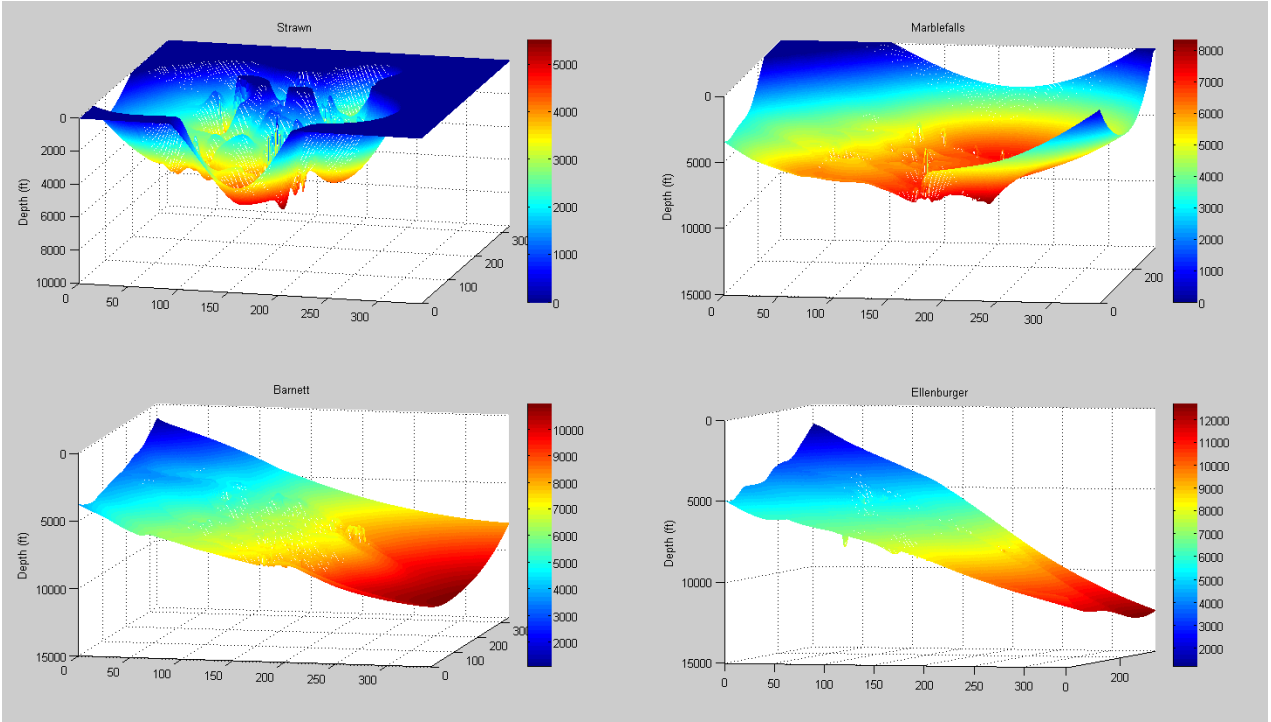

Figure 4. Interpolated Top Surfaces based on Green's Function Approach. The upturn of the Strawn and Marble Falls layers is considered an artifact of the contouring process in regions outside of data control (see Figure 3 for the regions with good data control).

The formation cross-sections in the simulator can be seen in Figure 5.

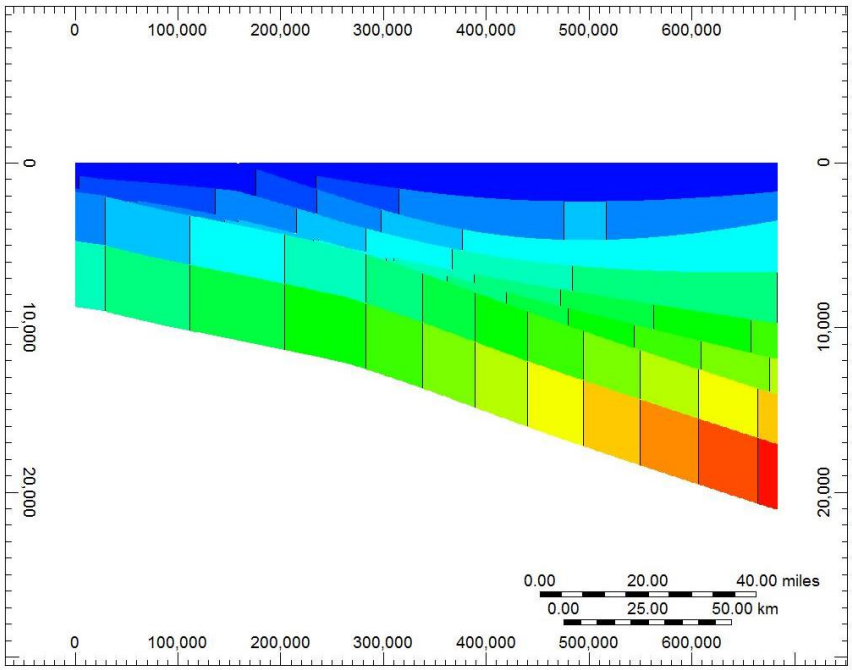

(a)

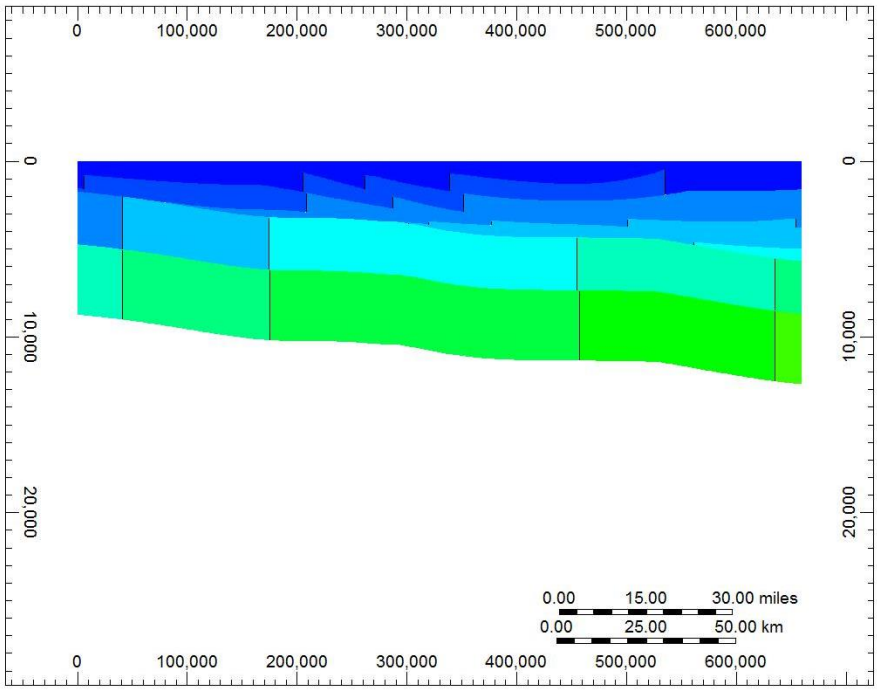

(b)

Figure 5. a) Formations Cross-section in the x-z Direction b) Formations Cross-section in the y-z Direction

8.3 Simulation Results and Analysis

Figure 6 shows the progression of the pore pressure over time in layer 8 (approximately the Ellenburger formation). Between 2004 and 2009, in the area pointed by the arrow, there is a 40 psi pressure increase, and between 2009 and 2012, there is an additional 15 psi pressure increase. Due to the complex formation of the basin, it is more difficult to see the pressure change due to the heterogeneity of the formation, which resulted in a wider range of pressure values, hence, making it harder to spot any changes in pressure. From the figure, it is clear that the pressure distribution is perturbed around some of the injectors (closed contours and higher gradients), but in much of the area the contours are fairly linear and uniformly spaced.

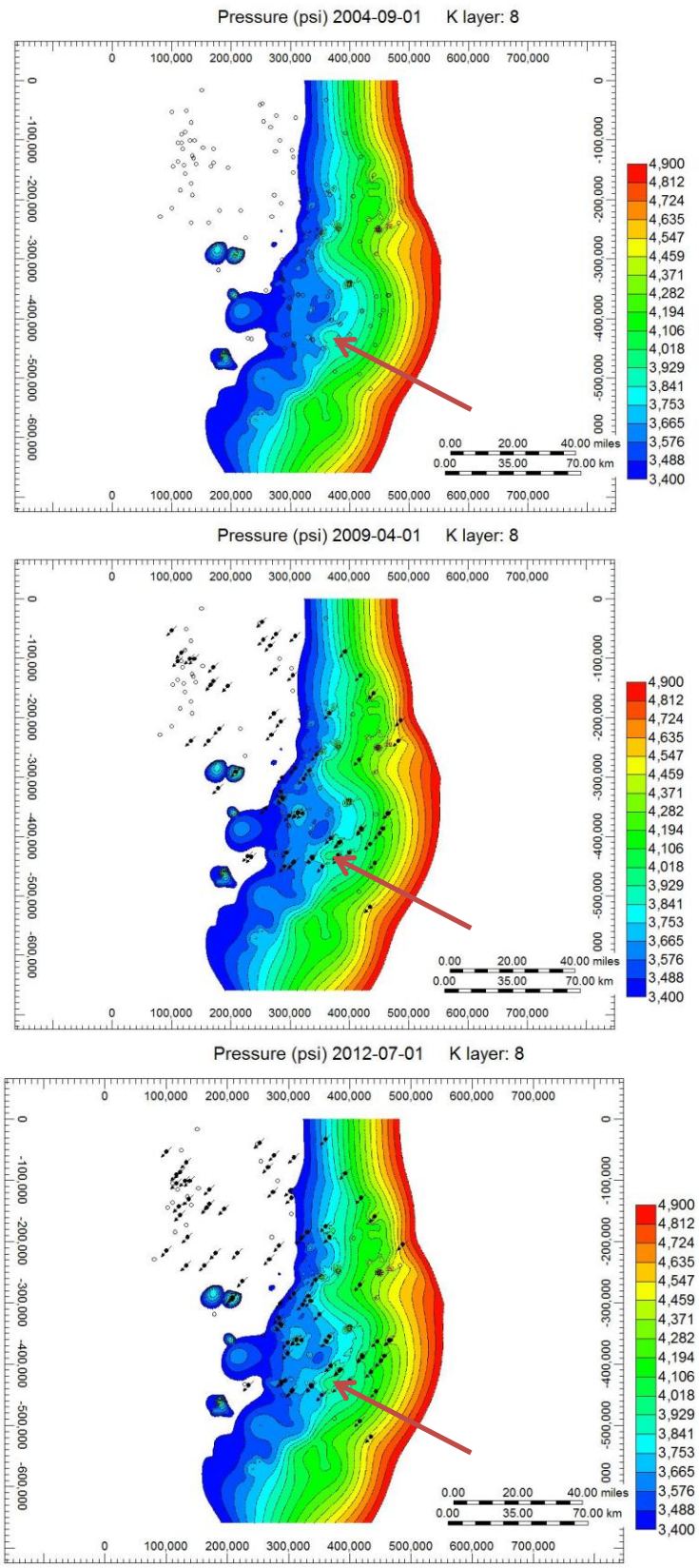

Figure 6. Pressure history in layer 8, the Ellenburger.

A simpler simulation was performed, where the entire simulation space was assumed to be homogenous the layer tops were horizontal. This simulation not so much measured formation response but indicated regions of high injection. Based on these results, it was easier to locate some spatial and temporal correlation between the increase pore pressure change and the occurrence of earthquakes. For instance, the 2012 earthquakes in Johnson County are in a region of pore pressure elevated by about 75 psi (Figure 7a). This exercise also illustrated the challenge of identifying the correlation between injectors and earthquakes. The 2013 earthquakes in Dallas County seem to occur in a region of no elevated pressure.

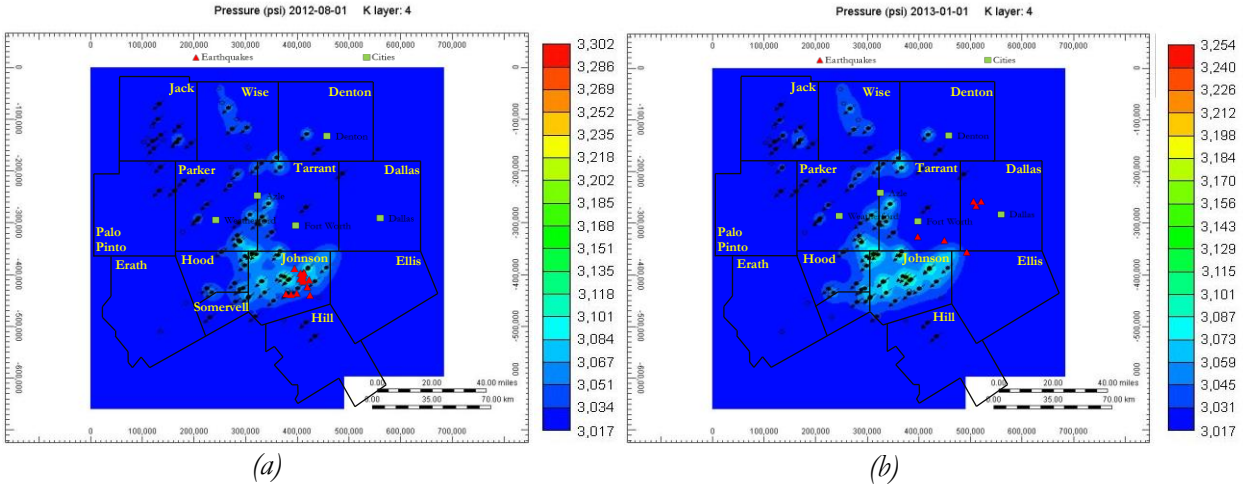

Figure 7. Homogeneous model pressure results.

Figures 8 and 9 show the simulated pore pressure for specific injection layers at the end of a cluster of earthquakes activities for layer 8. The simulation results showed some spatial and temporal correlations between earthquakes and injection well locations. However, in the maps of pressure throughout the layer, these changes are difficult to identify. Table 2 indicates magnitudes of pressure changes are specific earthquakes locations from 2008 through 2014. For example, around Azle, there is a pressure increase of around 15 psi between 2012 and 2014; however, there is a larger pressure increase of approximately 70 psi between 2010 and 2012.

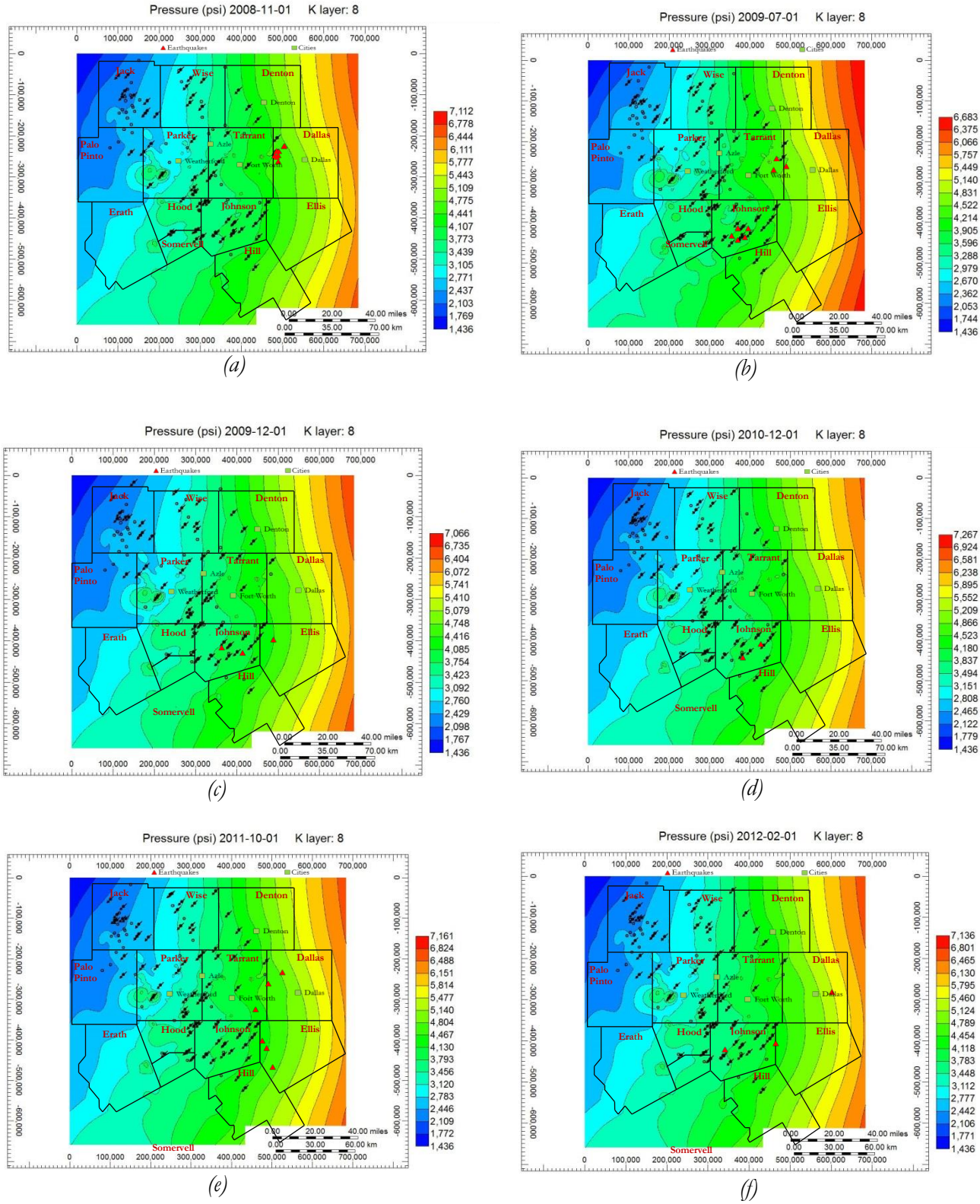

Figure 8. Pressure plots of layer 8 on dates where clusters of earthquakes were detected, 11/2008 through 2/2012.

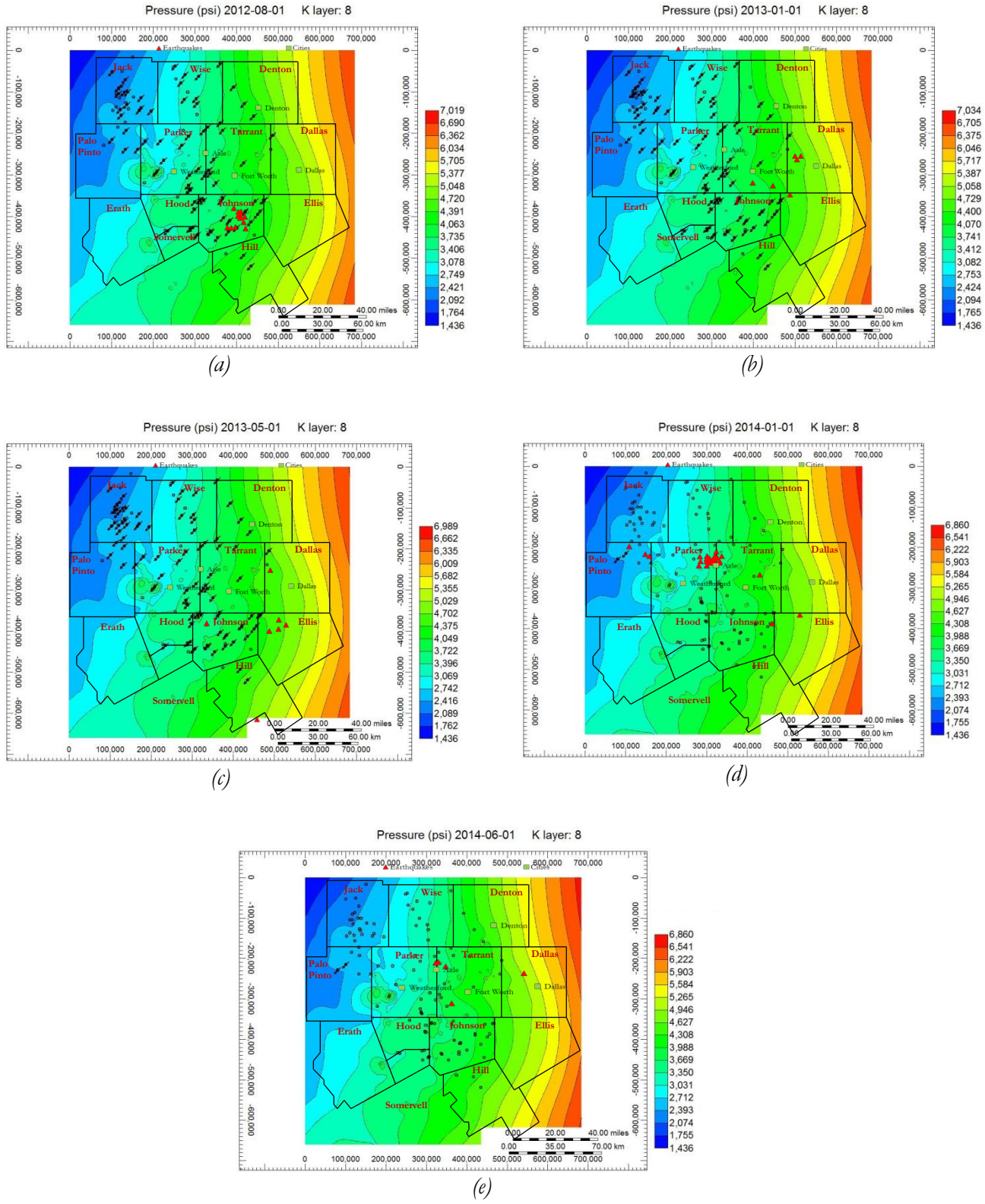

Figure 9. Pressure plots of layer 8 on dates where clusters of earthquakes were detected, 8/2012 through 6/2014.

Figure	Location	Date of Pressure Considered	Seismic Event Date	Starting Pressure (psi)	P@seismic (psi)	Pressure Increase (psi)
8a	Western Dallas County	12/1/2007	11/1/2008	3,789	3,830	41.1
8b	Southern Johnson County	12/2/2007	7/1/2008	3,070	3,092	22
8b	Eastern Tarrant County	12/3/2007	7/1/2009	3,670	3,686	16
8e	Southwestern Ellis County	7/1/2009	10/1/2011	3,729	3,749	20
9a	Middle of Johnson County	10/1/2011	8/1/2012	3,089	3,298	209

Table 2. Increase in pore pressure over time on location where seismic events occurred.

8.4 Modeling Limitations

Flow modeling of basin-wide wastewater injection is highly dependent on the input parameters. Basinwide geologic information has been difficult to collect, and the injection well data is not very detailed (typically we only have injection depth and monthly volumes). Nonetheless, this wide area approach does accentuate that apparently all high pressure regions do not have earthquakes and all earthquake areas don't have very high pressure. Also, it indicates that in some regions broad areas experience pore pressure change, and these areas might be those most susceptible to triggering large earthquakes if they were to occur.

Further modeling efforts should focus on using pressure data in companion with rate data to better estimate the permeability and thickness of injection intervals, and work is also needed on including more faults.

8.5 References

Blanchard, K. S., Denman, O., & Knight, A. S. (n.d.). Natural Gas in Atokna (Bend) Section of Northern Fort Worth Basin. 1446-1454.

Ewing, T. E. (1991). The Tectonic Map of Texas. Austin, TX: Bureau of Economic Geology.

Fountain, H. (2014, March 11). Ohio Looks at Whether Fracking Led to 2 Quakes. The New York Times.

Frohlich, C. (2012). Two-year Survey Comparing Earthquake Activity and Injection-Well Lcoations in the Barnett Shale, Texas. PNAS Early Edition.

Fu, Q., Horvath, S. C., Potter, E. C., ROberts, F., Tinker, S. W., Ikonnikova, S., . . . Yan, J. (2015). Log-derived Thickness and Porosity of the Barnett Shale, Fort Worth Basin, Texas: Implications for Assessment of Gas Shale Resources. AAPG Bulletin, 119-141.

Healy, J. H., Rubey, W. W., Griggs, D. T., & Raleigh, C. B. (1968). The Denver Earthquakes. Science, 1301-1310.

Hentz, T. F., Ambrose, W. A., & Carr, D. L. (2012). Reservoir Systems of the Pennsylvanian Lower Atoka Group (Bend Conglomerate), Northern Fort Worth Basin, Texas: High-resolution Facies Distribution, Structural Controls on Sedimentation, and Production Trends. AAPG Bulletin, 1301-1332.

Herkommer, M. A., & Denke, G. W. (1982). Stratigraphy and Hydrocarbons, Parker County, Texas. Dallas Geological Society.

Holland, A. A. (2013). Earthquakes Triggered by Hydraulic Fracturing in South-Central Oklahoma. Bulletin of the Seismological Society of America, 1784-1792.

Howe Justinic, A., Stump, B., Hayward, C., & Frohlich, C. (2013). Analysis of the Cleburne, Texas, Earthquake Sequence from June 2009 to June 2010. Bulletin of the Seismological Society of America, 3083-3093.

Jalali, M., Memarian, H., Zare, M., & Dusseault, M. B. (2008, July 2). Induced Seismicity Risk in Irani Oil and Gas Fields. American Rock Mechanics Association. San Francisco, CA.

Keranen, K. M., Weingarten, M., Abers, G. A., Bekins, B. A., & Ge, S. (2014). Sharp Increase in Central Oklahoma Seismicity Since 2008 Induced by Massive Wastewater Injection. Science .

Kim, W.-Y. (2013). Induced Seismicity Associated with Fluid Injection Into a Deep Well in Youngstown, Ohio. Journal of Geophysical Research, 3506-3518.

Panzar, J. (2014, November 27). Other States are Also Shaken, Sometimes Fracking May be to Blame for Earthquakes, but Not Always. Los Angeles Times. Lost Angeles, CA.

Pollastro, R. M., Hill, R. J., Jarvie, D. M., & Henry, M. E. (2003). Assesing Undiscovered Resources of the Barnett-Palezoic Total Petroleum System, Bend Arch-Fort Worth Basin Province, Texas. AAPG Southwest Section Meeting.

Pollastro, R. M., Jarvie, D. M., Hill, R. J., & Adams, C. W. (2007). Geologic Framework of the Mississippian Barnett Shale, Barnett-Palezoic Total Petroleum System, Bend Arch - Fort Worth Basin, Texas. AAPG Bulletin, 405-436.

Shapiro, S. A., Kummerow, J., Dinske, C., Asch, G., Rothert, E., Erzinger, J., . . . Kind, R. (2006). Fluid Induced Seismicity Guided by a Continental Fualt: Injection Experiment of 2004/2005 at the German Deep Drilling Site (KTB). Geophysical Research Letters.

Thompson, D. M. (1982). Atoka Group (Lower to Middle Pennsylvanian), Northern Fort Worth Basin, Texas: Terrigenous Depositional Systems, Diagenesis, and Reservoir Distribution Quality. Report of Investigations No. 125. Austin, TX: Bureau of Economic Geology.

USGS. (2015, 1 1). Induced Earthquakes. Retrieved from USGS Earthquake Hazards Program: http://earthquake.usgs.gov/research/induced/

van Poollen, H. K., & Hoover, D. B. (1970). Waste Disposal and Earthquakes at the Rocky Mountain Arsenal, Derby, Colorado. Journal of Petroleum Technology, 983-993.

Zoback, M. (1997). Inejction-induced Earthquakes and Crustral Stress at 9 km Depth at the KTB Deep Drilling Site, Germany. Journal of Geophysical Research, 18,477-18,491.

Zoback, M. (2012, April 17). Managing The Seismic Risk Posed by Wastewater Disposal. Earth.

9. Geological Synthesis

9.1 Introduction

This section was prepared by Julia Gale. It is the basis for a manuscript that will be submitted for publication in *2015*.

Task 7.0 – Building Fault Models in Selected Areas: Data Acquisition and Integration

Subtask 7.1 Selection of Key Areas for Geological Work

Subtask 7.2 Integration of Fault Data from Selected Areas

Geological work focused on two main areas; Timpson, East Texas and the wider Fort Worth Basin, Northern Texas. Geological input parameters were required for Task 8.0 of this project – Analysis of Fault Reactivation Potential for Selected Areas (Timpson, East Texas). The details of this geological work are reported in the Section 7 describing the Timpson study. A less detailed study of Williston Basin geology was also included in the analysis of events in that region (Frohlich et al., in press; see Section 4) and is not described again here.

In this section of the report we discuss the general geological factors influencing induced seismicity, using the Fort Worth Basin as our 'Key Area for Geological Work'. In particular we describe the challenges of fault analysis, as it pertains to induced seismicity, and present data for the Fort Worth Basin at a range of scales. We also discuss the influence of depth of injection, and the permeability structure of the injection horizon and of the layers above and below.

9.2 Data Gathering

Observation of published fault maps at the county scale or larger reveals discrepancies in the location and morphology of faults (Fig. 9.1). Moreover, in some publications it is not clear which horizon is being mapped, making comparison of maps even more challenging. Yet precise fault characterization is essential for deterministic models of induced seismicity. The lack of comprehensive fault maps at different scales available in the public domain compromises our ability to model induced seismicity, and to identify higher risk regions or depths in a basin. We made many requests to industry for data on subsurface structure in the areas covered by this project in the hope of filling some of the data gap. We requested structural interpretations of 3D reflection seismic volumes. In addition to the larger faults that have high potential associated risk we hope to gain information on smaller faults near the limits of reflection seismic detection. These data are of high value to companies, however, and none was forthcoming. One company has agreed to share reflection seismic data for small areas within the Fort Worth Basin, but we have not received it at the time of writing. We therefore relied on published maps, core and image log observations, and an in-house 3D reflection seismic volume from a small area on the border of Jack and Wise Counties in the Fort Worth Basin (referred to as the Boonsville data set). The lack of publically available reflection seismic data severely inhibited our ability to characterize the subsurface fault network in areas of interest. While we were able to map faults using our Boonsville data set, there has been no recorded seismicity in this area. Extrapolation to other areas that are

experiencing seismicity is not trivial because crustal structure in the area is not homogenous, and there is more than one fault set. We discuss findings, shortcomings, implications and recommendations in the following sections.

Well data and other geologic information was gathered using IHS databases for the different areas and State Survey and regulatory body databases for oil and gas; Texas Railroad Commission (TRRC) for Texas, SONRIS for Louisiana, and the North Dakota Department of Mineral Resources.

(a)

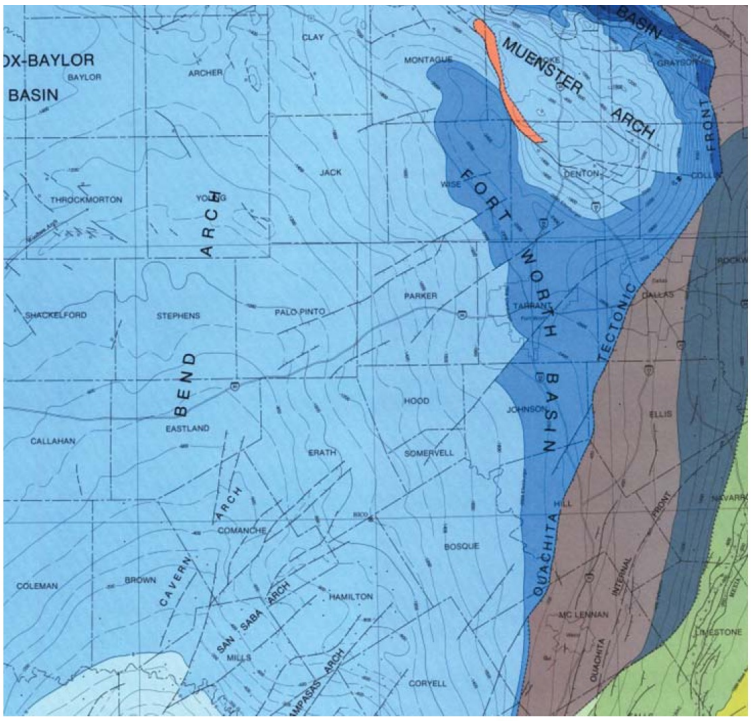

(b)

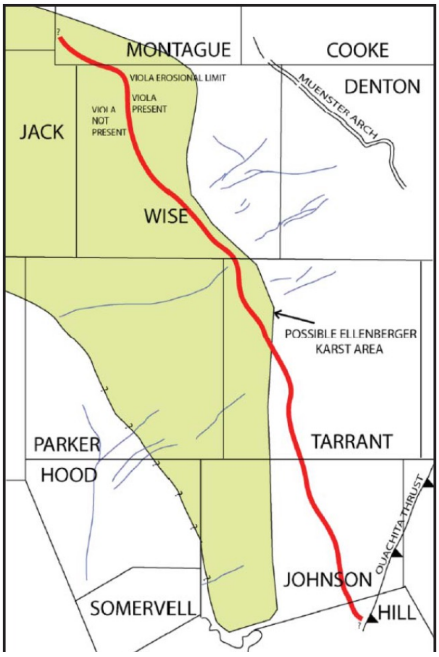

(c)

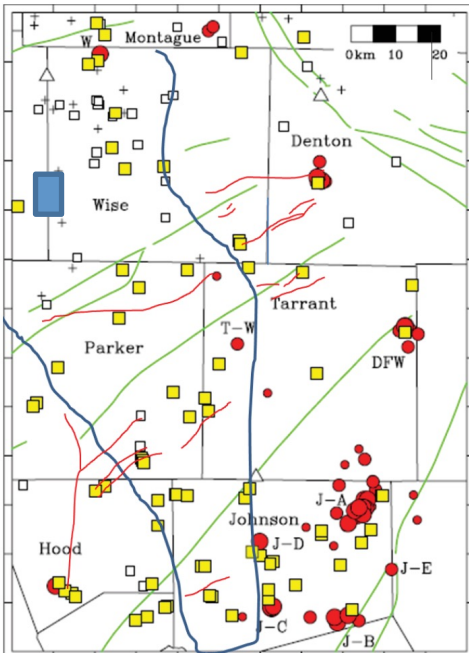

Fig. 9.1 Examples of published maps of faults in the Fort Worth Basin (a) faults on the top Ellenburger in the Tectonic Map of Texas (Ewing, 1991) (b) Mapped faults from Givens and Zhao (2005). Also shown is their interpretation of the extent of karsting in the Ellenburger Group (green shading) and the extent of the Viola Formation (red line) The structural level at which the faults are mapped is not stated. (c) Map from Frohlich (2012) showing faults taken from (a); green lines. The faults mapped in (b) are overlain red lines. The two mapped fault populations do not coincide for the most part, possibly because they are mapped at different structural depths or because they are different interpretations. Blue box indicates location of the Boonsville 3D reflection seismic volume.

9.3 Geologic parameters affecting the potential for induced seismicity

While there has been an increase in seismicity in the Fort Worth basin since 2008, events tend to be localized and limited in number to a few 10s of events in any one location. In 2014, for example there have been 13 events of M2.5 +, with 9 of those occurring in November and December near the town of Irving. By contrast there are hundreds of injection wells in operation across the basin (Fig. 9.2). In his 2012 study, Frohlich noted the heterogeneity of seismic activity in the basin, given the widespread injection, and speculated that the local geology was perhaps different. The purpose of this section is to examine the geologic factors that may influence the potential for induced seismicity in the central part of the Fort Worth basin (Jack, Wise, Denton, Parker, Tarrant, Hood and Johnson Counties) in the context of the location and depth of injection wells.

There are several key geologic parameters that potentially affect whether an earthquake could be induced or triggered as a result of fluid injection. These are: in-situ stress, permeability of injection interval and surrounding layers, fault strength and orientation. These parameters are discussed in general in this section and then more specifically for the Fort Worth Basin.

9.3.1 Depth of injection and composition of the injection interval

Both depth of injection and the composition of the target interval have a bearing on the behavior of injected fluids. The depth will govern the location with respect to dipping faults, and the composition of the target interval will govern the rate and volume of fluid that may be pumped. Depth of injection is more commonly reported than the target interval in the general injection well databases for IHS and the TRRC. In order to obtain the target interval the identified wells can be searched through the more specific databases for W-14 and H-1 wells at the TRRC.

For modeling purposes stratigraphic information for the area is needed. The level of detail needed depends on the goals of the modeling. For the basin-wide modeling of injection in the Fort Worth Basin (Section 8, this report) only broad stratigraphic intervals were needed, but for the Timpson study more detail was required. In this case we made use of stratigraphic tops for the well, picked from electric logs and reported by the operator, published work and in house Petra databases on the East Texas field to the north. In the more general case we note that even if stratigraphic

tops have been picked the interpretation of stratigraphy from logs is not always straightforward and some tops may not be correct.

For the Fort Worth Basin we mapped injection wells by disposal formation (Fig. 9.2) and by maximum injection volume (Fig. 9.3). There is some heterogeneity but in general the deepest wells, injecting into the Ellenburger Group are in the southeast of the basin, while the shallower, lower volume wells injecting in to the Pennsylvanian section are in the northeast. The difference in depth is a result of the basin structure, but also in choice of disposal target (Fig. 9.4). The Ellenburger Group is a faulted and karsted carbonate. Studies of the effects of karst collapse on fault development in the overlying sequence up to the Pennsylvanian section suggest the karst is unevenly developed on a small scale in the Boonsville dataset (McDonnell et al., 2007). Givens and Zhao (2005) suggested a broader region of enhanced karsting (Fig. 1b, green shaded area) that includes the area covered by the Boonsville study. Permeability of the karsted Ellenburger is highly heterogeneous. Faults and opening mode fractures are also present, some are likely open and able to transport fluids along their length and transmit fluids across them (cf. Gomez and Gale, 2007, study of fractures in karsted Ellenburger in West Texas). This combination of karst and open fractures has made the Ellenburger a target for disposal, but its heterogeneity is problematic for understanding the movement of disposed fluids.

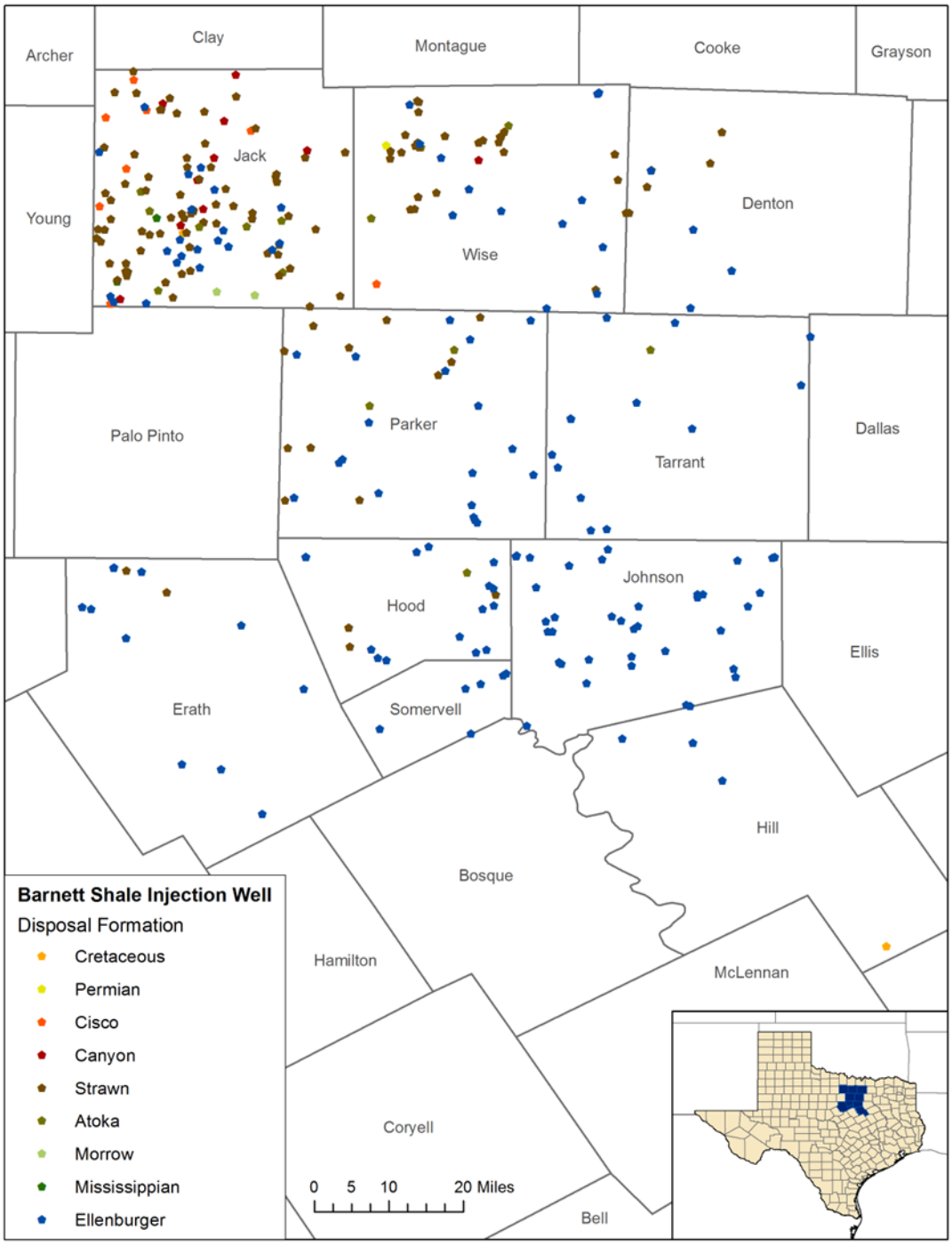

Fig. 9.2. Salt water disposal wells in the Fort Worth Basin identified through IHS and Texas Railroad Commission databases. Classes of well include W-14; disposal into a nonproductive zone and H-1; disposal into a productive zone. Color coding is for the Formation name of the disposal interval.

The Pennsylvanian section is dominated by clastic rocks, including the Bend, Strawn and Canyon group sandstone reservoirs.

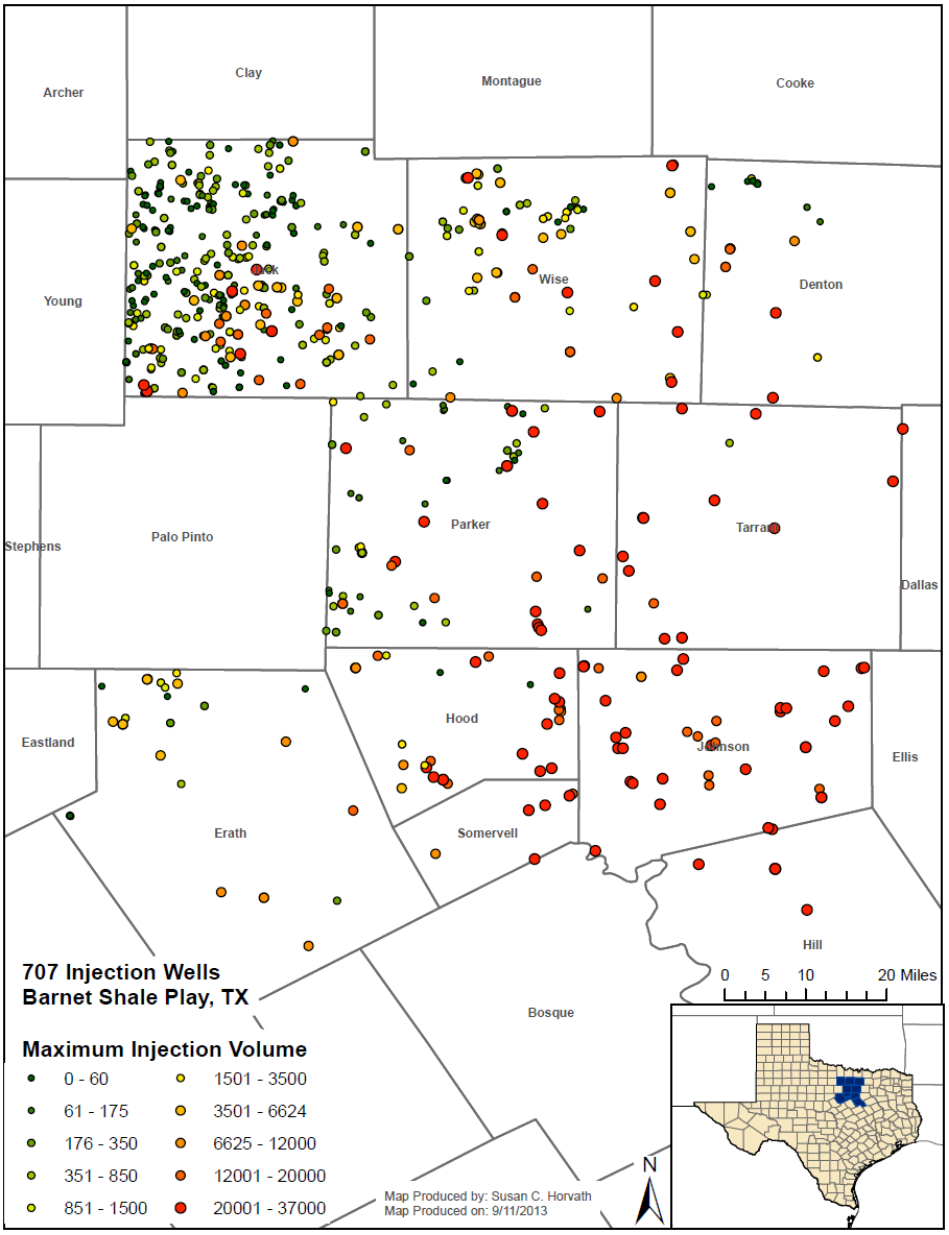

Fig. 9.3. Salt water disposal wells in the Fort Worth Basin identified through IHS and Texas Railroad Commission databases. Color coding is by maximum monthly injection volume (BWPM) .

9.3.2 Permeability of the injection zone

Information on the total volume and rate of injection, together with in-situ stress, can be used to model the pore-fluid pressure distribution around injection wells (e.g. Fan et al., this report). A key input parameter for models is the permeability of the rocks surrounding the well. Permeability is likely to be relatively high (a few 100s of md) in the injection horizon; the reason the horizon is chosen for injection is because porosity and permeability are high so that it can take large volumes of

water. The permeability may not be homogeneous, however, and if partly-open natural fractures or faults are present permeability may be heterogeneous. Permeability in the Ellenburger can range over several orders of magnitude depending on whether the formation has paleokarst; open fractures and connected vugs can produce channels with greater than darcy permeability, whereas the Ellenburger host rock may have very low permeability (Gomez and Gale, 2007). Permeability of layers above and below the injection horizon will govern the extent to which the fluids remain in the injection horizon. The stratigraphic architecture, which may not be "layer cake", will also affect the fluid dispersion. Constraining permeability is challenging in many subsurface flow problems, and the best that can be done is to capture uncertainty and conduct sensitivity analysis for measured ranges (cf. Fan et al., this report Section 7)

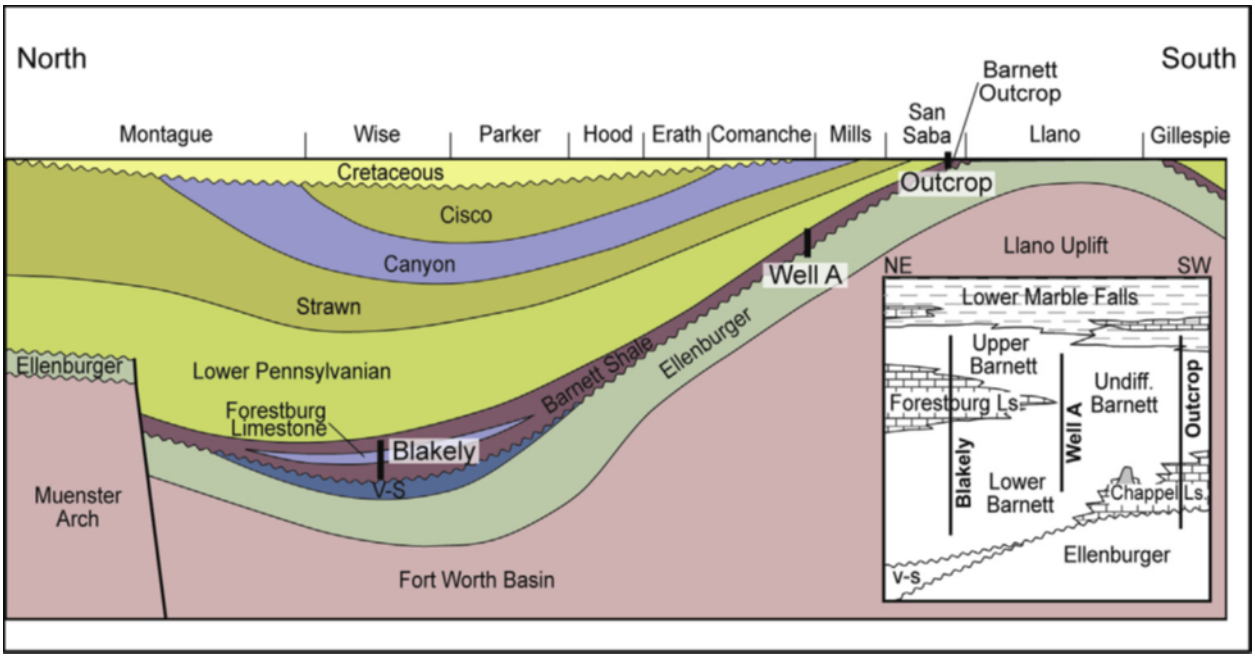

Fig. 9.4. Cross section through the Fort Worth Basin showing key stratigraphic intervals from Montague Co in the north to Gillespie Co. in the south. The section from Montague to Erath counties covers the area shown in Figs. 2 and 3. The Ellenburger Group and the Pennsylvanian Strawn section above the Barnett are the main disposal targets. From Gasparrini et al., (2014).

9.3.3 In situ stress

The in situ stress, together with the orientation of the fault governs fault criticality and thereby the degree to which faults present in an area are likely to slip, given a change in pore-fluid pressure. Some information on principal stress directions may be gained from borehole images of induced fractures and borehole breakouts. These may be available for nearby wells if not for the well in question. Minimum horizontal stress may be estimated from the breakdown pressure of the formation and vertical stress from the integration of density in the section. Maximum horizontal stress magnitudes are not routinely measured but a method using the width of the borehole breakout and the uniaxial compressive strength of the rock

can be used to estimate it. We used such methods to constrain in situ stress for the Timpson study (Section 7). For broad, basin-wide assessment the World Stress Map (Heidbach et al., 2009) is generally a useful source, but there are few data for the Fort Worth Basin; borehole breakouts to the southeast give consistent NE-SW trends for S_{Hmax} to the east, whereas data to the north on the border of Texas and Oklahoma are more variable in orientation (these data are also less robust) (Fig. 9.5). We have no data on magnitudes, but general indications from hydraulic fracturing practices in the Barnett Shale suggest a weak anisotropy in horizontal stresses, with dominant S_{Hmax} trending northeast. Local variation in this trend has been indicated by operators.

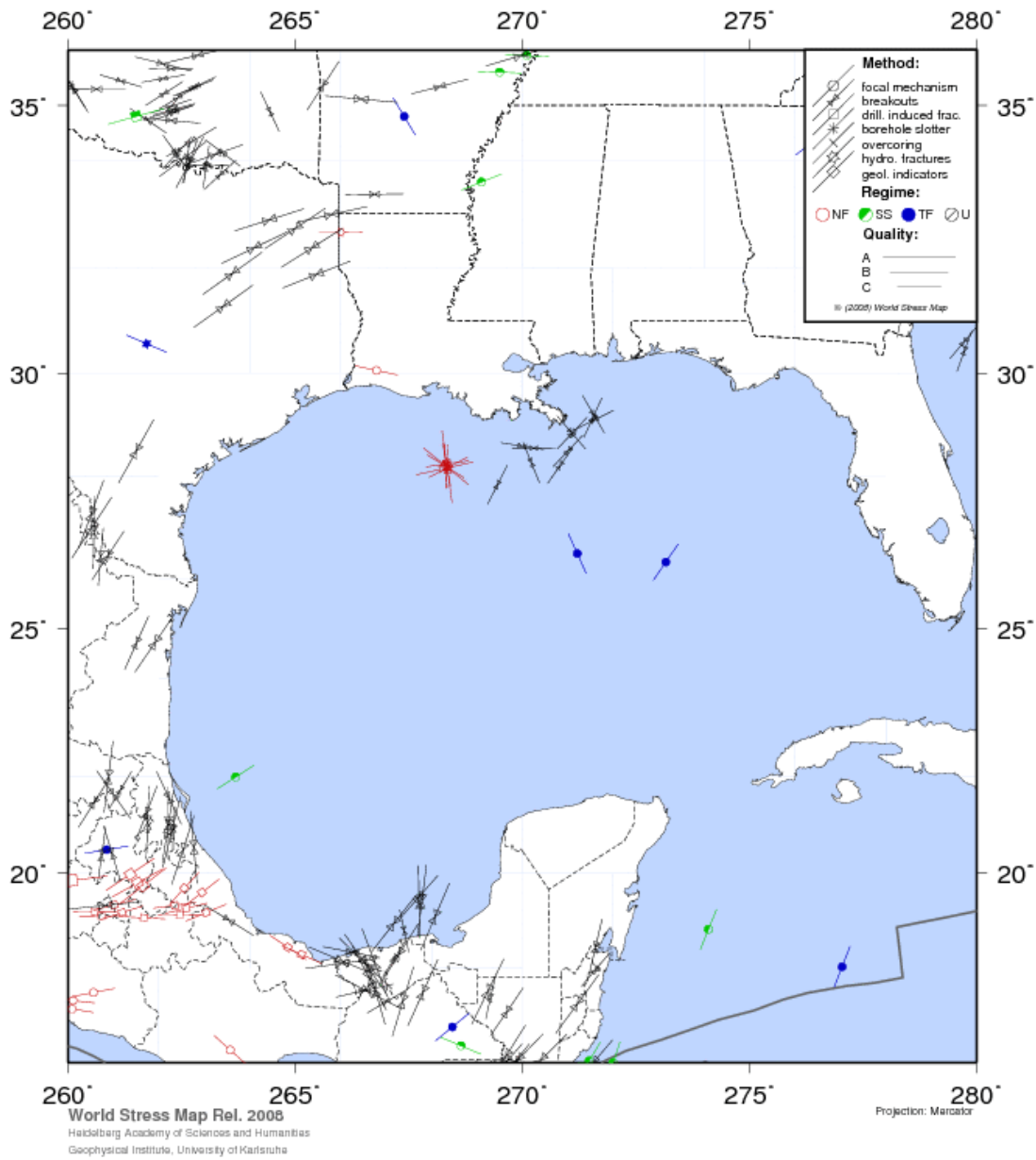

Fig. 9.5. World Stress Map for the Gulf of Mexico (Heidbach et al., 2009).

9.3.4 Fault populations

Movement on faults occurs when the stress on the fault is such that it overcomes the frictional shear-strength of the fault at a given location, and the fault reactivates. This can arise either because the far-field or local stress state changes, or because the normal stress across the fault is reduced due to an increase in pore-fluid pressure. Natural changes in tectonic stresses and pore fluids can occur. In addition to natural changes, human activity can affect both (Davies et al., 2014). In particular, fluid injected into disposal wells can increase pore fluid pressure. While the frictional properties of the fault can change if fluids are introduced along it giving rise to mineral reactions, this effect is highly specific to mineralogy, fluid composition, and PT conditions along the fault, and is secondary to the pore-fluid pressure effect on effective stress. The likelihood for reactivation depends not only on fault strength and stress on the fault, but also, crucially, on its orientation relative to the in-situ stress field. Some orientations are favored for slip, others less so. Where the stress on a fault is close to exceeding its strength the fault is termed 'critically stressed' (Barton et al., 1995). Critically stressed faults may not be present everywhere in a basin, but if they are present an increase in pore fluid pressure may be sufficient to trigger reactivation and an earthquake.

Faults are typically present at a range of scales from less than a meter to 10s of km in length and these populations demonstrate characteristic scaling (Walsh and Watterson, 1986; Cowie et al. 1996; Marrett et al., 1999). Many fault populations follow power-law cumulative frequency – displacement functions, for example Marrett et al. (1999) found fault displacements over five orders of magnitude for faults in the Paintbrush Group, Yucca Mountain, and large scale faults in Basin and Range in that vicinity. The total finite displacement on a fault is related to the fault length. Kim and Sanderson (2005) reviewed the relationships for different fault categories. For example, for normal faults the fault length is approximately 100 times the displacement. There is also a relationship between the size of a fault and the magnitude of the earthquake generated due to slip on that fault. The moment magnitude (which is the number reported for earthquake magnitude) is related to the seismic moment for that event, which is the area on the fault that has slipped multiplied by the amount of slip and the modulus of rigidity (shear modulus) of the rock. Zoback and Gorelick, (2012) summarized the relationships between magnitude, size, moment and stress drop. Faults with lengths of ~50 m to 10.0 km approximately correspond to earthquakes with magnitudes M2 to M5 depending on the stress drop (Fig. 9.6).

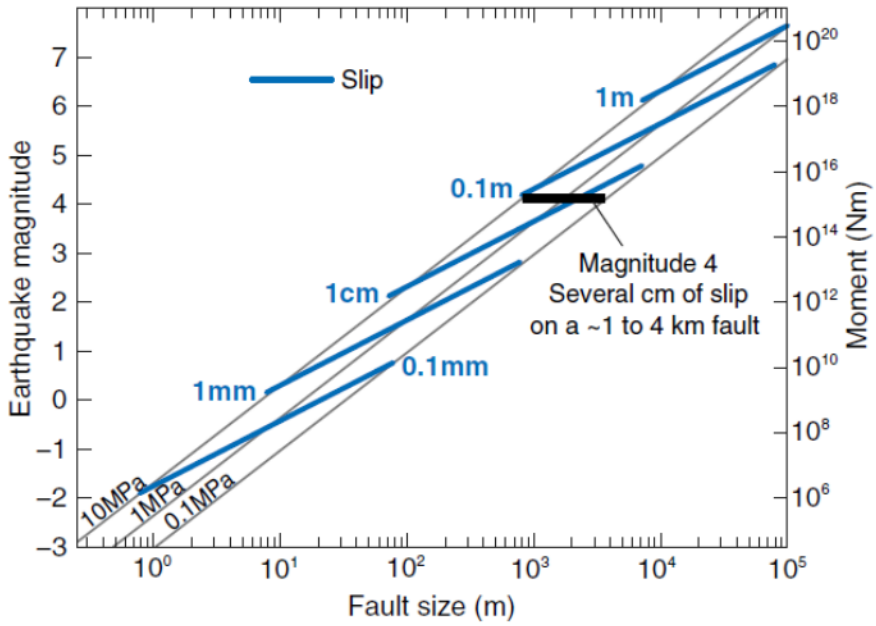

Fig. 9.6. Relationship between earthquake magnitude, fault size and moment for given stress drops (from Zoback and Gorelick, 2012).

A problem for diagnosing faults associated with events of 2-5 is that the total displacement may be less than would be seen on reflection seismic images. For example a normal fault with length 2 km has an offset of only 20 m according to the Kim and Sanderson (2005) length-displacement relationship. The result is a population of fault sizes relevant to the induced seismicity problem with smaller offsets than can be detected with existing tools.

Fault geometry presents a further challenge for understanding magnitudes of earthquakes likely for a given fault. The geometry of faults is generally more complex than typically represented on maps; they are commonly made up of multiple segments rather than single planes. Given that the size of the fault limits the size of the earthquake this might mean that for faults mapped as long, single planes the likelihood of a big event is reduced because the fault is actually made up of segments. Linkage of segments during a series of slip events has been the topic of numerous studies (e.g. Sibson, 1986). A small earthquake can occur where a small patch slips on a big fault, but a large earthquake will not occur on a small fault.

9.4 Fault Analysis in the Fort Worth Basin

9.4.1 Fault analysis from published maps

We examined fault population size characteristics for the FWB across a range of scales. Large-scale NE-striking faults are mapped on the top Ellenburger in Ewing's (1991) Tectonic Map of Texas (Fig. 9.7a). We measured the lengths of these faults in an area covering the central part of the Fort Worth basin and plotted their cumulative frequency (Fig. 9.7b). These data show a strong downward curvature at the large fault lengths (> 80 km), which is consistent with a censoring bias due to the size of the area investigated relative to the long fault lengths. For faults less than

~ 80 km long the data lie approximately along a straight line. The measured fault lengths range over less than one order of magnitude, however, so that the fit to the straight line is not well established; other curves could also be fitted to these data. The fault length versus apparent displacement relationship is also plotted but apparent displacement in the plane of the map is poorly constrained from the map alone, even assuming constantly dipping strata (Fig. 9.7c).

(a) (b)

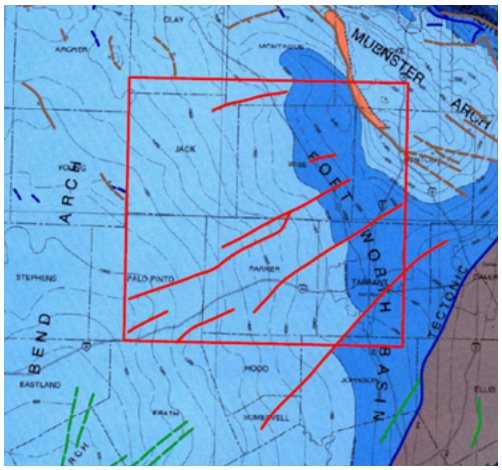

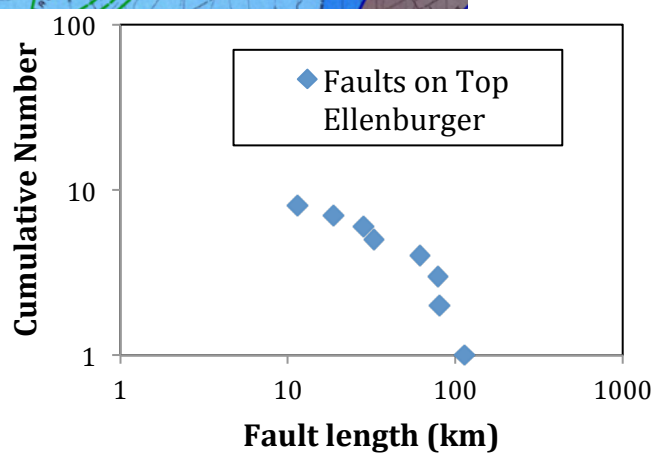

(c)

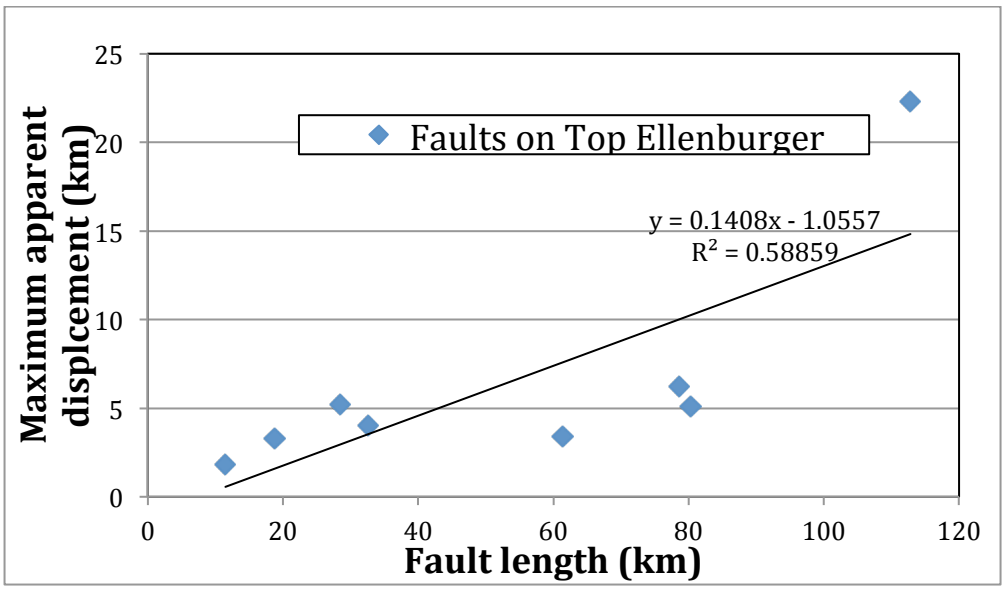

Fig. 9.7. (a) Faults on Ewing's 1991 map in Jack, Wise, Johnson counties are picked out in red; the area of investigation red box (b) Cumulative number fault length distribution plotted in log-log space. There is a power-law trend below around 80 km and likely a censoring artifact for faults longer than this. (c) Fault length is plotted against maximum apparent displacement, showing a correlation, albeit not strong.

In addition to the analysis of the Ewing (1991) map we measured faults on other maps of the area: 1) A map of the Ellenburger in the Fort Worth Basin by the J.M. Huber Corporation; 2) The Givens and Zhao (2005) map shown in Fig. 9.1; and 3) A map of Parker County by Hendricks (1955) that includes faults in outcrop in the Hill Creek Member of the Lazy Bend Formation in the Strawn Series. The Ellenburger faults trend mostly NE-SW, but faults in the Strawn showed a wide range of orientations. We compared fault length population distributions for a range of fault orientations centered on a NE trend (ENE-WSW through NNE-SSW) for the four maps by normalizing to map area for cumulative frequency (Fig. 9.8).

The cumulative frequencies for the two fault populations mapped in the Ellenburger are comparable; the earlier Huber map may have been in part a data source for the Ewing map. Interestingly the Givens and Zhao (2005) data show a continuation of the power-law straight line trend towards smaller faults in the Ellenburger, while they show a marked downturn in the larger fault population. This could be interpreted either as a function of the scale of their observation; in small seismic volumes the mapped faults will tend towards the smaller size, or as an indication that they saw evidence for smaller, linked faults rather than the longer ones mapped by Ewing. The broadly consistent trend on the plot gives us some basis for predicting frequency of smaller faults for the (dominant) NE-SW fault trend in this region of the Fort Worth Basin.

By contrast the mapped faults trending NE-SW in the Strawn show much higher frequency than fault populations in the Ellenburger. They also tend to be smaller length faults. Note how the slopes of the trends of both are similar (slope relates the number of small faults to large). We have no further mapped data to compare this result to, but in the next section will attempt to map faults in both Ellenburger and Strawn from a 3D reflection seismic volume.

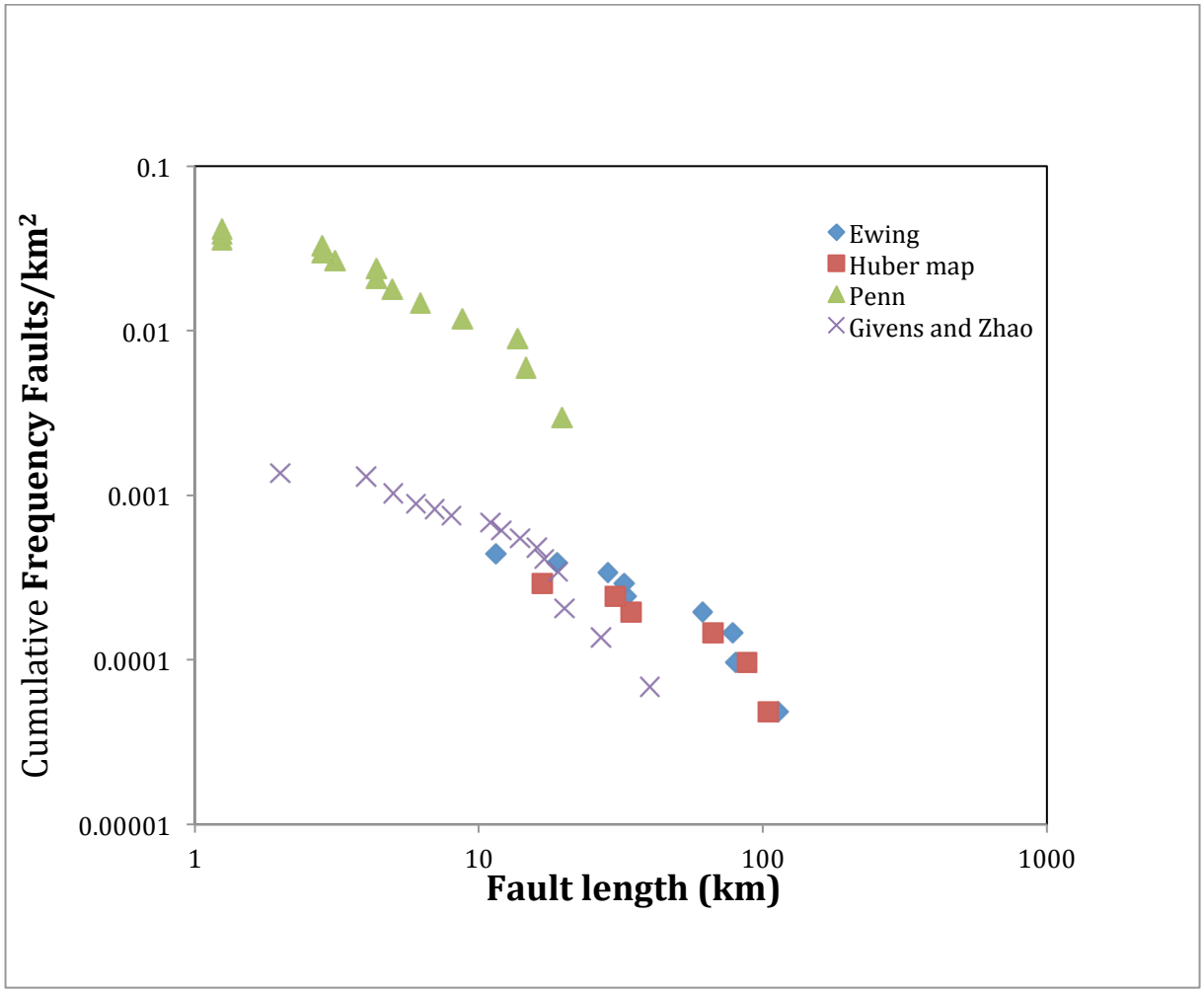

Fig. 9.8. Comparison of cumulative frequency fault length distributions for NE-SW trending faults in the Fort Worth Basin. Ewing, Huber and Givens and Zhao data are for faults mapped in the Ellenburger, the Penn data are for faults in outcrop in the Hill Creek Member of the Lazy Bend Formation in the Strawn Series.

9.4.2 Published fault analysis from reflection seismic data

There is extensive 3D reflection seismic coverage of the Fort Worth basin but this is not available to us. There are some published studies by other groups who have had access to these data, most notably from the group at The University of Oklahoma. Elebiju et al. (2010) link high-resolution aeromagnetic data, which captures basement structure, to seismic attributes on the Ellenburger at the top of the

basement delineating faults. They determined that much of the faulting is basement controlled and recognize to main trends; the northeast-southwest trend, parallel to the Ouachita orogenic belt, and the northwest-southeast trend, parallel to the Muenster Arch. Khawitada et al. (2013) also integrate 3D seismic, gravity, and magnetic data to image subbasement structures in the southeast Fort Worth basin. Their study area is in Wise and the western part of Denton counties.

McDonnel l et al. (2007) examined the circular faults that propagate up through the Pennsylvanian, with their origin likely in the collapsed karst of the Ellenburger. These faults are a different population from the large faults mapped by others on the top Ellenburger. The McDonnell et al. work utilized a small (67 km^2) 3D reflection seismic volume on the Jack/Wise county line (location, Fig. 9.1), termed the 'Boonsville' data set, and which belongs to the Bureau of Economic Geology at the University of Texas at Austin. We reanalyzed this data set using Landmark software, mapping faults with more planar geometries than the collapse faults in the McDonnell et al. study. We compare our results with those in the Khatiwada et al (2013) and Elejibu et al (2010) studies.

9.4.3 Fault analysis from the Boonsville seismic volume

We mapped faults in the Boonsville volume on the basis of where there is a discernable offset of reflectors and a signal in the coherency attribute. Fault attributes were measured and presented in Table 9.1 (appended). For fault height we used an average velocity of 16,800 ft/s for the entire interval since our faults penetrate from the basement into the Pennsylvanian and there is no good velocity information at or below the lower Ellenberger. The Pennslyvanian section is fairly slow (13000 ft/s) compared to the Ellenberger (21000 ft/s) so we used an average. Most of the faults cut through the Ellenberger and terminate in the Bend, some moving up into the Atoka, and a few into the Strawn.

The fault dimension and orientation data are included in An example of the mapped volume is illustrated in a 3D chair diagram showing vertical slices though the seismic amplitude and time slices on the top of the Ellenburger Group (red plane) and in the Pennsylvanian. The colored planes are mapped faults, which project up above the time slice and continue up into the Pennsylvanian.

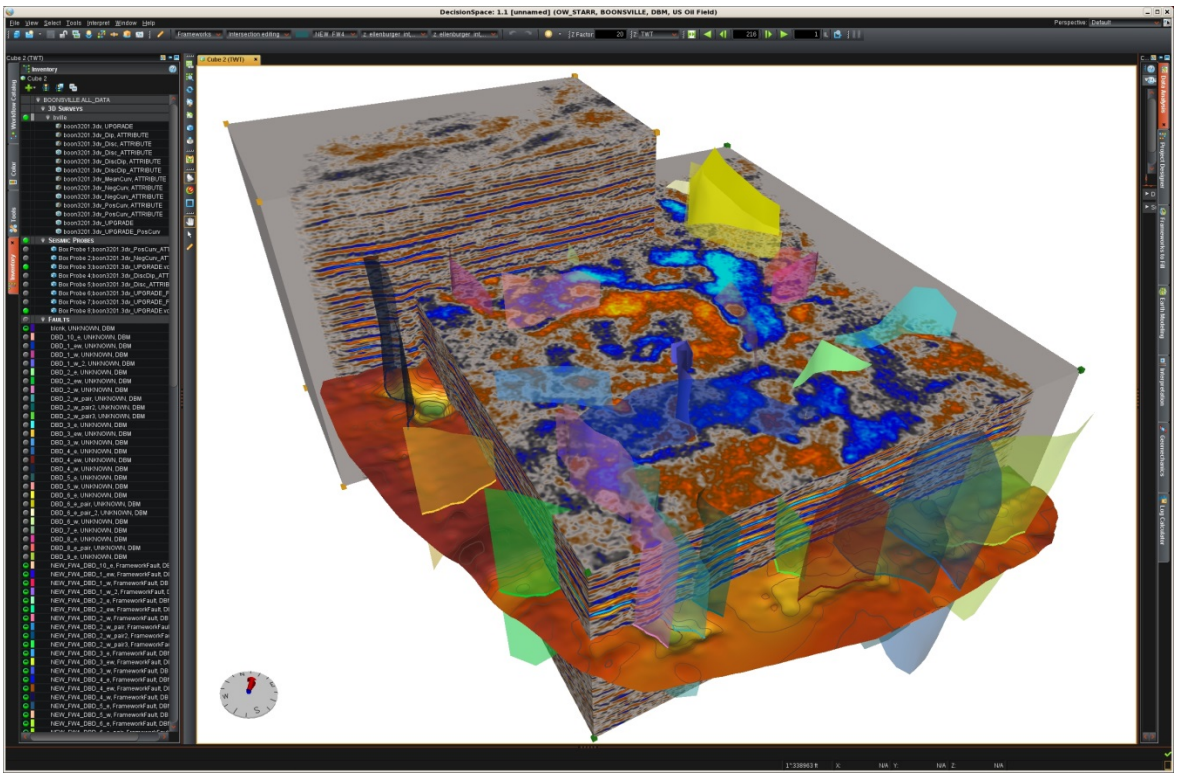

Fig. 9.9 A northeast-facing 3D view of the Top Ellenburger Structural Surface with transparently illuminated fault planes intersecting and terminating in Pennsylvanian-age stratigraphy.

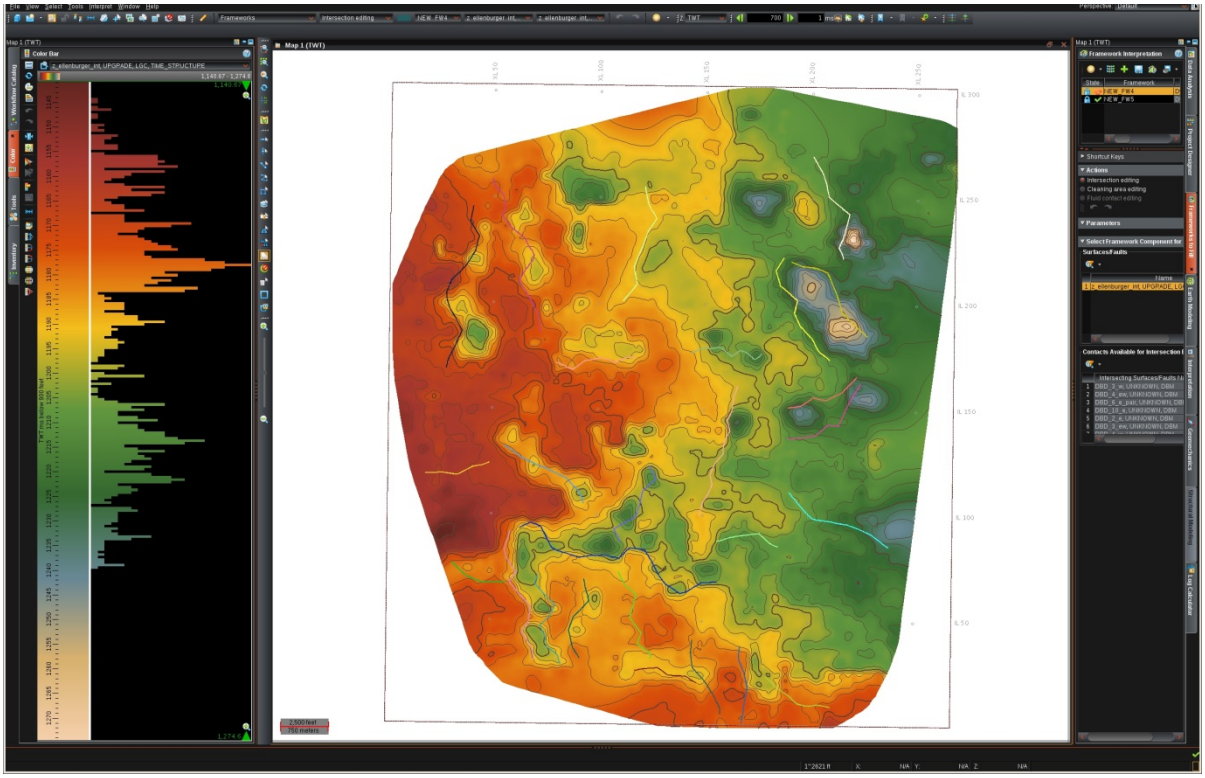

Fig. 9.10 Ellenberger structure map colored by depth with fault intersections marked as colored lines.

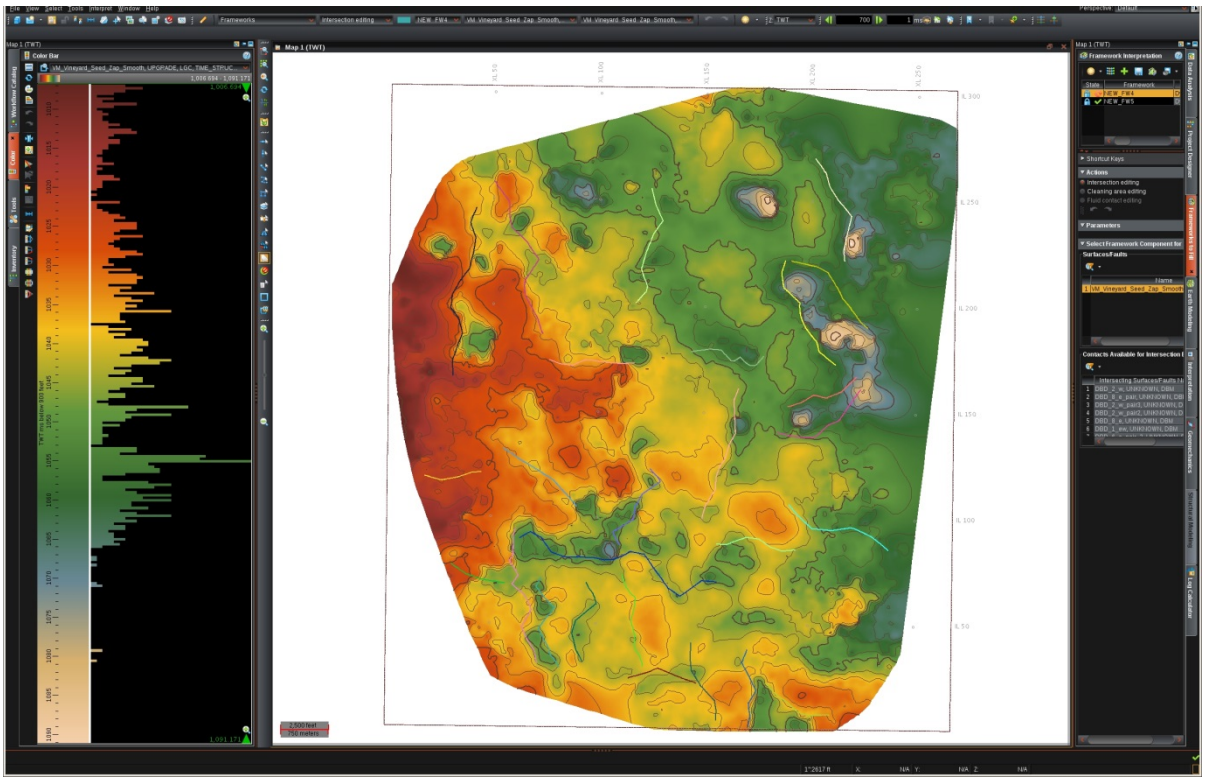

Fig. 9.11 Vineyard (Base of Bend Conglomerate) structure map colored by depth with fault intersections as for the Ellenburger marked as colored lines.

The structures are also shown in map view for the Ellenburger (Fig. 9.11) and for the Vineyard Formation, which is at the base of the Bend Conglomerate in the lower Pennsylvanian (Fig. 9.12). The faults and the sags are present in both horizons, suggesting they are large structures that have comparable heights and lengths. The heights, measured on the basis of the velocity conversion of TWT as described above, are of the order of 2500 to 5000 ft (750 to 1500 m), which is comparable to lengths of approximately 1 to 3 km (Table 9.1). It is likely that at least some of these structures comprise segments rather than individual faults of these dimensions. Our resolution is insufficient to determine this.

A further attribute that can help delineate structures is coherency. Coherency maps on the top Ellenburger and Vineyard show faults and collapse structures that are interpreted as such. There are also many other planar features (gray lines on the map) that might also be faults. These correspond to kinks or flexures in reflectors, but there is no clear break; they are below the limit of seismic resolution. We used to coherency maps in conjunction with the seismic amplitude to constrain faults to the best of our ability.

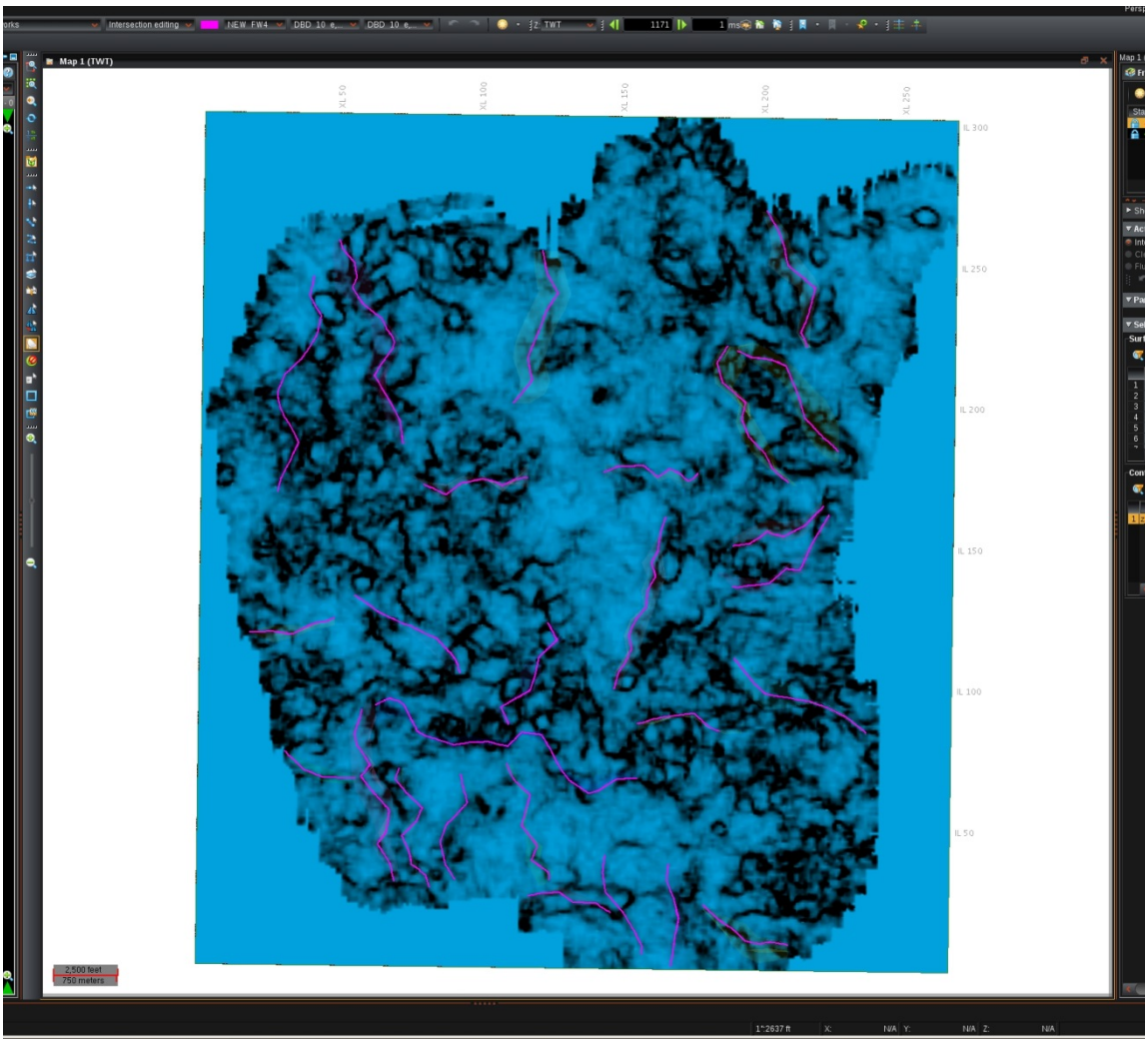

Fig. 9.12. Coherency time slice at 1171 ms below datum in Ellenburger-aged stratigraphy. Black represents areas of horizontal dissimilarity and blue represents areas of lateral continuity. Secondary collapse features are seen as black circles. Mapped faults from Fig. 9.10 are in pink.

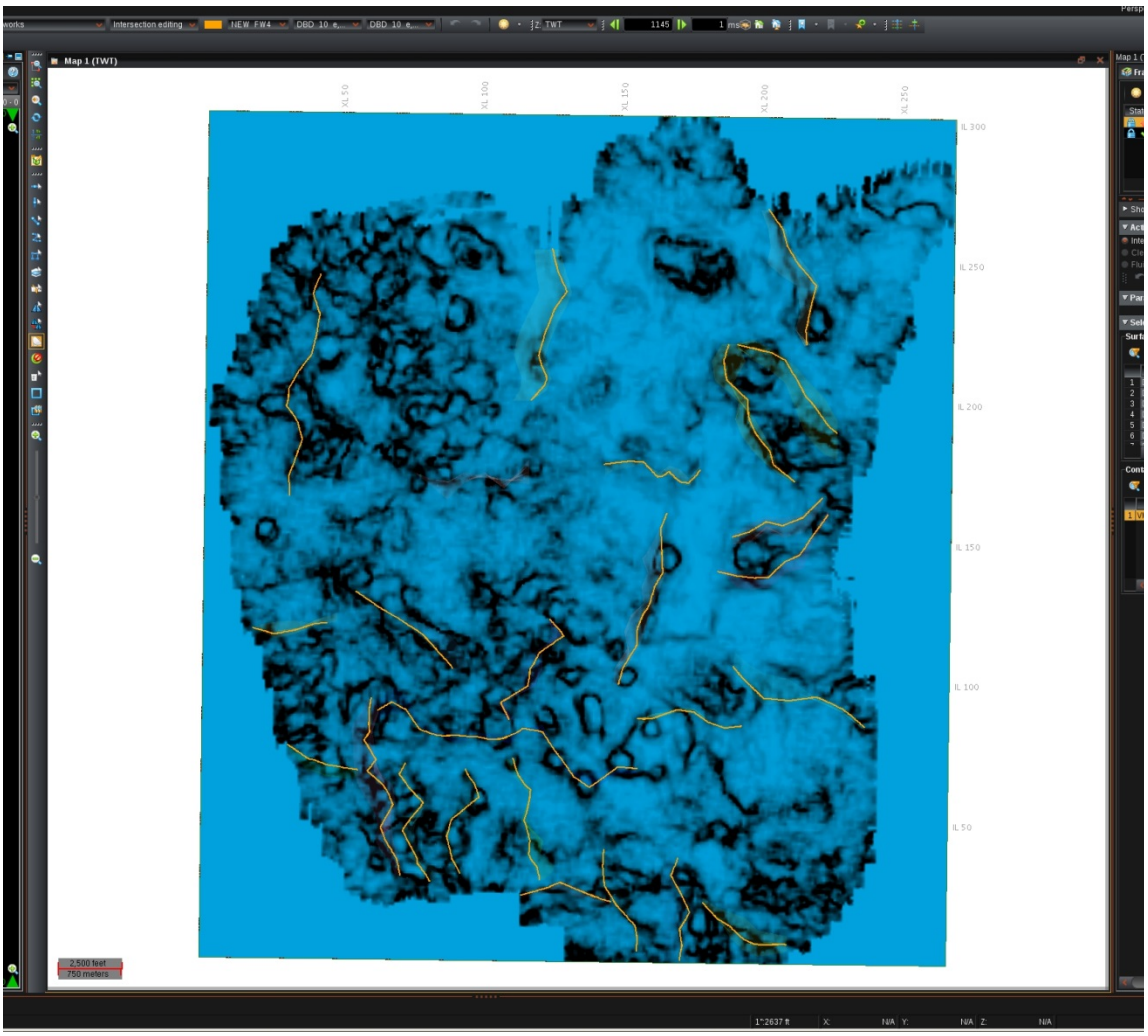

Fig. 9.13. Coherency time slice at 1145 ms below datum in Vineyard-aged stratigraphy. Black represents areas of horizontal dissimilarity and blue represents areas of lateral continuity. Secondary collapse features are seen as black circles. Mapped faults from Fig. 9.11 are in yellow.

We added the fault length data from the Boonsville analysis to the cumulative frequency plot for other data sets (Fig. 9.14). The Boonsville data plot with a steep slope at frequencies comparable to faults mapped in the Strawn outcrop in Parker County. Interpretation of the various datasets is challenging and there are many statistical sampling problems. Indeed, distinguishing between sampling artefacts and population attributes is a classic problem for interpretation of these types of data. One simple interpretation for the NE-trending fault set only is that the Ewing map captures the large faults in the population and the Boonsville seismic volume mapping captures the smallest faults. This relation might be represented on the plot by a power law, linking the two groups. The discrepancies for the other Ellenburger data could be regarded as truncation artefacts (resolution insufficient to capture all the faults at the small size) and the discrepancy for the Pennsylvanian outcrop data as a censoring problem where a particularly faulted horizon was mapped in more

detail than typical for that scale of map. The outcrop faults occur more densely in one part of the Parker County map than anywhere else. This simplistic interpretation assumes the fault population to be similarly developed across the different parts of the basin that we examined, (essentially Jack, Wise, Denton, Parker, Tarrant, Hood and Johnson Counties), which might not be the case. Accepting the interpretation implies that the frequency of NE-trending faults 1 km or more in length is approximately 0.1 /km^2.

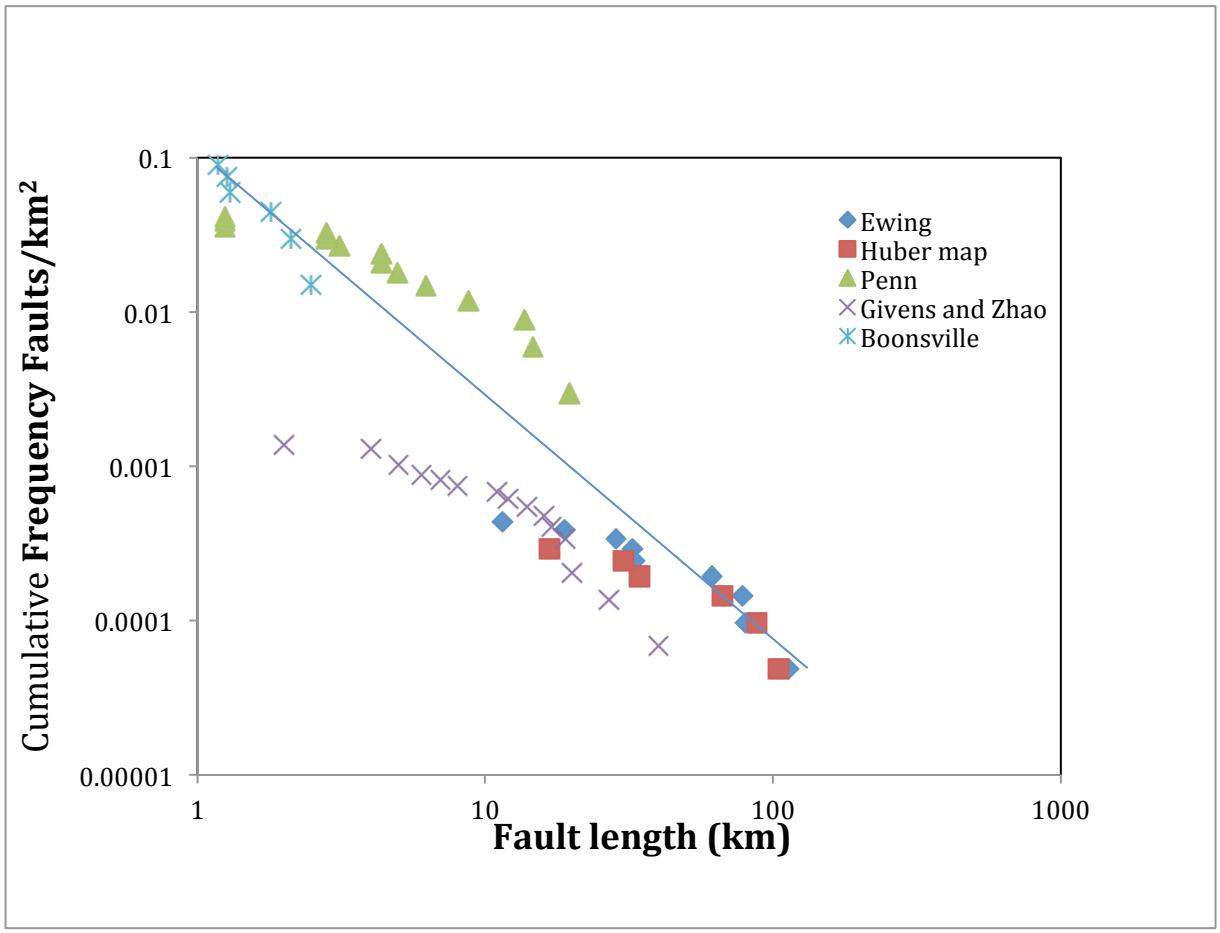

Fig. 9.14. Comparison of cumulative frequency fault length distributions for NE-SW trending faults in the Fort Worth Basin. Data are as for Fig. 9.8 but with the addition of the Boonsville data. The Boonsville NE-SW trending faults penetrate from basement to the Pennsylvanian section. Pale blue line links the smallest fractures mapped in the seismic volume with the largest structures mapped at basin scale.

Faults smaller than those on maps or in the seismic data are seen in some cores, and on image logs. It would be useful to be able to include these small faults on the cumulative frequency plot, but the sampling bias problems with them are potentially very great, because the structures are steeply dipping and there are relatively few cores or image logs available for analysis. Clustering of faults and fractures compounds the sampling bias problem, and orientation of faults in core is

commonly not known. Therefore although they are noted they cannot be included in the cumulative frequency plot.

9.5 Discussion and Recommendations

Critically stressed faults may not be present everywhere in the basin, and in fact the relative paucity of seismic activity in some areas suggests they are not. Our study, in addition to the Khatiwada et al (2013) and Elejibu et al (2010) studies are all in relatively quiescent parts of the basin (Fig. 9.1c). It would be useful to have reflection-seismic fault analyses in the more seismically active portion of the Fort Worth basin (Johnson County) to make some comparisons of fault populations in these areas. Of particular interest would be the deep Ellenburger structure in these regions, because the injection wells in the most seismically active region during the passage of the USArray are in the Ellenburger, and these are also the highest volume wells (Fig. 9.3)..

The main clusters of earthquakes in the Fort Worth basin have occurred in regions where injection has mostly been in the Ellenburger (Figs. 9.1, 9.2 and 9.3). We focused our analysis on the NE-trending set of faults because these are the dominant faults at the larger scale in the Ellenburger. We did not attempt to analyze the other fault orientations in a similar way because they number too few at the larger scale. The observations from the Boonsville data set, however, indicate several faults at the smaller scale in the NW-SE trend that extend from the Ellenburger up through the section to the Pennsylvanian, which is comparable to the findings of Elejibu et al. (2010) in their analysis of 3D seismic data. The frequency is similar to the NE-trending set. In the current stress field with relatively low anisotropy slip on either set could be possible. Our own experience with the Timpson study (section 7) shows that slip can occur on faults at orientations not generally favored for reactivation, but which are in close proximity to fluid injection activity.

The characterization of basin geology for assessing potential for induced seismicity is a necessary step in reducing risk. However, with the current tools available mapping of faults down to the scale required is challenging. It would be desirable to identify higher risk depths and regions basin-wide and to work towards more diligent fault mapping for planned disposal in those zones. In this study, because of limitations of data availability we were only able to map very crudely in different locations, and the smallest faults identified were approximately 1 km long. As per Fig. 9.6 we likely need data for the next scale down —faults around 100 m in length— and even these cannot be mapped with seismic data. However, such mapping activity would only provide some knowledge of fault styles, with perhaps ranges of intensity for different scales. There would be little information on fault clustering for example. There are alternative steps that could be taken to address the problem; one would be to improve technologies for fracture mapping, another would be to develop a stochastic model for fault risk assessment. For the remaining part of this study and into the future we will pursue the modeling approach.

The surface geology of the basin was not the focus of this project, but would be critical for assessing seismic hazard. Indeed, recommendations are now being

considered by USGS for inclusion of induced seismicity in their seismic hazard mapping initiative. The topic has recently been addressed in relation to hydraulic fracturing activities in the UK, where Westaway and Younger (2014) have suggested using the same critieria for permitted ground acceleration due to quarry blasting (peak ground velocities (PGV) in the seismic wavefield incident on any residential property of 10 mm s−1 during the working day, 2 mm s−1 at night, and 4.5 mm s−1 at other times). Clearly the topic merits further work.

Acknowledgements to RPSEA for funding, Landmark software usage, David Smith, Susan Horvath, Cari Breton for injection well data, Valerie Gono for generating the injection formation data, the Sloan Foundation Barnett Shale resource evaluation team at BEG , Dan Steward, Jon Huggins, Peter Hennings for technical discussions.

References

Barton, C. A., Zoback, M. D. and Moos, D., 1995, Fluid flow along potentially active faults in crystalline rock. Geology, v. 23, p.683–686.

Cowie, P. A., R. J. Knipe and I. G. Main, eds., 1996. Scaling laws for fault and fracture populations—Analyses and applications: Journal of Structural Geology 18: 135–383.

Davis, R., Foulger, G., Bindley, A. and Styles, P. 2014 Induced seismicity and hydraulic fracturing for the recovery of hydrocarbons. Marine and Petroleum Geology, v. 45, p.171–185.

Elebiju, O. O., Keller, G. R., and Marfurt K. J. (2010) Investigation of links between Precambrian basement structure and Paleozoic strata in the Fort Worth basin, Texas, U.S.A., using high-resolution aeromagnetic (HRAM) data and seismic attributes. Geophysics, v. 75, no. 4, p. B157–B168.

Ewing, T. E 1991, compiler, Tectonic map of Texas, Bureau of Economic Geology . SM0001. Scale 1:750,000. 4 oversized sheets, Lambert Conformal Conic projection based on standard parallel 33 degrees and 45 degrees. Accompanied by a text booklet, The Tectonic Framework of Texas, 36 p., 1991.

Frohlich, C. 2012, Two-year survey comparing earthquake activity and injection-well locations in the Barnett Shale, Texas. PNAS August 28, 2012 vol. 109 " no. 35, p. 13934-13938.

Givens, N., and Zhao, H. 2005, The Barnett Shale: not so simple after all. Expanded Abstract, AAPG Annual Meeting and Exhibition.

Gale, J.F.W., and Gomez, L.A., 2007. Late opening-mode fractures in karst-brecciated dolostones of the Lower Ordovician Ellenburger Group, west Texas: recognition, characterization, and implications for fluid flow. AAPG Bulletin v.91, p.1005–1023.

Heidbach, O., M. Tingay, A., Barth, J., Reinecker, D., Kurfeß and B. Müller (2009). The World Stress Map, equatorial scale 1:46,000,000: Commission for the Geological Map of the World, doi:10.1594/GFZ.WSM.Map2009.

Khawitada , M., Keller, G. R., and Marfurt, K. J., 2013, A window into the Proterozoic: Integrating 3D seismic, gravity,and magnetic data to image subbasement structures in the southeast Fort Worth basin, Interpretation, Vol. 1, No. 2, p. T125–T141, doi.org/10.1190/INT-2013-0041.1.

Kim, Y-S., and Sanderson, D. J., 2005, The relationship between displacement and length of faults: a review. Earth Science Reviews, v. 68, p.317–334.

Marrett, R., Ortega, O., Kelsey, C., 1999. Extent of power-law scaling for natural fractures in rock. Geology, v. 27, p.799–802.

Sibson, R. H., 1986, Brecciation processes in fault zones: inferences from earthquake rupturing. Pure and Applied Geophysics., v. 124, p. 159–175.

Walsh, J. J. & Watterson, J. 1988. Analysis of the relationship between displacements and dimensions of faults. Journal of Structural Geology 10, 239-247.

Westaway, R. and Younger, P. L., 2014 Quantification of potential macroseismic effects of the induced seismicity that might result from hydraulic fracturing for shale gas exploitation in the UK. Quarterly Journal of Engineering Geology and Hydrogeology, online first http://dx.doi.org/10.1144/qjegh2014-011

Zoback, M. D. and Gorelick, S. M., 2012, Earthquake triggering and large-scale geologic storage of carbon dioxide. http://www.pnas.org/content/109/26/10164 accessed 12/29/2014.

Appendix I: Earthquake Locations Determined in this Project

Table A1-1. Epicenters located within the Fort Worth Basin during this investigation (see Section 2). ID is identification number used by author to catalog event data; dep is focal depth (fixed at 5 km); mag is magnitude – values marked with '*' are magnitudes reported by the NEIC; rms is root mean square residual for location; gap is azimuthal gap of stations used in location; Q is location quality (see Data and Methods in text); events marked with '*' in ANF column appear in Array Network Facility catalog; group is epicentral cluster as labeled in Fig. 2-1 and Table 2.1.

ID	*year*	*mo*	*da*	*hr*	*mi*	*sec*	*lat*	*lon*	*dep*	*mag*	*rms*	*gap*	*Q*	*ANF*	*group*
115	2009	12	05	5	30	13.07	32.368	-97.082	5	2.9*	0.62	229	B	*	J-E
240	2009	12	22	5	20	26.55	32.454	-97.193	5		0.80	312	C		J-A
300	2009	12	30	9	6	50.89	32.263	-97.161	5		0.24	258	B		J-B
325	2010	01	01	23	47	30.67	32.416	-97.222	5		0.97	314	C		J-A
330	2010	01	02	8	6	47.05	32.474	-97.164	5	2.1	0.42	276	B		J-A
570	2010	01	27	9	20	22.30	32.614	-97.161	5	1.9	0.46	327	C		J-A
680	2010	02	06	3	53	2.94	32.552	-97.128	5		0.53	295	C		J-A
1725	2010	05	25	4	35	45.06	32.531	-97.121	5	2.1	0.46	292	B		J-A
1735	2010	05	26	5	54	55.73	32.858	-97.038	5		0.70	174	B		DFW
2025	2010	06	17	8	2	9.04	32.270	-97.279	5		0.47	136	B		J-B
2290	2010	07	11	10	33	5.31	32.966	-97.505	5		1.46	209	C		Tarrant W
2565	2010	07	30	10	31	11.54	33.416	-97.787	5		0.69	96	A	*	Wise
2830	2010	08	16	20	23	52.32	32.263	-97.218	5		0.45	102	B		J-B
3220	2010	09	30	10	48	44.77	32.288	-97.372	5		0.26	82	A	*	J-C
3240	2010	10	01	4	21	10.17	32.259	-97.213	5		0.47	104	A		J-B
3255	2010	10	03	11	25	44.64	32.270	-97.220	5		0.43	101	A		J-B
3400	2010	10	15	11	36	1.74	32.511	-97.148	5		0.61	72	A	*	J-A
3510	2010	11	01	11	1	15.67	32.822	-97.042	5		0.51	181	B	*	DFW
3580	2010	11	08	4	5	55.46	32.293	-97.372	5	2.5*	0.28	83	A	*	J-C
3585	2010	11	08	7	29	49.49	32.290	-97.374	5		0.30	82	A	*	J-C
3635	2010	11	12	9	3	51.86	32.290	-97.374	5	2.1*	0.34	82	A		J-C
3710	2010	11	20	15	35	57.79	33.158	-97.242	5	2.3	0.34	142	B		Denton
3720	2010	11	21	9	24	12.93	33.155	-97.252	5	2.1	0.58	112	B	*	Denton
3761	2010	11	23	19	59	54.05	32.334	-97.895	5		0.09	115	A	*	Hood
3765	2010	11	23	20	2	25.62	32.848	-97.018	5	2.4	0.80	156	B		DFW
3775	2010	11	24	0	49	23.90	33.156	-97.264	5		0.57	111	B	*	DFW
3785	2010	11	26	9	33	1.95	33.159	-97.252	5		0.53	81	A		Denton
3950	2010	12	11	2	29	50.08	33.160	-97.251	5	2.3	0.58	81	A	*	Denton
3976	2010	12	13	7	48	14.01	32.855	-97.064	5	2.5	0.32	117	B	*	Denton
3990	2010	12	13	21	7	32.76	33.167	-97.262	5		0.51	79	A	*	Denton
3995	2010	12	14	10	31	19.10	33.198	-97.256	5		0.44	139	B		Denton
4121	2010	12	29	4	32	38.64	33.463	-97.525	5		0.41	134	B	*	Montague
4126	2010	12	29	12	5	26.97	33.471	-97.514	5		0.43	130	B		Montague
4170	2011	01	04	0	17	36.42	33.162	-97.259	5		0.48	124	C		Denton
4900	2011	03	25	7	49	7.05	32.540	-97.209	5		0.45	217	B		J-A
5515	2011	05	23	3	57	25.66	32.469	-97.020	5		0.72	164	C		J-A
5595	2011	06	01	21	0	25.03	32.292	-97.368	5		0.37	120	A		J-C
5615	2011	06	03	0	54	7.82	32.425	-97.401	5		0.24	89	A		J-D
5620	2011	06	03	20	27	55.72	32.274	-97.187	5		0.49	104	A		J-B
5630	2011	06	06	10	23	54.51	32.271	-97.443	5		1.30	183	C		J-C
5636	2011	06	06	10	28	6.04	32.462	-97.187	5		0.26	151	A		J-A
5650	2011	06	06	23	55	5.24	32.513	-97.146	5		0.63	173	B	*	J-A
5660	2011	06	07	0	27	55.58	32.491	-97.145	5	2.2	0.66	207	B		J-A
5655	2011	06	07	0	15	44.39	32.582	-97.195	5		0.45	227	C		J-A
5661	2011	06	07	0	31	50.74	32.470	-97.178	5	2.2	0.60	210	B		J-A
5665	2011	06	07	7	41	36.08	32.465	-97.187	5		0.78	102	B		J-A
5670	2011	06	07	7	44	51.92	32.484	-97.157	5		0.62	162	B		J-A
5705	2011	06	07	21	19	24.48	32.454	-97.289	5		1.03	310	C		J-A

5712	2011	06	07	21	47	38.71	32.496	-97.130	5	2.2	0.71	284	C		J-A
5715	2011	06	07	21	51	20.97	32.504	-97.143	5	2.4	0.56	170	B		J-A
5720	2011	06	07	22	10	42.93	32.547	-97.127	5		0.47	186	B		J-A
5721	2011	06	07	22	11	36.50	32.502	-97.149	5		0.62	169	B		J-A
5722	2011	06	07	22	19	4.25	32.511	-97.140	5		0.61	116	A		J-A
5725	2011	06	07	23	35	17.90	32.493	-97.145	5	2.4	0.66	111	A		J-A
5730	2011	06	09	6	6	54.74	32.500	-97.146	5		0.60	168	B		J-A
5740	2011	06	10	6	32	17.21	32.828	-97.455	5		0.73	81	B	*	Tarrant W
5760	2011	06	12	16	51	49.80	32.495	-97.151	5	2.7*	0.58	74	A	*	J-A
5840	2011	06	25	5	38	52.62	32.480	-97.151	5	2.4*	0.71	76	A	*	J-A
5970	2011	07	09	3	14	56.84	32.483	-97.149	5		0.29	162	B		J-A
6005	2011	07	13	11	51	23.25	32.520	-97.029	5		1.05	180	C		J-A
6045	2011	07	17	6	58	1.08	32.488	-97.171	5	3.0*	0.63	94	A	*	J-A
6050	2011	07	17	8	23	56.10	32.494	-97.161	5		0.61	114	A	*	J-A
6055	2011	07	17	10	29	51.56	32.593	-97.147	5		0.22	194	B		J-A
6206	2011	08	01	4	33	30.80	32.865	-97.049	5	2.2*	0.24	115	A	*	DFW
6296	2011	08	07	4	45	31.87	32.864	-97.050	5	2.6*	0.27	115	A	*	DFW
6380	2011	08	12	18	50	59.75	32.728	-97.382	5		1.17	214	C		Tarrant W
6395	2011	08	14	7	14	51.83	32.483	-97.215	5		1.21	186	B		J-A

Table A1-2**.** Epicenters located within the Eagle Ford and surrounding areas during this investigation (see Section 3). 'EvID' is event identification number; identification numbers preceded by 'N' and 'A' are events reported by the NEIC and the Array Network Facility (ANF), respectively; 'mo da hr mi sec' are origin time month, day, hour, minute and second; 'lat lon' are latitude and longitude; 'dep' is focal depth (fixed at 5 km); 'rms' is root mean square residual of location (in seconds); 'gap' is azimuthal gap (in degrees); 'mag' is magnitude. Letter in 'Fig. 3-4', 'Fig. 3-8' and 'Fig. 3-3' columns indicates cluster in Figs. 3-3, 3-4 and 3-8.

Fashing Group

EvID	*year*	*mon*	*da*	*hr*	*mi*	*sec*	*lat*	*lon*	*dep*	*rms*	*gap*	*mag*	*Fig.3-4*
1242	2010	Mar	8	23	46	56.30	28.988	-97.970	5	0.91	110	3.00	F
N1243	2010	Mar	8	23	47	29.12	28.994	-97.962	5	0.89	113	2.85	F
A3438	2010	Aug	11	19	37	12.62	28.877	-98.199	5	0.93	81	2.29	D
N4956	2010	Dec	21	13	53	23.68	28.894	-98.187	5	0.88	82	3.00	D
N5166	2011	Jan	10	1	14	24.83	29.027	-97.959	5	1.05	118	2.60	F
5220	2011	Jan	15	5	28	31.70	28.966	-98.343	5	0.53	121	1.94	B
5379	2011	Feb	11	1	23	54.77	28.550	-98.024	5	0.96	89	2.18	E
A5532	2011	Mar	3	22	19	14.58	28.881	-98.192	5	1.16	80	2.63	D
5535	2011	Mar	4	6	36	38.64	28.868	-98.221	5	0.93	81	2.20	D
5754	2011	Apr	3	8	6	51.15	28.952	-98.184	5	0.88	97	1.94	C
5778	2011	Apr	7	9	42	4.54	29.259	-97.761	5	1.05	75	1.76	G
5781	2011	Apr	7	10	23	21.14	29.262	-97.766	5	1.00	74	1.84	G
5784	2011	Apr	7	10	39	8.04	29.260	-97.766	5	0.99	74	1.82	G
A5805	2011	Apr	9	4	47	16.22	29.246	-97.761	5	1.09	73	2.40	G
5880	2011	Apr	26	1	4	15.16	28.951	-98.189	5	0.75	98	2.01	C
5886	2011	Apr	26	8	41	4.51	28.945	-98.201	5	0.84	99	1.78	C
5887	2011	Apr	26	8	42	42.02	28.951	-98.191	5	0.84	98	1.78	C
5888	2011	Apr	26	8	43	45.82	28.952	-98.186	5	0.88	97	1.78	C
5889	2011	Apr	26	8	45	44.75	28.949	-98.191	5	0.85	98	1.78	C
5895	2011	Apr	27	0	29	27.98	28.951	-98.190	5	0.84	98	1.96	C
5898	2011	Apr	27	0	49	25.20	28.952	-98.190	5	0.81	98	1.93	C
5946	2011	May	4	2	44	14.48	28.956	-98.193	5	0.80	97	1.94	C
5949	2011	May	4	8	5	19.61	28.952	-98.191	5	0.79	97	1.84	C
5952	2011	May	4	9	54	47.03	28.959	-98.195	5	0.81	96	1.97	C

A6045	2011	May	19	8	43	11.05	29.354	-97.412	5	1.00	79	2.11		H
6051	2011	May	20	5	5	8.23	29.351	-97.413	5	0.96	75	2.16		H
6054	2011	May	20	16	21	37.73	29.351	-97.415	5	1.01	75	2.49		H
A6060	2011	May	21	7	27	11.30	28.846	-98.225	5	0.83	78	2.66	D	
6063	2011	May	21	7	44	36.28	28.933	-98.615	5	1.04	79	1.75		A
6069	2011	May	22	17	36	56.87	29.361	-97.420	5	1.05	74	2.62		H
A6081	2011	May	25	5	57	2.44	29.348	-97.417	5	1.21	75	2.36		H
6192	2011	Jun	22	10	47	21.89	28.875	-98.173	5	0.91	78	2.37	D	
6264	2011	Jul	5	10	4	31.89	28.954	-98.196	5	0.72	97	2.12	C	
6600	2011	Aug	26	23	4	30.22	28.924	-98.623	5	1.15	105	1.82		A
A6750	2011	Sep	22	7	30	28.66	29.017	-97.870	5	0.89	149	2.48	F	

Dimmit Group .

EvID	*year*	*mon*	*da*	*hr*	*mi*	*sec*	*lat*	*lon*	*dep*	*rms*	*gap*	*mag*	*Fig.3-8*
558	2010	Jan	13	20	21	27.26	28.478	-99.998	5	0.82	192	1.32	K
A 705	2010	Jan	26	9	39	0.52	28.491	-100.003	5	0.78	194	2.39	K
990	2010	Feb	25	23	25	19.12	28.486	-100.002	5	0.87	193	1.72	K
A1224	2010	Mar	8	12	4	18.42	28.490	-100.003	5	0.76	194	2.98	K
A1941	2010	Apr	22	9	20	28.92	28.479	-100.001	5	0.75	193	1.82	K
1962	2010	Apr	23	1	55	54.09	28.391	-100.058	5	0.41	227	1.72	L
1968	2010	Apr	23	12	5	18.27	28.386	-100.057	5	0.66	228	1.61	L
1989	2010	Apr	25	10	18	46.53	28.388	-100.048	5	0.47	223	1.78	L
1992	2010	Apr	26	5	31	44.00	28.385	-100.055	5	0.58	227	1.83	L
2037	2010	Apr	30	13	49	0.66	28.386	-100.053	5	0.70	226	1.49	L
2055	2010	May	1	0	16	27.51	28.490	-100.001	5	0.79	193	1.68	K
2679	2010	Jun	20	7	46	30.47	28.486	-100.000	5	0.84	193	1.59	K
4728	2010	Nov	29	2	4	13.82	28.606	-99.985	5	0.76	187	1.52	J
6174	2011	Jun	17	17	28	16.61	28.221	-99.672	5	0.80	134	2.45	M
6186	2011	Jun	21	2	1	11.15	28.214	-99.671	5	0.82	135	2.34	M
6222	2011	Jun	25	7	1	27.41	28.212	-99.661	5	0.65	135	2.00	M
6225	2011	Jun	25	14	54	11.86	28.211	-99.668	5	0.75	136	2.39	M
6228	2011	Jun	25	17	0	47.34	28.214	-99.676	5	0.72	136	2.20	M
A6231	2011	Jun	26	22	49	34.38	28.212	-99.681	5	0.74	137	2.72	M
6250	2011	Jun	30	9	35	12.61	28.206	-99.673	5	0.82	137	1.88	M
6255	2011	Jun	30	18	46	22.37	28.199	-99.681	5	0.89	140	2.35	M
6291	2011	Jul	9	15	25	31.71	28.182	-99.714	5	0.65	149	2.38	M

Other events (see Fig. 3-3) – Event #1986 location is from Frohlich et al. (2012)..

EvID	*year*	*mon*	*da*	*hr*	*mi*	*sec*	*lat*	*lon*	*dep*	*rms*	*gap*	*mag*	*Fig.3.3*
N1986	2010	Apr	25	2	10	42.69	27.71	-97.85	5			3.9	Alice
A3906	2010	Sep	18	3	20	44.05	30.637	-98.401	5	0.10	153	1.77	434A
A3909	2010	Sep	18	23	58	54.34	30.639	-98.409	5	0.13	151	1.88	434A
4484	2010	Nov	2	3	24	57.11	29.617	-96.851	5	0.20	302	2.29	636A
4828	2010	Dec	9	15	51	24.94	29.608	-96.855	5	0.19	301	2.54	636A

Table A1-3. Locations of earthquakes identified in this study in the Williston Basin and surrounding regions (see Section 4). Key: ID is identification number; dep is focal depth (fixed at 5 km for location); mag is magnitude; rms is root mean square residual; gap is azimuthal gap. Column labeled loc is location; events labeled Bk have epicenters within the shaded region in Fig. 4.1; events labeled CC are along the Cedar Creek Anticline.

ID	*year*	*mo*	*da*	*hr*	*mi*	*sec*	*lat*	*long*	*dep*	*mag*	*rms*	*gap*	*loc*
200	2008	11	02	22	49	19.48	46.410	-107.766	5	1.9	0.39	75	
360	2009	01	20	20	49	26.03	46.134	-105.484	5	1.8	0.21	107	

640	2009	07	15	5	14	7.15	47.439	-105.961	5	1.9	0.49	60	
680	2009	08	05	6	5	45.68	46.416	-107.760	5	1.9	0.36	76	
826	2009	08	31	1	24	22.78	47.632	-102.382	5	1.9	0.50	94	Bk
2090	2010	03	21	16	56	40.55	47.984	-103.978	5	2.5	0.27	72	Bk
2175	2010	04	27	5	7	58.84	46.585	-104.445	5	2.1	0.30	66	CC
2306	2010	06	14	7	58	3.46	46.034	-103.960	5	1.4	0.51	64	CC
2720	2011	04	06	11	23	49.39	48.418	-104.841	5	2.6	0.21	304	Bk

Table A1-4. Locations of earthquakes identified in this study in the Haynesville and surrounding regions (see Section 5).

Year	Month	Day	Hour	Min.	Sec.	Latitude	Longitude	Depth	Mag
2010	4	22	3	0	40.26	31.884224	-94.456665	1.88	1.59
2010	6	17	20	5	26.64	31.884182	-94.457186	1.953	2
2010	6	20	6	17	15.77	31.744706	-94.220117	7.581	1.88
2010	6	20	9	23	27.02	31.744702	-94.220093	7.576	1.73
2010	6	21	4	42	28.72	31.744686	-94.220125	7.576	1.68
2010	6	21	7	36	36.67	31.744718	-94.220117	7.569	1.62
2010	6	27	3	8	6.82	31.744722	-94.220036	7.574	1.67
2010	8	12	19	0	21.24	31.884204	-94.459318	2.153	1.98
2010	8	29	19	58	25.06	31.65259	-93.701172	1.764	1.89
2010	8	30	14	5	31.12	31.652464	-93.701465	1.759	2.85
2010	8	30	15	7	3.79	31.652629	-93.700944	1.764	2.09
2010	8	30	21	38	39.32	31.652572	-93.701237	1.734	2.08
2010	10	10	21	11	13.96	31.884267	-94.457275	1.979	1.91
2010	12	1	4	5	47.52	31.745003	-94.221566	8.25	2.32
2011	7	4	2	36	36.4	31.871753	-94.490999	13.50	2.81
2011	8	3	11	8	50.49	30.187105	-91.988721	27.36	2.75
2011	8	8	9	18	11.64	32.356769	-93.281144	5.948	1.28
2011	8	13	18	15	8.84	32.356419	-93.281177	6.068	2.27
2011	8	14	21	53	37.24	32.356732	-93.281315	6.08	1.58
2011	8	15	4	12	30.05	32.356989	-93.280623	6.378	2.21
2011	8	16	0	56	31.89	32.356791	-93.281396	6	1.48
2011	8	16	8	48	26.64	32.356722	-93.281104	6.055	1.65
2011	8	27	3	53	54.9	32.356858	-93.281226	6.054	1.5
2011	9	5	11	52	14.53	32.356486	-93.24091	9.682	1.76
2011	9	7	3	24	45.17	32.355516	-93.244775	5.987	1.66
2011	9	9	4	48	35.52	32.356423	-93.240991	9.721	2.11
2011	9	9	9	34	2.46	32.356242	-93.241227	9.894	1.37
2011	9	27	6	39	43.29	32.356852	-93.281063	6.117	2.19
2011	9	27	9	17	36.08	32.364537	-93.285107	13.39	2.36
2011	10	14	22	31	22.94	32.356801	-93.280981	6.063	2.15
2011	10	15	10	55	43.7	32.360225	-93.271395	2.419	2.74
2011	10	29	9	19	28.68	32.356639	-93.281217	6.014	1.74
2011	11	26	21	22	13.84	31.905288	-94.503035	17.78	3.05
2012	2	23	1	21	3.16	31.884127	-94.457959	1.991	2.42
2012	5	10	15	15	40.86	31.88395	-94.492098	14.11	4.63
2012	5	11	8	35	45.87	31.883734	-94.491895	13.89	2.5
2012	5	14	7	37	9.37	31.883811	-94.491895	13.9	2.34
2012	5	17	8	12	2.46	31.871297	-94.547599	20.13	5.45
2012	5	17	8	46	6.63	31.856077	-94.571672	22.69	2.1
2012	5	17	10	58	54.13	31.852708	-94.571118	22.81	2.72
2012	5	17	14	9	21.29	31.855332	-94.571411	22.73	2.3

2012	5	19	16	37	12.87	31.88387	-94.457926	1.947	2.1
2012	5	20	18	28	35.24	31.862244	-94.470524	13.35	3.53
2012	5	20	19	8	58.46	31.883927	-94.456323	1.935	1.92
2012	5	26	5	42	24.76	31.832074	-94.545345	27.87	2.51
2012	5	27	17	35	28.44	31.907774	-94.505005	17.67	2.69
2012	5	28	3	31	23.25	31.905904	-94.50271	17.73	1.69
2012	6	7	0	34	48.31	31.861226	-94.470719	13.53	2.36
2012	6	16	8	58	13.3	31.871682	-94.490194	13.39	2.82
2012	7	19	19	8	0.3	31.861208	-94.470638	13.53	2.84

Appendix II: Publications Resulting from this Project

Note: The publications marked '**' report research efforts initiated as a pilot project to prepare this proposal to RPSEA, but completed prior to initiation of RPSEA funding. Publications marked '*' concerned induced earthquakes, but primary authors were at other institutions and did not mention RPSEEA funding in article acknowldgements.

**Frohlich, C., Two-year survey comparing earthquake activity and injection well locations in the Barnett Shale, Texas, *Proc. National Acad. Sci.*,*109*, 13934-13938, 2012, doi:10.1073/pnas.1207728109

Frohlich, C., and M. Brunt, Two-year survey of earthquakes and injection/production wells in the Eagle Ford Shale, Texas, prior to the MW4.8 20 October 2011 earthquake, (Reprinted in: *Earth Planet. Sci. Lett.*, 402, 257-264, doi:10.1016/j.epsl.2014.06.006, 2014), *Earth Planet. Sci. Lett.*, *379*, 53-63, 2013, doi:10.1016/j.epsl.2013.07.02

Frohlich, C., W. Ellsworth, W. A. Brown, M. Brunt, J. H. Luetgert, T. MacDonald, and S. Walter, The 17 May 2012 M4.8 earthquake near Timpson, east Texas: An event possibly triggered by fluid injection, *J. Geophys. Res. Solid Earth*, *119*, 581-593, 2014, doi:10.1002/2013JB010755

**Frohlich, C., and E. Potter, What further research could teach us about "close encounters of the third kind": Intraplate earthquakes associated with fluid injection, in *Critical Assessment of Shale Resource Plays*, edited by J. Chatellier and D. Jarvie, *AAPG Memoir*, *103*, 109-119, 2013

Frohlich, C., J. I. Walter, and J. F. W. Gale, Earthquakes are scarce near injection wells in the Willeston Basin, 2008-2011, *Seismol. Res. Lett., 86,* 2015, doi: 10.1785/0220140180

*Gan, W., and C. Frohlich, Gas injection may have triggered earthquakes in the Cogdell oil field, Texas, *Proc. National Acad. Sci.*, *110*, 18786-18791, 2013, doi:10.1073/pnas.1311316110

*Hornbach, M. J., H. R. DeShon, W. L. Ellsworth, B. W. Stump, C. Hayward, C. Frohlich, H. R. Oldham, J. E. Olson, M. B. Magnani, C. Brokaw, and J. H. Luetgert. Causal factors for seismicity near Azle, Texas, *Nature Communications*, *(in press)*, 2015

*Justinic, A. H., B. Stump, C. Hayward, and C. Frohlich, Analysis of the Cleburne, Texas, earthquake sequence from June 2009 to June 2010, *Bull. Seismol. Soc. Amer.*, *103*, 3083-3093, 2013, doi:10.1785/0120120336

Appendix III: Technology Transfer Efforts Undertaken During this Project

2013 Apr 1 – Austin Geological Society meeting, Austin, TX: Frohlich, C. (invited), Texas earthquakes: Natural and manmade

2013 Apr 3 - GSA South Central Annual Meeting, Austin, TX: Frohlich, C. (keynote speaker), Texas earthquakes: Natural and manmade

2013 Apr 19 - Seismological Society of America Annual Meeting, Salt Lake City, UT: Brown, W., C. Frohlich, M. Brunt, W. Ellsworth and J. H. Luetgert, Investigating the cause of the 17 May 2012 M4.8 earthquake near Timpson, east Texas

2013 May 7 – Friends/Alumni of the Jackson School of Geosciences, Petroleum Club, Dallas, TX: Frohlich, C. (invited), Texas earthquakes: Eagle Ford and elsewhere: Natural and manmade

2013 Aug 5 - ECI sponsored conference Overcoming the Technical and Community Challenges of Hydraulic Fracturing for Shale Gas, Boulder, CO: Frohlich, C. (invited) Earthquake activity and injection/extraction in Texas

2013 Sep 9 - National Research Council workshop on Development of Unconventional Hydrocarbon Resources in the Appalachian Basin, Morgantown WV: Frohlich, C. (invited),

2013 Sep 16 - FRAC research consortium meeting, Austin, TX: Frohlich, C. (invited), Earthquake activity and injection/extraction in Texas

2013 Oct 24 - National Research Council workshop on Geoengineering Climate, Irvine, CA: Frohlich, C. (invited), What can injection-triggered earthquakes tell us about carbon sequestration as an earthquake hazard?

2013 Nov 11 - Scholia (Univ. Texas dinner club), Austin, TX: Frohlich, C. (invited), Texas earthquakes: Natural and manmade

2013 Nov 20 – Incorporated Research Institutions for Seismology webinar: Frohlich, C. (invited), Induced/Triggered Earthquakes: Examples from Texas

2013 Dec 11 - *American Geophysical Union meeting, San Francisco, CA:* Gan, W. and C. Frohlich. Did CO2 injection induce 2006-2011 earthquakes in the Cogdell oil field, Texas?

2013 Dec 11 - *American Geophysical Union meeting, San Francisco, CA:* Frohlich, C. (invited). Induced earthquakes are not all alike: Examples from Texas since 2008, Fall 2013

2014 Feb 20 – NETL webinar: Frohlich, C. (invited), Triggered earthquakes in Texas: "Everything you know is wrong"

2014 April 3 - Geophysical Society of Houston, Houston, TX: Frohlich, C. (invited), Triggered earthquakes in Texas: Everything you know is wrong

2014 Apr 7 - AAPG meeting: Gale, J., C. Frohlich, P. Eichhubl, J. Olson, Z. Fan, V. Gono, D. Smith, S. Horvatch, C. Breton and Marcy Davis, Relationships between induced seismicity and fluid injection: Development of strategies to manage injection

2014 April 15: Texas Geological Society, Dallas, TX: Frohlich, C. (invited) Triggered earthquakes in Texas: Everything you know is wrong

2014 Apr - European Geosciences Union General Assembly, Vienna, Austria: Eichhubl, P., C. Frohlich, J. Gale, J. Olson, Z. Fan and V. Gono, Induced and triggered seismicity: Theory and Observations

2014 Jul 8 - Petroleum Systems Engineering International Summer School, Austin, TX: Frohlich, C. and J. Olson (invited), What mother never told you about human-caused earthquakes

2014 Jul 10 - Texas Society of Professional Engineers, Dallas, TX: Frohlich, C. (invited) Triggered earthquakes in Texas: Everything you know is wrong

2014 Nov 5 - Earthquake Engineering Research Institute, Univ. Texas Austin, TX: Frohlich, C. Human-caused earthquakes in Texas and elsewhere: Everything you know is wrong. Invited seminar,

2014 Nov 12 - Workshop: Hydrocarbons and Seismicity in Italy, Rome, Italy: Astiz, L., J. H. Dietrich, C. Frohlich, B. H. Hager, R. Juanes and J. H. Shaw. Multidisciplinary study on the potential of induced seismicity due to oil and gas extraction activities: Geomechanical modeling as a tool to manage and monitor phenomena

2014 Nov 19 - Center for Petroleum and Geosystems Engineering Webinar, Austin, TX: Frohlich, C. and J. Olson (Invited). Induced seismicity: A multidisciplinary perspective.

2014 Dec 2 - TOPCORP short course for policymakers and regulators, Austin, TX: Frohlich, C. and J. Olson (Invited). Induced earthquakes and seismic hazards

2014 Dec 19 - American Geophysical Union meeting, San Francisco, CA: DeShon, H. R., M. J. Hornbach, W. L. Ellsworth, H. R. Oldham, C. Hayward, B. W. Stump, C. Frohlich, J. E. Olson and J. H. Luetgert. Understanding North Texas seismicity: A joint analysis of seismic data and 3D pore pressure modeling

2014 Dec 19 - American Geophysical Union meeting, San Francisco, CA: Fan, Z., P. Eichhubl, J. Gale, C. Frohlich and V. Gono. Was the Timpson, Texas, M4.8 event induced by fluid injection?

2014 Dec 19 - American Geophysical Union meeting, San Francisco, CA: Frohlich, C., J. I. Walter and J. Gale. Induced seismicity in the Bakken: Much ado about almost nothing

2015 Feb 2 –Petroleum and Geosystems Engineering, Univ. Texas Austin TX: Frohlich, C. Human-caused earthquakes in Texas and elsewhere: All alike in that they are all different.